



National Library
of Canada

Acquisitions and
Bibliographic Services Branch

395 Wellington Street
Ottawa, Ontario
K1A 0N4

Bibliothèque nationale
du Canada

Direction des acquisitions et
des services bibliographiques

395, rue Wellington
Ottawa (Ontario)
K1A 0N4

Your file - Votre référence

Our file - Notre référence

NOTICE

The quality of this microform is heavily dependent upon the quality of the original thesis submitted for microfilming. Every effort has been made to ensure the highest quality of reproduction possible.

If pages are missing, contact the university which granted the degree.

Some pages may have indistinct print especially if the original pages were typed with a poor typewriter ribbon or if the university sent us an inferior photocopy.

Reproduction in full or in part of this microform is governed by the Canadian Copyright Act, R.S.C. 1970, c. C-30, and subsequent amendments.

AVIS

La qualité de cette microforme dépend grandement de la qualité de la thèse soumise au microfilmage. Nous avons tout fait pour assurer une qualité supérieure de reproduction.

S'il manque des pages, veuillez communiquer avec l'université qui a conféré le grade.

La qualité d'impression de certaines pages peut laisser à désirer, surtout si les pages originales ont été dactylographiées à l'aide d'un ruban usé ou si l'université nous a fait parvenir une photocopie de qualité inférieure.

La reproduction, même partielle, de cette microforme est soumise à la Loi canadienne sur le droit d'auteur, SRC 1970, c. C-30, et ses amendements subséquents.

Canada

UNIVERSITY OF ALBERTA

**DIRECT ANALYSIS OF SOLID MATERIALS BY ELEMENTAL MASS
SPECTROMETRY**

by

XINBANG FENG



**A Thesis Submitted to the Faculty of Graduate Studies and Research in Partial
Fulfillment of the Requirements for the Degree of Doctor of Philosophy**

DEPARTMENT OF CHEMISTRY

EDMONTON, ALBERTA

FALL, 1994



National Library
of Canada

Acquisitions and
Bibliographic Services Branch

395 Wellington Street
Ottawa, Ontario
K1A 0N4

Bibliothèque nationale
du Canada

Direction des acquisitions et
des services bibliographiques

395, rue Wellington
Ottawa (Ontario)
K1A 0N4

Vous le / Votre référence

Vous le / Notre référence

The author has granted an irrevocable non-exclusive licence allowing the National Library of Canada to reproduce, loan, distribute or sell copies of his/her thesis by any means and in any form or format, making this thesis available to interested persons.

L'auteur a accordé une licence irrévocable et non exclusive permettant à la Bibliothèque nationale du Canada de reproduire, prêter, distribuer ou vendre des copies de sa thèse de quelque manière et sous quelque forme que ce soit pour mettre des exemplaires de cette thèse à la disposition des personnes intéressées.

The author retains ownership of the copyright in his/her thesis. Neither the thesis nor substantial extracts from it may be printed or otherwise reproduced without his/her permission.

L'auteur conserve la propriété du droit d'auteur qui protège sa thèse. Ni la thèse ni des extraits substantiels de celle-ci ne doivent être imprimés ou autrement reproduits sans son autorisation.

ISBN 0-315-95180-X

Canada

Name Xinbang FENG

Dissertation Abstracts International is arranged by broad, general subject categories. Please select the one subject which most nearly describes the content of your dissertation. Enter the corresponding four-digit code in the spaces provided.

0486 U·M·I
SUBJECT CODE

SUBJECT TERM

Subject Categories

THE HUMANITIES AND SOCIAL SCIENCES

COMMUNICATIONS AND THE ARTS

Architecture 0729
Art History 0377
Cinema 0900
Dance 0378
Fine Arts 0357
Information Science 0723
Journalism 0391
Library Science 0399
Mass Communications 0708
Music 0413
Speech Communication 0459
Theater 0465

EDUCATION

General 0515
Administration 0514
Adult and Continuing 0516
Agricultural 0517
Art 0273
Bilingual and Multicultural 0282
Business 0688
Community College 0275
Curriculum and Instruction 0727
Early Childhood 0518
Elementary 0524
Finance 0277
Guidance and Counseling 0519
Health 0680
Higher 0745
History of 0520
Home Economics 0278
Industrial 0521
Language and Literature 0279
Mathematics 0280
Music 0522
Philosophy of 0998
Physical 0523

Psychology 0525
Rending 0535
Religious 0527
Sciences 0714
Secondary 0533
Social Sciences 0534
Sociology of 0340
Special 0529
Teacher Training 0530
Technology 0710
Tests and Measurements 0288
Vocational 0747

LANGUAGE, LITERATURE AND LINGUISTICS

Language 0679
 General 0289
 Ancient 0290
 Linguistics 0291
 Modern 0401
Literature 0294
 General 0295
 Classical 0297
 Comparative 0298
 Medieval 0316
 Modern 0591
 African 0305
 American 0352
 Asian 0355
 Canadian (English) 0593
 Canadian (French) 0311
 English 0312
 Germanic 0315
 Latin American 0313
 Middle Eastern 0314
 Romance 0370
 Slavic and East European

PHILOSOPHY, RELIGION AND THEOLOGY

Philosophy 0422
Religion 0318
 General 0321
 Biblical Studies 0319
 Clergy 0320
 History of 0322
 Philosophy of 0469
Theology 0323

SOCIAL SCIENCES

American Studies 0324
Anthropology 0326
 Archaeology 0327
 Cultural 0310
 Physical 0272
Business Administration 0770
 General 0454
 Accounting 0338
 Banking 0385
 Management 0501
 Marketing 0503
Canadian Studies 0505
Economics 0508
 General 0509
 Agricultural 0510
 Commerce-Business 0511
 Finance 0358
 History 0366
 Labor 0351
 Theory 0578
Folklore 0366
Geography 0351
Gerontology 0578
History 0578
 General

Ancient 0579
Medieval 0581
Modern 0582
Black 0328
African 0331
Asia, Australia and Oceania 0332
Canadian 0334
European 0335
Latin American 0336
Middle Eastern 0333
United States 0337
History of Science 0585
Law 0358
Political Science 0615
 General 0616
 International Law and Relations 0617
 Public Administration 0814
Recreation 0452
Social Work 0626
Sociology 0627
 General 0938
 Criminology and Penology 0631
 Demography 0628
 Ethnic and Racial Studies 0629
 Individual and Family Studies 0630
 Industrial and Labor Relations 0629
 Public and Social Welfare 0700
 Social Structure and Development 0344
 Theory and Methods 0709
Transportation 0999
Urban and Regional Planning 0453
Women's Studies

THE SCIENCES AND ENGINEERING

BIOLOGICAL SCIENCES

Agriculture 0473
 General 0285
 Agronomy 0475
 Animal Culture and Nutrition 0476
 Animal Pathology 0359
 Food Science and Technology 0478
 Forestry and Wildlife 0479
 Plant Culture 0480
 Plant Pathology 0817
 Plant Physiology 0777
 Range Management 0746
 Wood Technology 0306
Biology 0287
 General 0308
 Anatomy 0309
 Biostatistics 0379
 Botany 0329
 Cell 0353
 Ecology 0369
 Entomology 0793
 Genetics 0410
 Limnology 0307
 Microbiology 0317
 Molecular 0416
 Neuroscience 0433
 Oceanography 0821
 Physiology 0778
 Radiation 0472
 Veterinary Science 0786
 Zoology 0760
Biophysics 0786
 General 0760
 Medical

Geodesy 0370
Geology 0372
Geophysics 0373
Hydrology 0388
Mineralogy 0411
Paleobotany 0345
Paleoecology 0426
Paleontology 0418
Paleozoology 0985
Palynology 0427
Physical Geography 0368
Physical Oceanography 0415

HEALTH AND ENVIRONMENTAL SCIENCES

Environmental Sciences 0768
Health Sciences 0566
 General 0300
 Audiology 0992
 Chemotherapy 0567
 Dentistry 0350
 Education 0769
 Hospital Management 0758
 Human Development 0982
 Immunology 0364
 Medicine and Surgery 0347
 Mental Health 0569
 Nursing 0570
 Nutrition 0380
 Obstetrics and Gynecology 0354
 Occupational Health and Therapy 0381
 Ophthalmology 0571
 Pathology 0419
 Pharmacology 0572
 Pharmacy 0382
 Physical Therapy 0573
 Public Health 0574
 Radiology 0575
 Recreation

Speech Pathology 0460
Toxicology 0383
Home Economics 0386

PHYSICAL SCIENCES

Pure Sciences
Chemistry 0485
 General 0749
 Agricultural 0486
 Analytical 0487
 Biochemistry 0488
 Inorganic 0738
 Nuclear 0490
 Organic 0491
 Pharmaceutical 0494
 Physical 0495
 Polymer 0754
 Radiation 0405
Mathematics 0605
Physics 0986
 General 0606
 Acoustics 0608
 Astronomy and Astrophysics 0748
 Atmospheric Science 0607
 Atomic 0607
 Electronics and Electricity 0798
 Elementary Particles and High Energy 0759
 Fluid and Plasma 0609
 Molecular 0610
 Nuclear 0752
 Optics 0756
 Radiation 0611
 Solid State 0463
Statistics 0346
Computer Science 0984

Engineering 0537
 General 0538
 Aerospace 0539
 Agricultural 0540
 Automotive 0541
 Biomedical 0542
 Chemical 0543
 Civil 0544
 Electronics and Electrical 0348
 Heat and Thermodynamics 0545
 Hydraulic 0546
 Industrial 0547
 Marine 0794
 Materials Science 0548
 Mechanical 0743
 Metallurgy 0551
 Mining 0552
 Nuclear 0549
 Packaging 0765
 Petroleum 0554
 Sanitary and Municipal System Science 0790
 Geotechnology 0796
 Operations Research 0795
 Plastics Technology 0994
 Textile Technology

PSYCHOLOGY

General 0621
Behavioral 0384
Clinical 0622
Developmental 0620
Experimental 0623
Industrial 0624
Personality 0625
Physiological 0989
Psychobiology 0349
Psychometrics 0632
Social 0451



**UNIVERSITY OF ALBERTA
RELEASE FORM**

NAME OF AUTHOR: XINBANG FENG
TITLE OF THESIS: DIRECT ANALYSIS OF SOLID MATERIALS
BY ELEMENTAL MASS SPECTROMETRY
DEGREE: Ph.D.
YEAR THIS DEGREE GRANTED: 1994

Permission is hereby granted to the University of Alberta Library to reproduce single copies of this thesis and to lend or sell such copies for private, scholarly or scientific research purposes only.

The author reserves all other publication and other right in association with the copyright in the thesis, and except as hereinbefore provided neither the thesis nor any substantial portion thereof may be printed or otherwise reproduced in any material form whatever without the author's prior written permission.

Xinbang Feng

.....
(Student's Signature)

Permanent Address:

#301, 10726-85 Avenue

Edmonton Alberta

Canada T6E 2K8

August 29, 1994
Date:

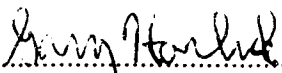
**Ask and it will be given to you;
seek and you will find;
knock and the door will be opened to you.**

St. Matthew 7:7

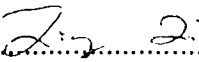
UNIVERSITY OF ALBERTA


FACULTY OF GRADUATE STUDIES AND RESEARCH

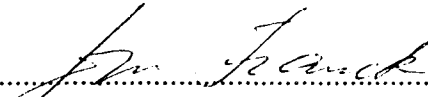
The undersigned certify that they have read, and recommend to the for acceptance, a thesis entitled DIRECT ANALYSIS OF SOLID MATERIALS BY ELEMENTAL MASS SPECTROMETRY submitted by XINBANG FENG in partial fulfillment of the requirements for the degree of Doctor of Philosophy.



.....
Dr. G. Horlick, Supervisor


.....
Dr. F. F. Cantwell


.....
Dr. L. Li


.....
Dr. R. B. Jordan


.....
Dr. J. P. Franck


.....
Dr. C. B. Boss, External Examiner

Date: Aug 29, 1994

**This thesis is dedicated to the memory of
Professor Baojun Wang and Professor Tiansheng Huang**

Abstract

The application of glow discharge-mass spectrometry (GD-MS), inductively coupled plasma-mass spectrometry (ICP-MS) and laser ablation-inductively coupled plasma-mass spectrometry (LA-ICP-MS) to the analysis of aluminum alloys is presented. The spectral characteristics of these three techniques are compared and contrasted. Both GD-MS and LA-ICP-MS are direct solid sampling methods, while ICP-MS as used in this work is based on a solution aspirated method. For the most part, GD mass spectra are simpler than ICP mass spectra in that species originating from the components of air, water and solution solutes are essentially absent in GD mass spectra. However, GD spectra show the presence of multiply-charged argon species, and matrix and analyte based argide species are more prevalent than oxide species, the opposite being the case with solution based ICP. The spectral complexity of LA-ICP-MS spectra seem to be on a par with GD-MS spectra, and tend to be much simpler than solvent-based ICP-MS, since almost no metal mono-oxides are observed from spectra for this dry plasma.

For these techniques, potential spectral interferences are evaluated and matrix effects are illustrated. For solution based ICP-MS analyses, it is shown that matrix effects can be minimized by adjustment of the nebulizer gas flow rate and by the use of an internal standard which is easy to add to the dissolved samples. For GD-MS based analyses, a matrix effect exists between low and high alloy aluminum samples and it is shown that the signal from aluminum argide can be used as an internal standard to minimize this matrix effect. The techniques of ICP-MS and GD-MS were applied to the analysis of a range of

Alcan and Alcoa aluminum standards and the technique of LA-ICP-MS was applied to the analysis of metallic bulk samples including Alcoa aluminum and NIST steels. Several non-conducting solids such as macor, glaze and porcelain samples were also ablated and analyzed qualitatively with LA-ICP-MS.

A computer program, Alcan DataBase, has been developed for management and display of ICP-MS and GD-MS spectral data. Alcan DataBase is a graphically-oriented database which provides the ability to compare and contrast the different spectral characteristics of ICP-MS and GD-MS, and also has the capability to assist in the qualitative analysis of unknown aluminum samples.

Acknowledgements

I would like to express my grateful thanks to my supervisor Professor Gary Horlick for his impressive guidance and invaluable advice throughout my work. I would like to thank Dr. Youbin Shao for his enthusiasm help to start the ICP-MS and GD-MS work and Dr. Lyle Burton for his help to start my computer programming project with Pascal.

I would also like to thank my wife Lucy Huang for her encouragement, love and support during my graduate studies. Thanks to Linda, my lovely daughter whose sweet smile with two dimples always relieve me from hard work.

My Thanks also go to all members in the research group for their valuable assistance and thoughtful discussion, especially to the staff of the Chemistry Department Electronics, Machine and Glass shops for their expertise and patience.

Finally, I would like to acknowledge Department of Chemistry for their five years financial support.

CHAPTER	PAGE
3.2 Experimental	48
3.3 Results and Discussion	54
3.3.1 Qualitative Spectral Scan	54
3.3.2 Evaluation of Background Spectral Interferences	58
3.3.3 Internal Standardization	62
3.3.4 Analytical Results	69
3.4 Conclusions	75
References	76
4. Analysis of Low Alloy Aluminum Samples Using Inductively Coupled Plasma Mass Spectrometry	78
4.1 Introduction	78
4.2 Experimental	79
4.3 Results and Discussion	80
4.3.1 Qualitative Spectral Scan	80
4.3.2 Evaluation of Potential Spectral Interferences	85
4.3.3 Matrix Effect and Internal Standardization	90
4.3.4 Analytical Results	96
4.4 Conclusions	106
References	107
5. Comparison of the Spectral Characteristics of ICP-MS and GD-MS with Respect to Low Alloy Aluminum Samples	110
5.1 Introduction	110
5.2 Experimental	111
5.3 Discussion	112
5.3.1 Comparison of Background Spectral Features	112
5.3.2 Comparison of Analyte Spectral Features	122

CHAPTER	PAGE
5.3.3 Comparison of Detection Limits	125
5.4 Conclusions	126
References	127
6. Alcan DataBase: A Computer Program for Management and Display of ICP-MS and GD-MS Spectral Data	128
6.1 Introduction	128
6.2 Alcan DataBase	133
6.2.1 Menus	135
6.2.1.1 File Menu	135
6.2.1.2 Interferences Menu	135
i. Change Background	136
ii. View a Mass Interference Window	136
iii. Add a Mass Interference	136
iv. Delete a Mass Interference	136
6.2.1.3 Spectra Menu	137
6.2.1.4 Window Menu	137
6.2.1.5 Help Menu	139
6.2.2 Windows	139
6.2.2.1 Spectrum Windows	139
6.2.2.2 Periodic Table Window	139
6.2.2.3 Element Windows	142
6.2.2.4 Interference Windows	142
6.3 Conclusions	146
References	147
7. Analysis of Aluminum and Steel Samples Using Laser Ablation Inductively Coupled Plasma Mass Spectrometry	148

CHAPTER	PAGE
7.1 Introduction	148
7.2 Experimental	150
7.3 Results and Discussion	155
7.3.1 Effect of Operating Parameters on Analyte Signals	155
7.3.2 Evaluation of Potential Spectral Interferences	159
7.3.3 Qualitative Spectral Scans for Aluminum Samples	162
7.3.4 Qualitative Spectral Scans for Steel Samples	164
7.3.5 Quantitative Analysis	167
7.3.5.1 Aluminum Alloys	169
7.3.5.2 Steel Samples	171
7.3.6 Evaluation of Memory Effects	172
7.3.7 Comparison to GD-MS	175
7.4 Conclusions	177
References	178
8. Analysis of Non-Conducting Materials Using Laser Ablation Inductively	
Coupled Plasma Mass Spectrometry	180
8.1 Introduction	180
8.2 Experimental	182
8.3 Results and Discussion	183
8.3.1 Evaluation of Potential Spectral Interferences	183
8.3.2 Qualitative Spectral Scans for Non-Conducting Samples	185
8.3.2.1 Macor Sample	185
8.3.2.2 Porcelain Sample	188
8.3.2.3 Glaze Samples	190
8.4 Conclusions	195
References	196

CHAPTER	PAGE
9. Conclusions and Future Directions	197
9.1 Conclusions	197
9.2 Future Directions	200
References	203

LIST OF TABLES

TABLE		PAGE
2.1	Summary of the pin-type GD-MS instrumental parameters	44
3.1	Ion lens voltage setting	51
3.2	Composition of Alcan 1SCXG low alloy aluminum	58
3.3	Comparison of relative signal intensities of analytes (at the 1% level) between high and low alloy aluminum samples	63
3.4	Detection limits of trace elements directly in Alcan aluminum solids by GD mass spectrometry	72
3.5	Results for the analysis of 1SWL low alloy aluminum	73
3.6	Results for the analysis of SS-360-C high alloy aluminum	73
4.1	Ion lens voltage settings	79
4.2	Composition of Alcan 1SCXG low alloy aluminum standard and concentration of elements in a 0.01% Al solution	85
4.3	Basic spectral interferences for elements of major interest in aluminum alloys (natural abundances in parentheses)	86
4.4	Comparison of signal intensities (counts/sec) at nebulizer flow-rate yielding maximum signal or reduced matrix effects	92
4.5	Constants of calibration function for aqueous calibration curves with internal standards	100
4.6	Analysis of the 0.01% solution of low alloy aluminum samples from Alcoa. Results reported as % in aluminum; precision expressed as standard deviation (n=4). Aqueous calibration solutions used, with yttrium as the internal standard	101

TABLE	PAGE
4.7 Analysis of the 0.01% solutions of low alloy aluminum samples from Alcan with both low and high nebulizer flow-rates. Results reported as % in aluminum; precision expressed as standard deviation (n=4). Aqueous calibration solutions used, with Co or Rh used as the internal standards	102
4.8 Analysis of 0.01% solution of low alloy aluminum samples from Alcoa by using matrix matching method. Results reported as % in aluminum; precision expressed as standard deviation (n=4)	104
4.9 Analysis of 0.1% solutions of the standard reference aluminum from both Alcan and Alcoa in condition of nebulizer flow-rate 0.9 l/min using ICP-MS. Results reported as % in aluminum; precision expressed as standard deviation (n=6). Aqueous calibration solutions are used, without internal standard	105
5.1 Composition of Alcan 1SCXG low alloy aluminum	122
7.1 Typical operating condition of the LA-ICP-MS system	154
7.2 Composition of NIST SRM 1261 low alloy steel	164
7.3 Results for the analysis of SRM SS-360-C high alloy aluminum	171
7.4 Results for the analysis of NIST SRM 1262 low alloy steel	172
7.5 Results of memory effect check for external chamber LA-ICP-MS	175
8.1 Typical operating parameters for the LA-ICP-MS system	184
8.2 Signal levels of elements in porcelain sample and macor Sample	188
8.3 Signal levels of elements in glaze samples with 1 Hz Nd:YAG LA-ICP-MS ...	194

LIST OF FIGURES

FIGURE	PAGE
1.1 Schematic diagram of the Perkin-Elmer/SCIEX ELAN 250/500 ICP-MS system	3
2.1 Schematic representation of a glow discharge and associated components	17
2.2 Schematic diagram of a pin-type sample glow discharge ion source	21
2.3 Schematic diagram of a pin-type glow discharge device attached to an "ICP"-MS system and the interface voltage biasing arrangement	22
2.4 Dependence of ion counts on the dc power supply of glow discharge at argon pressure of 2.50 torr for (a) $^{24}\text{Mg}^+$, $^{55}\text{Mn}^+$, $^{64}\text{Zn}^+$, (b) $^{48}\text{Ti}^+$, $^{58}\text{Ni}^+$, $^{63}\text{Cu}^+$, and $^{27}\text{Al}^{40}\text{Ar}^+$ signals	29
2.5 Dependence of ion counts on the argon pressure at discharge potential of 1000 volts for (a) $^{24}\text{Mg}^+$, $^{55}\text{Mn}^+$, $^{64}\text{Zn}^+$, (b) $^{48}\text{Ti}^+$, $^{58}\text{Ni}^+$, $^{63}\text{Cu}^+$, and $^{27}\text{Al}^{40}\text{Ar}^+$ signals	31
2.6 Dependence of current on (a) dc power supply (b) argon pressure and (c) sampling depth for GD-MS	33
2.7 Effect of shadow stop bias on (a) $^{24}\text{Mg}^+$, (b) $^{58}\text{Ni}^+$, (c) $^{64}\text{Zn}^+$ and (d) $^{27}\text{Al}^{40}\text{Ar}^+$ ion signal intensities	35
2.8 Effect of anode bias on (a) $^{24}\text{Mg}^+$, (b) $^{55}\text{Mn}^+$, (c) $^{64}\text{Zn}^+$ and (d) $^{27}\text{Al}^{40}\text{Ar}^+$ ion signal intensities	36
2.9 Diagram of the ion lenses for SCIEX ELAN 250 mass spectrometer	38
2.10 Dependence of ion counts on einzel-lens voltage for (a) $^{24}\text{Mg}^+$, (b) $^{58}\text{Ni}^+$, (c) $^{120}\text{Sn}^+$ and (d) $^{208}\text{Pb}^+$ signals	40

FIGURE	PAGE
2.11 Dependence of ion counts on bessel plate voltage for (a) $^{24}\text{Mg}^+$, (b) $^{58}\text{Ni}^+$, (c) $^{120}\text{Sn}^+$ and (d) $^{208}\text{Pb}^+$ signals	41
2.12 Dependence of ion counts on bessel box voltage for (a) $^{24}\text{Mg}^+$, (b) $^{58}\text{Ni}^+$, (c) $^{120}\text{Sn}^+$ and (d) $^{208}\text{Pb}^+$ signals	42
2.13 Dependence of ion counts on the photon stop voltage for (a) $^{24}\text{Mg}^+$, (b) $^{58}\text{Ni}^+$, (c) $^{120}\text{Sn}^+$ and (d) $^{208}\text{Pb}^+$ signals	43
3.1 Schematic diagram of a pin-type sample glow discharge ion source ...	49
3.2 Effect of shadow stop bias (a) and anode stop bias (b) on $^{63}\text{Cu}^+$ ion signal intensity	52
3.3 Schematic diagram of a pin-type glow discharge device attached to an "ICP"-MS system and the interface voltage biasing arrangement	53
3.4 GD mass spectra of a low alloy aluminum sample from Alcan (1SCXG) in the 1 to 45 m/z range	55
3.5 GD mass spectra of a low alloy aluminum sample from Alcan (1SCXG) in the 40 to 85 m/z range	56
3.6 GD mass spectra of a low alloy aluminum sample from Alcan (1SCXG) in the 80 to 125 (a) and 190 to 220 (b) m/z range	57
3.7 Glow discharge mass spectrum of a high alloy aluminum sample from Alcoa (SS-319E) in the 81 to 125 m/z range	61
3.8 Signal intensity changes as a function of time for $^{63}\text{Cu}^+$ (a), $^{27}\text{Al}^{40}\text{Ar}^+$ (b) and the signal intensity ratio of copper to aluminum argide (c)	66
3.9 Relative standard deviation of the signal intensity ratio ($^{63}\text{Cu}^+ / ^{27}\text{Al}^{40}\text{Ar}^+$) as a function of time	67
3.10 Signal intensity changes (in arbitrary units) as a function of time for (a) $^{24}\text{Mg}^+$, (b) $^{58}\text{Ni}^+$, (c) $^{63}\text{Cu}^+$ for a pin-type aluminum sample with and without the use of $^{27}\text{Al}^{40}\text{Ar}^+$ as an internal standard	68

FIGURE	PAGE
3.11 Calibration curves for $^{51}\text{V}^+$ (a) and $^{69}\text{Ga}^+$ (b) in Alcan low alloy aluminum standards with $^{27}\text{Al}^{40}\text{Ar}^+$ (m/z 67) as the internal standard	71
3.12 Calibration curves for $^{24}\text{Mg}^+$ (a) and $^{63}\text{Cu}^+$ (b) in both high and low alloy aluminum standards with $^{27}\text{Al}^{40}\text{Ar}^+$ (m/z 67) as the internal standard	74
4.1 Spectra of the 0.01% aluminum alloy solution (Alcan 1SCXG) for the mass range 1 to 45 m/z	82
4.2 Spectra of the 0.01% aluminum alloy solution (Alcan 1SCXG) for the mass range 40 to 85 m/z	83
4.3 Spectra of the 0.01% aluminum alloy solution (Alcan 1SCXG) for the mass range (a) 80 to 125 and (b) 190 to 220 m/z	84
4.4 ICP mass spectra of an aluminum alloy sample (Alcan 1SWM) illustrating the overlap of elemental isotopes and metal mono-oxides (a) Actual spectra and (b) simulated spectrum	89
4.5 Ion count as a function of nebulizer flow-rate for (a) $^{48}\text{Ti}^+$, (b) $^{58}\text{Ni}^+$, and (c) $^{63}\text{Cu}^+$ in 5% HNO_3 and in a matrix containing 1000 $\mu\text{g}/\text{mL}$ of Al ...	91
4.6 Effect of increasing Al concentration on the Ni signal at the nebulizer flow-rate yielding maximum signal intensity (b) and at a reduced nebulizer flow-rate (c)	93
4.7 Effect of increasing Al concentration on (a) $^{24}\text{Mg}^+$, (b) $^{48}\text{Ti}^+$, and (c) $^{59}\text{Co}^+$ signals as a percentage matrix effect	95
4.8 Effect of increasing Al concentration on (a) $^{48}\text{Ti}^+$, (b) $^{55}\text{Mn}^+$, and (c) $^{64}\text{Zn}^+$ signals with $^{59}\text{Co}^+$ as an internal standard	97

FIGURE	PAGE
4.9 Signal intensity changes (in arbitrary units) as a function of time for (a) $^{48}\text{Ti}^+$, (b) $^{58}\text{Ni}^+$ and (c) $^{63}\text{Cu}^+$ in a 0.01% aluminum solution with and without the use of $^{59}\text{Co}^+$ as an internal standard	98
5.1 Mass spectra for (a) ICP-MS and (b) GD-MS of Alcan aluminum alloy (1SCXG) in the 1-45 m/z range	115
5.2 Mass spectra for (a) ICP-MS and (b) GD-MS of Alcan aluminum alloy (1SCXG) in the 40-85 m/z range	116
5.3 Mass spectra for (a) ICP-MS and (b) and (c) GD-MS of Alcan aluminum alloy (1SCXG) in the 1-45 m/z range	117
5.4 Mass spectra for (a) ICP-MS and (b) GD-MS of Alcan aluminum alloy (1SWL) in the 80-125 m/z range	120
5.5 Bar graphs of ass spectrum between ICP-MS and GD-MS in the mass range 1-83 m/z	121
5.6 Mass spectra for (a) ICP-MS and (b) GD-MS of Alcan aluminum alloy (1SCXG) in the 190-220 m/z range	124
6.1 Comparison of spectral characteristics of ICP-MS and GD-MS windows ..	130
6.2 MDI windows for qualitative elemental analysis of lead	132
6.3 Alcan DataBase (a) main frame window and (b) pull down menus	134
6.4 Tiled MDI Child windows in their main frame window	138
6.5 Alcan DataBase help index window	140
6.6 Alcan DataBase main frame window and the periodic table window .	141
6.7 (a) A nickel element window and (b) $^{58}\text{Ni}^+$ isotope windows for interferences in both ICP-MS and GD-MS	143
6.8 Mass 51 window is opened by double-clicking on the peak at m/z 51 in an ICP spectrum window	145

FIGURE	PAGE
7.1 Schematic diagram of external chamber laser ablation ICP-MS system	151
7.2 Schematic diagram of the quartz ablation chamber	152
7.3 Dependence of signal intensity on the central gas flow-rate for (a) $^{24}\text{Mg}^+$, (b) $^{58}\text{Ni}^+$, (c) $^{63}\text{Cu}^+$ and (d) $^{120}\text{Sn}^+$	156
7.4 Central Gas Flow-Rate - Power parameter behavior graph for $^{55}\text{Mn}^+$ ion	157
7.5 Dependence of signal intensity on sampling depth for (a) $^{24}\text{Mg}^+$, (b) $^{55}\text{Mn}^+$, (c) $^{63}\text{Cu}^+$ and (d) $^{208}\text{Pb}^+$	158
7.6 Dependence of signal intensity on the laser repetition rate for (a) $^{24}\text{Mg}^+$, (b) $^{55}\text{Mn}^+$, (c) $^{120}\text{Sn}^+$ and (d) $^{208}\text{Pb}^+$	160
7.7 Background mass spectra for a dry ICP from (a) 1 to 45 m/z and (b) 40 to 85 m/z	161
7.8 LA-ICP-MS spectra of a low alloy aluminum sample (Alcoa SA-909) .	163
7.9 LA-ICP-MS spectra of a low alloy steel sample (NIST 1261)	165
7.10 LA-ICP-MS spectra of a low alloy steel sample (NIST 1261)	166
7.11 Dependence of lead signal intensity on different laser ablation repetition rates at (a) 10 Hz, (b) 15 Hz and (c) 20 Hz	168
7.12 Calibration curves for (a) $^{24}\text{Mg}^+$, (b) $^{55}\text{Mn}^+$, (c) $^{63}\text{Cu}^+$ and (d) $^{66}\text{Zn}^+$ with $^{57}\text{Fe}^+$ as an internal standard in both high and low alloy aluminum standards	170
7.13 Calibration curves for $^{58}\text{Ni}^+$ with $^{57}\text{Fe}^+$ as an internal standard (a) before and (b) after correction for the interference of $^{58}\text{Fe}^+$	173
7.14 Calibration curves for (a) $^{52}\text{Cr}^+$, (b) $^{55}\text{Mn}^+$, (c) $^{60}\text{Ni}^+$ and (d) $^{98}\text{Mo}^+$ with $^{57}\text{Fe}^+$ as an internal standard in both low alloy and stainless steel standards	174

FIGURE	PAGE
8.1 LA-ICP-MS spectra of a macor sample with a 5 Hz repetition rate of the Nd:YAG laser	186
8.2 Continuous signals obtained by ablation of a macor sample with 5 Hz repetition rate of the Nd:YAG laser. Signals were observed at four m/z values (a) $^{24}\text{Mg}^+$, (b) $^{11}\text{B}^+$, $^{56}\text{Fe}^+$ and $^{120}\text{Sn}^+$	187
8.3 LA-ICP-MS spectra of the yellow glaze on a porcelain dish sample with 1 Hz repetition rate of the Nd:YAG laser	189
8.4 LA-ICP-MS spectra of a white glaze sample (#2) with 1 Hz repetition rate of the Nd:YAG laser	191
8.5 LA-ICP-MS spectra of a white glaze sample (#2) with 1 Hz repetition rate of the Nd:YAG laser	192
8.6 Relative signal levels of elements in glaze samples	193

Chapter 1

Introduction

The inductively coupled plasma (ICP) has developed into a dominant source for elemental analysis. While the ICP primarily has been developed and applied as an atomic emission source, during the last decade it also has been widely applied to elemental analysis as an ion source for mass spectrometry. The powerful technique that emerged was inductively coupled plasma-mass spectrometry (ICP-MS), which matured from laboratory experimentation to commercial development and widespread analytical application. A great number of reviews [1-4] and research papers [5-15] for ICP-MS were published in the recent 10-year period. The rapid development of ICP-MS is the result of three unique measurement capabilities for elemental analysis. First of all, the technique offers very low detection limits. The detection limits for the direct analysis of solution samples are in the range of 1 to 100 pg/mL for most elements. The detection limits are broadly achieved for almost all elements across the periodic table and they are 100 to 1000 times superior to those obtained by atomic emission and atomic fluorescence spectroscopy. Secondly, the mass spectra of the elements are very simple and unique. The natural isotope abundance spectral pattern provides quick and essentially immutable evidence for the qualitative identification of an element. This has facilitated the development of ICP-MS as a powerful technique for automated qualitative and semi-quantitative elemental analysis. Finally, inherent in the technique is the

ability to measure elemental isotope ratios [16-18], thus allowing the routine utilization of isotope ratio data and the isotope dilution technique to study and solve analytical problems [19, 20]. A schematic diagram of the Perkin-Elmer/Sciex Elan 250/500 ICP-MS system is presented in Figure 1.1.

The success and rapid development of ICP-MS have now lent considerable credibility to the utilization of MS for routine elemental analysis. However, ICP-MS is primarily a solution based technique. This has paved the way for the development and assessment of additional ion sources or different sampling methods for elemental analysis that would either complement or improve on the ICP. In particular, there is a need for techniques that can be directly applied to solid materials as many samples are natural solids which include bulk metal, alloy, geological, environmental and semi-conducting samples. Aluminum alloys are some of the most challenging samples for alternative solution-based methods because of difficulties in dissolution and the presence of refractory species. Thus, the direct analysis of aluminum alloys is an interesting topic for analytical chemists and some new analytical methods have been developed in recent years with respect to the analyses of solid aluminum-based alloys [21-26]. Two basic approaches may be considered for the direct solid analysis. One is the use of a source other than an ICP that is directly applicable to solid samples. This source can be a glow discharge device or an electrothermal vaporization (ETV) device. Thus, glow discharge-mass spectrometry (GD-MS) has been developed in recent years to meet the need of direct solid analysis [25-29]. The other is the use of sample introduction systems for the ICP that can directly handle solids. Solid samples can be ablated by a laser beam and then directly introduced into the ICP. Samples can also be held in an electrode and directly inserted into an ICP. Thus, laser ablation ICP-MS

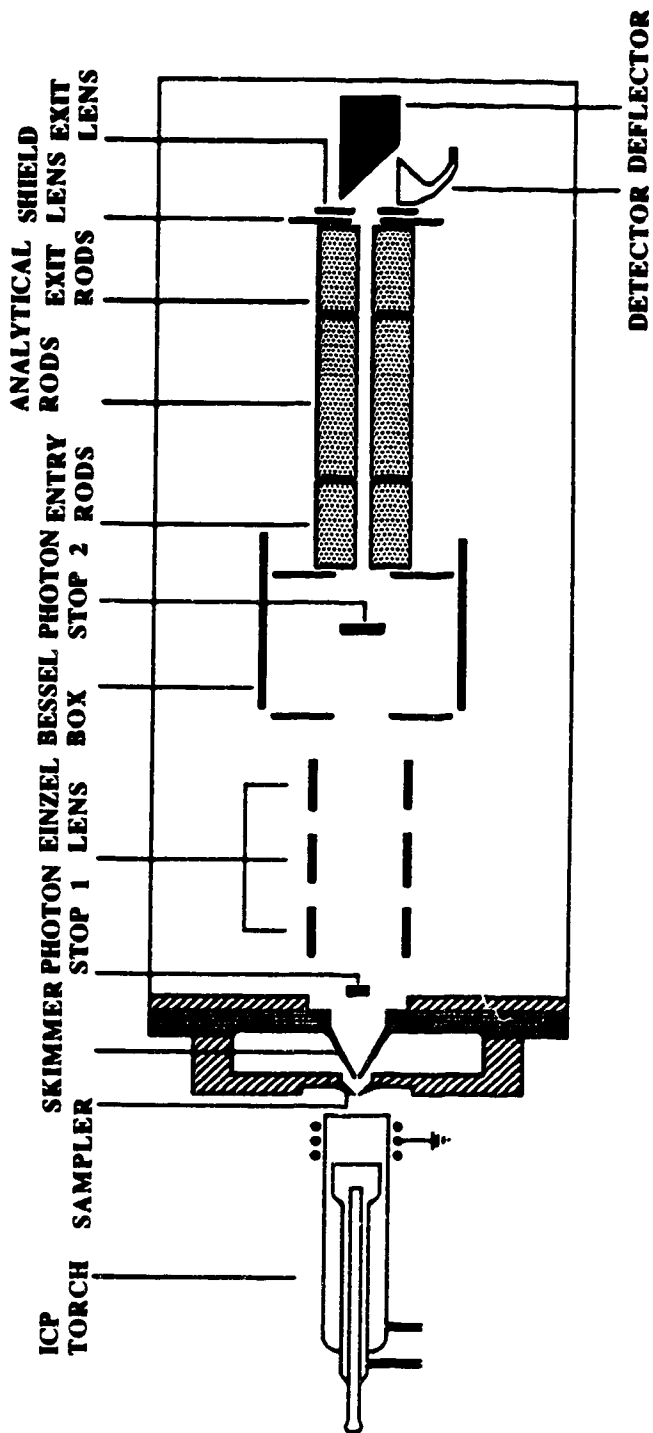


Figure 1.1 Schematic diagram of the Perkin-Elmer/SCIEX ELAN 250/500 ICP-MS system

[30-38] and direct sample insertion ICP-MS [39-42] have become powerful techniques to deal with the solid samples.

Direct solid sampling is an attractive method for sample introduction into atomic emission and mass spectrometry systems since it can avoid the time-consuming sample dissolution, digestion and preparation procedures usually required for the more common solution based sample introduction techniques. The direct analysis of solids can be carried out without the use of chemical reagents and without the processes of separation and pre-concentration which could introduce contamination or cause losses of the analyte. Solid sampling techniques have additional advantages when the sample is difficult or hazardous to digest. For instance, with high-purity aluminum or aluminum alloys, certain compounds of refractory carbides and oxides, silicate minerals and others do not readily digest, dissolve or remain in solution. Dissolution also dilutes the often already low concentrations of the sought-for-elements, lowering the power of detection. Also solution nebulization delivers only a small percentage of the sample into the plasma whereas direct solid injection sends most of the sample into the excitation or ionization source.

1.1 Glow Discharge Mass Spectrometry

Among known techniques of direct solid sampling, glow discharge mass spectrometry (GD-MS) provides considerable versatility in meeting elemental analysis needs. Its primary application has arisen in bulk solids analysis where the strong analytical advantages of the technique can be most directly and easily utilized. Studies so far with GD-MS show the following useful features: (1) one of the most important advantages is the direct analysis of metals and alloys with

little or no sample pre-treatment; (2) the analysis of nonconductors can be accomplished by compacting with a graphite or metal matrix; (3) the mass spectrum is responsive to both metallic and nonmetallic elements; (4) minimal matrix effects have been observed; (5) low parts-per-billion detection limits are attainable; (6) sensitivities are generally uniform for most elements; (7) isotopic information can be obtained; (8) spectra are much simpler than optical emission spectra; (9) the glow discharge is a stable, low-power discharge with an inert discharge environment; (10) the operation of GD-MS is quite economical with low gas and sample consumption rate; (11) and finally, rapid qualitative and quantitative analyses can be performed. The limitations of the method appear to be: (1) applicable primarily to solids (solutions require an intermediate evaporation step); (2) spectral interferences from the discharge gas and other background gases; (3) polyatomic interferences from sputtered matrix atoms in combination with other plasma species; and (4) increased cost and complexity as compared with emission techniques (*i.e.* a mass spectrometer).

The application of GD-MS to the analysis of various materials including bulk metals and compact powders has been studied in recent years. The analysis of metals and alloys has been the most frequent use to date of GD-MS. A typical bulk analysis application is the qualitative and quantitative analysis of steels, copper or brass [29, 43-44]. Relative sensitivity factors (RSFs) for the analysis of 56 elements by GD-MS have been determined from the multiple analyses of 30 standard reference materials representing six different matrix elements (*i.e.* Al, Ti, Fe, Ni, Cu and Pt alloys) [22]. The values of RSF for most elements were in the range of 0.3-6, which contradicts somewhat the common claim of uniform element sensitivity [27], but it was confirmed that the RSF values were independent of matrix [27]. GD-MS has also been used for the

routine quality control of high-purity aluminum [23] and has been compared with SIMS for the determination of U and Th in aluminum alloys [26]. In addition, a typical analysis of a pure semiconductor, indium, illustrated the sensitivity and element coverage of the technique [45]. Analysis of tellurium was faster by GD-MS than by spark source mass spectrometry (SSMS) [46], but sample preparation was more difficult and detection limits were better by SSMS. It was difficult to find an internal standard in both techniques but an isotope from matrix could be used in GD-MS.

The analysis of insulating materials such as glass and ceramics poses problems for GD-MS because of their inherent insulating properties. The use of a radio frequency generated plasma discharge has been shown to sputter insulators [47-49]. Besides the rf glow discharge, methods for insulators involve converting the insulator or non-conducting material into a conducting form. The mixing of an oxide powder with a copper host matrix (1:9) allows pressing of a disk sample for glow discharge sputtering [50]. This may be accomplished in the case of insulating powders, which can be mixed with a carefully chosen high purity metal binder [51, 52]. Several conducting matrices including graphite, copper, silver, iron, aluminum and tantalum have been studied as matrices for the analysis of non-conducting materials using pressed disks in GD-MS [53]. Plasma modification studies have been carried out using getter reagents as sample matrices in analyzing lanthanum oxide with GD-MS [54]. Solid insulators such as glass samples, however, require some other means of analysis. Secondary cathode GD-MS [55] has been used to promote sputtering of glass samples in a dc. glow discharge cell. Atomization of the glass sample is a result of redeposition of atoms from the metal cathode, creating a thin conducting film on the glass surface.

A important factor that can influence plasma chemistry is residual water in the glow discharge. Analysis of bulk metals has shown that water suppresses both sputtering yield and the ionization of the analyte in the glow discharge [56]. However, the population of elemental ions in a glow discharge is inversely proportional to the metal oxide bond strength. The formation of metal oxides in a glow discharge is usually a consequence of water impurities in the GD system, especially for compacted powder samples. The elements with higher M-O bond strength such as rare earth elements more readily form metal oxides. In the analysis of refractory elements such as Ti, Zr, Nb and the rare earths, metal mono-oxide ions (MO^+) may dominate the mass spectra. Plasma modifiers such as Ti, Ta and W can be used as sample matrices in analyzing oxide samples [52]. The host matrix not only provides the conducting medium, but also can remove the interferences from water vapor because of their higher affinity toward oxygen. Furthermore, the sputtering yield of these modifiers in glow discharge is not very low so that the matrix has a considerable population remaining in the gas phase.

1.2 Laser Ablation Inductively Coupled Plasma Mass Spectrometry

The first demonstration of the use of lasers in spectrochemical analysis took place in 1962 when a ruby laser was used for laser ablation of solid material, *i.e.*, the laser radiation was focused onto the material which resulted in evaporation and atomization of material, with subsequent detection of the atoms by emission spectrometry.

Laser ablation inductively coupled plasma mass spectrometry (LA-ICP-MS) [30-38] and laser ablation glow discharge mass spectrometry (LA-GD-MS) [25] are alternative methods of introducing solids into the plasma. The ability to directly analyze solid materials is a major asset of laser ablation, and this ability complements the solution sample-handling capability of the ICP. As the solid is not dissolved, little or no sample preparation is necessary and the solid is not diluted. Moreover, as no acid or solvent is used, the polyatomic interferences are less problematic and contamination effects are unlikely. The strength of LA-ICP-MS for the fast semiquantitative survey analysis of solids and pressed powders has been demonstrated [32]. Major and trace elements up to the ppm level can be determined in this way. Sample preparation and any knowledge about the composition is not necessary. Non conducting solids such as oxides, and geological refractory materials can be analyzed by laser ablation. Trace impurities in uranium oxide (U_3O_8) have been determined using LA-ICP-MS [33]. Zircon samples containing Hf, Y, Re, Th and U have been analyzed by both laser ablation and solution ICP-MS [34]. A novel surface analytical technique, resonant laser ablation (RLA), has been used to detect small quantities of aluminum in NIST SRM steel samples [35]. It was estimated that detection levels down to a few ppm were achievable by RLA-ICP-MS for aluminum in steel samples.

1.3 Thesis Outline

The first step in this thesis work was to characterize the parameter behavior of the glow discharge device (GDD) and the SCIEX ELAN mass spectrometer. These studies are presented in Chapter 2. From this work, we understand what is required to reach the desired operating conditions and know

the effect on signal intensities of the parameters including: power supply voltage, gas pressure, depth of sampling for a pin-type GDD, voltage bias of anode and shadow stop on the interface, and the ion lens settings in the mass spectrometer.

Bulk metal samples such as aluminum alloys were analyzed by using both ICP-MS and GD-MS, and both methods are described in Chapter 3 and 4, respectively. Both low and high alloy aluminum standards in the form of pins were directly analyzed with GD-MS, whereas only low alloy samples were determined by using ICP-MS after they were dissolved as 0.01% solutions. Qualitative spectral scans aid in identifying potential spectral interferences for both techniques. Instrument stability and matrix effects were addressed and the selection of an internal standard was discussed. It is quite easy to add an internal standard in ICP-MS, whereas a matrix species has to be chosen as an internal standard for GD-MS.

Comparison of the spectral characteristics of ICP-MS and GD-MS with respect to the analysis of low alloy aluminum samples is addressed in Chapter 5. An investigation was carried out comparing and contrasting both background and the analytical spectral features of ICP-MS and GD-MS. The results include the more intense background species originating from solvent and air in ICP-MS, and argides, dimers of argon, and multiply charged argon ions species in GD-MS.

Computers have become an essential part of spectrochemical research for both data acquisition and data processing. An effective computerized data base can be considered as one of the most useful tools for the management of

analytical results and analytical information [57]. A computer program, Alcan DataBase, for Microsoft Windows (IBM-PC) has been developed and is presented in Chapter 6. Alcan DataBase is a graphically-oriented database for the analysis of aluminum alloy samples with both ICP-MS and GD-MS. Five low alloy aluminum samples from Alcan used as standards were determined by ICP-MS and GD-MS, and the spectral data for these standards were acquired and then installed in this program. Alcan DataBase not only provides the ability to compare and contrast the different spectral characteristics between ICP-MS and GD-MS, but also can be used to support qualitative analysis for different aluminum samples.

In Chapter 7 and 8, an external chamber laser ablation ICP-MS technique is addressed. Both conducting and non-conducting bulk samples were ablated with a Nd:YAG laser and analytes were determined using ICP-MS. Qualitative spectral scans aid in identifying potential spectral interferences for the mass spectrum. Simultaneously multielement analyses of disk form samples of aluminum and stainless steels are presented with a particular emphasis placed on the utility of the minor isotope of iron (m/z 57) as an internal standard. Only qualitative analysis was carried out for non-conducting material such as macor, porcelain and glaze samples.

Thus, three general methods for both qualitative and quantitative analyses of aluminum alloy samples are addressed in this thesis. ICP-MS is a solution based method so that dissolution of samples and preparation of standard solutions is necessary. The directly solid sampling methods such as GD-MS and LA-ICP-MS seem more convenient than the solution based method. However, GD-MS analyses have time-consuming steps involving sample form

fabrication and pre-sputtering. Therefore, LA-ICP-MS is the simplest, most rapid and most effective method for the elemental analysis of solid samples with minimal matrix effects and memory effects. On the other hand, a laser is an expensive instrument, while a glow discharge device is more economic. Because of different sampling methods, the spectral characteristics and complexity for these three methods could be quite different. The background interferences should be much simpler in a dry plasma utilized in GD-MS and LA-ICP-MS. In this thesis, the three methodologies are compared and contrasted. For the most part, the important areas to address during the development of quantitative analytical method are similar for these techniques. They include qualitative and quantitative analyses, assessment of spectral overlaps, assessment of matrix effects, instrumental settings, and choice of an internal standard. However, details of each step for the three methods do differ, and in particular, spectral characteristics, matrix effects, and internal standardization have considerations unique to each technique.

References

1. D. J. Douglas and R. S. Houk, *Prog. Anal. At. Spectrosc.* **8**, 1 (1985).
2. R. S. Houk and J. J. Thompson, *Mass Spectrometry Reviews* **7**, 425 (1988).
3. D. J. Douglas, *Can. J. Spectrosc.* **34**, 38 (1989).
4. G. M. Hieftje and G. H. Vickers, *Anal. Chim. Acta* **216**, 1 (1989).
5. A. L. Gray, *Spectrochimica Acta* **40B**, 1525 (1985).
6. H. E. Taylor, *Spectroscopy* **1**, 20 (1986).
7. R. S. Houk, *Anal. Chem.* **58**, 97A (1986).
8. A. L. Gray, *J. Anal. At. Spectrom.* **1**, 403 (1986).
9. H. Kawaguchi, *Anal. Sciences (Japan)* **4**, 339 (1988).
10. J. Marshall and J. Franks, *J. Anal. At. Spectrom.* **6**, 591 (1991).
11. R. K. Winge, J. S. Crain and R. S. Houk, *J. Anal. At. Spectrom.* **6**, 601 (1991).
12. A. L. Gray, *J. Anal. At. Spectrom.* **7**, 1151 (1992).
13. S. J. Hill, M. J. Ford and Les Ebdon, *J. Anal. At. Spectrom.* **7**, 1157 (1992).
14. S. E. Hobbs and J. W. Olesik, *Anal. Chem.* **64**, 274 (1992).
15. H. Klinkenberg, T. Beeren and W. Van Born, *Spectrochimica Acta* **49B**, 171 (1994).
16. R. J. Anderson and A. L. Gray, *Proc. Anal. Div. Chem. Soc.*, **13**, 284 (1976).
17. A. L. Gray, *Dyn. Mass Spectrom.*, **5**, 106-113 (1978).
18. A. R. Date and A. L. Gray, *Int. J. Mass Spectrom. Ion Phys.*, **48**, 357(1983).
19. J. R. Garbarino and H. E. Taylor, *Anal. Chem.*, **59**, 1568 (1987).
20. J. W. McLaren, D. Beauchemin and S. S. Berman, *Anal. Chem.*, **59**, 610 (1987).

21. R. K. Marcus and D. C. Duckworth, paper presented at 1989 Pittsburgh Conference and Exposition on Analytical Chemistry and Applied Spectroscopy, Atlanta, GA, USA, 6-10 March 1989.
22. W. Vieth and J. C. Huneke, *Spectrochimica Acta* **46B**, 137 (1991).
23. L. F. Vassamillet, *J. Anal. At. Spectrom.* **4**, 451 (1989).
24. H. M. Shihomatsu and S. S. Iyer, *Nucl. Instrum. Methods Phys. Res. Sect. A*, **280**, 488 (1988).
25. W. W. Harrison, K. R. Hess, R. K. Marcus and F. L. King, *Anal. Chem.* **58**, 341A (1986).
26. W. W. Harrison and B. L. Bentz, *Prog. Analyt. Spectrosc.* **11**, 53 (1988).
27. W. W. Harrison, *J. Anal. At. Spectrom.* **3**, 867 (1988).
28. N. Jakubowski, D. Stuewer and G. Toelg, *Spectrochimica Acta* **46B**, 155 (1991).
29. Y. Shao and G. Horlick, *Spectrochimica Acta* **46B**, 165 (1991).
30. A. L. Gray, *Analyst*, **110**, 551 (1985).
31. P. Arrowsmith, *Anal. Chem.* **59**, 1437 (1987).
32. P. van de Weijer, W. L. M. Baeten, M. H. J. Bekkers and P. J. M. G. Vullings, *J. Anal. At. Spectrom.* **7**, 599 (1992).
33. J. S. Crain and D. L. Gallimore, *J. Anal. At. Spectrom.* **7**, 605 (1992).
34. W. T. Perkins, N. J. G. Pearce and R. Fuge, *J. Anal. At. Spectrom.* **7**, 611 (1992).
35. I. S. Borthwick, K. W. D. Ledingham and R. P. Singhal, *Spectrochim. Acta* **47B**, 1259 (1992).
36. R. J. Watling, H. K. Herbert, D. Delev and I. D. Abell, *Spectrochim. Acta* **49B**, 205 (1994).
37. V. V. Kogan, M. W. Hinds and G. I. Ramendik, *Spectrochim. Acta* **49B**, 333 (1994).

38. A. J. Walder, I. D. Abell, I. Platzner and P. A. Freedman, *Spectrochim. Acta* **49B**, 397 (1994).
39. S. A. Darke, S. E. Long, C. J. Pickford and J. F. Tyson, *J. Anal. At. Spectrom.* **4**, 715 (1989).
40. V. Karanassios and G. Horlick, *Spectrochim. Acta* **44B**, 1345 (1989).
41. V. Karanassios and G. Horlick, *Spectrochim. Acta* **44B**, 1361 (1989).
42. V. Karanassios and G. Horlick, *Spectrochim. Acta* **44B**, 1387 (1989).
43. R. C. Hutton and A. Raith, *J. Anal. At. Spectrom.* **7**, 623 (1992).
44. N. Jakubowski, D. Stuewer and W. Vieth, *Anal. Chem.* **59**, 1825(1987).
45. J. Clark, G. Ronan, T. Ainscough and D. Wheeler, paper presented at 1990 Pittsburgh Conference and Exposition on Analytical Chemistry and Applied Spectroscopy, New York, NY, USA, 5th-9th March, 1990.
46. K. Swenters, J. Verlinden and R. Gijbels, *Fresenius Z Anal Chem* **335**, 900 (1989).
47. D. C. Duckworth and R. K. Marcus, *Anal. Chem.* **61**, 1879 (1989).
48. D. L. Donohue and W. W. Harrison, *Anal. Chem.* **47**, 1528 (1975).
49. R. K. Marcus, *J. Anal. At. Spectrom.* **8**, 935 (1993).
50. M. R. Winchester and R. K. Marcus, *Applied Spectroscopy* **42**, 941 (1988).
51. G. Ehrlich, U. Stahlberg and V. Hoffmann, *Spectrochimica Acta* **46B**, 115 (1991).
52. H. Nickel, D. Guntur, M. Mazurkiewicz and A. Naoumidis, *Spectrochimica Acta* **46B**, 125 (1991).
53. S. L. Tong and W. W. Harrison, *Spectrochimica Acta* **48B**, 1237 (1993).
54. Y. Mei and W. W. Harrison, *Spectrochimica Acta* **46B**, 175 (1991).
55. D. M. P. Milton and R. C. Hutton, *Spectrochimica Acta* **48B**, 39 (1993).
56. T. J. Loving and W. W. Harrison, *Anal. Chem.* **54**, 1526 (1983).
57. G. B. King and G. Horlick, *Spectrochimica Acta* **47B**, E353 (1992).

Chapter 2

Effect of Operating Parameters on Analyte Signals in Glow Discharge Mass Spectrometry

2.1 Introduction

2.1.1 The glow discharge

The glow discharge is one of the oldest spectroscopic sources. It was first introduced as an optical emission source by Paschen [1] and Schuler [2] over 70 years ago, and it was studied as an early ion source by Thomson, Bainbridge, and Aston [3] in the 1930s, who used glow discharges as ready sources of ions to study and develop the earliest form of mass spectrometry. However, the signals from these high voltage early devices were rather unstable. The glow discharge sources available today are more compact and operate at considerably lower voltages and currents than earlier devices and stability and reproducibility are considered strengths compared with other sources. Hence, the glow discharge is a simple and reliable method of producing atoms, ions and photons characteristic of an analytical sample. Reconsideration of the glow discharge as an analytical ion source was primarily due to the studies of Coburn and co-workers [4-7] in the 1970s. Their work provided the incentive for the analytical

development of glow discharge mass spectrometry (GD-MS) [8-12], and eventual commercialization.

In general, the glow discharge is a simple two-electrode device, filled with a rare gas to about 0.1-10.0 torr. A few hundred volts applied across the electrodes causes breakdown of gas and formation of the ions, electrons and other species that make the glow discharge useful in analytical chemistry. Figure 2.1 is a simplified schematic diagram that shows the basic components and discharge regions. A solid sample to be analyzed serves as the cathode; while the anode material is not particularly critical.

Only two plasma zones need concern us here: the cathode dark space and the negative glow. The cathode dark space is a thin layer that shows relatively little light emission from electron atom collision. By contrast, the negative glow is a region of bright emission arising from excitation of atoms and ions. The negative glow region extends diffusely away from the cathode and, in the case of small analytical sources, tends to fill much of the remaining discharge volume. Nearly all of the discharge voltage is dropped across the cathode dark space, leaving the negative glow as an essentially field-free region.

The glow discharge can be considered a two-step system involving atomization by sputtering and then ionization/excitation. The sample usually serves as the cathode in a low pressure argon discharge, where positive argon ions are accelerated to the cathode, removing surface atoms of the sample by sputtering. Therefore, the glow discharge can be considered as an atom generator that produces a steady-state atomic density, with atoms being lost continually by diffusion to the source walls but replaced by the constant-rate of

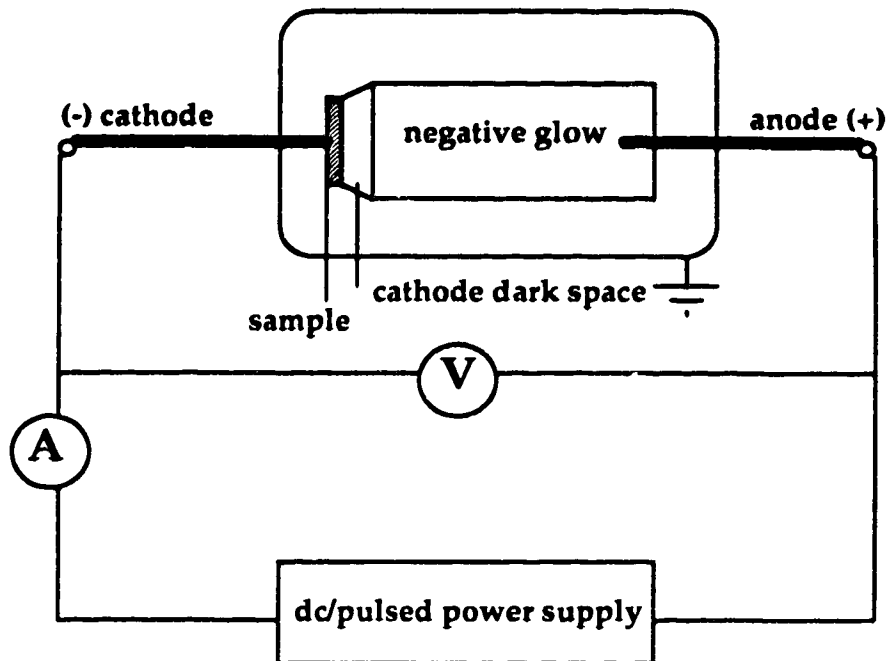


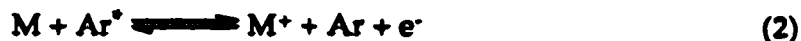
Figure 2.1 Schematic representation of a glow discharge and associated components

sputtering. As the atoms diffuse into the adjacent negative glow, they undergo collisions with many different types of species in the plasma. Impact by electrons, ions and metastable atoms can cause excitation of sputtered atoms, giving rise to optical emission. Sufficient energy to remove an electron completely from the atom creates the ion that forms the basis of GD-MS.

The glow discharge is a versatile source that lends itself to a wide range of analytical measurements [13]. The representative atoms, ions and photons in the plasma produce several analytical options. Atomic absorption (AA) can be carried out directly on the sputtered atoms [14-16]; atomic fluorescence (AF) by exciting atoms with an external energy source [17-20]; atomic emission (AE) from the internal plasma excitation [21-24]; and mass spectrometry (MS) based on generalized elemental ionization that occurs in the plasma [25-29]. Both atomic emission spectrometry (GD-AES) [21-24] and GD-MS [25-29] are excellent methods for direct solids elemental analysis. Especially, the ability of GD-MS to obtain rapidly and effectively a qualitative and quantitative isotopic survey of essentially all the elements in the Periodic Table has obvious analytical appeal [25].

2.1.2 Glow discharge as an ion source

As mentioned earlier, two steps are operative in the glow discharge, sputtering and ionization/excitation. Sputtering is removal of atoms from the cathode by bombardment with fast argon neutrals and ions. After sputtering, the atoms diffuse into the negative glow zone which contains energetic electrons, ions and metastable atoms. Generally, two major ionization steps occur in this zone; electron impact and Penning (metastable impact) ionization:



where Ar^* represents a metastable argon atom.

Electron densities of 10^{14} cm^{-3} have been reported in glow discharges [30-31]. Three different groups of electrons may be present in the negative glow [32]: fast electrons (energies $>25 \text{ eV}$), secondary electrons (energies of $\sim 7 \text{ eV}$, which derive from the direct ionization process), and ultimate electrons (those electrons which have been fully thermalized in the plasma). The large population of secondary-type electrons in the negative glow is sufficiently energetic to cause efficient excitation of the discharge gas, but has energies below the optimum cross section for efficient impact ionization. Between 0.01-0.1% of the sputtered neutral population may be expected to be ionized by electron impact [process (1)] in a conventional planar-diode dc glow discharge source. However, ionization of a ground state atom or molecule may occur by a collision with an excited atom whose total energy is equal to or greater than the first ionization potential of the neutral species. Penning ionization [process (2)] can be identified as the dominant ionization process in a glow discharge although the electron population is generally several orders of magnitude greater than the metastable population. Argon has metastable energy states at 11.55 and 11.72 eV, values exceeding nearly all of the elemental first-ionization potentials [30]. Besides electron impact and Penning ionization, other routes such as charge transfer process [see process (3)] might also contribute to the ionization of sputtered neutral species [30].



The analytical sample ions are then extracted from the glow discharge ion source for subsequent separation in a mass spectrometer according to their mass-to-charge ratio, m/z , allowing qualitative and quantitative analysis.

2.1.3 Glow discharge mass spectrometry instrumentation

Targeted directly at the elemental analysis market, a commercial GD-MS instrument named VG9000 from VG Isotopes Limited/Fisons (Cheshire, UK) first appeared in 1983. It is a very capable instrument with high resolution and is based on a double-focusing sector system. However, it is considerably more expensive than quadrupole-based inductively coupled plasma mass spectrometry (ICP-MS) instrumentation, thus limiting its widespread application. On the other hand, the success of quadrupole-based ICP-MS instrumentation has led to considerable interest in quadrupole GD-MS systems. In fact it is possible to construct GD ion sources that can be interfaced to the same spectrometers that are currently used for ICP-MS [29]. A glow discharge device (GDD) has been designed that can be bolted directly onto the front plate of a commercial ICP quadrupole-based mass spectrometer (Perkin-Elmer/SCIEX ELAN 250/500 ICP-MS system) to replace the ICP torch (see Figures 2.2 and 2.3) [29].

The glow discharge ion source provides a flowing gas load to the mass spectrometer. The interface between the GDD and the mass spectrometer is of critical importance because it has to be capable of sampling the plasma from a 1-5 torr source and then introduce the ions into a lower pressure analyzer chamber where approximate 10^{-6} - 10^{-7} torr is maintained under gas flow conditions. Fortunately, the gas flow rates can be quite low, typically a few cubic

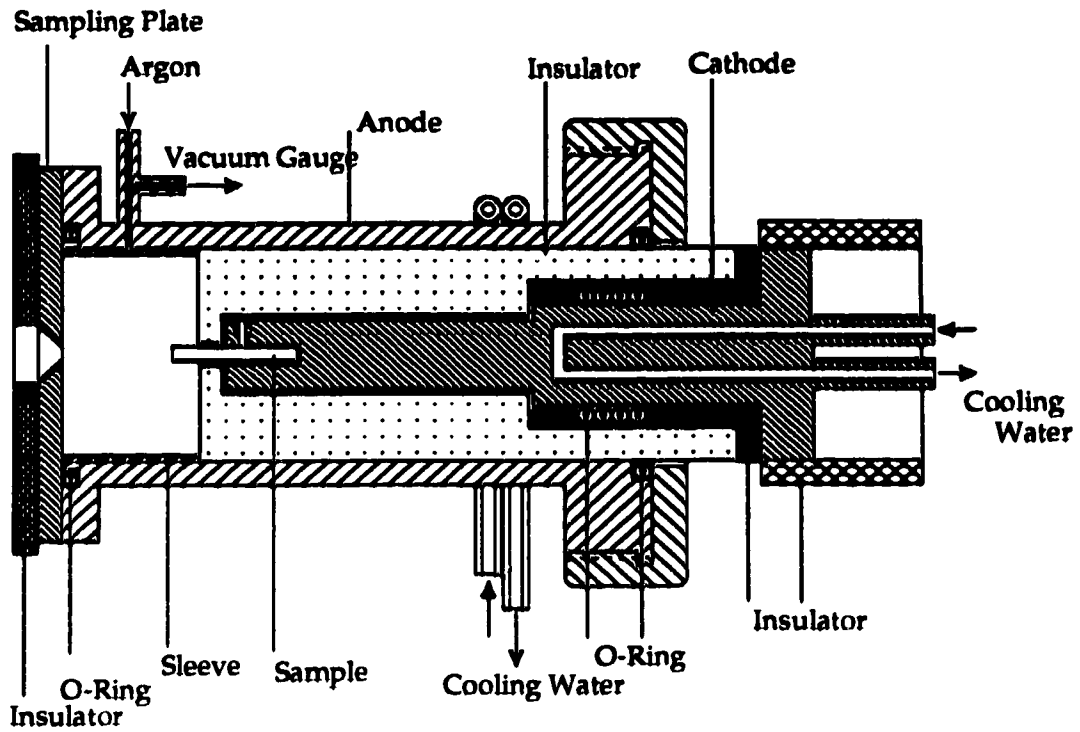


Figure 2.2 Schematic diagram of a pin-type sample glow discharge ion source

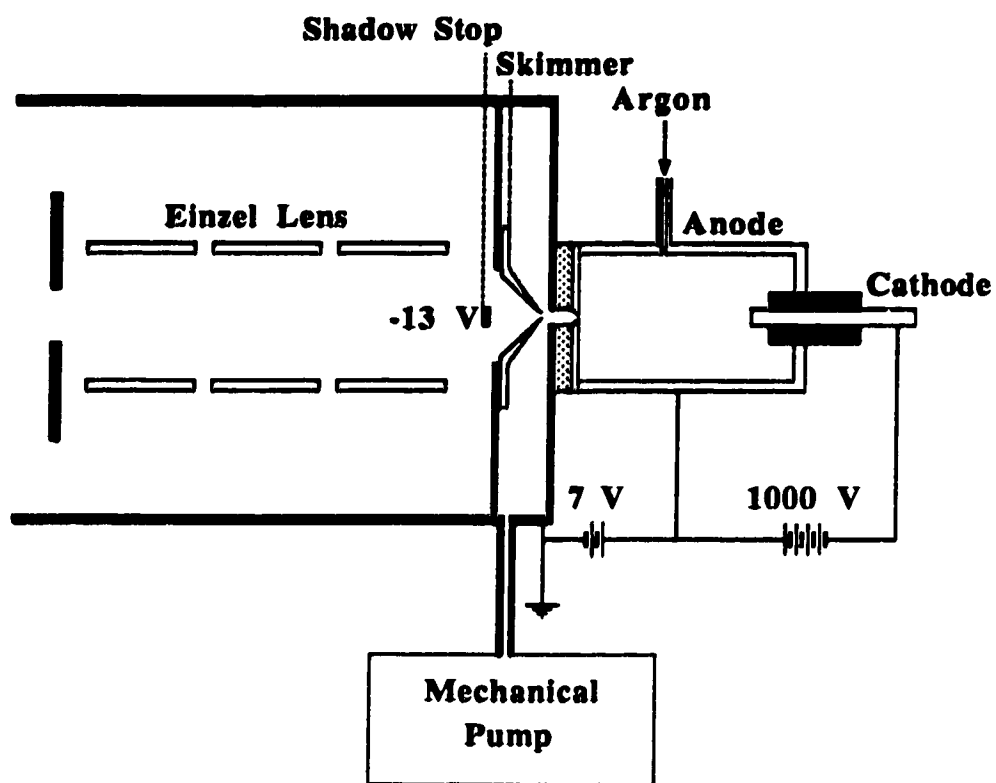


Figure 2.3 Schematic diagram of a pin-type glow discharge device attached to an "ICP"-MS system and the interface voltage biasing arrangement

centimeters per minute. In ICP-MS, the interface consists of two cones, a sampler and a skimmer, having orifices typically in the range of 0.9-1.4 mm. However, in GD-MS, the sampling cone is replaced by a sampling plate (1 mm orifice) which functions as the anode of the GDD and is electrically insulated from the front plate of the mass spectrometer. A skimmer (0.89 mm orifice) is still used to sample a central portion of the beam, allowing a fraction of the sample and discharge gas species to pass into the lower pressure analyzer chamber. The region between sampling plate and the skimmer can be pumped mechanically to approximate 0.1-0.2 torr, compared to the pressure between the sampler and skimmer in ICP-MS where the pressure is about 1 torr. The region behind the skimmer, where the photon stop ion lenses, quadrupole and detector are located, is cryo-pumped to a running pressure of approximately 10^{-6} - 10^{-7} torr in GD-MS while in ICP-MS the operating pressure in this region is as high as 10^{-5} torr.

The ions sampled from the GD source undergo a rather convoluted path in reaching the ion detector. Due to the photon noise from the GD emission, photon stops are included in the ion optics. In the SCIEX ELAN, there are two photon stops. The first one is located just downstream from the skimmer and shadows the second photon stop which is located inside the Bessel box. With a slight negative bias voltage setting, the first photon stop or so called shadow stop protects the second photon stop from being bombarded with too many ions which has a deleterious effect on the stability of the voltage of the second photon stop. In order for ions to reach the quadrupole mass analyzer, they must be traveling at an angle in order to avoid the first photon stop. Ion transfer optics (e.g. Einzel lens) are to enhance ion throughput and the voltages on each lens

element have to be set so that the ions pass through the Einzel lens into and through the Bessel box.

The Bessel box has been employed as a first stage for quadrupole based instruments. It functions as an energy pass filter which selects an energy window for transmission to the quadrupole for isotopic resolution. Ions of the selected energy are passed through the box while those of higher energies and lower energies are rejected. The second photon stop located in the center of the Bessel box prevents most of the neutral atoms and glow discharge photons from reaching the quadrupole and detector, thus reducing background noise.

Ion separation in GD-MS is also achieved using a quadrupole mass filter. The quadrupole is chosen for its simplicity, economy, with low sampling voltages and high ion transmission particularly in the low mass region. Ions are extracted from the quadrupole field through a circular aperture and detected by a continuous dynode channel electron multiplier, operated in a pulse counting mode. The detector is mounted off axis from the quadrupole, as a further aid, to reduce noise from the light emitted by the ion source. The SCIEX ELAN 250 is also designed to go into a shutdown mode to protect the detector if the ion signal becomes too intense.

2.1.4 Operating parameters of glow discharge mass spectrometry

Glow discharge mass spectrometry (GD-MS) is a good technique for the trace elemental analysis of conductive solid samples. In order to use any technique efficiently and to take full advantage of its capability, it is necessary to know the effect of instrument operating parameters on analytical signals. The

instrumentation involved in GD-MS is quite complicated and a great number of variables affect the analytical signal. The key parameters include the voltage setting of the dc power supply, the operating source pressure, and the sampling depth for a pin-type glow discharge device (GDD). The GD current is, in turn, affected by all these operating parameters.

Glow discharges require rather low power (current X voltage) to produce ions from solid samples. Generally, the power dissipation is of the order of 10 watts or less. The actual required voltages and currents are significantly affected by the operating source pressure. The voltage required to initiate and maintain the discharge varies inversely with pressure. At pressures below ~5 torr, discharge voltages may be in the 1000-2000 V range. A hollow cathode discharge, on the other hand, may require only ~300 volts at 1 torr pressure. Electrode geometry and choice of fill gas will also affect power needs. Argon gas is most often selected as the fill gas due to its low cost and good sputtering efficiency. A general purpose power supply for glow discharges should provide 1000-2000 V at currents of 10-50 mA, although this would not necessarily suffice for all glow discharge applications. One might also have use of a high voltage low current unit (3000-4000 V, 10 mA) and a low voltage, high current supply (500 V, 200 mA) in some applications [30].

The second and the third key set of variables in GD-MS, in addition to the GD parameters, are the settings of the mass spectrometer input ion-optic voltages, as well as the interface voltage biasing arrangement including the shadow stop bias and the anode bias. The effect of these operating parameters on analyte signals have already been studied for a quadrupole-based ICP mass spectrometer [31, 33-35]. The dependence of ion signals on input ion-optic

voltages [31, 35] and a computer simulation of the voltage settings on the input ion-lens has also been presented for ICP-MS [36]. However, the shadow stop bias voltage has not been altered in ICP-MS studies, where the shadow stop is usually at ground potential. In GD-MS, however, intense and reliable positive ion signals are obtained when the anode is bias slightly positive with respect to ground and when the shadow stop of the mass spectrometer is bias slightly negative with respect to ground [29].

The size of the orifice in the sampling cone of the interface in an ICP-mass spectrometer has a major impact on signal characteristics. In particular, for oxide forming elements, the MO^+/M^+ ratio is very dependent on orifice size. However, the effect of the orifice size of the skimmer is not as dramatic as the effect of the sampler orifice size [37]. In a glow discharge, the sampling cone is replaced by a sampling plate, which is not the region where oxide formation occurs in GD-MS. Thus, the effect of the orifice size of the skimmer on the signal is not critical for GD-MS.

2.2 Experimental

A pin-type glow discharge ion source designed by Shao and Horlick [29] was directly bolted onto the front plate of an ICP mass spectrometer (SCIEX/Perkin-Elmer Elan, Model 250) in place of the normal sampler (see Figure 2.2). The GD source was electrically insulated from the interface plate of the mass spectrometer by using a Teflon ring. This allows biasing of the anode at a potential above ground. The GD cavity was 10 mm in length. The sample used as the cathode in the GD cavity was machined in the form of a metallic pin, 3 mm in diameter and about 15 mm in length. The sample pin was inserted into

the GD cavity about 1 to 3 mm. A schematic diagram of the glow discharge device attached to the "ICP"-MS system is shown in Figure 2.3.

The argon gas introduced into the GD device was controlled by an SS22RS4 valve (Whitey Co., Ohio, USA). The pressure in the GD cavity was measured by a vacuum gauge which was an MKS Baratron Model 122A.

The power supply for this GD device was a BHK model 2000-0.1 M voltage supply (Kepco Inc., Flushing, N.Y.). It has a full scale rating of 2000 V at 100 mA.

Standard aluminum samples from the Aluminum Company of America (Alcoa) were chosen for this work. Both the effects of DC power supply voltage and argon fill gas pressure on analyte signals were studied. The experiments first involved variation of the discharge voltage from 600 to 1200 volts when the argon pressure was kept at a constant value of 2.50 torr. And then, the argon pressure was changed from 1.5 to 3.0 torr while the discharge voltage was fixed at 1000 volts. Signal intensities for $^{24}\text{Mg}^+$, $^{48}\text{Ti}^+$, $^{55}\text{Mn}^+$, $^{58}\text{Ni}^+$, $^{63}\text{Cu}^+$, $^{64}\text{Zn}^+$ and $^{27}\text{Al}^{40}\text{Ar}^+$ were acquired in order to assess the optimized operating conditions. Investigation of the aluminum argide ($^{27}\text{Al}^{40}\text{Ar}^+$) signal was also carried out since it might function as an internal standard in quantitative analysis.

Establishment of the interface voltage biasing arrangement is also critical for the operation of this GD-MS system (see Figure 2.3). Intense and reliable ion signals can be obtained only when the anode is biased slightly positive with respect to ground (7 V in Figure 2.3) and when the shadow stop of the ELAN mass spectrometer is biased slightly negative (-13 V in Figure 2.3) with respect to

ground [29]. The skimmer and the complete interface mounting plate are at ground potential. The first photon stop (shadow stop) is a normal interface component of the ELAN input ion optics [36]. It serves to "shadow" the photon stop in the center of the bessel box and is usually grounded when the system is used with an ICP source. The dependence of the ion signal on both shadow stop and GD anode bias potentials was investigated. The signals were acquired for $^{24}\text{Mg}^+$, $^{48}\text{Ti}^+$, $^{55}\text{Mn}^+$, $^{58}\text{Ni}^+$, $^{63}\text{Cu}^+$, $^{64}\text{Zn}^+$ and $^{27}\text{Al}^{40}\text{Ar}^+$ from an aluminum alloy pin. In this experiment the ion source was operated by varying either the shadow stop bias from 0 to -20 V or the anode bias from 0 to 20 V so that the maximum ion signal intensity could be obtained.

The effect of ion lens voltages on analyte signal were also studied. The change in analyte signal upon changing the voltage for each of the four accessible ion lens voltages was measured for a set of eight elements in one of aluminum standards covering a range of atomic masses. The results show that a compromise selection of the lens voltage settings to cover a large mass range is necessary.

2.3 Results and Discussion

2.3.1 Effect of glow discharge parameters

Glow discharge parameters mainly include the dc power supply voltage and the discharge gas pressure. The effect of dc power supply voltage on the analyte ion signals of $^{24}\text{Mg}^+$, $^{48}\text{Ti}^+$, $^{55}\text{Mn}^+$, $^{58}\text{Ni}^+$, $^{63}\text{Cu}^+$, $^{64}\text{Zn}^+$ and $^{27}\text{Al}^{40}\text{Ar}^+$ is illustrated in Figure 2.4. Other glow discharge conditions were fixed at 2.50 torr of argon pressure and 8 mm sampling depth for the pin-type

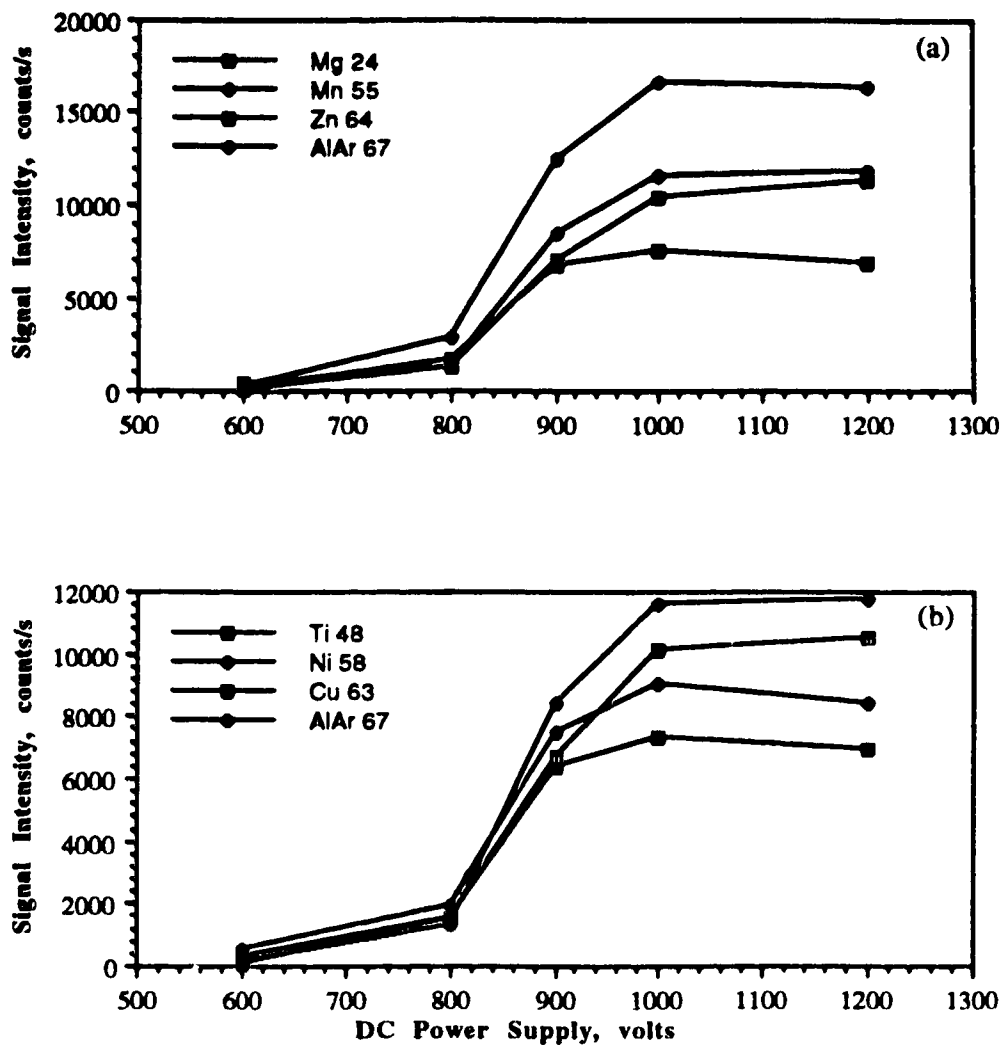


Figure 2.4

Dependence of ion counts on the dc power supply of glow discharge at argon pressure of 2.50 torr for (a) $^{24}\text{Mg}^+$, $^{55}\text{Mn}^+$, $^{64}\text{Zn}^+$, (b) $^{48}\text{Ti}^+$, $^{58}\text{Ni}^+$, $^{63}\text{Cu}^+$ and $^{27}\text{Al}^{40}\text{Ar}^+$ signals

GD device. All of the elements exhibit similar behavior when increasing the voltage from 600 to 1200 volts. The signals of the analytes rise slowly with an increase of the voltage between the anode and cathode of GD device from 600 to 800 volts. At 800 volts, signal intensities increase sharply. At voltages above 1000 volts, the signals have all plateaued.

The effect of argon pressure on the ion signals of the analytes was also studied. Plots of ion signal intensity *versus* argon pressure are shown in Figure 2.5. The discharge voltage was kept at a constant value of 1000 volts. The $^{24}\text{Mg}^+$, $^{48}\text{Ti}^+$, $^{55}\text{Mn}^+$, $^{58}\text{Ni}^+$, $^{63}\text{Cu}^+$, $^{64}\text{Zn}^+$ and $^{27}\text{Al}^{40}\text{Ar}^+$ signals increase as the argon pressure is increased until a particular value (about 2.5 torr) is reached, and then the signals start to slowly decrease. All of the above elements show the same behavior.

The sampling depth for a pin-type glow discharge also affects the intensity of the analytical signal in GD-MS. The sampling depth refers to the distance from the sampling plate to the end of sample pin (the cathode), while the sample insertion length measures the length of the sample pin which is inserted into the GD cavity. Thus the length of the GD cavity (10 mm) is equal to the sampling depth plus the insertion length. Normally, the shorter the sampling depth, the stronger the signal intensity. In other words, the longer the insertion length, the stronger the signal intensity. For aluminum samples, however, the insertion length cannot be too long. Otherwise, the shape of the glow is distorted, and an unstable glow is obtained. Usually, the limit of the insertion length is about 3 mm (*i.e.* sampling depth about 7 mm).

DC current in a pin-type glow discharge is a function of the operating

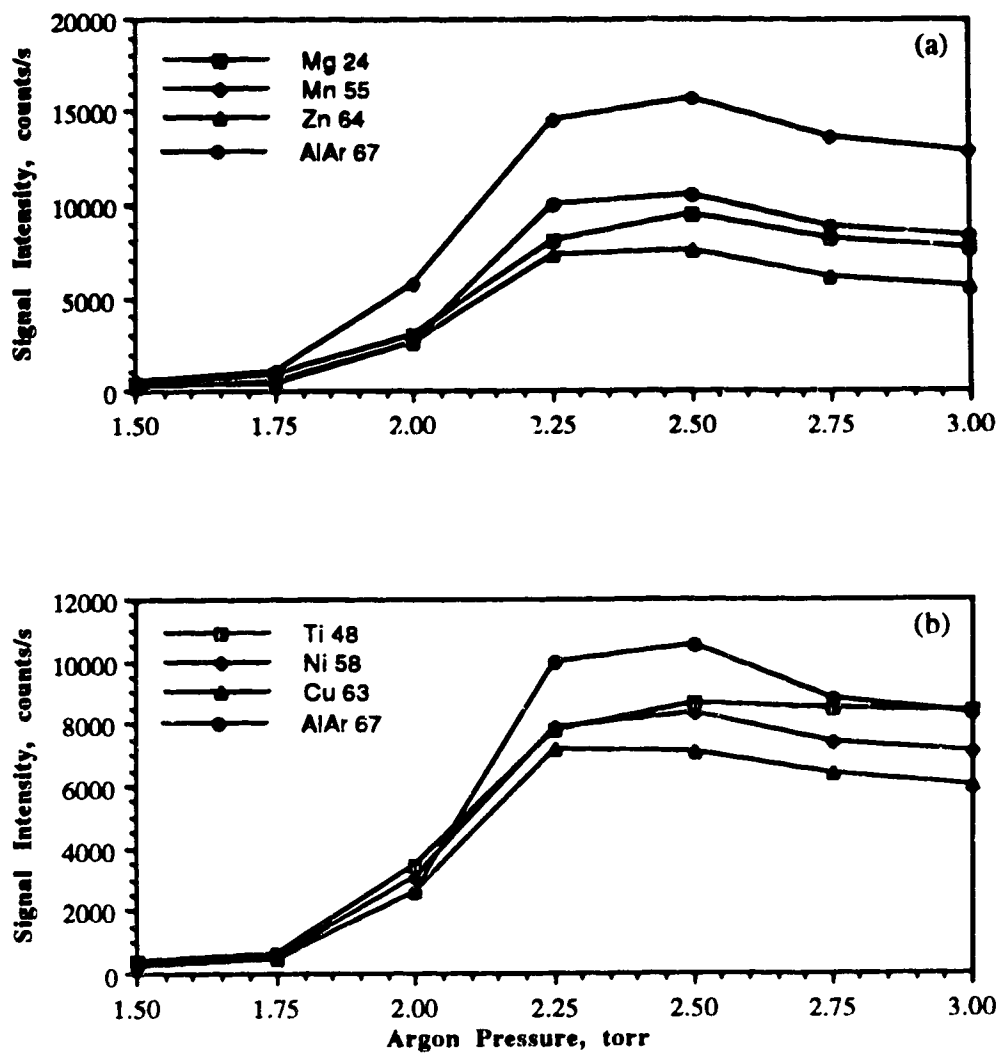


Figure 2.5 Dependence of ion counts on the argon pressure at discharge potential of 1000 volts for (a) $^{24}\text{Mg}^+$, $^{55}\text{Mn}^+$, $^{64}\text{Zn}^+$, (b) $^{48}\text{Ti}^+$, $^{58}\text{Ni}^+$, $^{63}\text{Cu}^+$ and $^{27}\text{Al}^{40}\text{Ar}^+$ signals

parameters which include the discharge voltage, the pressure of the argon gas, and the insertion length of the sample. Current increases with increasing voltage, pressure, and insertion length. The dependence of dc current on the discharge voltage, the pressure of argon, and the insertion length is shown in Figure 2.6. However, dc current is not proportional to the intensity of the analyte signal. Usually, an increase of the current does not correspond directly to an increase in the counts of the ion signal. Normally, the dc current in this pin-type glow discharge ion source was in the range of 6 to 9 mA.

A conventional dc glow discharge can be established by applying a potential of 500-1000 V between two planar conducting electrodes in a vacuum vessel at 1-10 torr pressure [30]. However, the cathodic sputtering in GD correspond directly to produce ion signals. Usually, 100-500 eV bombardment energies of primary ion (Ar^+) are required to sputter the cathode electrode. A sputtered atom must receive an energy that is sufficient to overcome its surface binding energy. A threshold energy is the minimum energy which is able to dislodge a target atom. Above the threshold energy, the sputtering yield rises first exponentially and then linearly with ion energy, reaches a flat maximum or plateau at about 1000 eV, and finally decreases with increasing ion energy [30]. Generally, the power dissipation for GD should be around 8-10 W to get strong ion signals; *i.e.* a potential of 800-1000 V is expected to be applied at current of ~10 ma. Below 800 V, the dissipation power is low and the sputtering efficiency is relatively poor. Thus a lower level of the ion signals is obtained. However, increase of the fill gas pressure increases the ion current, in turn, increases the dc current. Therefore, when the dissipation power of the glow discharge increases, the ion signal is expected to be increased.

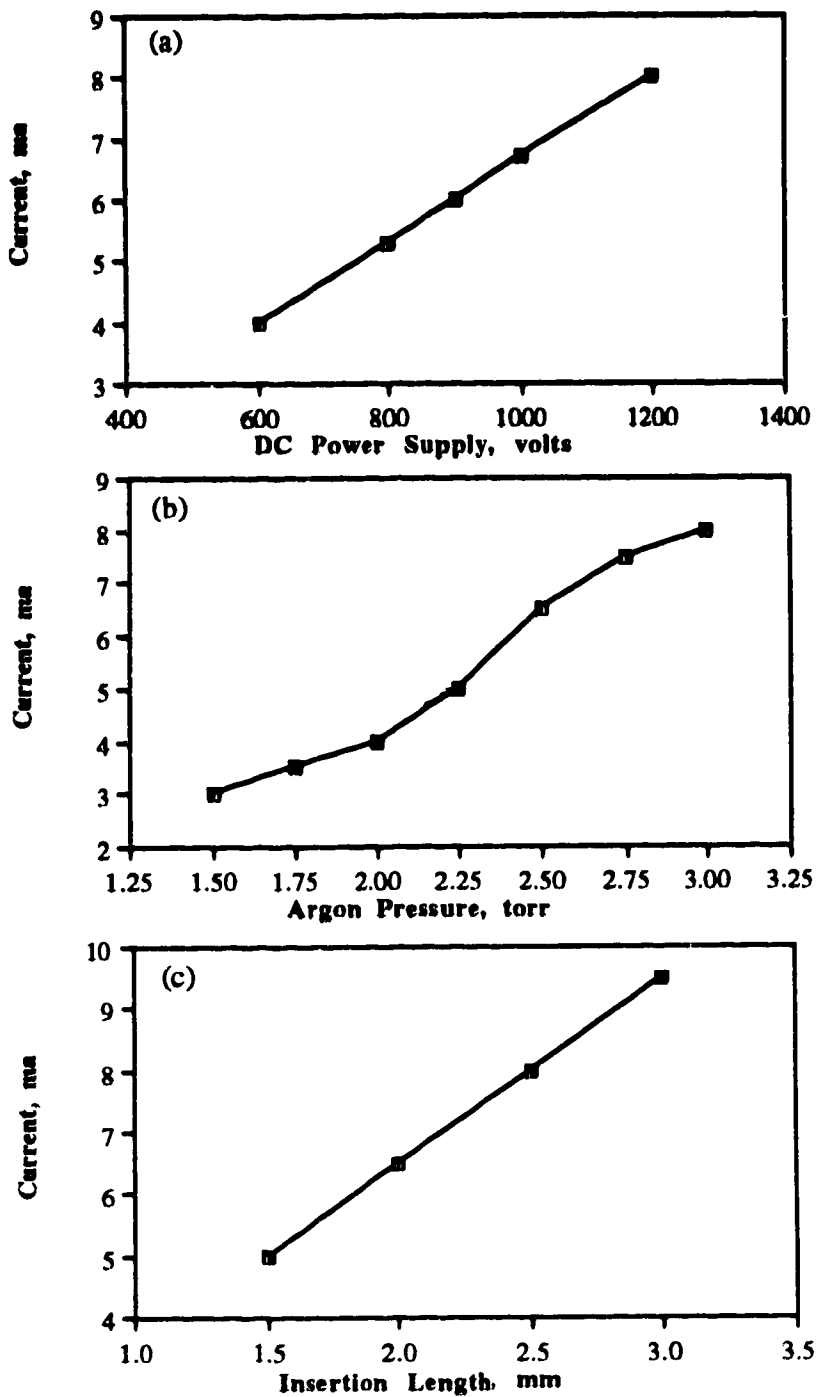


Figure 2.6 Dependence of current on (a) dc power supply (b) argon pressure and (c) sampling depth for GD-MS

2.3.2 Effect of interface parameters

The interface parameters include the anode bias voltage for the glow discharge source and the shadow stop bias voltage for mass spectrometer. These two bias potentials affect the intensity of the analytical signals in GD-MS. The dependence of the $^{24}\text{Mg}^+$, $^{58}\text{Ni}^+$, $^{64}\text{Zn}^+$ and $^{27}\text{Al}^{40}\text{Ar}^+$ ion signals on shadow stop bias is shown in Figure 2.7. Except for the lighter element ^{24}Mg which requires a more negative bias potential, the signals for most elements in this aluminum sample pin require a bias potential of -13 V on the first photon stop to reach maximum counts. The effect of anode bias on analytical signal intensity is more critical than that of the shadow stop bias. Plots of signal intensity (logarithm scale) *versus* anode bias voltage are shown in Figure 2.8. All the analyte signals show the same behavior and the analytical signals require a bias potential of +7 V with respect to ground on the anode of the GD to reach maximum counts. This value is the same as that determined when the pin-type GD was used to analyze steel and brass samples [29]. Thus, both these bias potentials seem to be independent of the sample material to be analyzed. By floating the potential 7 volts above ground, the anode repels the positive ions produced in the GD cavity and pushes the ions through the skimmer which is grounded. Opposite to the anode bias, the negative shadow stop voltage attracts the positive ions from the GD cavity into the mass spectrometer. Signal counts of ions increase with increasing the bias potential because of increasing the kinetic energy of the ions. However, the signal intensity is not proportional to the bias potentials. There is a maximum bias value for each potential shown in Figures. 2.7 and 2.8. The light element such as $^{24}\text{Mg}^+$ requires a more negative bias potential (see Figure 2.7) since light mass results in a high velocity of the ion (*i.e.* signal counts) at a constant potential. The space charge effect makes the signal counts drop when

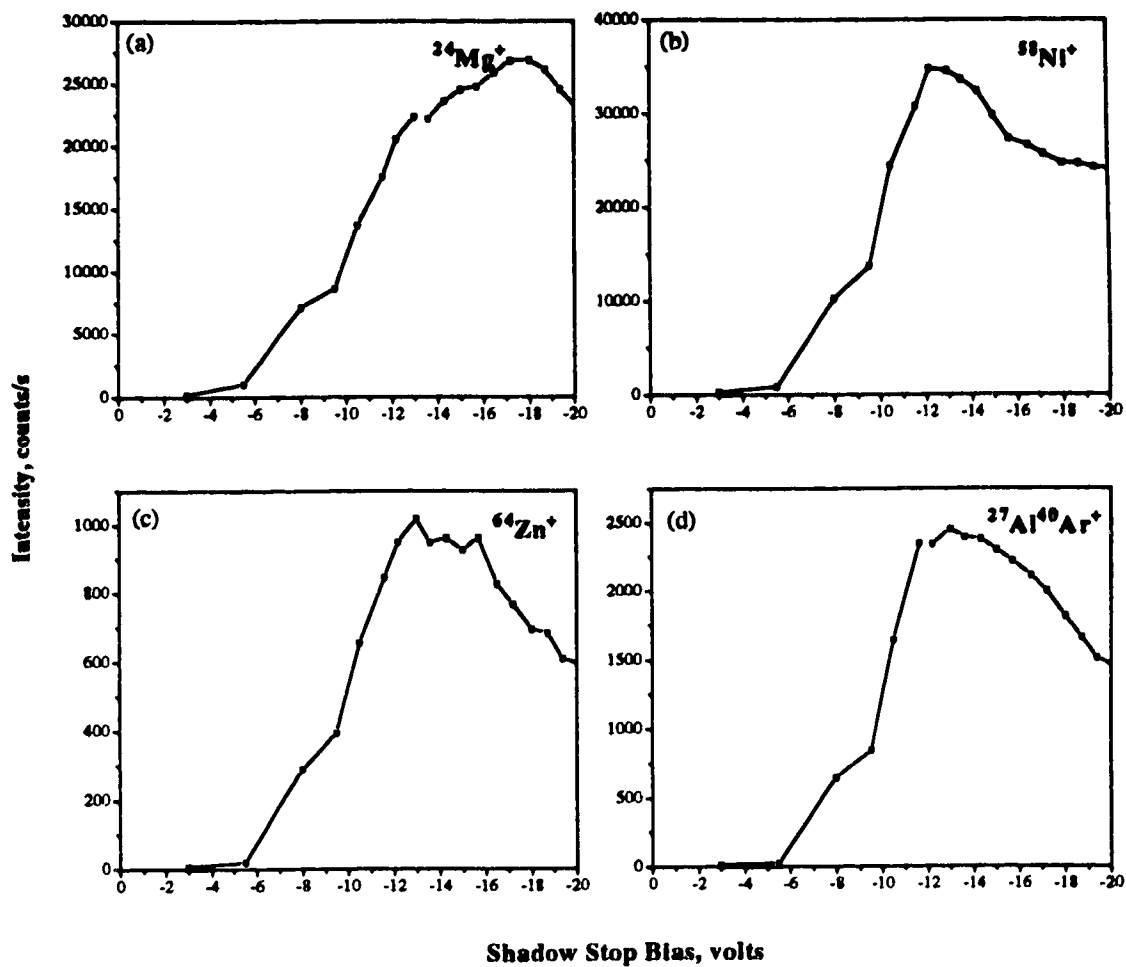


Figure 2.7 Effect of shadow stop bias on (a) $^{24}\text{Mg}^+$, (b) $^{58}\text{Ni}^+$, (c) $^{64}\text{Zn}^+$ and (d) $^{27}\text{Al}^{40}\text{Ar}^+$ ion signal intensities

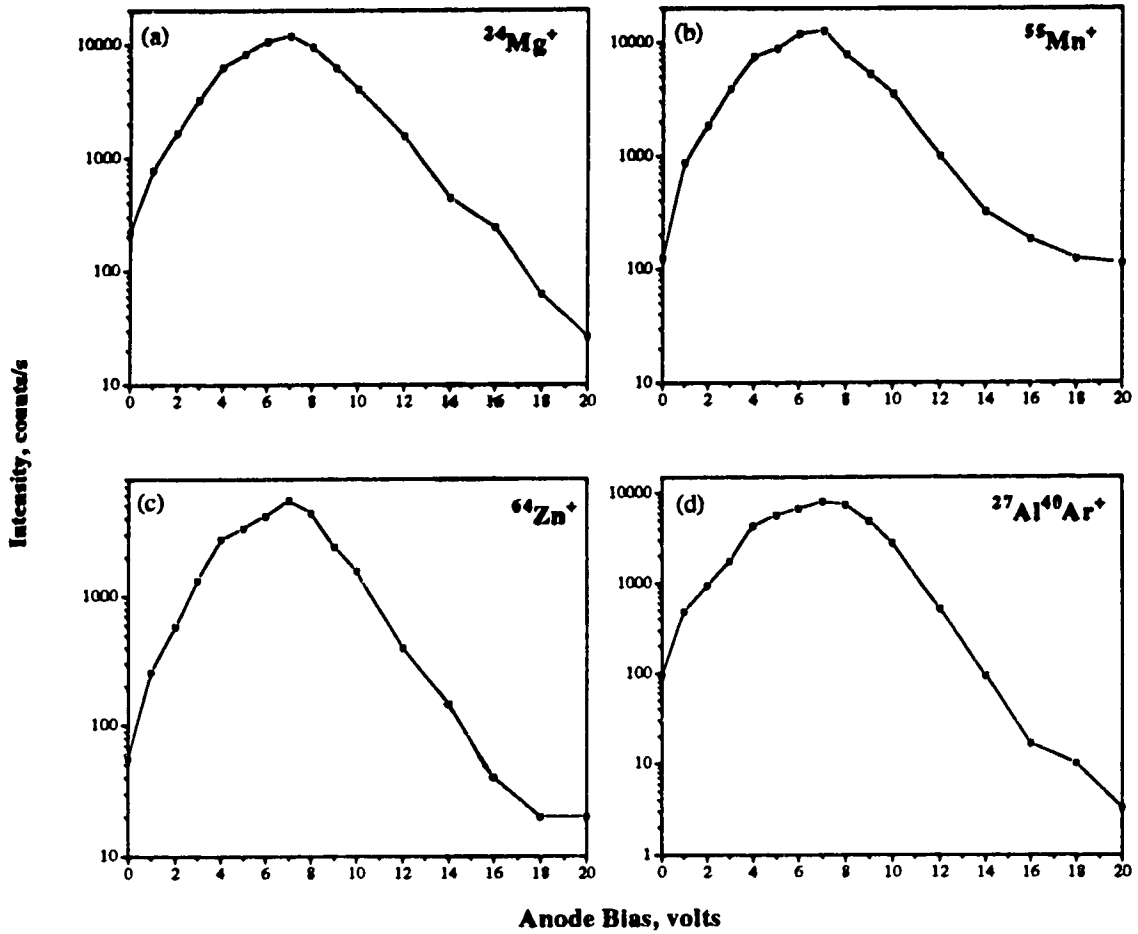


Figure 2.8 Effect of anode bias on (a) $^{24}\text{Mg}^+$, (b) $^{55}\text{Mn}^+$, (c) $^{64}\text{Zn}^+$ and (d) $^{27}\text{Al}^{40}\text{Ar}^+$ ion signal intensities

bias potential increases further. The positive ions would repel each other in the space. Both bias values might, however, be different when different configurations of glow discharges such as disk, Grimm and hollow-cathode sources are utilized [29].

2.3.3 Effect of ion lens voltages

The ions formed in the glow discharge are extracted by the sampling plate, pass through the skimmer and into the ion transfer optics. The ion optics include an einzel lens which is used to enhance the ion throughput. At the exit from the einzel lens assembly, the ion beam enters into an analyzer chamber called a bessel box. It functions as an energy pass filter which selects an energy window for transmission to the quadrupole for isotopic resolution. Ions of the selected energy are passed through the box while those of higher energies and lower energies are rejected. The plate unit and the barrel of the bessel box, together, make ions flow around the second photon stop and then into the entrance of the quadrupole rods. The second photon stop located in the center of the bessel box prevents most of the neutral atoms and glow discharge photons from reaching the quadrupole and detector, thus reducing background noise. A schematic diagram of the input ion optics of the SCIEX ELAN is shown in Figure 2.9. The elements for which the voltages can be varied are referred to as: E1, the cylinders 1 and 3 of the einzel lens (0 to -20 V); P, the front and back bessel plates (0 to -60 V); B, the bessel barrel (0 to +10 V); and S2, the second photon stop (0 to -20 V) which is located in the bessel box. Four push-button indexing switches are used to adjust the voltages. The voltage of the center cylinder of the einzel lens is not accessible to the user, it was set by the manufacturer at -130 V. The change in analyte signal upon changing the voltage of each of the four accessible

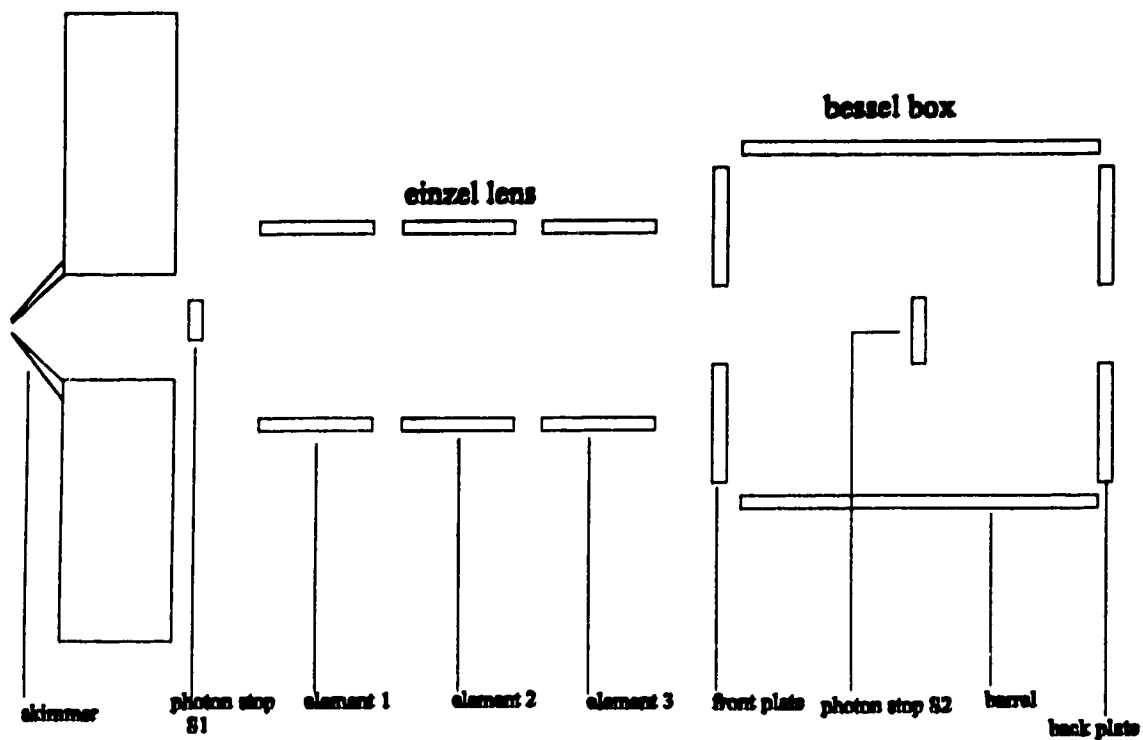


Figure 2.9 Diagram of the ion lenses for SCIEX ELAN 250 mass spectrometer

ion lens voltages was measured for a set of eight elements covering a range of atomic masses. The elements chosen were $^{24}\text{Mg}^+$, $^{48}\text{Ti}^+$, $^{55}\text{Mn}^+$, $^{58}\text{Ni}^+$, $^{63}\text{Cu}^+$, $^{64}\text{Zn}^+$, $^{120}\text{Sn}^+$ and $^{208}\text{Pb}^+$, ranging in atomic mass from 24 to 208 m/z.

The dependence of signal intensity on einzel-lens voltage (E1) for four ions ($^{24}\text{Mg}^+$, $^{58}\text{Ni}^+$, $^{120}\text{Sn}^+$ and $^{208}\text{Pb}^+$) is presented in Figure 2.10. This is the potential applied on cylinders 1 and 3 of the einzel-lens. For elements such as Mg, Ni and Sn, more negative voltage applied to the lens results in higher signal counts. The plot for the heavier element such as Pb has a maximum at -17 V. The effect of the voltage on ion counts for different masses is not too severe so that a compromise voltage setting of -18 to -20 V on the einzel-lens is satisfactory, but may have to be reduced a couple of volts for the heavier analytes.

The effect of bessel box plate voltage (P) on the ion signal is displayed in Figure 2.11. Every element has a peak type response. The lighter the element, the more negative the voltage at which the peak maxima occurs. The maxima for these elements occur over a voltage range from -12 to -22 V. Typically, a compromise voltage setting such as -18 to -20 V was chosen.

The graphs of signal intensity *versus* the bessel box barrel potential (B) are shown in Figure 2.12. The maxima for these elements occur over a voltage range from 3.5 to 6 V. In general, a compromise voltage setting of 4 to 5 V on the barrel was found to be acceptable.

Finally, the plots of signal intensity *versus* the second photon stop voltage (S2) are shown in Figure 2.13. Maximum signals are obtained at a lens voltage

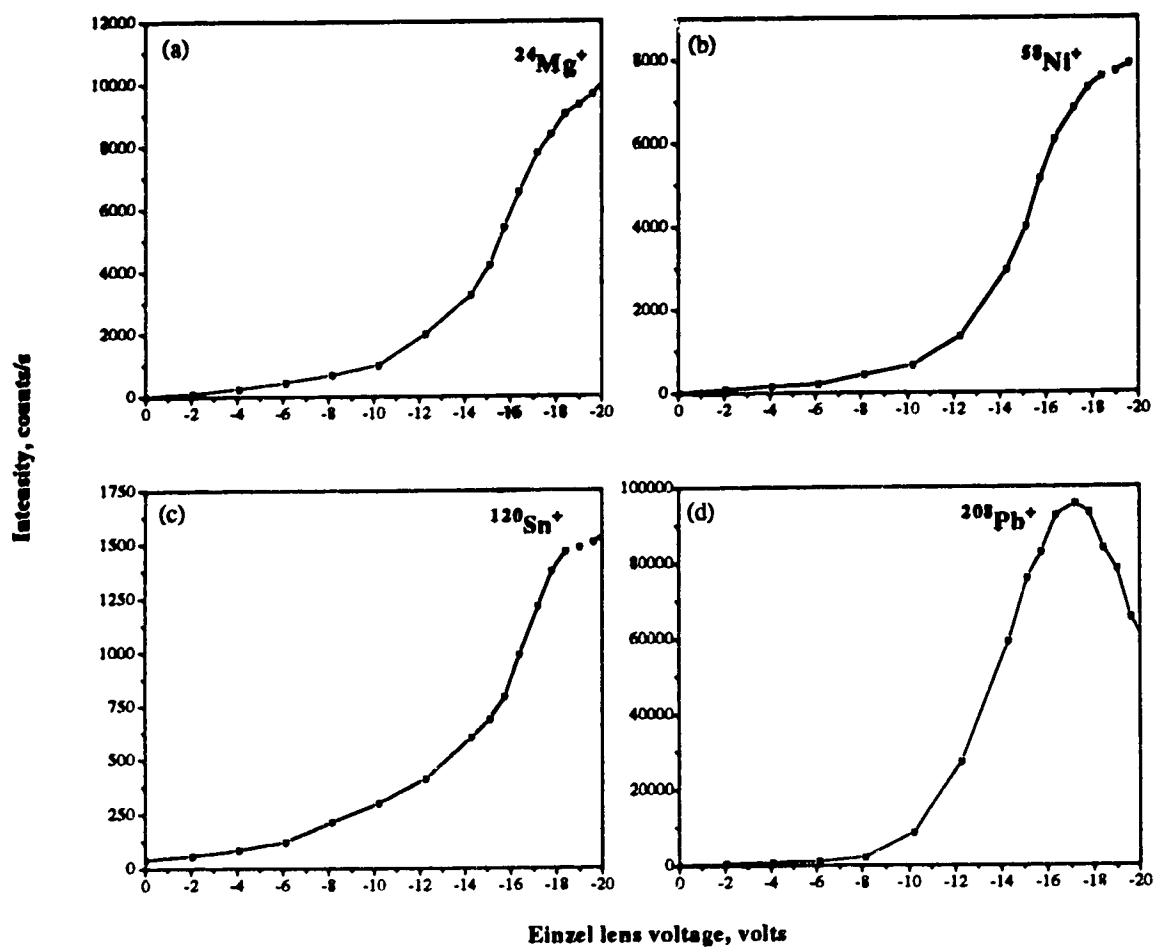


Figure 2.10 Dependence of ion counts on einzel-lens voltage for (a) $^{24}\text{Mg}^+$, (b) $^{58}\text{Ni}^+$, (c) $^{120}\text{Sn}^+$ and (d) $^{208}\text{Pb}^+$ signals

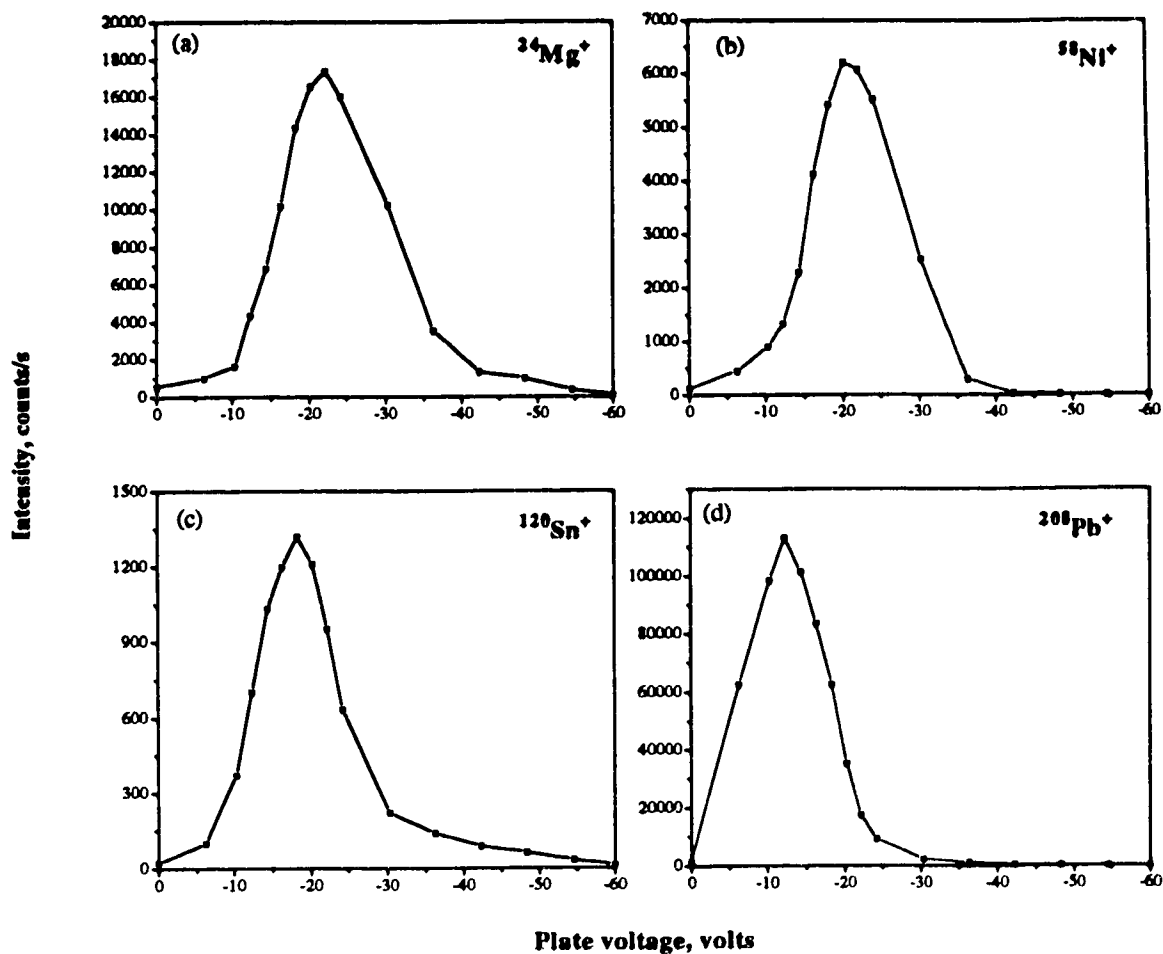


Figure 2.11 Dependence of ion counts on Bessel plate voltage for (a) $^{24}\text{Mg}^+$, (b) $^{58}\text{Ni}^+$, (c) $^{120}\text{Sn}^+$ and (d) $^{208}\text{Pb}^+$ signals

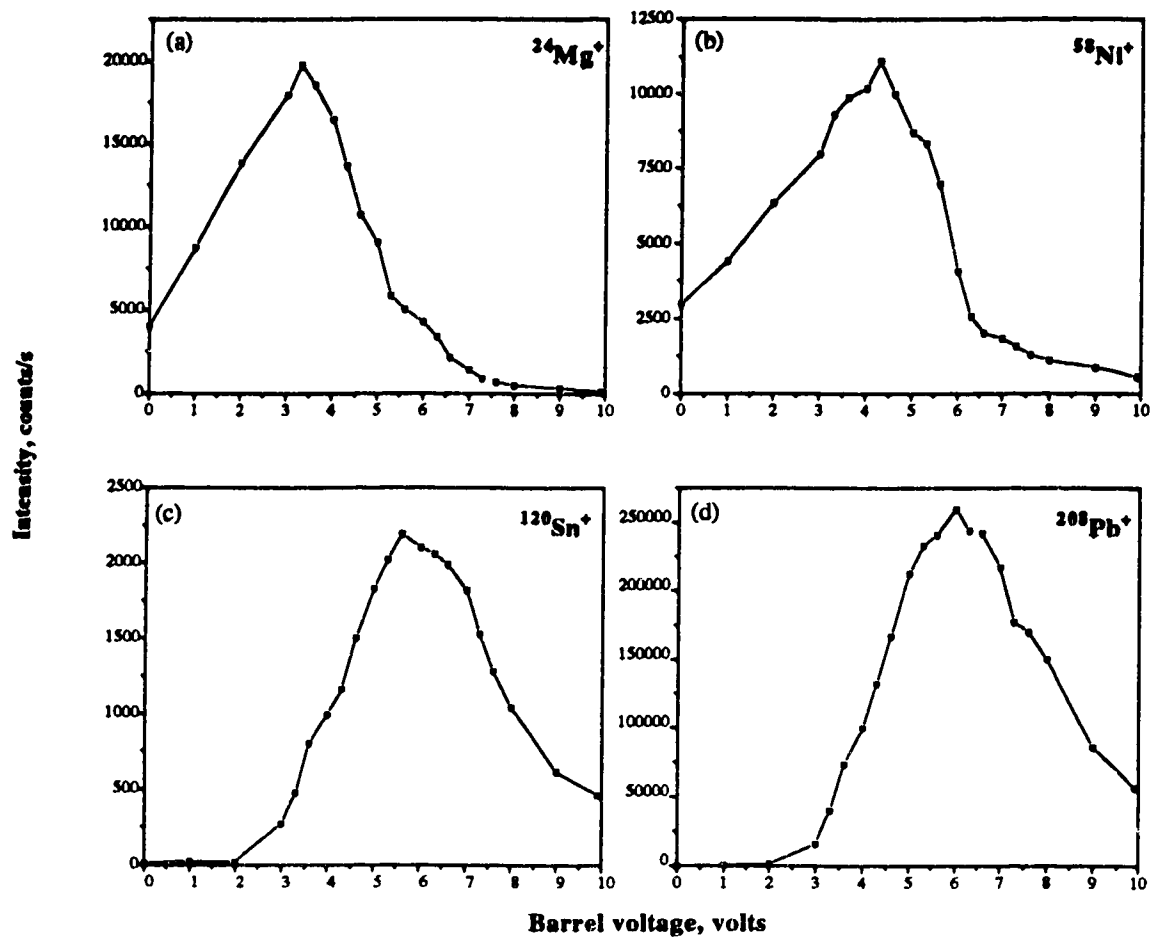


Figure 2.12 Dependence of ion counts on bessell box voltage for (a) $^{24}\text{Mg}^+$, (b) $^{58}\text{Ni}^+$, (c) $^{120}\text{Sn}^+$ and (d) $^{208}\text{Pb}^+$ signals

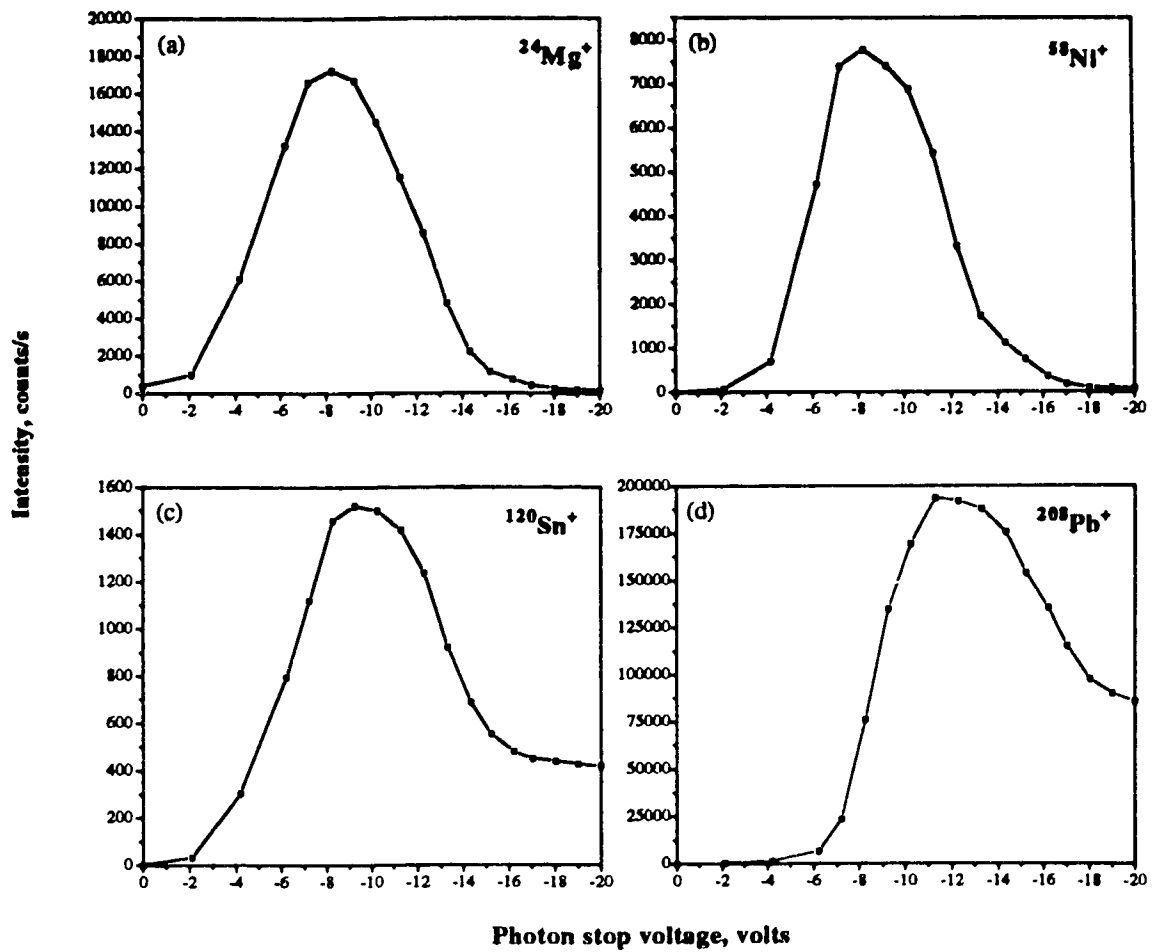


Figure 2.13 Dependence of ion counts on the photon stop voltage for (a) $^{24}\text{Mg}^+$, (b) $^{58}\text{Ni}^+$, (c) $^{120}\text{Sn}^+$ and (d) $^{208}\text{Pb}^+$ signals

range from -8 to -11 V. A compromise voltage setting on the photon stop in the range of -8 to -9 V was normally used.

The results for the effect of ion lens voltages in GD-MS are relatively similar to those established in ICP-MS. Thus, there is no significant difference on ion-lens voltage setting between ICP-MS and GD-MS. This implies that the ion energies of the ions extracted from the GD source are comparable to those for the ICP source.

2.4 Conclusions

The basic running conditions for the pin-type glow discharge device and the mass spectrometer are summarized in Table 2.1. The most compromised settings with respect to differential analyte signal response are those associated with the ion lenses (E1, P, B and S2). In particular, these must be adjusted if heavy analytes are being determined (See Figures 2.10 to 2.13).

Table 2.1 Summary of the pin-type GD-MS instrumental parameters.

A. Glow Discharge Device:		
dc Voltage (cathode)		-1000 V
Fill Gas Pressure (Argon)		2.5 torr
B. Interface:		
Anode Bias		+7 V
Shadow Stop Bias		-13 V
C. Mass Spectrometer:		
Einzel Lens(E1)		-18 to -20 V
Bessel Box Plates(P)		-18 to -20 V
Bessel Box Barrel(B)		4 to 5 V
Photon Stop(S2)		-8 to -9 V

References

1. F. Paschen, *Ann. Phys.* **50**, 901 (1916).
2. H. Schuler, *Z. Phys.* **72**, 423 (1931).
3. F. W. Aston, *Mass Spectra and Isotopes*, 2nd ed., Longmans, Green and Co., New York, 1942.
4. J. W. Coburn and E. Kay, *Appl. Phys. Lett.* **19**, 350 (1971).
5. J. W. Coburn and E. Kay, *J. Appl. Phys.* **43**, 4965 (1972).
6. J. W. Coburn E. Taglauer and E. Kay, *J. Appl. Phys.* **45**, 1779 (1975).
7. J. W. Coburn E. Eckstein and E. Kay, *J. Appl. Phys.* **46**, 2828 (1975).
8. W. W. Harrison and C. W. Magee, *Anal. Chem.* **46**, 461 (1974).
9. C. G. Bruhn, B. L. Bentz and W. W. Harrison, *Anal. Chem.* **50**, 373 (1978).
10. J. W. Coburn and W. W. Harrison, *Appl. Spectrosc. Rev.* **17**, 95 (1988).
11. N. Jakubowski, D. Stuewer and W. Vieth, *Anal. Chem.* **59**, 1825 (1987).
12. W.W. Harrison, *J. Anal. At. Spectrom.* **3**, 867 (1988).
13. J. A. C. Broekaert, *J. Anal. At. Spectrom.* **2**, 537 (1987).
14. D. C. McDonald, *Anal. Chem.* **49**, 1336 (1977).
15. M. R. Winchester and R. K. Marcus, *Applied Spectroscopy* **42**, 941 (1988).
16. C. L. Chakrabarti, K. L. Headrick, J. C. Hutton and P. C. Bertels, *Spectrochimica Acta* **46B**, 183 (1991).
17. H. G. C. Human, N. P. Ferreira, R. A. Kruger and L. R. P. Butler, *Analyst* **103**, 469 (1986).
18. B. W. Smith, N. Omenetto and J. D. Winefordner, *Spectrochimica Acta* **39B**, 1389 (1984).
19. B. M. Patel and J. D. Winefordner, *Spectrochimica Acta* **41B**, 469 (1986).

20. S. A. Dashin, Yu. A. Karpov, O. A. Kushlyansky, I. A. Mayorov and M. A. Bolshov, *Spectrochimica Acta* **46B**, 467 (1991).
21. A. Quentmeier, H. Bubert, R. P. H. Garten, H. J. Heinen, H. Puderbach and S. Storp, *Mikrochim. Acta, Suppl.* **11**, 89 (1985).
22. K. H. Koch, M. Kretschmer and D. Grunenberg, *Mikrochim. Acta*, **2**, 225 (1983).
23. G. Ehrlich, U. Stahlberg and V. Hoffmann, *Spectrochimica Acta* **46B**, 115 (1991).
24. H. Nickel, D. Guntur, M. Mazurkiewicz and A. Jaoumidis, *Spectrochimica Acta* **46B**, 125 (1991).
25. W. W. Harrison, K. R. Hess, R. K. Marcus and F. L. King, *Anal. Chem.* **58**, 341A (1986).
26. S. Tanguay and R. Sacks, *Spectrochimica Acta* **46B**, 217 (1991).
27. N. Jakubowski, D. Stuewer and G. Toelg, *Spectrochimica Acta* **46B**, 155 (1991).
28. W. Vieth and J. C. Huneke, *Spectrochimica Acta* **46B**, 137 (1991).
29. Y. Shao and G. Horlick, *Spectrochimica Acta* **46B**, 165 (1991).
30. W. W. Harrison and B. L. Bentz, *Prog. Analyt. Spectrosc.* **11**, 53 (1988).
31. M. A. Vaughan, G. Horlick and S. H. Tan, *J. Anal. At. Spectrom.* **2**, 765 (1987).
32. F. Howorka and M. Pahl, *Z. Naturforsch.*, **27A**, 1425 (1972).
33. G. Horlick, S. H. Tan, M. A. Vaughan and C. A. Rose, *Spectrochim. Acta* **40B**, 1555 (1985).
34. G. Zhu and R. F. Browner, *Appl. Spectrosc.* **41**, 56 (1987).
35. A. L. Gray and J. G. Williams, *J. Anal. At. Spectrom.* **2**, 599 (1987).
36. M. A. Vaughan and G. Horlick, *Spectrochim. Acta* **45B**, 1301 (1990).
37. M. A. Vaughan and G. Horlick, *Spectrochim. Acta* **45B**, 1289 (1990).

Chapter 3

Analysis of Aluminum Samples Using Glow Discharge Mass Spectrometry

3.1 Introduction

Glow discharge mass spectrometry (GD-MS) has been used for the direct determination of trace levels of elements in various types of solid samples [1]. The applications include analysis of nonconductors such as glasses and ceramics using radio frequency powered GD-MS [2], determination of C, N, O, P and S in semiconductors [3], the direct analysis of metals, alloys (such as steels and brass) [4, 5], and the analysis of superconductors [6]. Aluminum alloys are some of the most challenging samples for alternative solution-based methods because of difficulties in dissolution and the presence of refractory species. Thus, analytical methods using GD-MS have been developed in recent years with respect to the analyses of solid aluminum-based alloys. The method of quantitation was based on the use of relative sensitivity factors (RSF's) determined from an aluminum standard for each of the analytes and it was confirmed that RSF values were independent of matrix [7, 8]. In addition, GD-MS was also used for the routine quality control of high-purity aluminum [9] and has been compared with SIMS for the determination of U and Th in aluminum [10]. In this report,

simultaneous multielement analysis of alloy aluminum samples is presented with a particular emphasis placed on the utility of aluminum argide as an internal standard. A pin-type GD ion source which was interfaced to a commercial ICP mass spectrometer (SCIEX/Perkin-Elmer ELAN Model 250 ICP-MS) was employed for this work.

3.2 Experimental

A pin-type GD ion source (Figure 3.1) designed by Shao and Horlick [5] was used for this work. This ion source can be directly bolted onto an external interface plate of the mass spectrometer (SCIEX/Perkin-Elmer Elan, Model 250) in place of normal sampling cone. The whole source is electrically insulated from the interface plate of the mass spectrometer by a Teflon ring. This allows biasing of the anode and the sampling plate at a potential other than ground potential which is necessary for the successful operation of the device. The sampling plate and the anode are normally operated at the same potential. The central orifice diameter in the sample plate is 1 mm.

Five standard aluminum samples from the Aluminum Corporation of Canada (Alcan) and eight standard aluminum samples from the Aluminum Company of America (Alcoa) were chosen for this work. The aluminum samples, which were used as the cathode in the GD cavity, were machined in the form of a metallic pin, 3 mm in diameter and about 15 mm in length. The sample pin was inserted into the GD cavity about 3 mm so that the distance from the sampling plate to the end of sample pin was 7 mm, since the GD cavity is 10 mm in length.

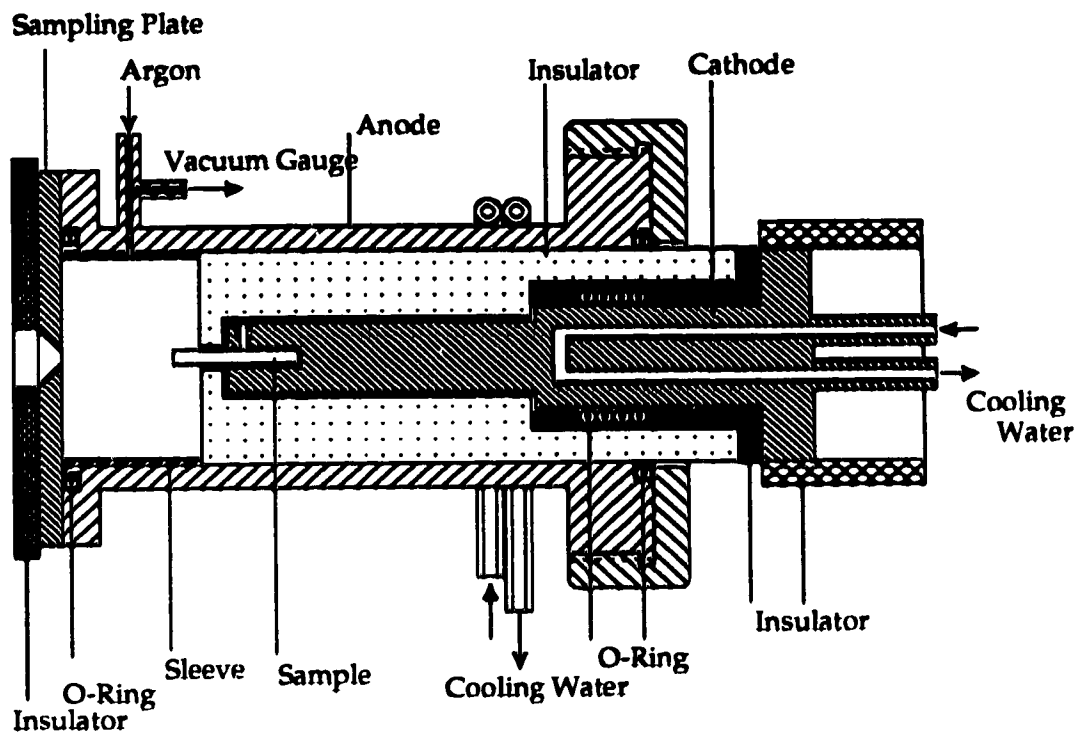


Figure 3.1 Schematic diagram of a pin-type sample glow discharge ion source

Argon introduced into the GD device was controlled by an SS22RS4 valve (Whitey Co., Ohio, USA). The system was pumped with the normal mechanical vacuum pump connected to the interface of the ICP mass spectrometer. No extra pump was needed for this GD device. This pin-type GD device was water cooled. The cooling water connections are shown in Figure 3.1.

Typical operating pressures were 2.5 torr for the GD device, 0.1 to 0.2 torr for the region between the sampling plate and the skimmer and 10^{-7} to 10^{-6} torr for the mass spectrometer. These pressures were lower compared to the typical operating pressures for this system as an ICP-MS, where the pressure is about 1 torr between the sampling cone and the skimmer and the mass spectrometer operates at about 10^{-5} torr. The vacuum gauge used on the GD device was an MKS Baratron Model 122A.

The power supply for GD devices was a BHK Model 2000-0.1 M voltage supply (Kepco Inc., Flushing, N.Y.). It has full scale ratings of 2000 V and 100 mA. Typical operating conditions ranged 800-1200 V and 7.5-9.5 mA for most aluminum samples, with an operating pressure of 2.5 torr.

Establishment of the correct voltage biasing arrangement for the interface components was critical for the successful operation of the GD device. Shao and Horlick [5] reported that intense and reliable ion signals were only obtained when the anode was biased slightly positive with respect to ground and when the shadow stop of the ELAN was biased slightly negative with respect to ground. The shadow stop is a normal component interface of the ELAN input ion optics [5]. It serves to obscure the photon stop in the center of the Bessel box

and is usually grounded when the system is used with an ICP source. The dependence of the ion signal on both the shadow stop and anode bias potentials is shown in Figure 3.2. The signal is for $^{63}\text{Cu}^+$ in an aluminum alloy pin. Therefore, this pin-type ion source was usually operated with the shadow stop biased at -13.0 V and the anode biased at 7.0 V, the conditions at which the maximum ion signal intensity was obtained. The interface voltage biasing arrangement is shown in Figure 3.3 and the ion focusing lens voltages listed in Table 3.1 were a compromise chosen to cover a large mass range. The ion lens voltage settings shown in Table 3.1 are different from the values of the pin-type GD-MS instrumental parameters which were described in Chapter 2 (Table 2.1) since a different mass spectrometer was used to obtain maximum ion signals for this experiment.

Table 3.1 Ion lens voltage setting

<u>Lens</u>	<u>Setting</u>	<u>Voltage (V)</u>
Bessel box barrel(B)	62	6.5
Bessel box plates(P)	48	-30.9
Einzel lens(E1)	99	-22.4
Photon stop(S2)	40	-8.6

Aluminum is one of the active metals and it is easily oxidized. Thus, the surface of an aluminum alloy pin is covered with a tenacious thin film of aluminum oxide after it is exposed to air. Whenever a fresh aluminum surface is created and exposed to either air or water, a surface film of aluminum oxide forms at once. The normal surface film present in air is about 5 nm thick [11].

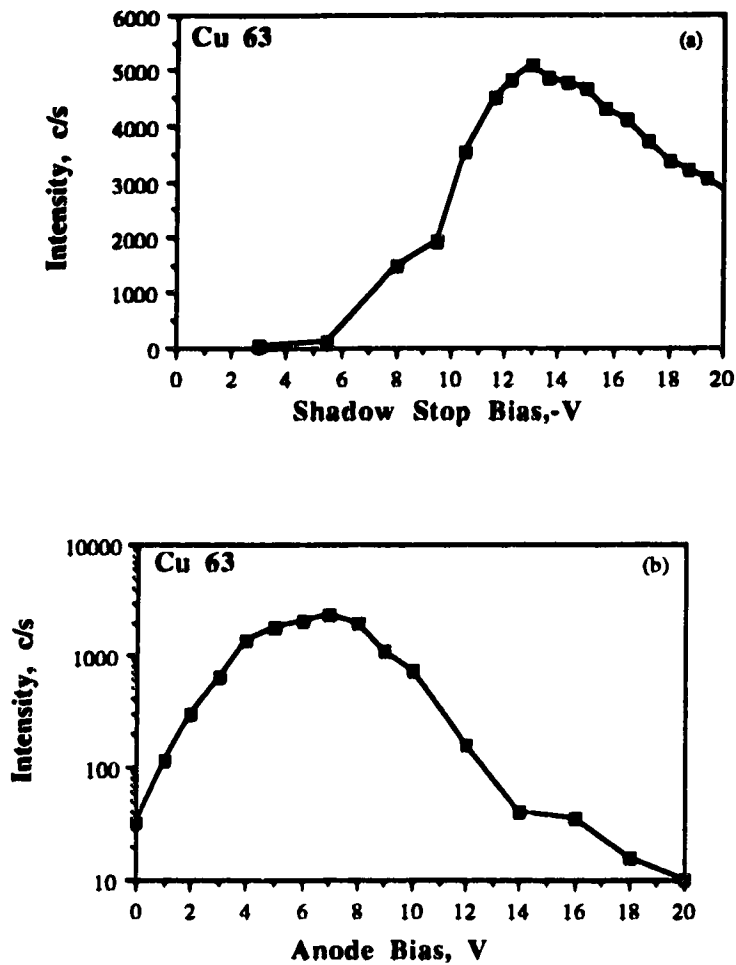


Figure 3.2 Effect of shadow stop bias (a) and anode stop bias (b) on $^{63}\text{Cu}^+$ ion signal intensity

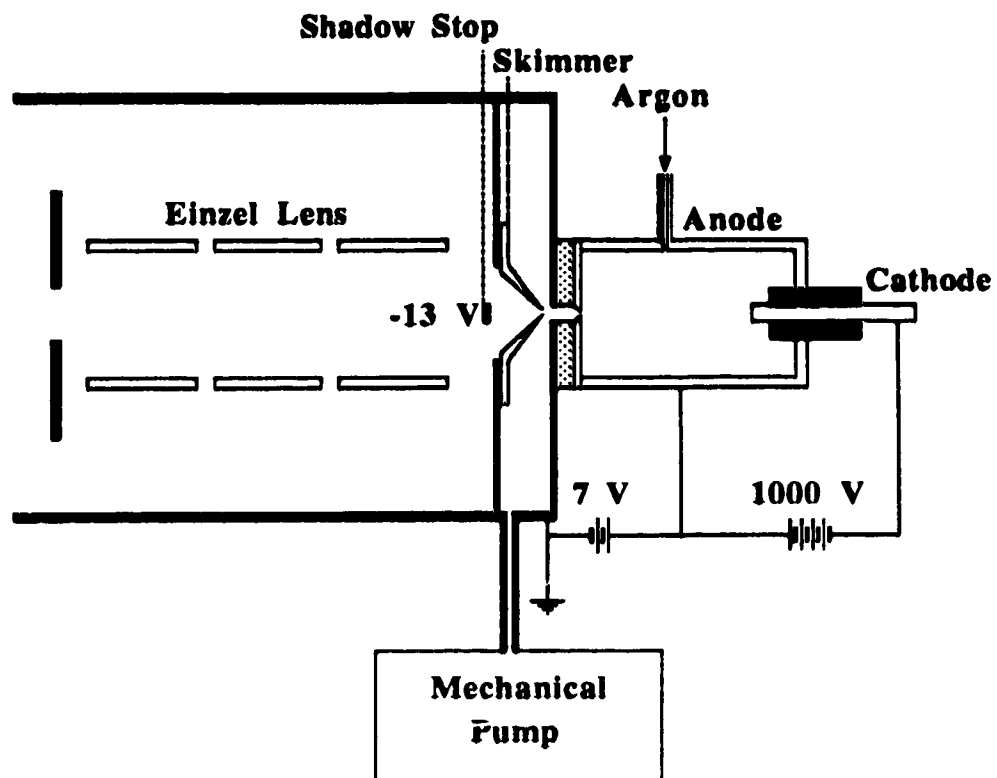


Figure 3.3 Schematic diagram of a pin-type glow discharge device attached to an "ICP"-MS system and the interface voltage biasing arrangement

An extended sputter induction period is required for surface cleaning and subsequent efficient sputter atomization of the bulk aluminum. Therefore, it is necessary to pre-sputter a sample pin for a quite long time. Each aluminum alloy pin was pre-sputtered for about 40-min before a measurement in order to reach stable conditions for all determined elements. This is in contrast to a steel or a brass sample, which was normally pre-sputtered for just 10-min [5]. However, it is possible in a routine analysis to shorten this time significantly by increasing pressure and/or power during pre-burning. Sometimes, however, that procedure will not be successful because an unstable arc may occur in the glow discharge.

3.3 Results and Discussion

3.3.1 Qualitative Spectral Scans

One of the key features of GD-MS is the ease with which the elements in a sample can be determined qualitatively [12, 13]. Mass spectra for one of the low alloy aluminum samples (1SCXG) are shown in Figures 3.4, 3.5 and 3.6. This sample was in the form of a pin. The certified composition values are listed in Table 3.2. Most elements were less than 0.03% by weight except Mg, Si and Fe. The presence of all elemental components could be easily verified using these spectra except for Li and Ca because of their lower concentration and the isobaric overlap with argon background species such as $^{40}\text{Ar}^{6+}$ at m/z 6.67 and $^{40}\text{Ar}^+$ at m/z 40. A small peak for Na could still be observed at m/z 23 although the composition of Na is at a very low level (0.0026%). Some elements such as

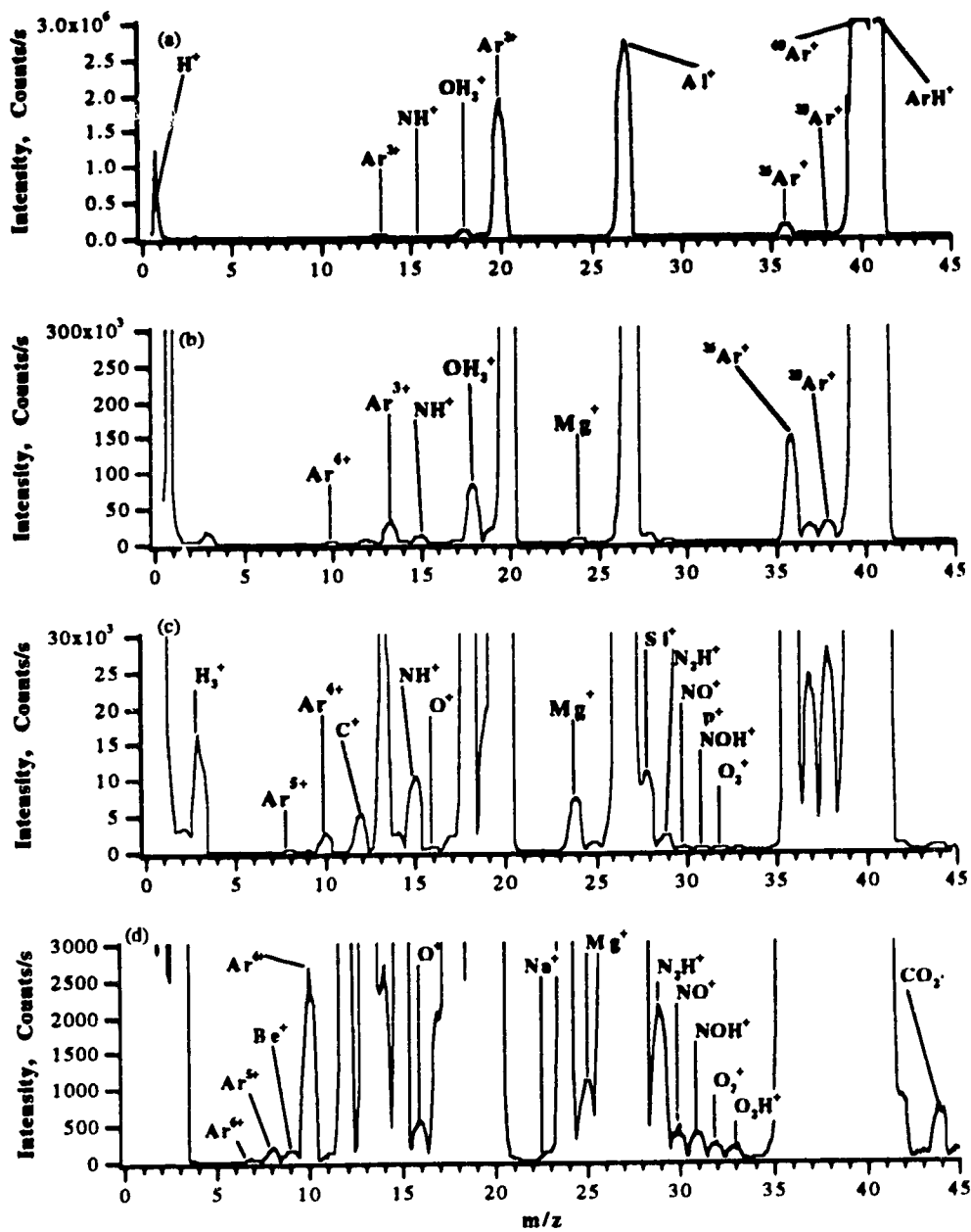


Figure 3.4 GD mass spectra of a low alloy aluminum sample from Alcan (1SCXG) in the 1 to 45 m/z range

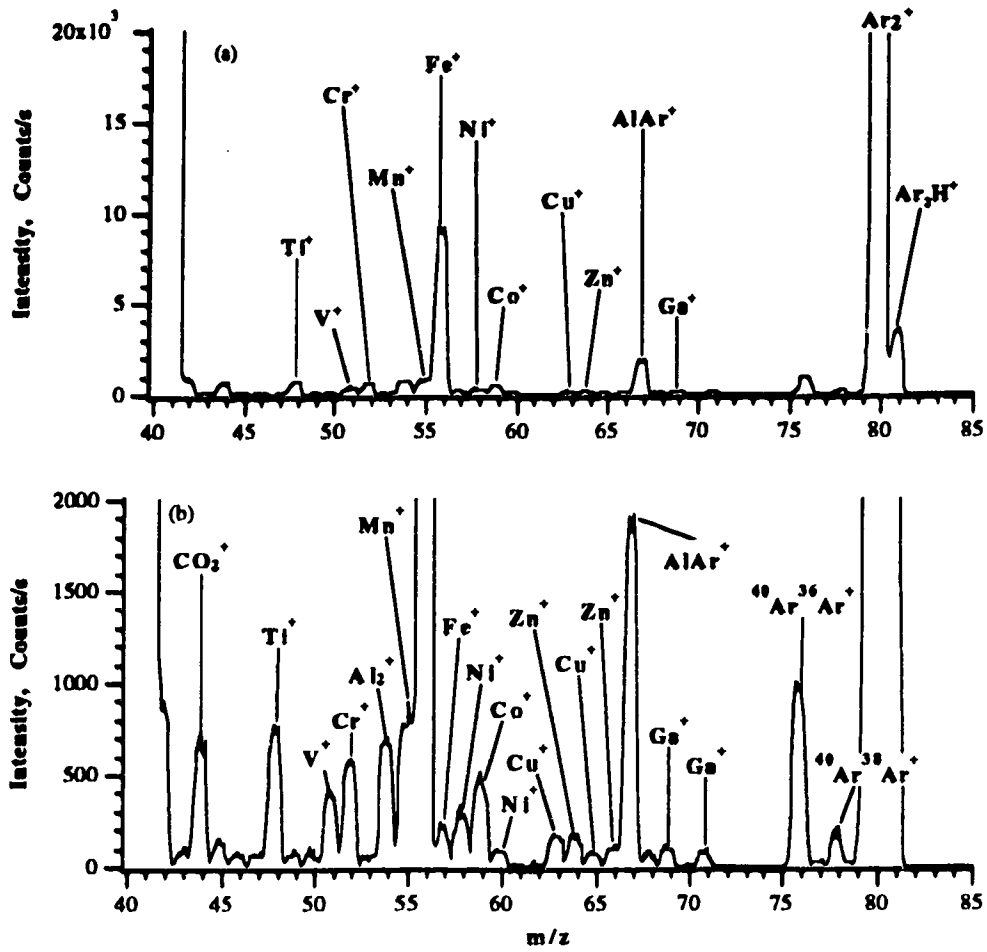


Figure 3.5

GD mass spectra of a low alloy aluminum sample from Alcan (1SCXG) in the 40 to 85 m/z range

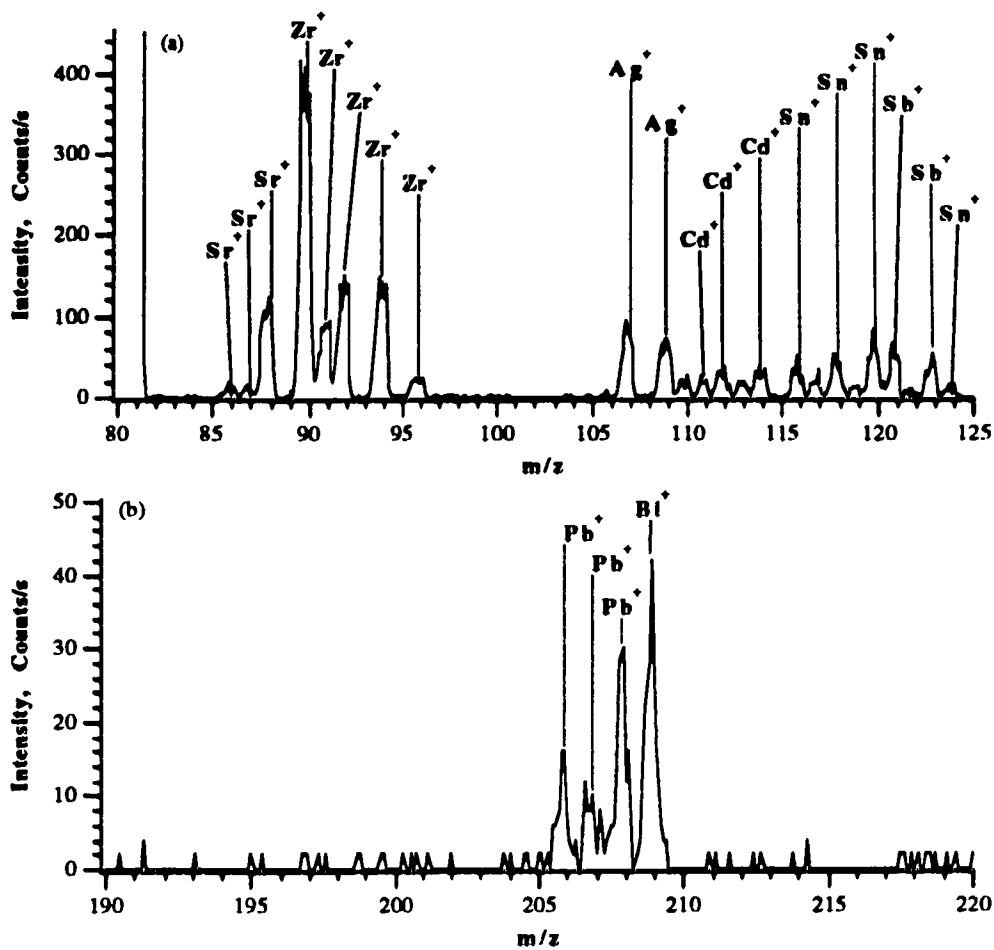


Figure 3.6 GD mass spectra of a low alloy aluminum sample from Alcan (1SCXG) in the (a) 80 to 125 and (b) 190 to 220 m/z range

Sr, Ag and Sb were found in this measurement, which were not tabulated by Alcan.

Table 3.2 **Composition of Alcan 1SCXG low alloy aluminum**

Element	Composition (%by weight)	Element	Composition (%by weight)
Be	0.007	Bi	0.022
Ca	0.0058	Cd	0.018
Co	0.02	Cr	0.018
Cu	0.022	Fe	0.33
Ga	0.015	Li	0.0021
Mg	0.25	Mn	0.026
Na	0.0026	Ni	0.023
Pb	0.019	Si	0.2
Sn	0.024	Ti	0.02
V	0.008	Zn	0.027
Zr	0.034		

3.3.2 Evaluation of Background Spectral Interferences

A problem that glow discharge mass spectrometry shares with its optical counterparts is the presence of spectral interferences. These species arise from polyatomic (or molecular) ions of the same nominal mass as the atomic ions of interest [14]. The basic background species in GD-MS come mainly from argon.

These argon-based background species in GD-MS seem more complicated than those in ICP-MS. The major species not only include the normal species such as $^{40}\text{Ar}^+$, $^{40}\text{ArH}^+$, $^{40}\text{ArN}^+$, $^{40}\text{ArO}^+$ and $^{40}\text{ArOH}^+$ which appear in ICP-MS but also include the dimers of argon ($^{40}\text{Ar}_2^+$, $^{40}\text{Ar}^{36}\text{Ar}^+$ and $^{40}\text{Ar}^{38}\text{Ar}^+$) which are less obvious and severe in ICP-MS. In addition to the dimers, the multiply ionized species of argon such as Ar^{2+} , Ar^{3+} , Ar^{4+} and even Ar^{5+} and Ar^{6+} can be observed in GD-MS, while they are absent in ICP-MS. The presence of some of these argon-based background species create some spectral overlap problems which include $^7\text{Li}^+$ (Ar^{6+}), $^{40}\text{Ca}^+$ (Ar^+), $^{54}\text{Fe}^+$ (ArN^+), $^{56}\text{Fe}^+$ (ArO^+), $^{57}\text{Fe}^+$ (ArOH^+), $^{76}\text{Se}^+$, $^{76}\text{Ge}^+$ ($^{40}\text{Ar}^{36}\text{Ar}^+$), $^{78}\text{Se}^+$ ($^{40}\text{Ar}^{38}\text{Ar}^+$), and $^{80}\text{Se}^+$ ($^{40}\text{Ar}_2^+$).

Other background species originating from water and air seem less important in GD-MS compared to ICP-MS. The signal levels of O^+ , O_2^+ , N^+ , N_2^+ , NO^+ and NOH^+ are much lower in GD-MS than those in ICP-MS so that it is not a serious problem to identify $^{28}\text{Si}^+$ and $^{31}\text{P}^+$ by GD-MS. However, it is difficult to always insure that water and air are completely removed from the system and gas supply. Background species such as O^+ , OH^+ , OH_2^+ and OH_3^+ still can be observed in GD-MS with OH_2^+ being the most intense, although its signal level is much weaker than that in ICP-MS.

Since GD is a direct solid sampling technique, there is no need to dissolve a sample. Therefore, the background species arising from nitric, sulfuric or hydrochloric acids that may be used to dissolve samples for ICP-MS can be avoided. This makes it possible, for example, to identify V, Cr and As by using GD-MS which are free from the interference of chlorine-based species such as $^{35}\text{ClO}^+$, $^{35}\text{ClOH}^+$, $^{37}\text{ClO}^+$ and $^{35}\text{Cl}^{40}\text{Ar}^+$ which occur when HCl is used as a

dissolution acid which is common for aluminum samples. These interferences are considered serious problems in ICP-MS.

There is little interference problem from the Al matrix. Al is a monoisotopic element and mono-oxide and mono-hydroxide species (MO^+ and MOH^+) of metals are normally very weak components in GD-MS compared to their intensity in ICP-MS. The small peak at m/z 43 is likely from $^{27}\text{AlO}^+$, although it could also be an isotope of Ca ($^{43}\text{Ca}^+$). In low alloy aluminum samples, other mono-oxide species from constituents in the alloy cannot be seen as they are usually at low levels [5].

In this experiment, the presence of argides and dimers of aluminum were not a serious problem from the point of view of spectral interference. The dimer of aluminum, $^{27}\text{Al}_2^+$, could interfere with $^{54}\text{Fe}^+$ and the argide of aluminum, $^{27}\text{Al}^{40}\text{Ar}^+$, could interfere with $^{67}\text{Zn}^+$. The level of this argide ($^{27}\text{Al}^{40}\text{Ar}^+ / ^{27}\text{Al}^+$) was about 0.06%. No other dimers or argides were found in the spectra of the low alloy aluminum samples. Argides of minor components in aluminum alloys were only observed in GD-MS for high alloy aluminum samples. A section of a mass spectrum for one of the high alloy samples (SS-319E) is shown in Figure 3.7. Several metal argides such as MnAr^+ , FeAr^+ , NiAr^+ , CuAr^+ and ZnAr^+ were observed in the 80 to 125 m/z region. The level of these argides ($\text{MAr}^+ / \text{M}^+$) was normally less than 1% although the signals for both isotopes of CuAr^+ (m/z 103 and 105) were higher since the composition of copper in this alloy was relatively high (3.83%).

Multiply ionized aluminum species were observed in this experiment but were not easy to verify. The presence of Al^{2+} at m/z 13.5 could be considered,

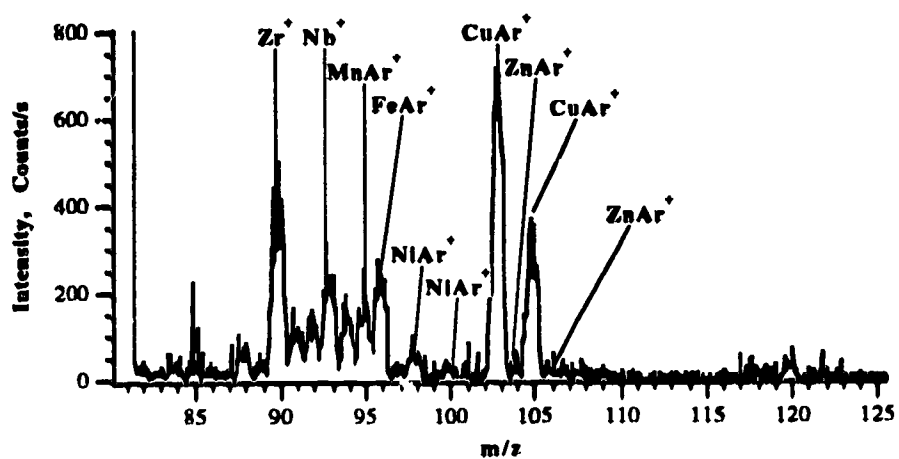


Figure 3.7 Glow discharge mass spectrum of a high alloy aluminium sample from Alcoa (SS-319E) from 81 to 125 m/z range.

but it can be affected by a multiply charged argon species Ar^{3+} located at m/z 13.3. The small peak at m/z 9 is likely from Al^{3+} but it also can result in an isobaric overlap with an isotope of beryllium ($^9\text{Be}^+$). Therefore, there is no clear-cut evidence to confirm the presence of multiply charged aluminum species from the spectra shown in Figure 3.4. However, by checking the GD-MS spectra from other Alcan samples such as 1SXD and 2SDZ, where no peak was found at m/z 9 since they do not contain beryllium. Thus it does seem that these multiply ionized aluminum species may not be for real.

3.3.3 Internal Standardization

In ICP-MS, suppression of analyte signals can be observed because of the presence of a high concentration of a matrix element [15]. GD-MS, however, is supposed to be relatively free of matrix effects [13,14]. In the glow discharge, the sputtering atomization is quite consistent from sample to sample. If the net momentum and lattice disruption forces of an incoming ion are sufficient to normalize widely varying lattice binding energies, then matrix effects would be removed or at least minimized [13]. In this experiment, however, significantly different signal sensitivities for analytes were observed between the spectra of low and high alloy aluminum. Relative signal intensities of analytes for both alloys are shown in Table 3.3. They were obtained by dividing the signal intensity by the concentration of a component (i.e. Intensity/%Concentration). Therefore, the relative intensity can be considered as the intensity when the concentration of an analyte is 1%.

Table 3.3 Comparison of relative signal intensities of analytes (at the 1% level) between high and low alloy aluminum samples

Mass	Analyte	Intensity / % Concentration		Loss in intensity For low alloy Al
		High Alloy (90%Al)	Low Alloy (99%Al)	
24	Mg	210000	120000	43%
48	Ti	280000	150000	46%
55	Mn	290000	150000	48%
58	Ni	140000	70000	50%
63	Cu	110000	60000	45%
64	Zn	126000	64000	49%
67	AlAr	8000*	4000	50%

*Intensity of AlAr for the high alloy is corrected by $7200/0.90=8000$.

From Table 3.3, we can notice that the relative intensities of analytes are much higher for a high alloy aluminum than those for a low alloy aluminum. The loss in signal intensity is about 50% for most of the elements. This might not be a matrix effect arising in the discharge. A reasonable explanation is that there could be different sputtering rates between the low and high alloy aluminum samples. As we know, the sample is first atomized into the discharge by a process called sputtering, and then these sputtered atoms are ionized in the negative glow by electron impact or Penning processes, where Penning ionization has been identified as the dominant ionization process in glow discharge configurations [12]. As the nature of the target material (lattice or crystal structure, binding energy of surface atoms, etc.) strongly influences the

sputtering yield, where sputtering rate is proportional to the sputtering yield [12], the preferential sputtering, i.e., the effect of individual sputtering rates of a multi-element system on the composition of the surface and on the overall sputtering rate, then comes into play in mixed metal samples or alloys. In effect, the surface is enriched with elements possessing low sputter yields, whereas the surface coverage of elements with high sputter yields is decreased. In this fashion, the overall sputtering rate is limited by and equal to that of the component having the slowest rate [12]. Aluminum is an element that has a low sputtering yield and the overall sputtering rate is controlled by the sputtering rate of Al so that aluminum is more difficult to sputter than other alloy components in glow discharge. In this experiment, although low aluminum alloys are softer than high alloys, they seem more difficult to sputter in a glow discharge with a low overall sputtering rate. On the other hand, high alloys are less soft. However, they are much easier to sputter with a higher overall sputtering rate, so that higher signal sensitivities can be observed in GD-MS. In addition, we also found different signal intensities for aluminum argide ($^{27}\text{Al}^{40}\text{Ar}^+$) at m/z 67 from the low and high alloy aluminum samples. Low alloy aluminum is almost a pure sample (99% Al). This contrasts with a high alloy aluminum where the composition of aluminum is about 90% or even less. As a result, the formation of aluminum argide from a low alloy aluminum in a glow discharge plasma should be higher than that from a high alloy aluminum. Comparing the intensity of signals from spectra for both low and high aluminum alloys, however, the opposite result is found. The argide signal in the GD mass spectrum is much lower for the low aluminum alloys than that for the high aluminum alloys. This is further evidence that there is a difference in sputtering rates between low and high aluminum alloys in a glow discharge. The sputtering rates were measured by pre-burning both low and high alloys.

Each sample was pre-sputtered twice for a one-hour period for the first time and a two-hour period for the second time. The difference in weight of loss between these two runs was obtained and then the sputtering rate was calculated. In this experiment, the sputtering rate for one of the low alloy aluminum samples (SA-909) was about $40 \pm 3 \mu\text{g}/\text{min}$, while the sputtering rate for one of the high alloys (SS-319E) was about $57 \pm 3 \mu\text{g}/\text{min}$. Therefore, the different sputtering rates result, in part, in the different relative signal intensities between high and low alloy aluminum samples.

It took more than 30-min to pre-burn a sample pin before analysis. The signal profiles as a function of time for both copper and aluminum argide are shown in Figure 3.8. Both signals were quite low during the pre-burning period. After about 15 min, the signal increased rapidly to reach a maximum and then leveled off at a lower level. A plot of the ratio of copper signal to aluminum argide signal with respect to the time is also shown in Figure 3.8(c). The signal ratio fluctuates in the pre-sputtering period, and then, becomes very stable. The plot of the relative standard deviation (%RSD) of the signal ratio ($^{63}\text{Cu}/^{27}\text{Al}^{40}\text{Ar}^+$) versus the time is displayed in Figure 3.9. The relative standard deviation decreases exponentially and reaches about 1-2% after 40-min pre-burning.

The change in signal intensity over a 40-min period was also investigated. Data for this medium-term drift were acquired while sputtering an aluminum pin sample after a 30 min pre-burn. Plots of medium-term drift with and without the use of AlAr^+ as an internal standard are shown in Figure 3.10. The unratiod ion counts show a continuous downward drift with respect to time. However, when AlAr^+ is used as an internal standard, the drift in signal

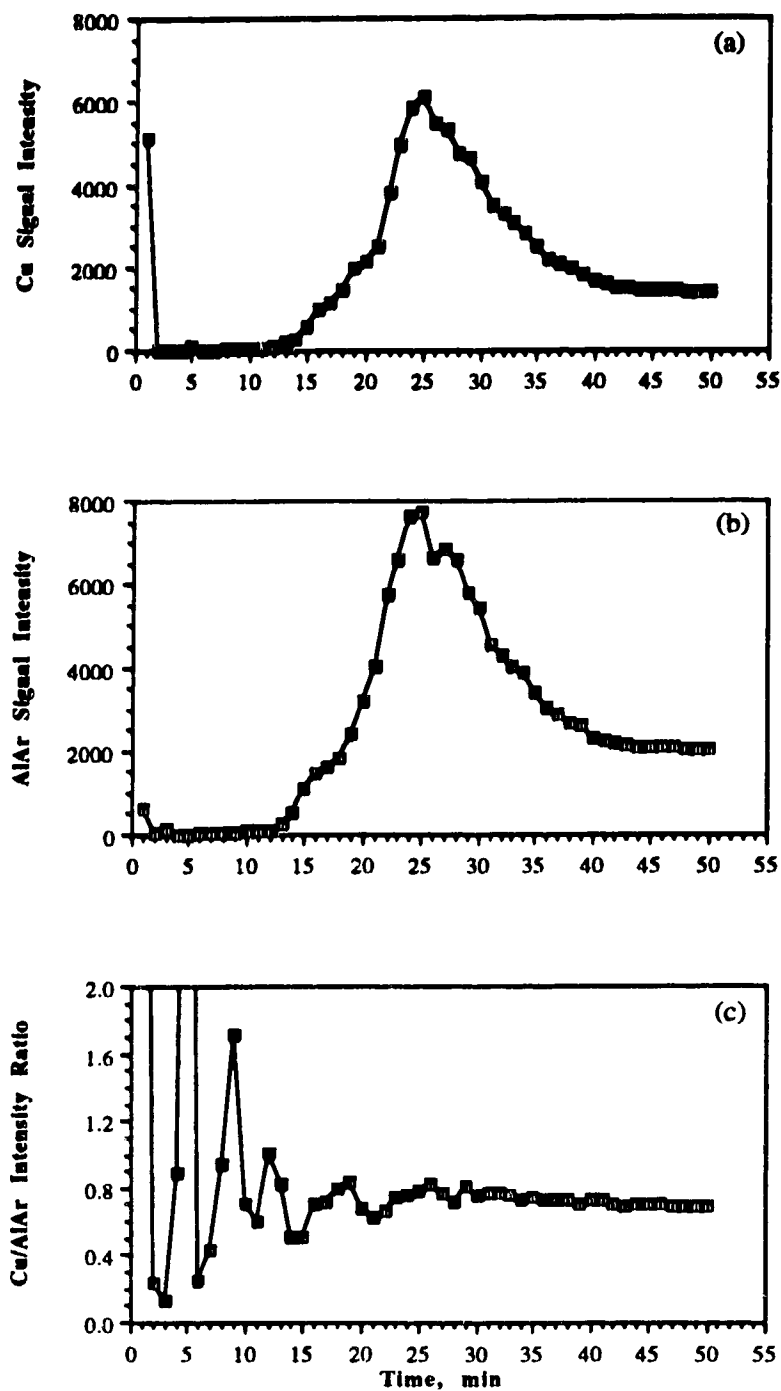


Figure 3.8 Signal intensity changes as a function of time for (a) $^{63}\text{Cu}^+$, (b) $^{27}\text{Al}^{40}\text{Ar}^+$ and (c) the signal intensity ratio of copper to aluminium argide.

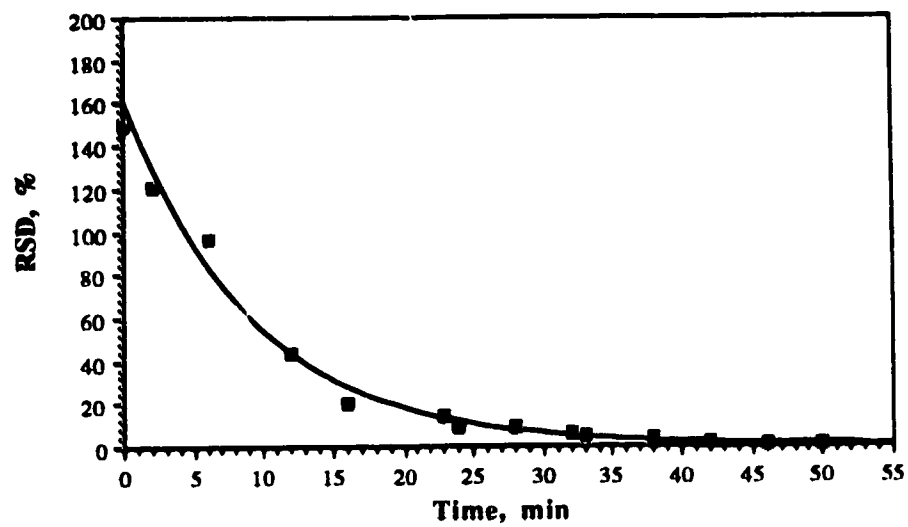


Figure 3.9 Relative standard deviation of the signal intensity ratio ($^{63}\text{Cu}^+ / ^{27}\text{Al}^{40}\text{Ar}^+$) as a function of time.

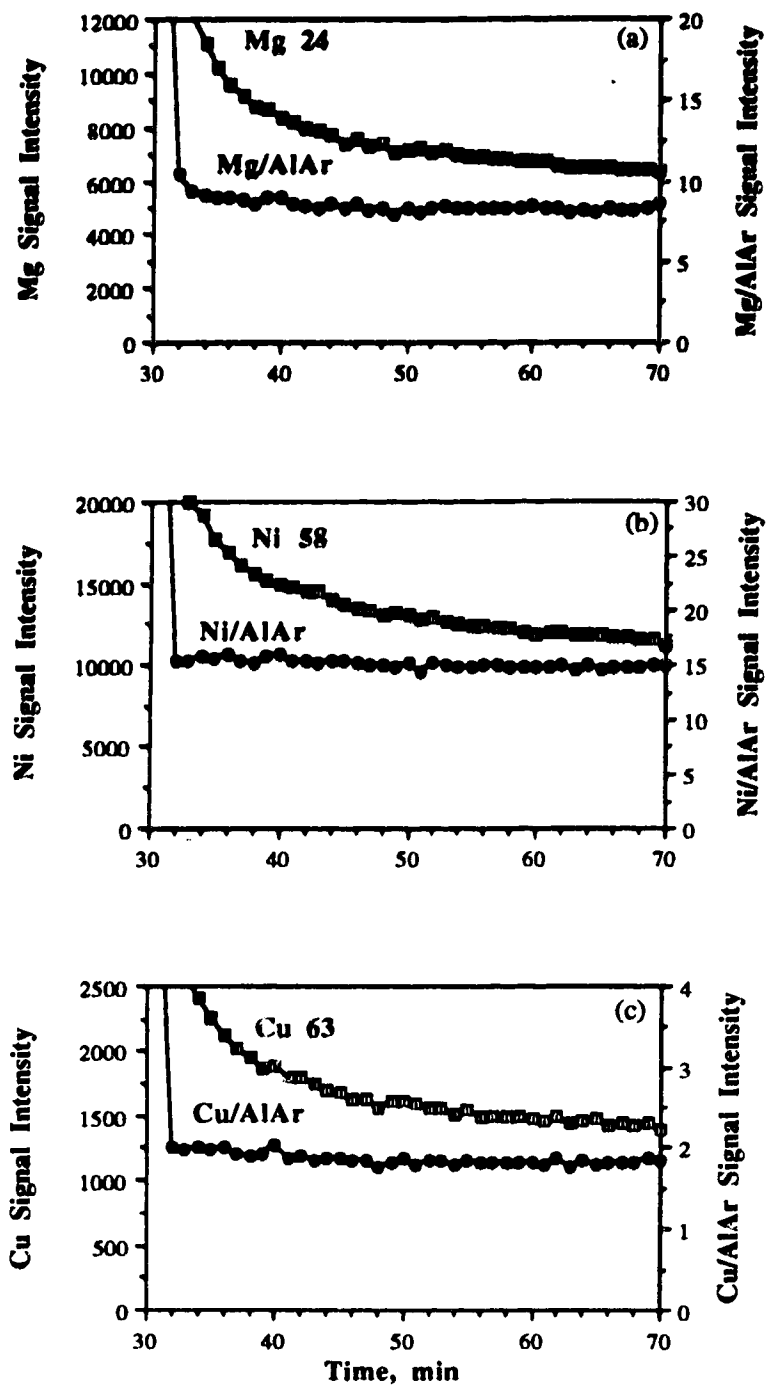


Figure 3.10 Signal intensity changes (in arbitrary units) as a function of time for (a) $^{24}\text{Mg}^+$, (b) $^{58}\text{Ni}^+$ and (c) $^{63}\text{Cu}^+$ for a pin-type aluminum sample with and without the use of $^{27}\text{Al}^{40}\text{Ar}^+$ as an internal standard.

intensity with time is essentially eliminated.

Since it is impossible to add an element as an internal standard for solid samples, usually, a matrix based element such as a minor isotope of a major component, an argide or another molecular matrix based species can be used for this purpose. Aluminum argide (AlAr^+) was the only choice as the internal standard in this experiment for several reasons. First of all, it is a matrix based argide with a signal that seems to correctly mimic analyte signal in different matrices *i.e.* between high and low alloy aluminum samples. Secondly, it is in the mid-mass range (m/z 67), a compromise position for any mass effects. Finally, it not only experiences a similar degree of matrix effect to all other analytes, but also drifts in a same direction as the analytes drift as shown by the data presented in Figures 3.8 and 3.10. Therefore, both the sputtering rate differences and instrument drift problems can be compensated by the use of this internal standard.

3.3.4 Analytical Results

GD-MS can be applied to the quantitative analysis of aluminum alloys. A group of calibration curves was established using the Alcan low alloy aluminum standards 1SCXG, 1SWL, 1SWM, 1SXD and 2SDZ for the determination of Mg, Ti, V, Mn, Ni, Co, Cu, Zn, Ga, Zr, Sn, Pb and Bi. The concentration for these components in the standards was normally in the range of 0.001% to 0.030% except for one of the standards which contained 0.25% magnesium. The slopes of the log-log plots for the calibration curves were in the range of 0.95 to 1.06. Examples of two analytical curves for $^{51}\text{V}^+$ and $^{69}\text{Ga}^+$ with AlAr^+ as the internal standard are shown in Figure 3.11. The slopes of the log-log plots in Figure 3.11

are 1.04 and 1.06, respectively. The detection limits for the determination of these components were evaluated from this group of calibration curves as linear plots. They were evaluated using the standard deviation of background and the sensitivity of analyte signal. The detection limits were all in the range of 10-100 p.p.b. directly in the solid and are summarized in Table 3.4. The low alloy aluminum sample 1SWL was analyzed for all the above components as an "unknown". The results are listed in Table 3.5 and the standard deviations for the results were calculated based on $n=6$.

Another group of calibration curves was established using both low and high alloy aluminum standards from Alcoa for the determination of Mg, Ti, Mn, Ni, Cu and Zn. The seven standards used were SA-909, SA-1170, SA-1169, SS-356-B, SS-A132AA, SS-D132-A and SS-319E. The composition of the components for Alcoa standards was in the range of 0.03% to 1.3% for magnesium, 0.03% to 2.5% for nickel and 0.03 to 3.8% for copper, and the slopes of the log-log plots for the standard curves were usually in the range of 0.85 to 0.95 using aluminum argide as the internal standard. Examples of two calibration curves for $^{24}\text{Mg}^+$ and $^{63}\text{Cu}^+$ with AlAr^+ as the internal standard are presented in Figure 3.12. The slopes of the log-log plots in Figure 3.12 are 0.90 and 0.89, respectively. A high alloy aluminum sample (SS-360-C) was analyzed as an "unknown" sample. The results listed in Table 3.6 agree well with the certified values. The precision data were obtained based on $n=6$.

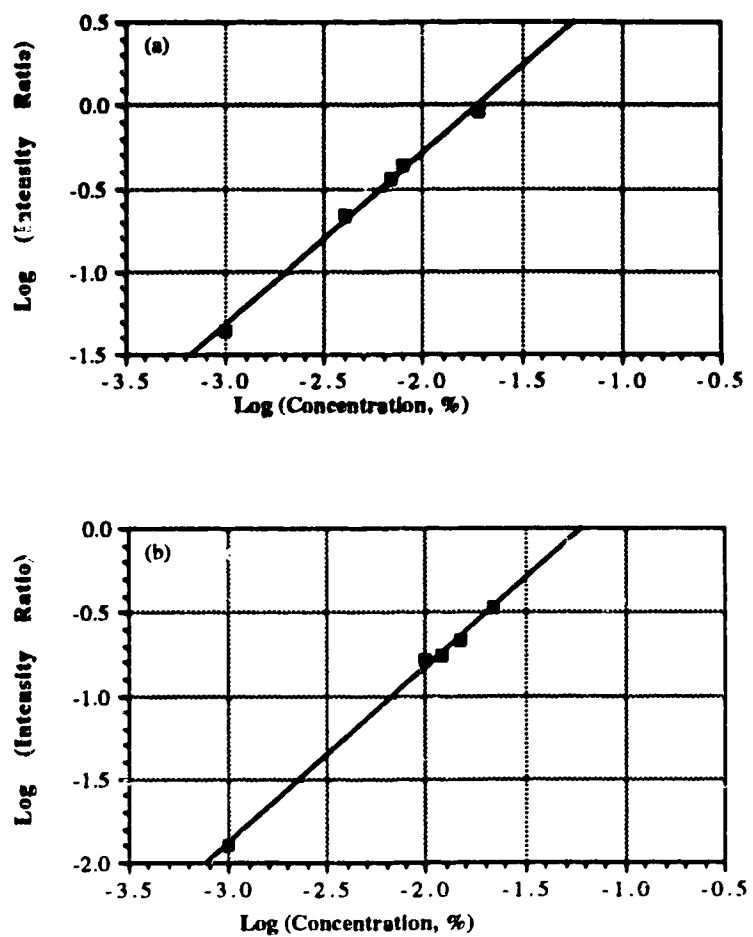


Figure 3.11 Calibration curves for $^{51}\text{V}^+$ (a) and $^{69}\text{Ga}^+$ (b) in Alcan low alloy aluminum standards with AlAr^+ (m/z 67) as the internal standard.

Table 3.4 Detection limits of trace elements directly in Alcan aluminum solids by GD mass spectrometry

Elements	Mass	Detection limits(p.p.b.)
Mg	24	108
Ti	48	42
V	51	31
Mn	55	30
Ni	58	59
Co	59	30
Cu	63	63
Zn	64	58
Ga	69	44
Zr	90	10
Sn	120	41
Pb	208	87
Bi	209	56

Table 3.5 Results for the analysis of 1SWL low alloy aluminum

Element	Certified Value(%)	Result(%±σ)	%rsd
Mg	0.015	0.0145±0.0004	2.5
Ti	0.025	0.0230±0.0002	0.9
V	0.019	0.0160±0.0002	1.2
Mn	0.023	0.0202±0.0004	2.0
Ni	0.022	0.0205±0.0005	2.4
Co	0.001	0.0013±0.0001	5.8
Cu	0.030	0.0278±0.0009	3.2
Zn	0.023	0.0209±0.0006	2.9
Ga	0.012	0.0107±0.0003	2.8
Zr	0.013	0.0129±0.0002	1.6
Sn	0.024	0.0225±0.0006	2.7
Pb	0.018	0.0195±0.0001	0.6
Bi	0.018	0.0193±0.0005	2.4

Table 3.6 Results for the analysis of SS-360-C high alloy aluminum

Element	Certified Value(%)	Result(%±σ)	%rsd
Mg	0.52	0.503±0.018	3.6
Ti	0.079	0.076±0.001	1.3
Mn	0.22	0.224±0.008	3.6
Cu	0.31	0.308±0.009	2.9
Zn	0.25	0.248±0.009	3.6

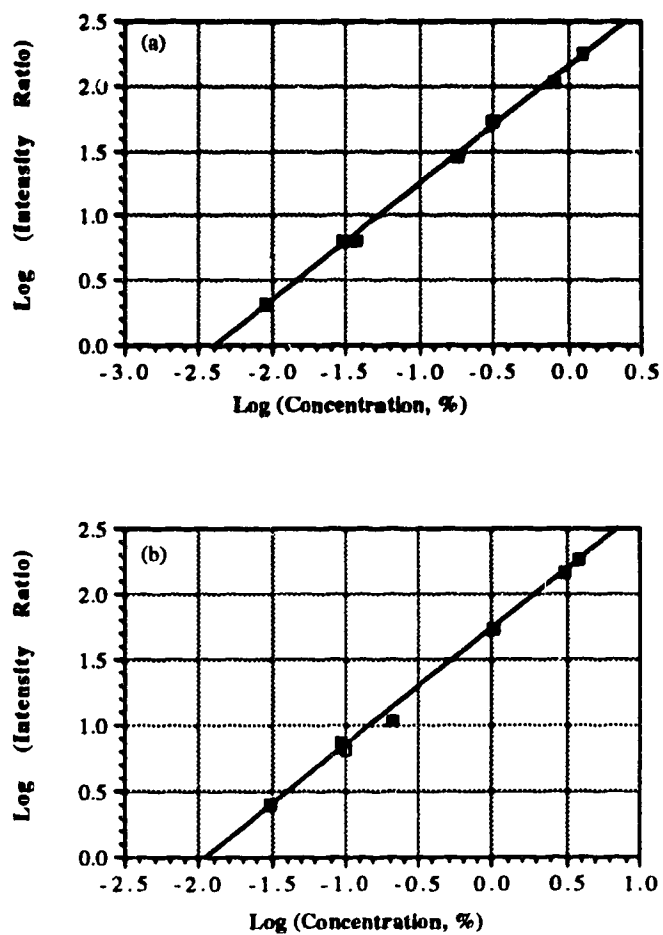


Figure 3.12 Calibration curves for $^{24}\text{Mg}^+$ (a) and $^{63}\text{Cu}^+$ (b) in both high and low alloy aluminum standards with AlAr^+ (m/z 67) as the internal standard.

3.4 Conclusion

One of the most important advantages of glow discharge mass spectrometry is the ability to do direct solids analysis. GD-MS can be used successfully for the analysis of solid alloy aluminum samples both qualitatively and quantitatively. Almost all of the trace elements can be identified directly from the mass spectra. The basic spectral interferences seem less important in GD-MS than those in ICP-MS although the argon based background species in GD-MS are more complicated than those in ICP-MS. Some matrix effect problems exist as different signal sensitivities of analytes between low and high alloy aluminum were observed. It is suggested that there is a difference in sample sputtering rates between these alloys. It has been shown that internal standardization is important, not only to compensate for instrument drift, but also to help compensate for the different sputtering rates. In addition, calibration curves were established using both Alcan and Alcoa aluminum alloy standards. Essentially, all elements can be determined simultaneously and p.p.b. limits of detection can be obtained. With careful consideration of instrument settings, spectral interferences, matrix effects and internal standardization, excellent quantitative results can be obtained for most elements in aluminum alloy samples.

References

1. W. W. Harrison, K. R. Hess, R. K. Marcus and F. L. King, *Anal. Chem.* **58**, 341A (1986).
2. D. C. Duckworth and R. K. Marcus, *Anal. Chem.* **61**, 1879 (1989).
3. J. Clark, G. Ronan and R. C. Hoodless, paper presented at 1989 11th International Symposium on Microchemical Techniques, Wiesbaden FRG. 28th Aug. - 1st Sept. 1989.
4. N. Jakubowski, D. Stuewer and W. Vieth, *Anal. Chem.* **59**, 1825 (1987).
5. Y. Shao and G. Horlick, *Spectrochimica Acta* **46B**, 165 (1991).
6. M. Tanaka, H. Saisho, H. Nobumasa and K. Shimizu, paper presented at 1989 Pittsburgh Conference and Exposition on Analytical Chemistry and Applied Spectroscopy, Atlanta, GA, USA, 6-10 March 1989.
7. R. K. Marcus and D. C. Duckworth, paper presented at 1989 Pittsburgh Conference and Exposition on Analytical Chemistry and Applied Spectroscopy, Atlanta, GA, USA, 6-10 March 1989.
8. W. Vieth and J. C. Huneke, *Spectrochimica Acta* **46B**, 137 (1991).
9. L. F. Vassamillet, *J. Anal. At. Spectrom.* **4**, 451 (1989).
10. H. M. Shihomatsu and S. S. Iyer, *Nucl. Instrum. Methods Phys. Res. Sect. A*, **280**, 488 (1988).
11. J. E. Hatch, *Aluminum: Properties and Physical Metallurgy*, American Society for metals, p. 242 (1984).
12. W. W. Harrison and B. L. Bentz, *Prog. Anal. At. Spectrosc.* **11**, 53 (1988).
13. W. W. Harrison, *J. Anal. At. Spectrom.* **3**, 867 (1988).
14. F. L. King, A. L. McCormack and W. W. Harrison, *J. Anal. At. Spectrom.* **3**, 883 (1988).

15. S. H. Tan and G. Horlick, *J. Anal. At. Spectrom.* **2**, 745 (1987).
16. N. Furuta, *Spectrochimica Acta* **41B**, 1115 (1986).

Chapter 4

Analysis of Low Alloy Aluminum Samples Using Inductively Coupled Plasma Mass Spectrometry

4.1 Introduction

Inductively coupled plasma mass spectrometry (ICP-MS) has been used for the determination of trace and/or ultra trace amounts of elements in different kinds of samples that include geochemical samples [1-4], body tissues and fluids [5-8], environmental [9-12] and biological materials [13-20] (including water [17, 19] and food samples [16, 20]) as well as industrial materials [21-28]. In fact the industrial applications of ICP-MS have increased significantly in recent years. For instance, the applicability of ICP-MS to the analysis of SRM steel samples has been investigated [27] and ultra trace amounts of uranium and thorium in high purity aluminum were determined by using ICP-MS [28].

The quantitatively analytical methodology developed for ICP-MS normally includes the use of internal standardization [13, 27] and matrix matching methods. In this report, these areas are addressed with respect to the analysis of low alloy aluminum samples. This solution-based analysis will also provide a contrast to the direct solid technique of GD-MS just presented in the last chapter. Direct comparison of these two techniques will be presented in the following chapter.

4.2 Experimental

All analyses were performed using a SCIEX (Perkin Elmer-Sciex) Elan Model 250 ICP mass spectrometer. A standard MAK optical emission ICP torch was used in connection with a Meinhard nebulizer and a Scott-type spray chamber. Compromise conditions for power and nebulizer flow-rate can be easily obtained for a range of elements. The flow rate yielding the maximum ion count for a given power and sampling depth is essentially the same for most elements. For this work, a sampling depth of 15 mm from the load coil was chosen with a plasma forward power of 1.3 kW. Two nebulizer flow-rates were utilized (1.10 and 0.90 L/min), since matrix effects could be decreased at the lower nebulizer flow-rate setting. Some sacrifice in optimum signal intensity had to be accepted in order to decrease the matrix effect caused by aluminum. The ion focusing lens voltages were a compromise chosen to cover a large mass range. The ion lens voltages used are listed in Table 4.1.

Table 4.1 Ion lens voltage settings.

<u>Lens</u>	<u>Setting</u>	<u>Voltage (V)</u>
Bessel Box Barrel(B)	55	6
Bessel Box Plates(P)	49	-32
Einzel Lens(E1)	95	-22
Photon Stop(S2)	34	-7

Five standard aluminum samples from the Aluminum Corporation of Canada (Alcan) and three standard aluminum samples from the Aluminum Corporation of America (Alcoa) were chosen for this work. The samples SRM 1SCXG, 1SWL, 1SWM, 1SXD and 2SDZ were from Alcan and SRM SA-909, SA-1170 and SA-1169 were from Alcoa.

All low alloy aluminum samples were simply dissolved in 6 mol/L hydrochloric acid as described by Ward and Marciello [29]. A sample of 100 mg was transferred into a 250-mL glass beaker. Ten milliliters of 6 mol/L hydrochloric acid was added and the solution was heated until the reaction subsided (about 5-10 min). In this experiment no black specks of silicon could be seen in the solution after dissolution because the samples were low alloys with more than 99% aluminum and less than 0.25% silicon. The solution then was cooled and diluted to 100 ml (0.1% Al solution) with de-ionized water. The 0.01% Al sample was prepared by taking 10.0 ml of 0.1% Al solution and diluting it to 100 ml. The hydrochloric acid used to dissolve the aluminum samples was of analytical-reagent grade and all standards were prepared from ICP grade standard solutions obtained from Leco Corporation.

4.3 Results and Discussion

4.3.1 Qualitative Spectral Scans

Qualitative analysis is one of the primary features of ICP-MS and the elements in a sample can be easily identified. The ICP mass spectrum compared to the atomic emission spectrum for these aluminum samples is quite simple. The complexity of the atomic emission spectra of aluminum samples is well

known [29], but the mass spectra clearly illustrate the ease with which the elemental composition of such samples can be determined. ICP mass spectra for one of the Alcan aluminum samples (SRM 1SCXG) are shown in Figures 4.1, 4.2 and 4.3. All the spectra shown in these figures were obtained using a solution that had a total aluminum composition of 0.01%. The certified composition of this sample and the concentration of the elements in this 0.01% Al solution are listed in Table 4.2. Most of the elements such as Li, Be, Na, Mg, Ti, Mn, Ni, Co, Cu, Zn, Ga, Zr, Cd, Sn, Pb and Bi could be readily identified using these mass spectra. Both Li and Na were in the lowest concentration in this aluminum sample solution (0.0021 and 0.0026 $\mu\text{g}/\text{mL}$), however, the peak at m/z 23 was much higher than that at m/z 7. Na seemed likely an impurity from HCl, while Li might be real. In contrast, GD mass spectra showed very weak peaks at m/z 7 and 23 (see chapter 3) although there was a small interference of Ar^{6+} located at m/z 6.67. Some elements such as Sr, Ag and Sb were identified, but are not certified or mentioned in the Alcan data provided for this standard.

The mass spectra shown in Figures 4.1-4.3 also illustrate some of the potential problems that arise when using ICP-MS for the analysis of aluminum samples. In general, spectral interference problems can arise from background, solvent, oxide and hydroxide species as shown in Figure 4.2 and 4.3(a). These problems and additional spectral interference problems will be discussed in the next section.

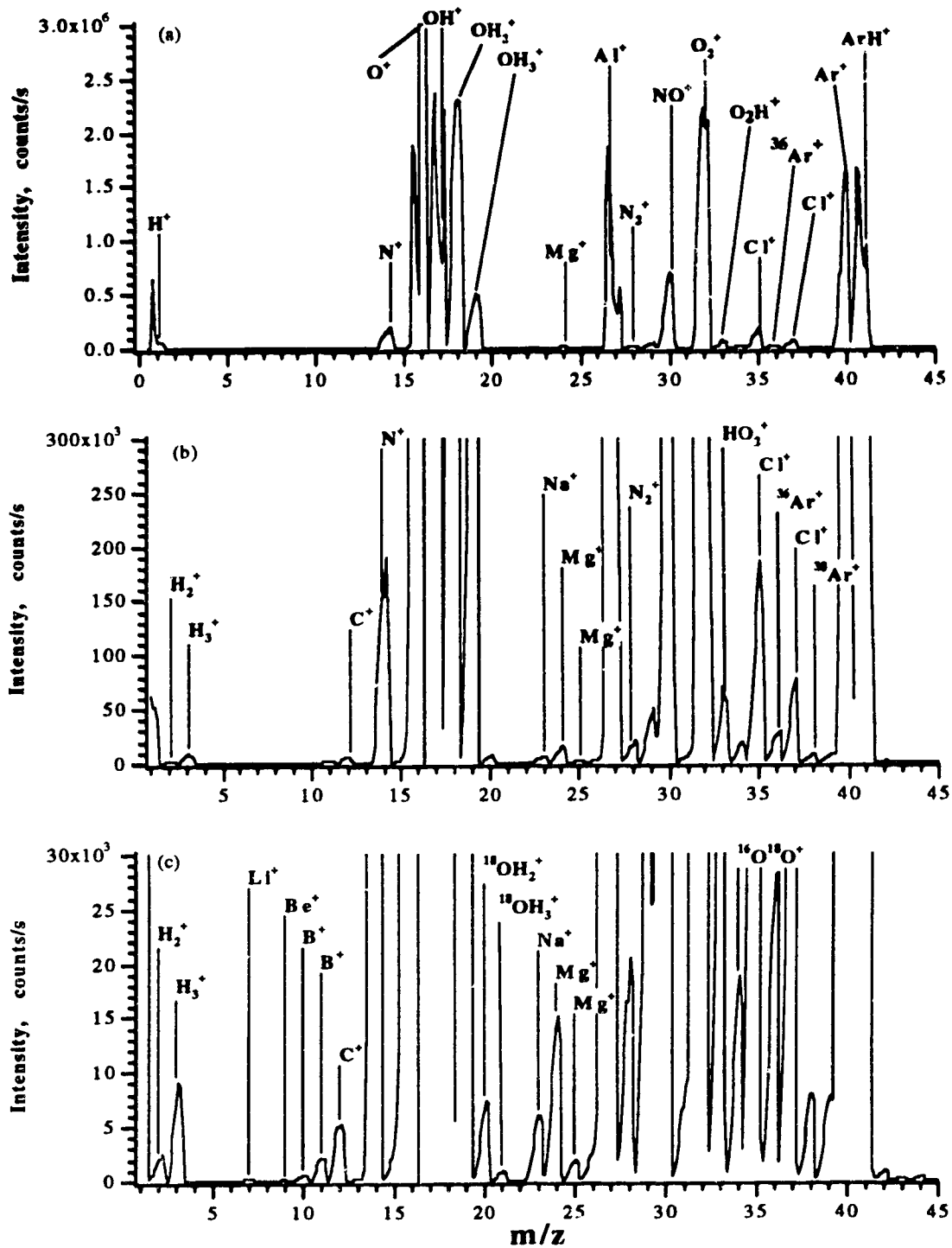


Figure 4.1

Spectra of the 0.01% aluminum alloy solution (Alcan 1SCXG) for the mass range 1 to 45 m/z .

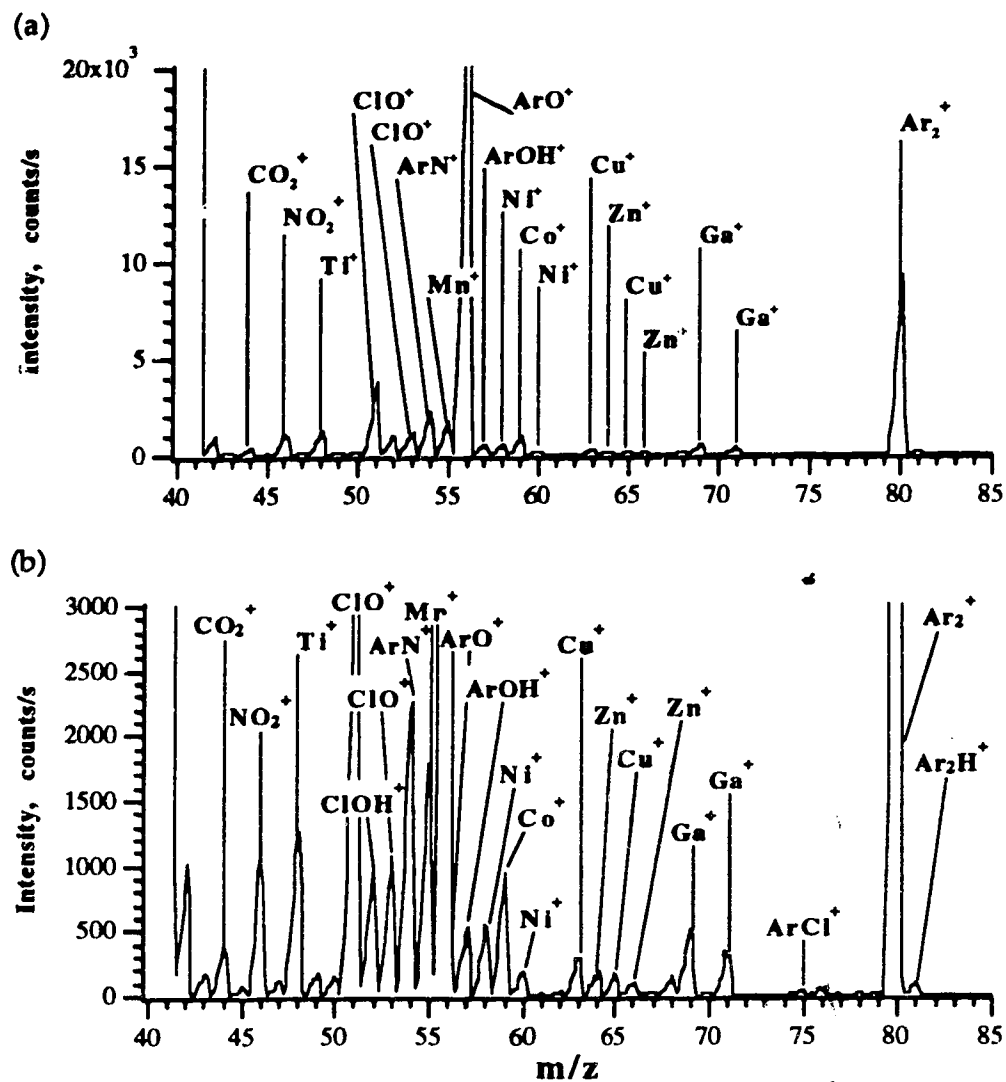


Figure 4.2 Spectra of the 0.01% aluminum alloy solution (Alcan 1SCXG) for the mass range 40 to 85 m/z .

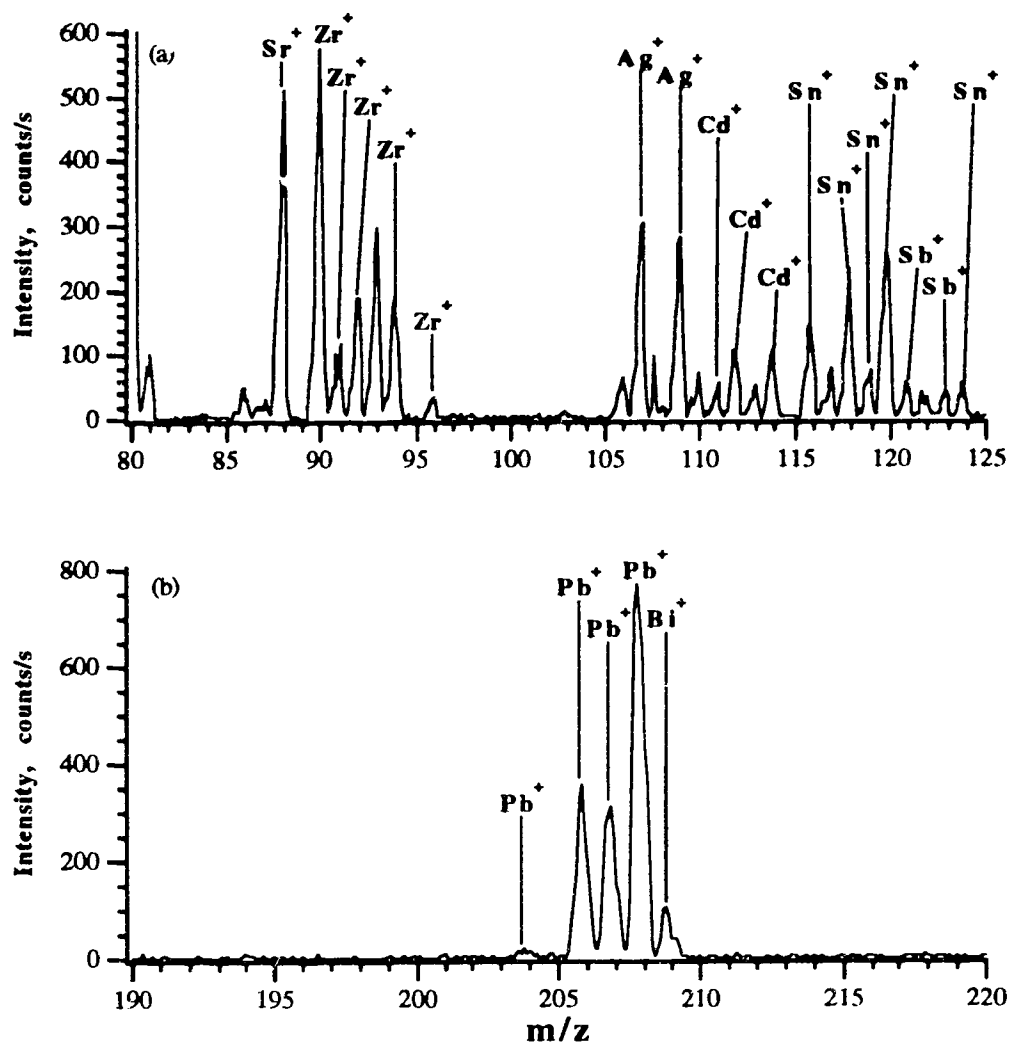


Figure 4.3 Spectra of the 0.01% aluminum alloy solution (Alcan 1SCXG) for the mass range (a) 80 to 125 and (b) 190 to 220 m/z .

Table 4.2 Composition of Alcan 1SCXG low alloy aluminum standard and concentration of elements in a 0.01% Al solution

Element	Composition (%by weight)	Concentration $\mu\text{g/mL}$	Element	Composition (%by weight)	Concentration $\mu\text{g/mL}$
Be	0.007	0.007	Bi	0.022	0.022
Ca	0.0058	0.0058	Cd	0.018	0.018
Co	0.02	0.02	Cr	0.018	0.018
Cu	0.022	0.022	Fe	0.33	0.33
Ga	0.015	0.015	Li	0.0021	0.0021
Mg	0.25	0.25	Mn	0.026	0.026
Na	0.0026	0.0026	Ni	0.023	0.023
Pb	0.019	0.019	Si	0.2	0.2
Sn	0.024	0.024	Ti	0.02	0.02
V	0.008	0.008	Zn	0.027	0.027
Zr	0.034	0.034			

4.3.2 Evaluation of Potential Spectral Interferences

The basic isobaric and background spectral interferences in ICP-MS have been well documented [30, 31]. Some of the major problem species are summarized in Table 4.3 for the more common elements that are determined in aluminum alloys. Only the major background species are listed for water, diluted nitric acid, sulfuric acid and hydrochloric acid solutions, and the tables of Tan and Horlick [31] should be consulted for more details.

Table 4.3 Basic spectral interferences for elements of major interest in aluminum alloys (natural abundances in parentheses)

Element	Isobaric Overlap	Background Species		
		H ₂ O, HNO ₃	H ₂ SO ₄	HCl
7Li(92.5)				
9Be(100)				
23Na(100)				
24Mg(78.8)				
25Mg(10.15)				
27Al(100)				
28Si(92.21)		14N ₂ , 12C ¹⁶ O		
31P(100)		14N ¹⁶ OH		
32S(95.02)		16O ₂	32S	
40Ca(96.94)	40Ar(99.60)			
46Ti(8.01)	46Ca(0.004)	14N ¹⁶ O ₂		
48Ti(73.98)	48Ca(0.19)		34S ^N , 32S ^O	
51V(99.76)				35Cl ^O , 37Cl ^N
52Cr(83.76)		40Ar ¹² C, 36Ar ¹⁶ O	36S ¹⁶ O	35Cl ¹⁶ OH
53Cr(9.51)				37Cl ¹⁶ O
54Fe(5.82)	54Cr(2.38)	40Ar ¹⁴ N		37Cl ¹⁶ OH
55Mn(100)		40Ar ¹⁴ NH		
56Fe(91.66)		40Ar ¹⁶ O		
57Fe(2.19)		40Ar ¹⁶ OH		
58Ni(67.77)	58Fe(0.33)			
59Co(100)				
60Ni(26.16)				
62Ni(3.66)				
63Cu(69.1)				
64Zn(48.89)	64Ni(1.16)		32S ^O ₂ , 32S ₂	
65Cu(30.9)			33S ^O ₂ , 32S ³³ S	
66Zn(27.81)				
69Ga(60.16)				37Cl ¹⁶ O ₂
71Ga(39.84)				36Ar ³⁵ Cl
88Sr(82.58)				
90Zr(51.45)				
120Sn(32.59)	120Te(0.1)			
208Pb(52.35)				
209Bi(100)				

Unfortunately, some of the key elements of interest in aluminum metallurgy (such as Si and P) cannot be easily identified because of spectral overlaps with species present in the ICP discharge. These molecular background ions include $^{14}\text{N}_2^+$ and $^{14}\text{N}^{16}\text{OH}^+$ which affect the major isotopes of Si and P. Iron and calcium are also problem elements. With iron its major isotope ($^{56}\text{Fe}^+$) is affected by ArO^+ , and its next two most abundant isotopes, $^{54}\text{Fe}^+$ and $^{57}\text{Fe}^+$, are affected by ArN^+ and ArOH^+ , respectively. Finally, the least abundant isotope, $^{58}\text{Fe}^+$, has an isobaric overlap with the major isotope of nickel. The most serious problem concerns calcium, where all of its six isotopes are affected. The major isotope ($^{40}\text{Ca}^+$) is affected by $^{40}\text{Ar}^+$ and its third most abundant isotope ($^{42}\text{Ca}^+$) is affected by ArH_2^+ , both isotopes of $^{46}\text{Ca}^+$ (0.004) and $^{48}\text{Ca}^+$ (0.187) suffer from the interference of NO_2^+ and isobaric overlap from $^{46}\text{Ti}^+$ and $^{48}\text{Ti}^+$. Even the next least abundant isotope $^{43}\text{Ca}^+$ (0.14) and the next most abundant isotope $^{44}\text{Ca}^+$ (2.09) are affected by aluminum oxide ($^{27}\text{AlO}^+$) and aluminum hydroxide ($^{27}\text{AlOH}^+$), as well as by the background species CO_2^+ .

Molecular background species can also be formed from the components of the over-all sample solution matrix. Sulphur- and chlorine-containing components can be particularly troublesome. For example, the use of HCl presents some major potential problems. Two key elements that can be affected are vanadium and chromium. A chlorine-containing matrix results in the formation of $^{35}\text{ClO}^+$, $^{35}\text{ClOH}^+$ and $^{37}\text{ClO}^+$, which interfere with both $^{51}\text{V}^+$ and $^{52}\text{Cr}^+$ as well as $^{53}\text{Cr}^+$. These are serious problems (see Figure 4.2) because $^{50}\text{V}^+$ is the only other naturally occurring isotope of V and it has a natural abundance of only 0.25%. $^{50}\text{Cr}^+$ is the only remaining isotope of Cr with a natural abundance of 4.34%, whereas both $^{50}\text{V}^+$ and $^{50}\text{Cr}^+$ suffer from isobaric overlaps from $^{50}\text{Ti}^+$, $^{36}\text{ArN}^+$, $^{35}\text{Cl}^{15}\text{N}^+$ and $^{34}\text{S}^{16}\text{O}^+$ background species.

In addition to N, C, Ar, Cl and Al, other sample components may also cause MO and MOH spectral interference problems. For example, it can be seen from Figure 4.4(a), that some masses of cadmium suffer spectral overlap from ZrO^+ species. $^{93}NbO^+$ can also interfere with one of the silver isotopes ($^{109}Ag^+$). In order to show these interferences clearly, the mass spectrum of another aluminum standard (Alcan 15WM) which does not contain silver is shown in Figure 4.4(a). These problems are illustrated in detail by the bar graph simulated spectrum shown in Figure 4.4(b), which shows that the group of peaks of ZrO^+ well agrees with the isotopic pattern observed. The level of these oxides was pretty high, the ratios of $^{90}Zr^{16}O^+ / ^{90}Zr^+$ and $^{93}Nb^{16}O^+ / ^{93}Nb^+$ were about 9.6% and 7.5%, respectively, because both zirconium and niobium oxides are refractory and both have a high M-O bond dissociation energy. The signal intensity of metal oxides in ICP-MS is usually proportional to the metal oxide bond strength. The elements with higher M-O bond strength such as rare earth elements more readily form metal oxides. For the analysis of aluminum samples which contain refractory elements such as Ti, Zr, Nb and/or rare earth elements, metal mono-oxide ions may present in the mass spectra.

Fortunately, the number of oxide and hydroxide species of aluminum are minimal since aluminum is a monoisotopic element and most of the elements in aluminum are low M-O bond strength elements except for Ti, Zr and Nb. In this experiment, although $^{48}TiO^+$, $^{48}TiOH^+$ and $^{55}MnO^+$ would affect ^{64}Zn , ^{65}Cu and ^{71}Ga respectively. But no other severe MO^+ and MOH^+ spectral interference problems could be observed from the mass spectra for low alloy aluminum samples. Since the range of reported oxide levels was about 0.1-2.5% for the low M-O bond energy elements [32-35], whereas the concentrations of trace elements

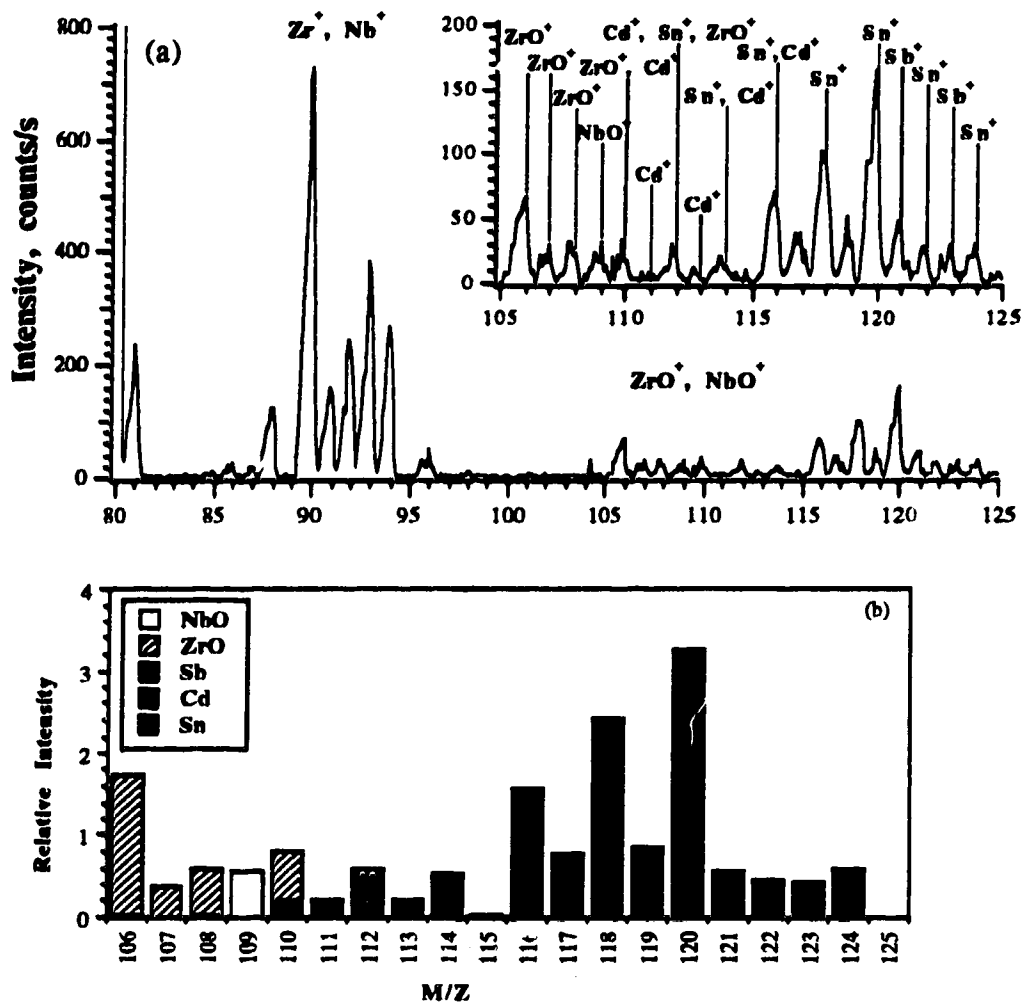


Figure 4.4 ICP mass spectra of an aluminium alloy sample (Alcan 1SWM) illustrating the overlap of elemental isotopes and metal mono-oxides. (a) actual spectra and (b) simulated spectrum.

in 0.01% aluminum solutions were less than 0.03 $\mu\text{g}/\text{ml}$, the signal levels of the oxide species in these sample solutions could be much less than 50 counts/sec. Therefore, the oxide and hydroxide spectral interferences are not very important for analysis of low alloy aluminum samples.

4.3.3 Matrix effect and internal standardization

In ICP-MS, a high concentration of a matrix element is known to affect analyte sensitivity and suppressions of analyte signals have been observed [36-39]. Thus, for the analysis of aluminum, the effect of high Al concentrations on analyte sensitivity should be evaluated. A set of graphs demonstrating the effect of 1000 $\mu\text{g}/\text{ml}$ of Al on Ti, Ni and Cu signals is shown in Figure 4.5. Signal intensities are plotted as a function of nebulizer flow-rate with the solid line corresponding to the analyte solution (0.1 $\mu\text{g}/\text{ml}$) containing no aluminum, and the broken line corresponding to a solution containing 1000 $\mu\text{g}/\text{ml}$ of aluminum and 0.1 $\mu\text{g}/\text{ml}$ of analyte. As shown by Tan and Horlick [36], a severe suppression occurs at the nebulizer flow-rate corresponding to the maximum analyte signal intensity. Previous results have indicated that heavy matrix elements cause the most severe matrix effect and light analytes are more seriously affected than heavier analytes [36]. As well, elements with low ionization potentials cause more serious matrix effects. Al is a relatively light matrix ion, but it has a low ionization potential (5.968 eV) and a high degree (98.92%) of ionization in the ICP [40]. Therefore, over-all, the suppression of signals is severe in an aluminum matrix.

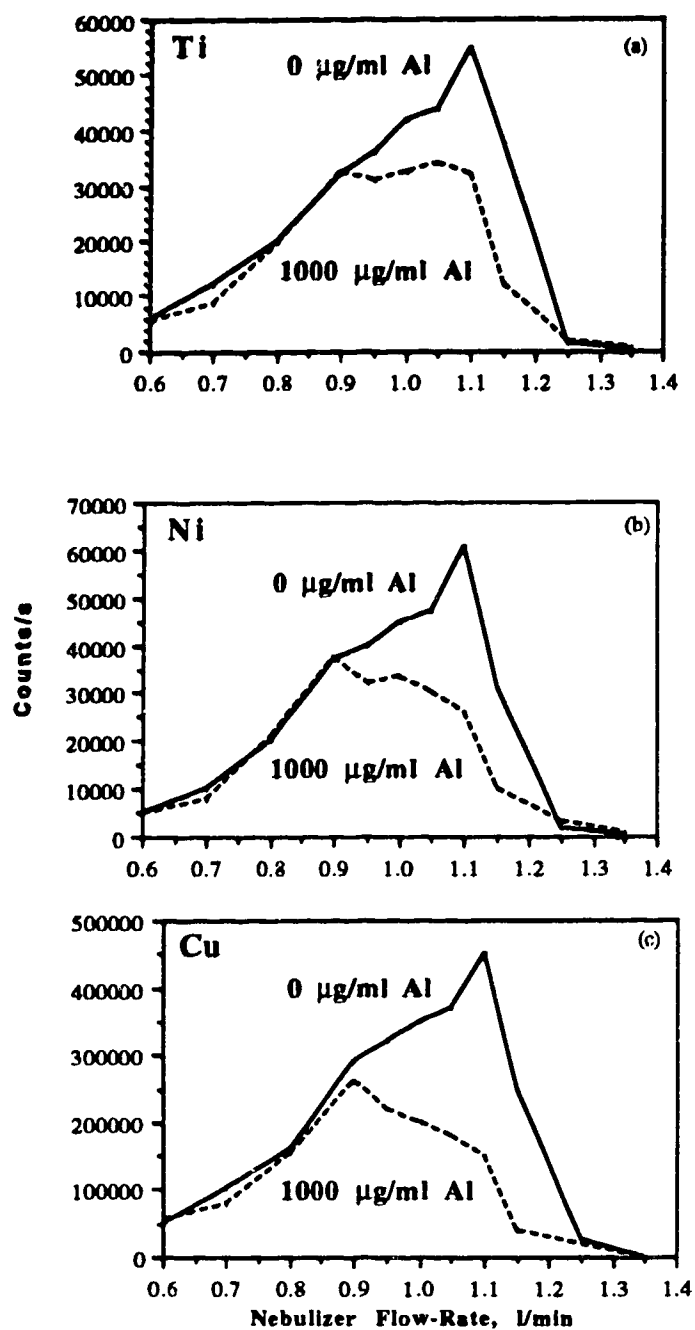


Figure 4.5 Ion count as a function of nebulizer flow-rate for $^{48}\text{Ti}^+$, $^{58}\text{Ni}^+$ and $^{63}\text{Cu}^+$ in 5% HNO_3 and in a matrix containing 1000 $\mu\text{g}/\text{mL}$ of Al

The matrix effect, as a result of the high concentration of Al, can be minimized by a small reduction in nebulizer flow-rate from that which results in the maximum analyte signal. The dependence of the matrix effect on nebulizer flow-rate and Al concentration is shown in Figure 4.6 for Ni. At the nebulizer flow-rate yielding the maximum analyte signal, the Ni signal is suppressed by increasing amounts of Al, but the matrix effect is eliminated at the low nebulizer flow-rate. This reduction in matrix effect does, however, result in a minor loss in analyte sensitivity, as shown in Table 4.4 for a number of analytes. In the worst instance, the sacrifice in signal intensity was only 45%. This makes it possible to do quantitative analysis of the trace elements at a higher matrix concentration (1000 µg/ml) with a lower nebulizer flow-rate (0.90 L/min).

Table 4.4 Comparison of signal intensities (counts/sec) at nebulizer flow-rate yielding maximum signal or reduced matrix effects

Element	Signal at flow-rate for maximum intensity	Signal at flow-rate for reduced matrix effects	Loss in signal intensity, %
Mg	110000	60000	45
Ti	55000	32000	41
Mn	80000	50000	38
Ni	60000	35000	42
Co	60000	35000	42
Cu	45000	25000	44
Zn	10000	7000	30
Y	80000	50000	38

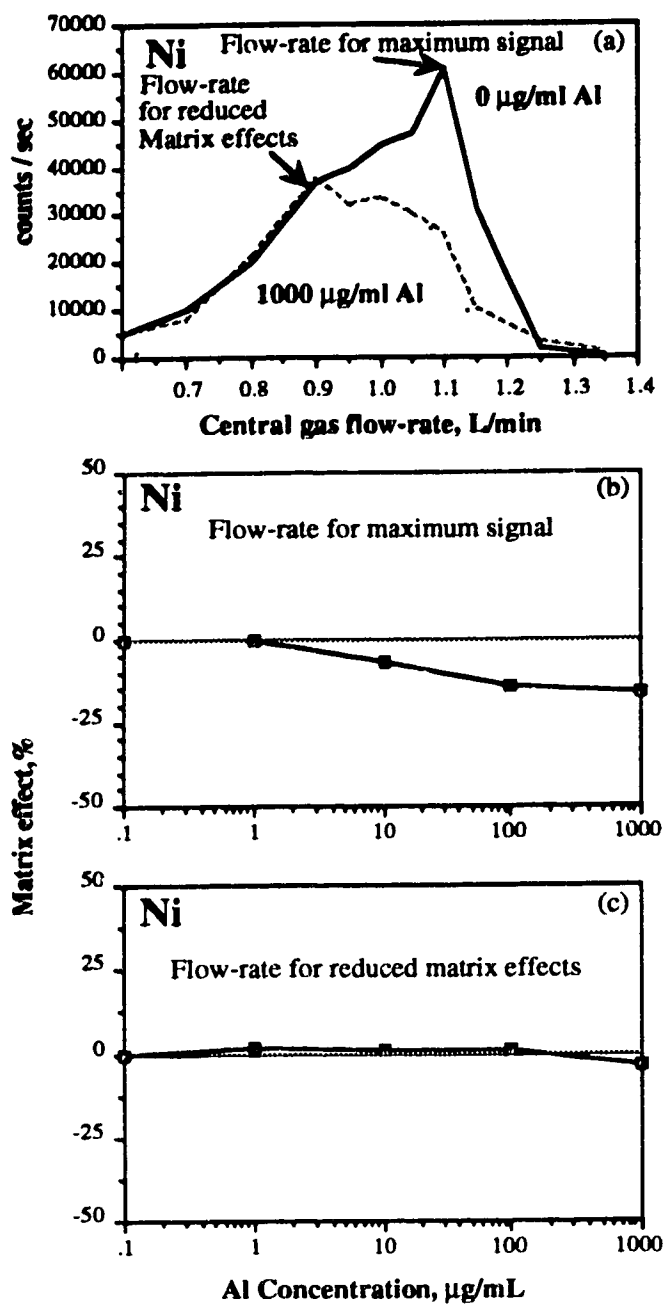


Figure 4.6 Effect of increasing Al concentration on the Ni signal at the nebulizer flow-rate yielding maximum signal intensity (b) and at a reduced nebulizer flow-rate (c).

Vaughan and Horlick suggested that the degree of the matrix effect changed slowly as a function of mass over a modest mass range of analytes, and for a relatively light matrix element, all analytes experience a similar effect [27]. However, in this experiment, a light element such as Mg and heavy elements such as Sn and Pb were determined. The degree of the matrix effect was different between light and heavy elements. Therefore, the suppressions of the signal intensities were different between light and heavy elements. One consequence of this is that two internal standards should be used to compensate for matrix effects so that a wider mass range of analytes can be determined.

Several criteria should be followed for selection of an internal standard in the analysis of aluminum samples. First of all, an internal standard should be an element which is not present in the aluminum samples. Secondly, it should be monoisotopic, so that there are no extra isobaric corrections to be made on account of the internal standard and it should not form strong oxides. Finally, it should be in the mid-mass range, a compromise position for any mass effect. In this experiment, yttrium was chosen as an internal standard for mid-mass range element determinations. Alternatively, both cobalt and rhodium were also selected as internal standards for the determination of both lighter and heavier elements. As some of the samples from Alcan contained a small amount of cobalt, an isobaric correction had to be made on account of the internal standard when Co was used as an internal standard.

Matrix effect data are shown in Figure 4.7 for Co (internal standard) and two analytes (Mg and Ti) as a function of the Al concentration. These data were obtained at a nebulizer flow-rate giving the maximum analyte signal response. The matrix effect is clearly similar for all species. Thus, when Co is used as an

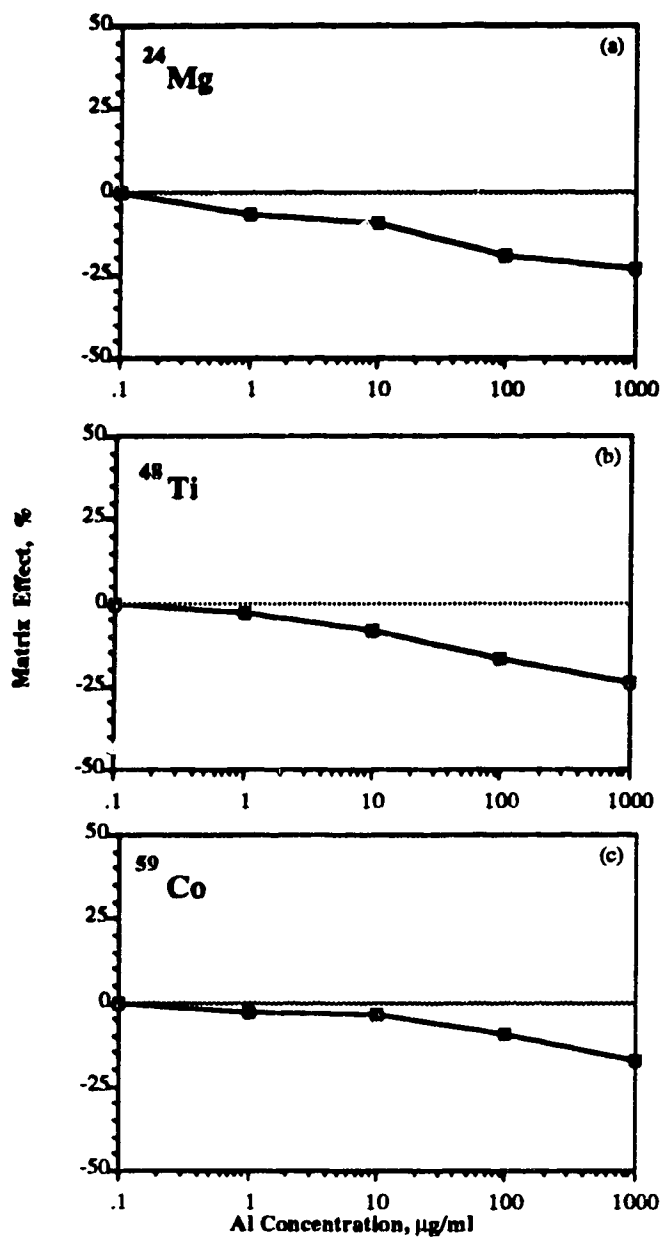


Figure 4.7 Effect of increasing Al concentration on (a) $^{24}\text{Mg}^+$, (b) $^{48}\text{Ti}^+$ and (c) $^{59}\text{Co}^+$ signal as a percentage matrix effect.

internal standard it compensates for the Al induced matrix effect (Figure 4.8). This type of compensation for the matrix effect is only effective if the analyte and the internal standard experience the same matrix effect. Therefore, two internal standards are recommended when a wide mass range of analytes is determined.

Both short-term and medium-term stabilities of the ICP-MS instrument were investigated by Vaughan and Horlick [27]. It was reported that in the medium term, the internal standard improved the standard deviation of the signal significantly, from 10.9% on average, to 2.3% [27].

The change in signal intensity over a 25-min period was also investigated in this experiment. Data for this medium-term drift were acquired while aspirating the 0.01% Al solution over 25 min. Plots of the medium-term drift with and without the use of Co as internal standard are shown in Figure 4.9. The unratiod ion signal intensity shows a continuous downward drift with respect to time. However, when Co is used as an internal standard, the drift in signal intensity with time is improved significantly. In this medium-term (25 min) experiment, the internal standard reduces the relative standard deviation (%rsd) of the signal from 5% to 2 %.

4.3.4 Analytical Results

Aqueous calibration curves for both internal standard and matrix matching methods were employed for the determination of Mg, Ti, Mn, Ni, Cu and Zn in both Alcoa and Alcan aluminum samples. For the internal standard method, both yttrium and/or cobalt were chosen as the internal standard.

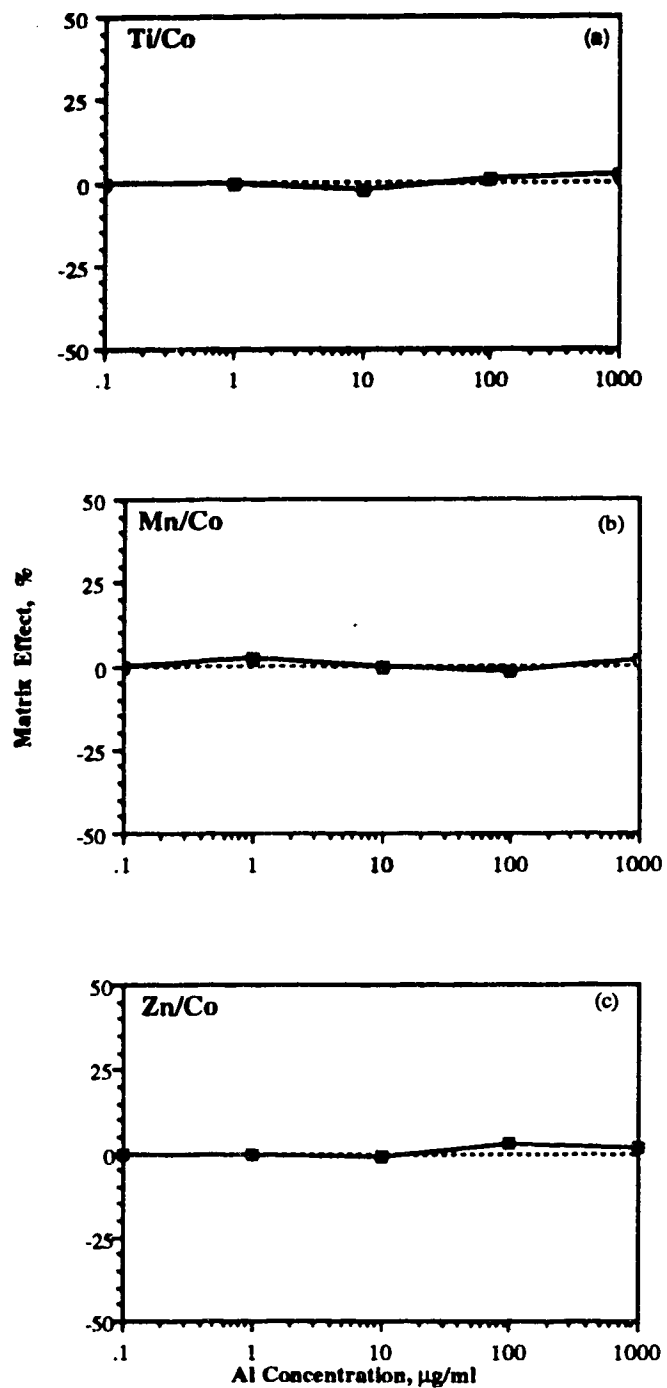


Figure 4.8 Effect of increasing Al concentration on the (a) $^{48}\text{Ti}^+$, (b) $^{55}\text{Mn}^+$ and (c) $^{64}\text{Zn}^+$ signals with $^{59}\text{Co}^+$ as an internal standard.

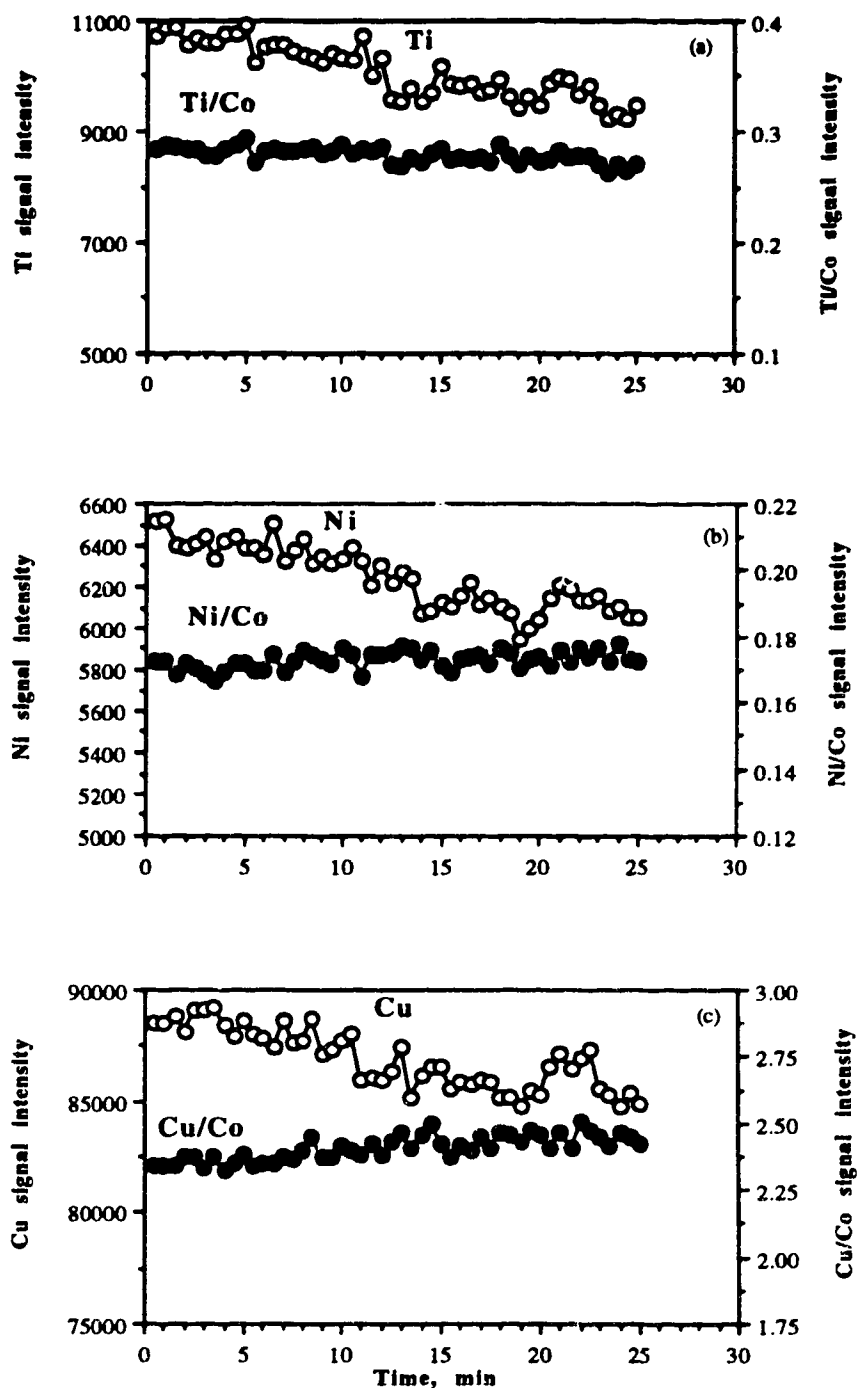


Figure 4.9 Signal intensity changes (in arbitrary units) as a function of time for (a) $^{48}\text{Ti}^+$, (b) $^{58}\text{Ni}^+$ and (c) $^{63}\text{Cu}^+$ in a 0.01% aluminium solution with and without the use of $^{59}\text{Co}^+$ as an internal standard.

Rhodium was also used as the internal standard for the determination of heavier elements. The intensity ratios of analyte to internal reference were obtained with respect to the concentration ($\mu\text{g}/\text{ml}$) of the standard solutions. The calibration graphs were linear over the two orders of magnitude needed for the samples. The concentration range was from 0.003 to 0.3 $\mu\text{g}/\text{ml}$. The slopes (b) of log-log plots for the calibration function ($\log(\text{intensity ratio}) = a + b \cdot \log(\text{concentration})$) are presented in Table 4.5 and the analytical results and the certified values are given in Tables 4.6 and 4.7. The experimental results are in good agreement with the certified values except the results of both $^{63}\text{Cu}^+$ and $^{65}\text{Cu}^+$ isotopes. In Table 4.6, the results of the copper were higher than the certified value of a low concentration sample (SA-909) and lower than the certified value of a higher concentration sample (SA-1169). There might be a contamination of copper on the ion lenses of the mass spectrometer which was used to work as a GD mass spectrometer for copper samples. With a lower nebulizer flow-rate (0.9 L/min), the internal standard was used here to improve and compensate for the instrumental drift.

Table 4.5 Constants of calibration function for aqueous calibration curves with internal standards

Element/Internal Standard	Calibration function* Slope	Correlation Coefficient
$^{24}\text{Mg}/^{89}\text{Y}$	0.97	0.999
$^{48}\text{Ti}/^{89}\text{Y}$	0.97	0.999
$^{55}\text{Mn}/^{89}\text{Y}$	0.98	0.999
$^{58}\text{Ni}/^{89}\text{Y}$	0.96	0.999
$^{60}\text{Ni}/^{89}\text{Y}$	0.98	0.999
$^{63}\text{Cu}/^{89}\text{Y}$	0.93	1.000
$^{64}\text{Zn}/^{89}\text{Y}$	0.97	1.000
$^{65}\text{Cu}/^{89}\text{Y}$	0.93	0.999
$^{66}\text{Zn}/^{89}\text{Y}$	0.98	1.000
$^{48}\text{Ti}/^{59}\text{Co}$	0.98	1.000
$^{55}\text{Mn}/^{59}\text{Co}$	0.91	0.999
$^{58}\text{Ni}/^{59}\text{Co}$	0.92	0.999
$^{60}\text{Ni}/^{59}\text{Co}$	0.94	1.000
$^{63}\text{Cu}/^{59}\text{Co}$	0.93	0.999
$^{64}\text{Zn}/^{59}\text{Co}$	0.90	0.998
$^{65}\text{Cu}/^{59}\text{Co}$	0.90	0.999
$^{66}\text{Zn}/^{59}\text{Co}$	0.89	0.998
$^{69}\text{Ga}/^{59}\text{Co}$	0.99	1.000
$^{90}\text{Zr}/^{103}\text{Rh}$	0.99	0.997
$^{120}\text{Sn}/^{103}\text{Rh}$	0.98	1.000

*Calibration function: $\log y = a + b \log x$

Table 4.6 Analysis of the 0.01% solution of low alloy aluminum samples from Alcoa. Results reported as % in aluminum; precision expressed as standard deviation (n=4). Aqueous calibration solutions used, with yttrium as the internal standard

Sample	SA-909	SA-1170	SA-1169
²⁴ Mg	0.02980±0.00040	0.00810±0.00020	0.03800±0.00030
Certified	0.030	0.009	0.038
⁵⁵ Mn	0.02480±0.00070	0.01950±0.00020	0.06600±0.00260
Certified	0.031	0.027	0.076
⁵⁸ Ni	0.03110±0.00040	0.00570±0.00008	0.00437±0.00004
Certified	0.034	-	-
⁶⁰ Ni	0.03160±0.00080	0.00300±0.00007	0.00306±0.00011
Certified	0.034	-	-
⁶³ Cu	0.05570±0.00240	0.10700±0.00320	0.19410±0.00890
Certified	0.031	0.100	0.210
⁶⁴ Zn	0.03160±0.00040	0.03800±0.00070	0.02000±0.00030
Certified	0.030	0.039	0.021
⁶⁵ Cu	0.05520±0.00140	0.10400±0.00180	0.19410±0.00070
Certified	0.031	0.100	0.210
⁶⁶ Zn	0.03090±0.00080	0.03890±0.00050	0.02200±0.00040
Certified	0.030	0.039	0.021

Table 4.7 Analysis of the 0.01% solutions of low alloy aluminum samples from Alcan with both low and high nebulizer flow-rates. Results reported as % in aluminum; precision expressed as standard deviation (n=4). Aqueous calibration solutions used, with Co or Rh used as the internal standards

Nebulizer Flow-rate: 0.9 L/min

Mass\Samples	1SCXG	1SWL	1SWM	1SXD	2SDZ
Mg 24/59	.2143 ±.0034	.0193 ±.0004	.0109 ±.0003	.0132 ±.0011	.0366 ±.0010
Certified	.25	.015	.005	.006	.035
Ti 48/59	.0178 ±.0004	.0250 ±.0004	.0051 ±.00004	.0131 ±.0008	.0393 ±.0015
Certified	.02	.025	.005	.013	.041
Mn 55/59	.0173 ±.0005	.0208 ±.0006	.0056 ±.0002	.0064 ±.0003	.0382 ±.0008
Certified	.026	.023	.005	.005	.042
Ni 58/59	.0161 ±.0004	.0210 ±.0004	.0055 ±.0001	.0068 ±.0004	.0445 ±.0008
Certified	.023	.022	.006	.005	.045
Zn 64/59	.0330 ±.0007	.0274 ±.0005	.0216 ±.0001	.0175 ±.0003	.0538 ±.0010
Certified	.027	.023	.016	.005	.046
Ga 69/59	.0118 ±.0001	.0116 ±.0002	.0089 ±.0002	.0018 ±.0002	.0237 ±.0009
Certified	.015	.012	.01	.001	.022
Sn 120/103	.0242 ±.0011	.0237 ±.0005	.0055 ±.0003	.0059 ±.0006	.0477 ±.0011
Certified	.024	.024	.006	.006	.045

Nebulizer Flow-rate: 1.1 L/min

Mass\Samples	1SCXG	1SWL	1SWM	1SXD	2SDZ
Mg 24/59	.193 ±.003	.0180 ±.0003	.0103 ±.0004	.0119 ±.0004	.0336 ±.0009
Certified	.25	.015	.005	.006	.035
Ti 48/59	.0174 ±.0003	.0251 ±.0002	.0051 ±.0002	.0129 ±.0003	.0397 ±.0003
Certified	.02	.025	.005	.013	.041
Mn 55/59	.0175 ±.0003	.0210 ±.0002	.0051 ±.0005	.0052 ±.0001	.0372 ±.0004
Certified	.026	.023	.005	.005	.042
Ni 58/59	.0162 ±.0003	.0209 ±.0003	.0049 ±.0001	.0060 ±.0001	.0443 ±.0007
Certified	.023	.022	.006	.005	.045
Zn 64/59	.0299 ±.0004	.0262 ±.0006	.0184 ±.0004	.0153 ±.0005	.0492 ±.0002
Certified	.027	.023	.016	.005	.046
Ga 69/59	.0115 ±.0001	.0112 ±.0001	.0089 ±.0001	.0010 ±.0001	.023 ±.0003
Certified	.015	.012	.01	.001	.022
Sn 120/103	.0227 ±.0006	.0230 ±.0005	.0056 ±.0004	.0055 ±.0002	.0451 ±.0006
Certified	.024	.024	.006	.006	.045

Matrix matching was also tried at both high and low nebulizer flow-rates without use of internal standards. Standard solutions were prepared and Al was added with a concentration of 100 $\mu\text{g}/\text{ml}$ in order to match the 0.01% Al sample solutions. The results for 0.01% solution of low alloy aluminum samples from Alcoa by using matrix matching method are shown in Table 4.8. Since the matrix effect of aluminum on analyte signals was significantly reduced at a lower nebulizer flow-rate (0.90 L/min), 0.1% sample solutions were also aspirated in order to compensate the loss in intensity of the analyte signals at the reduced flow-rate setting. As a result, the ability to detect analytes was enhanced significantly so that it was possible to determine the ultra trace elements in the low alloy aluminum samples. The analytical results using the matrix matching method with both high and low nebulizer flow-rates are given in Table 4.8, and the results for the 0.1% solutions of the standard reference aluminum from both Alcoa and Alcan at a nebulizer flow-rate of 0.9 L/min are also presented in Table 4.9. The agreement between the experimental and certified values was good, especially, for the results of Alcan 1SWM and 1SXD low alloys where the compositions of the most analytes are normally in a range of 0.001% to 0.006%. Because of their lower concentrations in the 0.01% aluminum solutions, the accuracy for most analytes in 1SWM and 1SXD shown in Tables 4.7 is relatively poor. The results are significantly higher than the certified values. As shown in Table 4.9, however, the accuracy of the results is significantly improved for the 0.1% Al solutions.

Table 4.8 Analysis of 0.01% solution of low alloy aluminum samples from Alcoa by using matrix matching method. Results reported as % in aluminum; precision expressed as standard deviation (n=4).

Samples	SA-909	SA-1170	SA-1169
Nebulizer flow-rate: (0.9 L/min)			
²⁴Mg	0.0316±0.0013	0.0057±0.0007	0.0401±0.0008
Certified	0.030	0.009	0.038
⁵⁵Mn	0.0319±0.0005	0.0245±0.0004	0.0782±0.0015
Certified	0.031	0.027	0.076
⁵⁸Ni	0.0353±0.0012	0.0061±0.0006	0.0044±0.0003
Certified	0.034	-	-
⁶⁰Ni	0.0296±0.0014	0.0016±0.0001	0.0018±0.0003
Certified	0.034	-	-
⁶³Cu	0.0316±0.0012	0.0996±0.0009	0.2092±0.0037
Certified	0.031	0.10	0.21
⁶⁴Zn	0.0321±0.0009	0.0415±0.0013	0.0203±0.0019
Certified	0.030	0.039	0.021
⁶⁵Cu	0.0302±0.0014	0.1028±0.0011	0.2096±0.0003
Certified	0.031	0.10	0.21
⁶⁶Zn	0.03150±0.0016	0.04330±0.0018	0.0207±0.0023
Certified	0.030	0.039	0.021
Nebulizer flow-rate: (1.1 L/min)			
²⁴Mg	0.0249±0.0003	0.0075±0.0002	0.0361±0.0007
Certified	0.030	0.009	0.038
⁵⁵Mn	0.0278±0.0009	0.0248±0.0007	0.0770±0.0012
Certified	0.031	0.027	0.076
⁵⁸Ni	0.0361±0.0007	0.0085±0.0002	0.0056±0.0001
Certified	0.034	-	-
⁶⁰Ni	0.0362±0.0006	0.0042±0.0003	0.0030±0.0002
Certified	0.034	-	-
⁶³Cu	0.0320±0.0007	0.1060±0.0024	0.2078±0.0031
Certified	0.031	0.10	0.21
⁶⁴Zn	0.0313±0.0007	0.0358±0.0005	0.0194±0.0008
Certified	0.030	0.039	0.021
⁶⁵Cu	0.0317±0.0007	0.1059±0.0031	0.2069±0.0037
Certified	0.031	0.10	0.21
⁶⁶Zn	0.0308±0.0009	0.0388±0.0008	0.0205±0.0004
Certified	0.030	0.039	0.021

Table 4.9 Analysis of the 0.1% solutions of the standard reference aluminium from both Alcoa and Alcan in condition of nebulizer flow-rate 0.9 l/min by using ICP-MS. Results reported as % in aluminium; precision expressed as standard deviation (n=6). Aqueous calibration solutions are used, without internal standard.

Samples:	1SCXG	1SWL	1SWM	1SXD	SA-909	SA-1170	SA-1169	
Mg 24	Measured	0.1881±0.0150	0.0142±0.0005	0.0052±0.0003	0.0059±0.0005	0.0268±0.0010	0.0069±0.0001	0.0348±0.0002
	Certified	0.25	0.015	0.005	0.006	0.030	0.009	0.038
Ti 48	Measured	0.0208±0.0018	0.0243±0.0005	0.0055±0.0003	0.0113±0.0007	0.0251±0.0009	0.0153±0.0001	0.0156±0.0001
	Certified	0.02	0.025	0.005	0.013	0.030	0.039	0.021
Mn 55	Measured	0.0238±0.0015	0.0229±0.0004	0.0065±0.0003	0.0054±0.0004	0.0286±0.0007	0.0220±0.0002	0.0719±0.0012
	Certified	0.026	0.023	0.005	0.005	0.031	0.027	0.076
Ni 60	Measured	0.0225±0.0015	0.0225±0.0005	0.0060±0.0003	0.0060±0.0004	0.0332±0.0013	0.0028±0.0002	0.0032±0.0001
	Certified	0.023	0.023	0.006	0.005	0.034	-	-
Cu 63	Measured	0.0234±0.0010	0.0340±0.0005	0.0099±0.0003	0.0149±0.0007	0.0343±0.0013	0.0981±0.0012	0.2127±0.0026
	Certified	0.022	0.03	0.006	0.013	0.031	0.10	0.21
Zn 64	Measured	0.0296±0.0017	0.0260±0.0006	0.0185±0.0006	0.0080±0.0005	0.0342±0.0006	0.0373±0.0003	0.0206±0.0003
	Certified	0.027	0.023	0.016	0.005	0.030	0.039	0.021
Cu 65	Measured	0.0230±0.0008	0.0335±0.0007	0.0097±0.0006	0.0145±0.0010	0.0341±0.0005	0.1006±0.0024	0.2168±0.0041
	Certified	0.022	0.03	0.006	0.013	0.031	0.10	0.21
Zn 66	Measured	0.0279±0.0020	0.0243±0.0004	0.0184±0.0009	0.0062±0.0005	0.0335±0.0012	0.0379±0.0006	0.0212±0.0007
	Certified	0.027	0.023	0.016	0.005	0.030	0.039	0.021
Ga 69	Measured	0.0129±0.0008	0.0111±0.0003	0.0100±0.0004	0.0010±0.00003			
	Certified	0.015	0.012	0.01	0.001			
Zr 90	Measured	0.0257±0.0013	0.0130±0.0002	0.0195±0.0009				
	Certified	0.034	0.013	0.018				
Sn 120	Measured	0.0146±0.0006	0.0173±0.0003	0.0044±0.0002	0.0038±0.0002	0.0246±0.0012		
	Certified	0.024	0.024	0.006	0.006	0.026		

4.4 Conclusions

Inductively coupled plasma mass spectrometry can be used successfully for the analysis of low alloy aluminum samples. However, basic spectral interferences make the determination of some important elements (Si and P) difficult. In addition, ArN^+ , ArO^+ and ArOH^+ from the argon gas may cause important spectral interferences on the major isotopes of Fe, and the ClO^+ and ClOH^+ species from the solution matrix may cause severe interference on the V and Cr signals. The Al induced matrix effects are an important aspect of ICP-MS analyses in this experiment and suppressions of analyte signals were observed. It was shown that the matrix effect could be reduced significantly with a lower nebulizer flow-rate setting so that 0.1% Al sample solutions can be determined without the use of internal standards but with matrix matching. Moreover, it was also shown that internal standardization is very useful, not only to compensate for instrumental drift but also to help compensate for matrix effects. Matrix matching was also applied to match the 0.01% Al sample solutions. Excellent results can be obtained for determination of most elements in aluminum alloy samples.

References

1. K. E. Jarvis *J. Anal. At. Spectrom.* **4**, 563 (1989).
2. J. M. Richardson, A. P. Dickin, R. H. McNutt, J. I. McAndrew and S. B. Beneteau, *J. Anal. At. Spectrom.* **4**, 465 (1989).
3. K.E. Jarvis and J. G. Williams, *Chem. Geol.* **77**,53 (1989).
4. G. E. M. Hall, J. G. Pelchat and J. Loop, *J. Anal. At. Spectrom.* **5**, 339 (1990).
5. T. J. Brotherton, W. L. Shen and J. A. Caruso, *J. Anal. At. Spectrom.* **4**, 39 (1989).
6. M. Dever, D. W. Hausler and J. E. Smith, *J. Anal. At. Spectrom.* **4**, 361 (1989).
7. T. D. B. Lyon and G. S. Fell, *J. Anal. At. Spectrom.* **5**, 135 (1990).
8. P. Tothill, L. M. Matheson and J. F. Smyth, *J. Anal. At. Spectrom.* **5**, 619 (1990).
9. M. J. Campbell and H. T. Delves, *J. Anal. At. Spectrom.* **4**, 235 (1989).
10. X. Wang, A. Lásztity, M. Viczián, Y. Isreal and R.M. Barnes, *J. Anal. At. Spectrom.* **4**, 727 (1989).
11. A. Lásztity, X. Wang, M. Viczián, R.M. Barnes, *J. Anal. At. Spectrom.* **4**, 737 (1989).
12. N. Furuta, *J. Anal. At. Spectrom.* **6**, 199 (1991).
13. Y. Igarashi, H. Kawamura, K. Shiraishi and Y. Takaku, *J. Anal. At. Spectrom.* **4**, 571 (1989).
14. B. T. G. Ting, C. S. Mooers and M. Janghorbani, *Analyst*, **114**, 667 (1989).
15. D. Beauchemin, K. W. Siu and S.S. Berman, *Anal. Chem.* **60**, 2587 (1988).
16. R. D. Statzger, *Anal. Chem.* **60**, 2500 (1988).

17. J. M. Henshaw, E. M. Heithman and T.A. Hinnners, *Anal. Chem.* **61**, 335 (1989).
18. J. K. Friel, C. S. Skinner, S. E. Jackson and H. P. Longerich, *Analyst*, **115**, 269 (1990).
19. D. C. Gregoire, *J. Anal. At. Spectrom.* **5**, 623 (1990).
20. K. Shiraishi, Y. Takaku, K. Yoshimizu, Y. Igarashi, K. Masuda, J. F. McInroy and G. Tanaka, *J. Anal. At. Spectrom.* **6**, 335 (1991).
21. H. M. Al-Swaidan, *Anal. Lett.* **21**, 1487 (1988).
22. S. J. Stotesbury, J. M. Pickering and M. A. Grifferty, *J. Anal. At. Spectrom.* **4**, 457 (1989).
23. V. Vandecasteele, G. Wauters and R. Dams, *J. Anal. At. Spectrom.* **4**, 461 (1989).
24. C. J. Amarasiriwardena, B. Gercken, M. D. Argentine, R. M. Barnes, *J. Anal. At. Spectrom.* **5**, 457 (1990).
25. R. C. Hutton, M. Bridenne, E. Coffre, Y. Marot and F. Simondet, *J. Anal. At. Spectrom.* **5**, 463 (1990).
26. A. Zurhaar and L. Mullings, *J. Anal. At. Spectrom.* **5**, 661 (1990).
27. M. A. Vaughan and G. Horlick, *J. Anal. At. Spectrom.* **4**, 45 (1989).
28. K. Takeda, T. Yamaguchi, H. Akiyama and T. Masuda, *Analyst* **116**, 501 (1991).
29. A. F. Ward and L. F. Marciello, *Anal. Chem.* **51**, 2264 (1979).
30. M. A. Vaughan and G. Horlick, *Appl. Spectrosc.* **40**, 434 (1986).
31. S. H. Tan and G. Horlick, *Appl. Spectrosc.* **40**, 445 (1986).
32. J. W. McLaren, D. Beauchemin and S. S. Berman, *J. Anal. At. Spectrom.* **2**, 277 (1987).
33. J. Takahashi, R. Hara, *Anal. Sci.* **4**, 331 (1988).
34. G. Zhu and R. F. Browner, *Appl. Spectrosc.* **41**, 349 (1987).

35. S. J. Jiang, M. D. Palmiery, J. S. Fritz and R. S. Houk, *Anal. Chim. Acta* **200**, 559 (1987).
36. S. H. Tan and G. Horlick, *J. Anal. At. Spectrom.* **2**, 745 (1987).
37. D. C. Gregoire, *Spectrochim. Acta* **42B**, 895 (1987).
38. H. P. Longerich, *J. Anal. At. Spectrom.* **4**, 665 (1989).
39. J. R. Pretty, E. H. Evans, E. A. Blubaugh, W. L. Shen, J. A. Caruso and 29. G. H. Vickers, D. A. Wilson And G. M. Hieftje, *J. Anal. At. Spectrom.* **4**, 749 (1989).
40. N. Furuta, *Spectrochim. Acta* **41B**, 1115 (1986).

Chapter 5

Comparison of the Spectral Characteristics of ICP-MS and GD-MS with Respect to Low Alloy Aluminum Samples

5.1 Introduction

As was seen in the last two chapters, both inductively coupled plasma mass spectrometry (ICP-MS) and glow discharge mass spectrometry (GD-MS) are applicable to the determination of the elemental composition of aluminum alloys. In contrast to the solution-based ICP-MS methodology, the direct solids analysis capability of GD-MS is an obvious advantage. Both techniques also are substantially different with respect to the spectral characteristics of the basic mass spectra obtained and to the nature of the basic spectral interferences. In particular, the species observed from the support gas (argon), other background gases, polyatomic interferences from matrix elements by themselves and in combination with other plasma species can be quite different between the two techniques.

In this report, both background and analyte spectral characteristics for both mass spectra (ICP-MS and GD-MS) will be compared with respect to the analysis of low alloy aluminum samples.

5.2 Experimental

Both experiments were carried out by using a SCIEX (Perkin Elmer-Sciex) Elan Model 250 ICP quadrupole mass spectrometer. For ICP-MS, a standard MAK optical emission ICP torch was used in connection with a Meirhard nebulizer and a Scott-type spray chamber. A sampling depth of 15 mm from the load coil was chosen with a plasma forward power of 1.3 kW. The nebulizer flow-rate for argon was 1.10 L/min. The ion lens voltages were a compromise chosen to cover a large mass range (see Chapters 2 and 4). For GD-MS, a pin-type GD device was designed [1] and it was bolted directly onto an external interface plate of the quadrupole mass spectrometer in place of the normal sampling cone used in ICP-MS. This GD source was electrically isolated from the interface plate of the mass spectrometer by a disk insulator. It was usually operated with the shadow stop biased at -13.0 V and the anode biased at 7.0 V, at which the maximum ion signal intensity can be obtained. The power supply for the GD device was a BHK Model 2000-0.1 M voltage supply (Kepco Inc., Flushing, N.Y.) with full scale ratings of 2000 V and 100 mA. Typical operating conditions were 1000 V and 7-9 mA. For GD-MS, the typical operating pressures were 2.5 torr argon for the GD device, 0.1 to 0.2 torr for the region between the sampling plate and the skimmer and 10^{-7} to 10^{-6} torr for the mass spectrometer. These pressures are lower compared with the typical operating pressures for this system as an ICP-MS, where the pressure is about 1 torr between the sampling cone and the skimmer and the mass spectrometer operates at about 10^{-5} torr. The vacuum gauge used on the GD device was an MKS Baratron Model 122A.

Standard low alloy aluminum samples from the Aluminum Corporation of Canada (Alcan) were chosen for this work. For ICP-MS, a sample of 100 mg

aluminum chip was transferred into a 250-mL glass beaker. Ten milliliters of 6 mol/L HCl was added and the solution was heated until the reaction subsided (about 5-10 min). The solution then was cooled and diluted to 100 ml (0.1% Al solution) with de-ionized water. A 0.01% Al sample was prepared by taking 10.0 mL of 0.1% Al solution and diluting it to 100 mL. The hydrochloric acid used to dissolve the aluminum samples was of analytical-reagent grade.

For GD-MS, the aluminum standard was machined in the form of a metallic pin, 3 mm in diameter and about 15 mm in length. The sample pin was inserted into the GD cavity about 3 mm so that the distance from the sampling plate to the end of sample pin was 7 mm since the GD cavity is 10 mm in length. This sample pin was the cathode of the glow discharge.

5.3 Discussion

This discussion is focused on the different spectral characteristics between ICP-MS and GD-MS for the analysis of low alloy aluminum samples. The discussion is divided into three different parts. One is a comparison of background spectral features, another is a comparison of analyte spectral features and the other is a comparison of the detection limits.

5.3.1 Comparison of background spectral features

Mass spectroscopic interference effects arise from overlaps of: isobaric isotopes of elements; basic plasma background species; matrix induced background species; hydrides; oxides; hydroxides; doubly charged species; and from overlaps with argon gas based species [2,3]. Background species in ICP-MS

normally originate from the plasma gases, from air entrainment, and from the sample and/or solvent (water). The background spectral features of ICP-MS have been the subject of numerous investigations [2-6]. For example, Tan and Horlick [2] showed background spectra for distilled water and for three acidic matrices (i.e. 5% HCl, HNO₃, H₂SO₄). The spectral complexity depends upon the solvent used and they tabulated a number of the isotopic combinations of background species that could potentially interfere with major and minor isotopes of elements.

In marked contrast to pneumatic nebulizer based solution sample introduction systems such as ICP-MS, GD-MS involves the introduction of solid sample directly into a low pressure "dry plasma", i.e. a plasma in which almost no water and air are present. Thus the solvent and/or air dependent background species should be significantly reduced in GD-MS systems. However, the spectral interferences from discharge gas and other background gases; polyatomic interferences from sputtered matrix atoms in combination with other plasma species could still be present in GD-MS. With respect to the spectral scans of a low alloy aluminum sample (1SCXG/Alcan) using both ICP-MS and GD-MS shown in this chapter, the background spectral interferences from several specific sources are compared between ICP-MS and GD-MS. These include: the basic background from air or solvent; the background species induced from argon gas; the background from the aluminum based matrix; as well as oxide and hydroxide species.

The basic background species originating from water and air seem less important in GD mass spectra. The signal levels of N⁺, O⁺, OH⁺, OH₂⁺, OH₃⁺, N₂⁺, CO⁺, NO⁺, O₂⁺ and O₂H⁺ are much lower in GD-MS than in ICP-MS. Since

solvents are not used in GD devices, the resulting mass spectra tend to be much simpler (at least in the 14 to 75 m/z region) than for ICP-MS. Figures 5.1 and 5.2 show the spectra for the aluminum standard sample from both ICP-MS and GD-MS. As hydrochloric acid is needed to dissolve the sample for ICP-MS, the background species arising from the acid can not be avoided. Not only can both isotopes of $^{35}\text{Cl}^+$ and $^{37}\text{Cl}^+$ be observed (Figure 5.1a), but also the interferences of chlorine-based species such as $^{35}\text{ClO}^+$, $^{35}\text{ClOH}^+$, $^{37}\text{ClO}^+$ and $^{40}\text{Ar}^{35}\text{Cl}^+$ can be found in the ICP mass spectrum (Figure 5.2a). They are considered as serious problems for determinations of $^{51}\text{V}^+$, $^{52}\text{Cr}^+$, $^{53}\text{Cr}^+$ and $^{75}\text{As}^+$ in ICP-MS [2, 4, 6].

Another type of background species in ICP-MS and GD-MS are those coming from the argon support gas. These argon gas based background species in the GD-MS spectrum tend to be more complicated than those in ICP-MS. The major interferences not only include the normal species such as $^{40}\text{Ar}^+$, $^{40}\text{ArH}^+$, $^{40}\text{ArN}^+$ and $^{40}\text{ArO}^+$ which appear in ICP-MS but also the isotopes of argon ($^{36}\text{Ar}^+$ and $^{38}\text{Ar}^+$) and dimers of argon ($^{40}\text{Ar}_2^+$, $^{40}\text{Ar}^{36}\text{Ar}^+$ and $^{40}\text{Ar}^{38}\text{Ar}^+$) which are more obvious in GD-MS in a relative sense. That is, the signal intensities at 36, 38, 76, 78, 80 and 81 m/z are much weaker in ICP-MS than those in GD-MS (see Figures 5.1 and 5.2). This implies that the concentration of these ions (different isotopes and dimers of argon) are much higher in a "dry plasma". In addition, the multiply ionized species of argon such as Ar^{2+} , Ar^{3+} , Ar^{4+} and even Ar^{5+} and Ar^{6+} can be observed in GD-MS, whereas they are absolutely absent in ICP-MS. The presence of these multiply charged argon species in GD-MS is illustrated in Figure 5.3. For a 1000-V glow discharge, the average energy of fast electrons

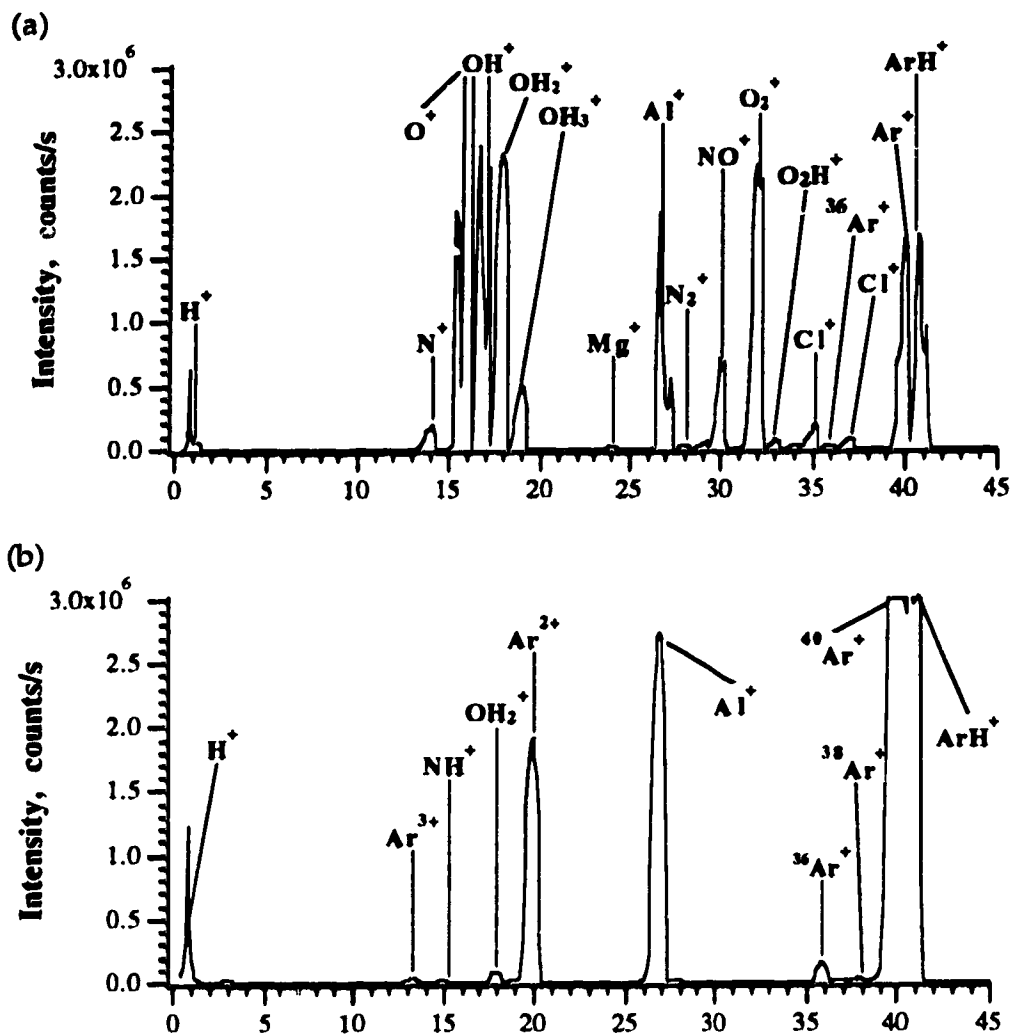


Figure 5.1 Mass spectra for (a) ICP-MS and (b) GD-MS of Alcan aluminum alloy (15CXG) in the mass range 1-45 m/z.

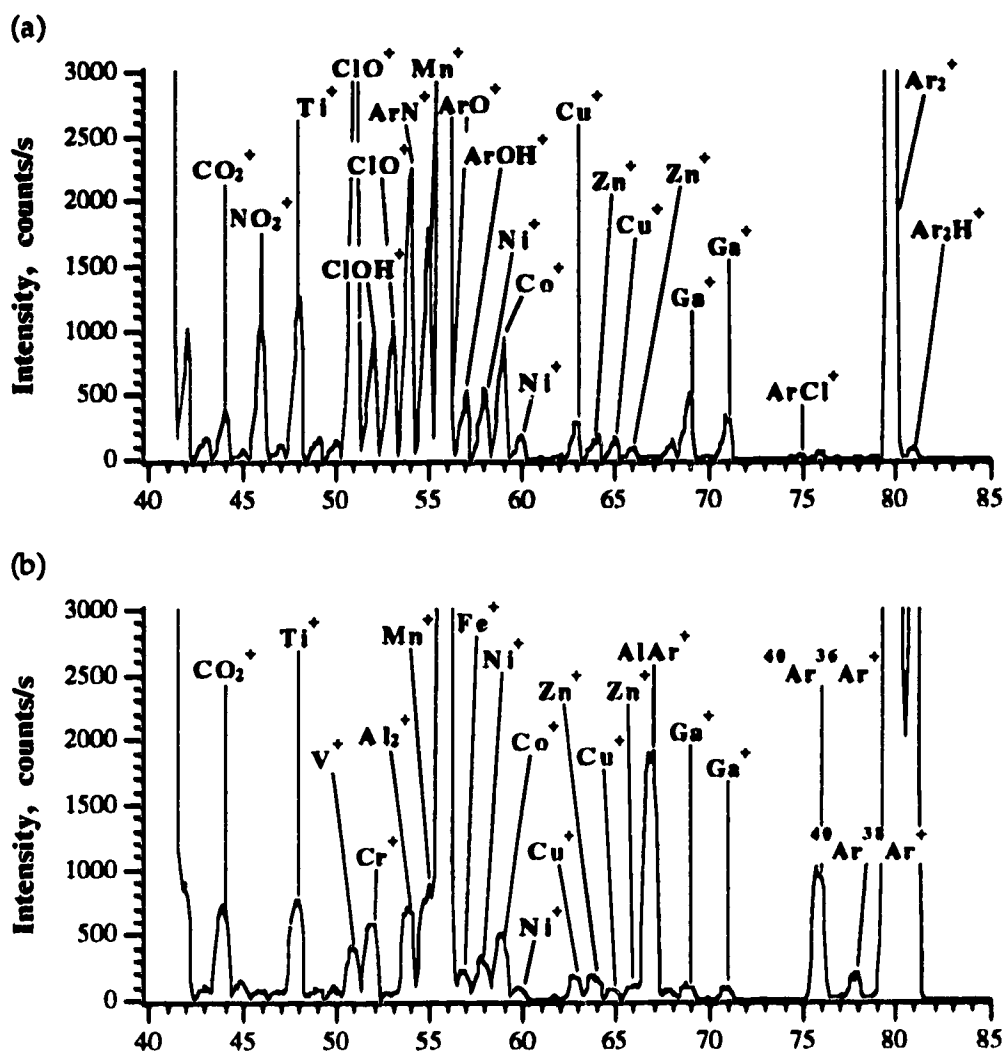


Figure 5.2 Mass spectra for (a) ICP-MS and (b) GD-MS of Alcan aluminum alloy (1SCXG) in the mass range 40-85 m/z.

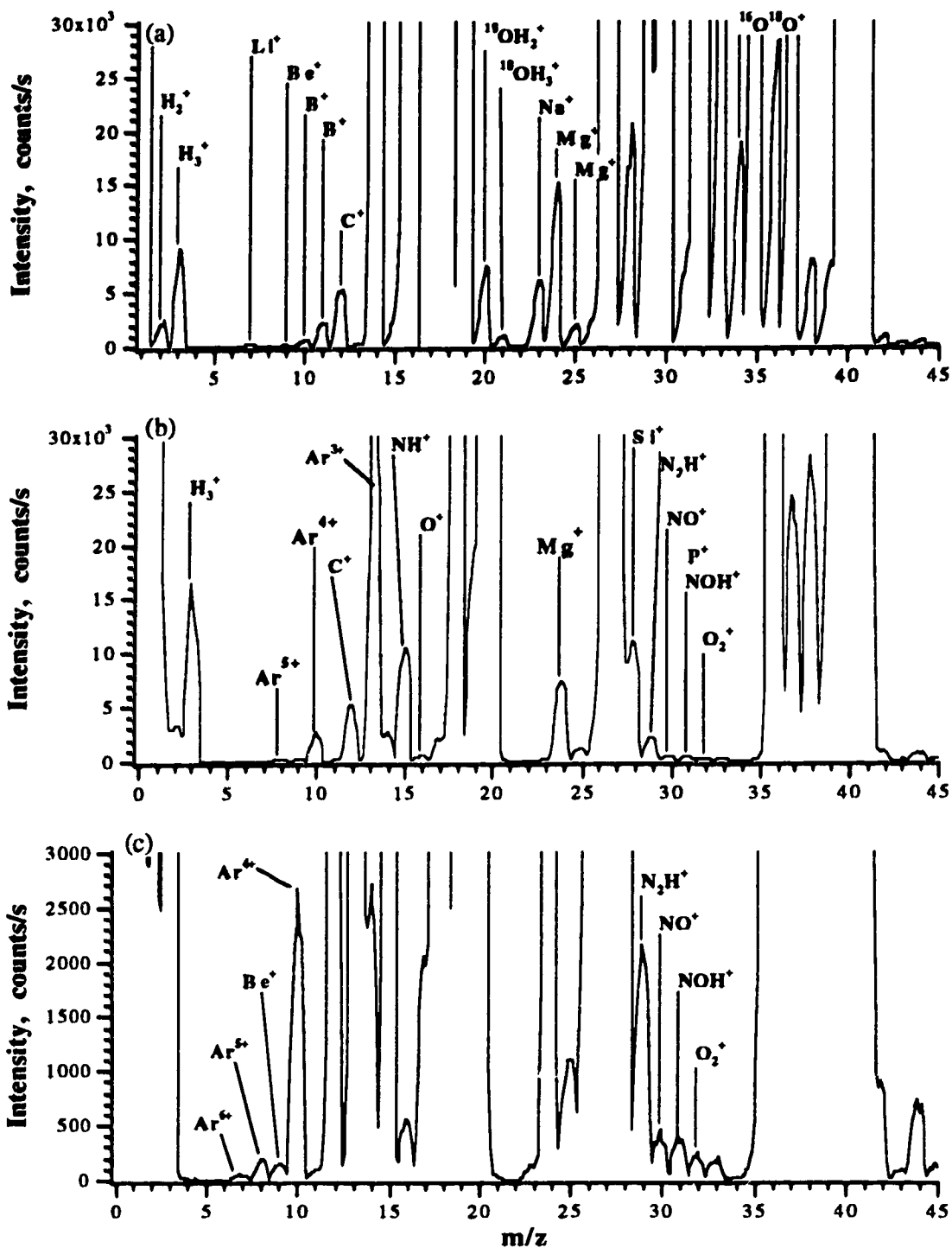


Figure 5.3 Mass spectra for (a) ICP-MS and (b) and (c) GD-MS of Alcan aluminum alloy (1SCXG) in the mass range 1-45 m/z .

might be about 200-400 eV [7]. This is sufficient energy to form the multiply charged argon ions in a stepwise manner. However, such high energy electrons do not occur in an ICP.

Aluminum based matrix species do not seem to be major components in either ICP-MS or GD-MS. Since Al is a monoisotopic element, less interference problems can, a priori, be expected. Mono-oxide and mono-hydroxide species of aluminum (AlO^+ and AlOH^+), the dimer of aluminum ($^{27}\text{Al}_2^+$) and multiply charged aluminum species (Al^{2+} and Al^{3+}) are relatively low in intensity. In both mass spectra (Figure 5.2), the small peak at mass 43 is likely from $^{27}\text{AlO}^+$, although it also can be overlapped with an isotope of Ca ($^{43}\text{Ca}^+$). Also, the presence of the mono-hydroxide and dimer of aluminum (AlOH^+ and Al_2^+) could not be confirmed since the large peaks at both mass 44 and 54 could also originate from the background components of CO_2^+ and $^{40}\text{ArN}^+$, which are much stronger in ICP-MS than those in GD-MS, as well as the isobaric overlap of $^{44}\text{Ca}^+$ and $^{54}\text{Fe}^+$ with natural abundances of 2.09% and 5.82%, respectively. The existence of doubly charged and triply charged aluminum species (Al^{2+} and Al^{3+}) at m/z 13.5 and 9 could be considered in GD-MS, but Al^{2+} can be affected by a multiply charged argon species Ar^{3+} with m/z 13.3 and also an isobaric overlap with beryllium (^9Be) may occur at m/z 9 (see Figure 5.3). Therefore, there is still no exclusive evidence to prove the presence of multiply charged aluminum species in GD-MS.

One of the most important different spectral features of GD-MS from ICP-MS is the enhanced presence of metal matrix based argides. Such argides tend to be almost completely absent in ICP-MS. In this GD-MS aluminum spectrum, the only significant argide is $^{27}\text{Al}^{40}\text{Ar}^+$ which interferes with $^{67}\text{Zn}^+$ (Figure

5.2b). The level of this argide ($^{27}\text{Al}^{40}\text{Ar}^+ / ^{27}\text{Al}^+$) is about 0.06%. No other argide was found in the GD-MS spectrum for this low alloy aluminum sample.

In addition to N, C, Ar, Cl and Al, other sample components or metals may also cause MO and MOH spectral interference problems in ICP-MS due to the effects of water and air. For example, it can be seen from Figure 5.4a for another aluminum standard (1SWL/Alcan), that some masses of cadmium suffer spectral overlap from ZrO^+ compounds. Interference from this metal oxide (MO) could not be found in GD-MS, although it is difficult to always insure that water and air are completely removed from the GD system and gas supply.

A group of bar graphs are used in Figure 5.5 to compare the different intensities of background signals between ICP-MS and GD-MS in the mass range from 1 to 83 m/z. In summary, for the background species coming from the effect of water (or solvent and acid) and air such as $^{14}\text{N}^+$, $^{16}\text{O}^+$, $^{16}\text{OH}^+$, $^{16}\text{OH}_2^+$, $^{16}\text{OH}_3^+$, $^{18}\text{OH}_3^+$, $^{14}\text{N}_2^+$, CO^+ , N_2H^+ , COH^+ , $^{14}\text{N}^{16}\text{O}^+$, NOH^+ , $^{16}\text{O}_2^+$, $^{16}\text{O}_2\text{H}^+$, $^{18}\text{O}^{16}\text{O}^+$, $^{35}\text{Cl}^+$, $^{37}\text{Cl}^+$, $^{14}\text{NO}_2^+$, $^{35}\text{ClO}^+$, $^{35}\text{ClOH}^+$, $^{37}\text{ClO}^+$, $^{40}\text{Ar}^{14}\text{N}^+$, $^{40}\text{ArNH}^+$, $^{40}\text{Ar}^{16}\text{O}^+$, $^{40}\text{ArOH}^+$ and $^{40}\text{Ar}^{35}\text{Cl}^+$, the signal intensities are obviously stronger in ICP-MS than in GD-MS. These background species severely affect some of the key elements of interest in aluminum alloys (Si, P, S, Ca, V, Cr, Fe and As). However, for the background species originating from argon gas, such as Ar^{6+} , Ar^{5+} , Ar^{4+} , Ar^{3+} , Ar^{2+} , $^{36}\text{Ar}^+$, $^{38}\text{Ar}^+$, $^{38}\text{ArH}^+$, $^{40}\text{ArH}^+$, $^{40}\text{ArH}_2^+$, $^{27}\text{Al}^{40}\text{Ar}^+$, $^{40}\text{Ar}^{36}\text{Ar}^+$, $^{40}\text{Ar}^{36}\text{ArH}^+$, $^{40}\text{Ar}^{38}\text{Ar}^+$, $^{40}\text{Ar}^{38}\text{ArH}^+$ and $^{40}\text{Ar}_2^+$, the signal intensities are much weaker or even missing in ICP-MS compared to GD-MS. Many of these are not considered to be a big problem in GD-MS since the multiply charged argon signals are located at a relatively low mass region (6-20 m/z) where the only affected element of interest in aluminum alloys is lithium ($^7\text{Li}^+$,

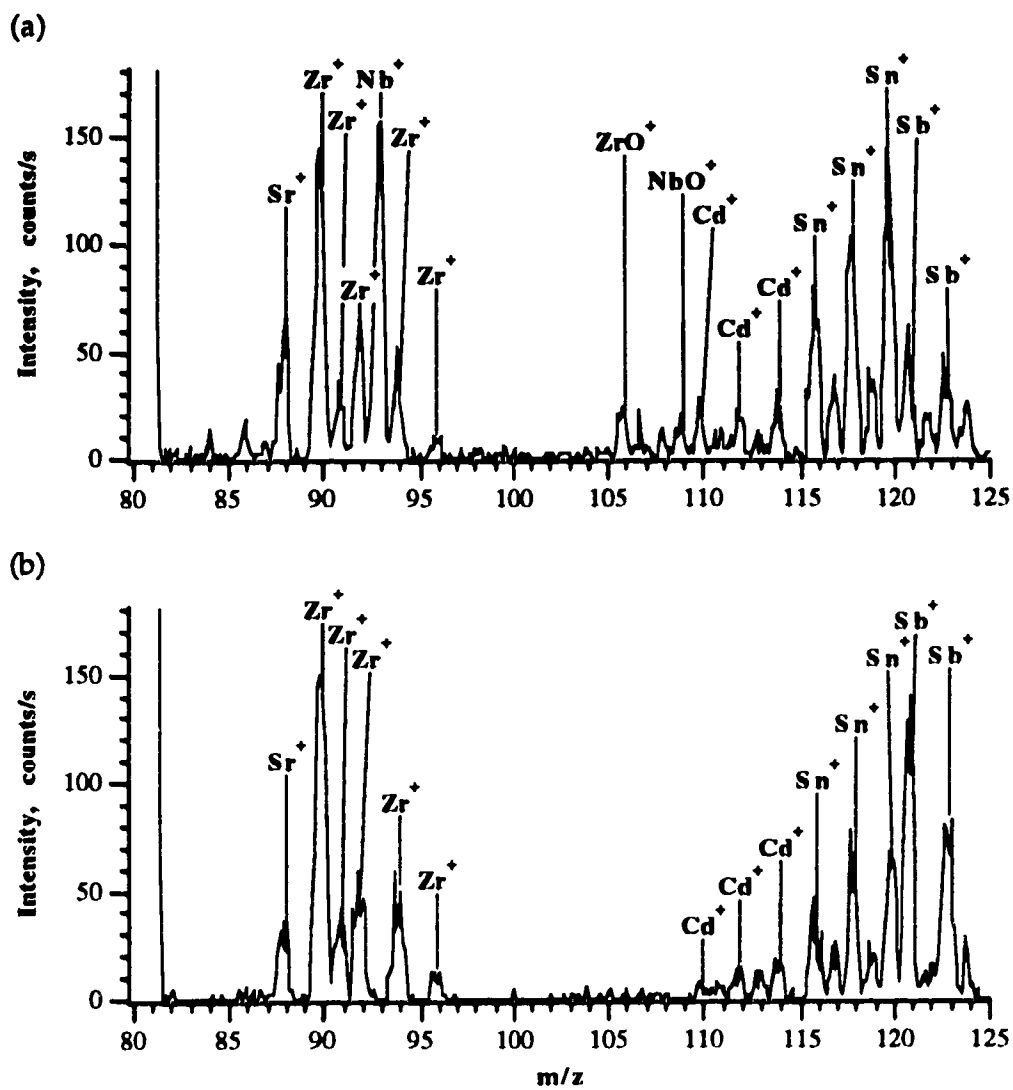


Figure 5.4 Mass spectra for (a) ICP-MS and (b) GD-MS of Alcan aluminum alloy (1SWL) in the mass range 80-125 m/z .

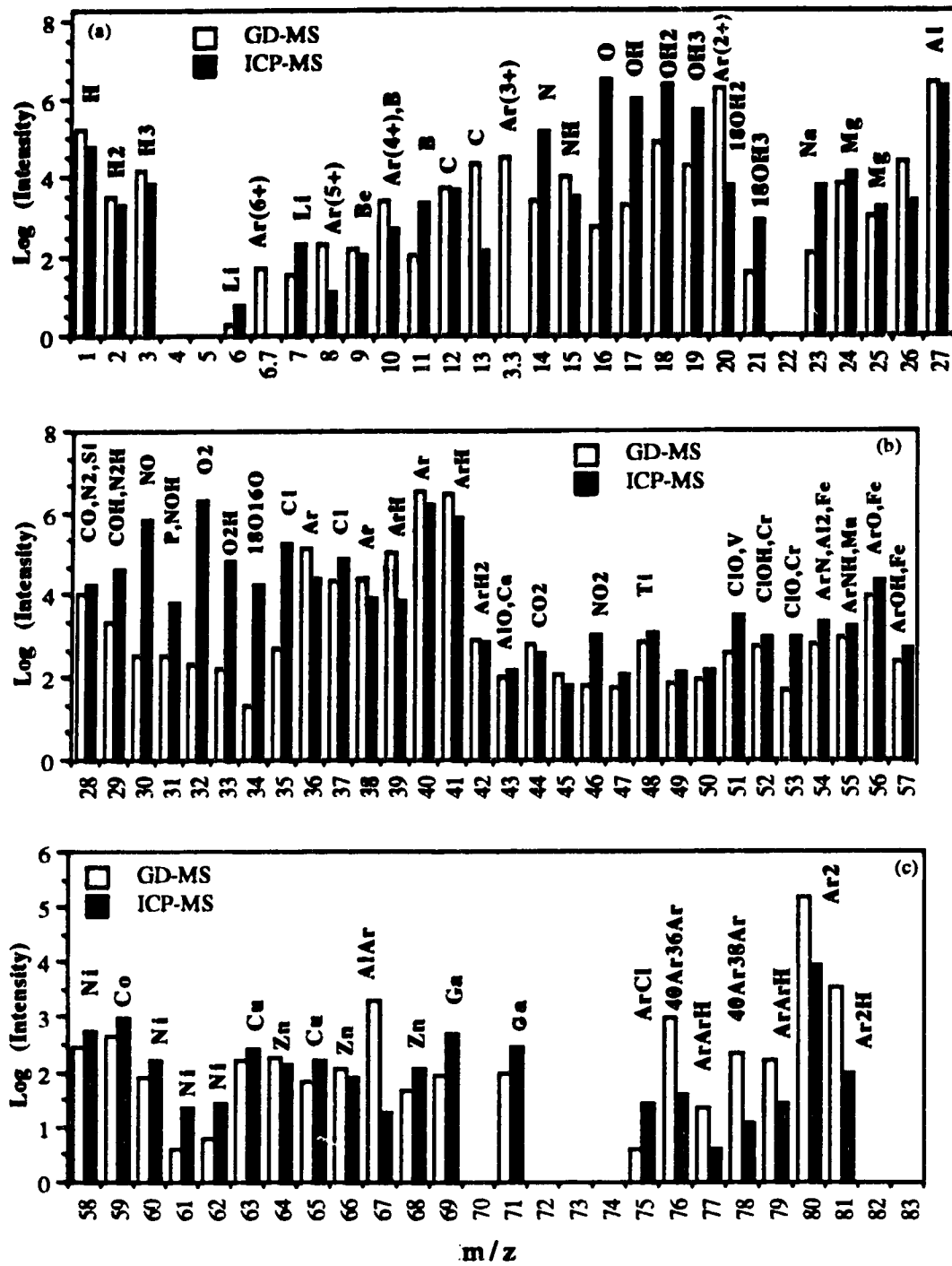


Figure 5.5 Bar graphs of mass spectrum between ICP-MS and GD-MS in the mass range 1-83 m/z

92.5%). The significant signal of aluminum argide ($^{27}\text{Al}^{40}\text{Ar}^+$) only affects a minor isotope of zinc ($^{67}\text{Zn}^+$) with a natural abundance of 4.11%.

5.3.2 Comparison of analyte spectral features

Both ICP-MS and GD-MS can be considered as useful sources for elemental analysis with low detection limits broadly achieved for almost all elements across the periodic table. Most of elements in the aluminum alloy can be identified readily from both mass spectra in this experiment. Although a 0.01% Al solution of the standard (see Table 5.1) was aspirated for ICP-MS, in general, the signal intensities are slightly higher in ICP-MS than those in GD-MS (see Figure 5.5). Thus even with the dilution associated with dissolution, ICP-MS is superior to GD-MS in terms of sensitivities (see next section).

Table 5.1 Composition of Alcan 1SCXG low alloy aluminum

Element	Composition (%by weight)	Element	Composition (%by weight)
Be	0.007	Bi	0.022
Ca	0.0058	Cd	0.018
Co	0.02	Cr	0.018
Cu	0.022	Fe	0.33
Ga	0.015	Li	0.0021
Mg	0.25	Mn	0.026
Na	0.0026	Ni	0.023
Pb	0.019	Si	0.2
Sn	0.024	Ti	0.02
V	0.008	Zn	0.027
Zr	0.034		

An interesting difference in analyte signal intensities between ICP-MS and GD-MS shown in Figure 5.6 is the different intensity ratio of $^{208}\text{Pb}^+$ to $^{209}\text{Bi}^+$. In ICP-MS, $^{208}\text{Pb}^+$ signal is much higher than that of $^{209}\text{Bi}^+$. However, in GD-MS, the opposite situation can be observed, where the signal of ^{209}Bi is slightly higher than that of $^{208}\text{Pb}^+$. This suggests that the degree of ionization is higher for Pb than that for Bi in the ICP (97.93% for Pb contrasts to 94.14% for Bi in one report [8]) although the compositions of two elements are almost the same in this sample (Bi 0.022% and Pb 0.019%). The sputter step inherent in glow discharges ablates atoms of all elements generally in a uniform manner and the various collision mechanisms in the plasma are sufficiently energetic to ionize indiscriminately, so that both Pb and Bi could be released readily and ionized uniformly. That is perhaps why there is no significant difference in intensity between both signals in GD-MS. Again, a similar circumstance can be noticed in Figure 5.4 where the ratio of $^{120}\text{Sn}^+$ to $^{121}\text{Sb}^+$ in GD-MS is totally different from that in ICP-MS, with the GD-MS results indicating a more uniform response. An opposite situation can be observed in Figure 5.3, where $^{23}\text{Na}^+$ signal shows the different intensity between ICP-MS and GD-MS. Both Li and Na are the lowest components in the aluminum standard (see Table 5.1). However, the signal for $^{23}\text{Na}^+$ in ICP-MS is much higher than that in GD-MS, while the $^7\text{Li}^+$ signal is obscured by a multiply charged argon species (Ar^{6+}) in GD-MS. The source of the Na might come from the dissolution of the aluminum sample with hydrochloric acid.

Another difference noted is the absence of the niobium signal at m/z 93 in the GD-MS spectrum (Figure 5.4). There might be a difference in sputtering yield between Zr and Nb, i.e., niobium seems much more difficult to sputter than

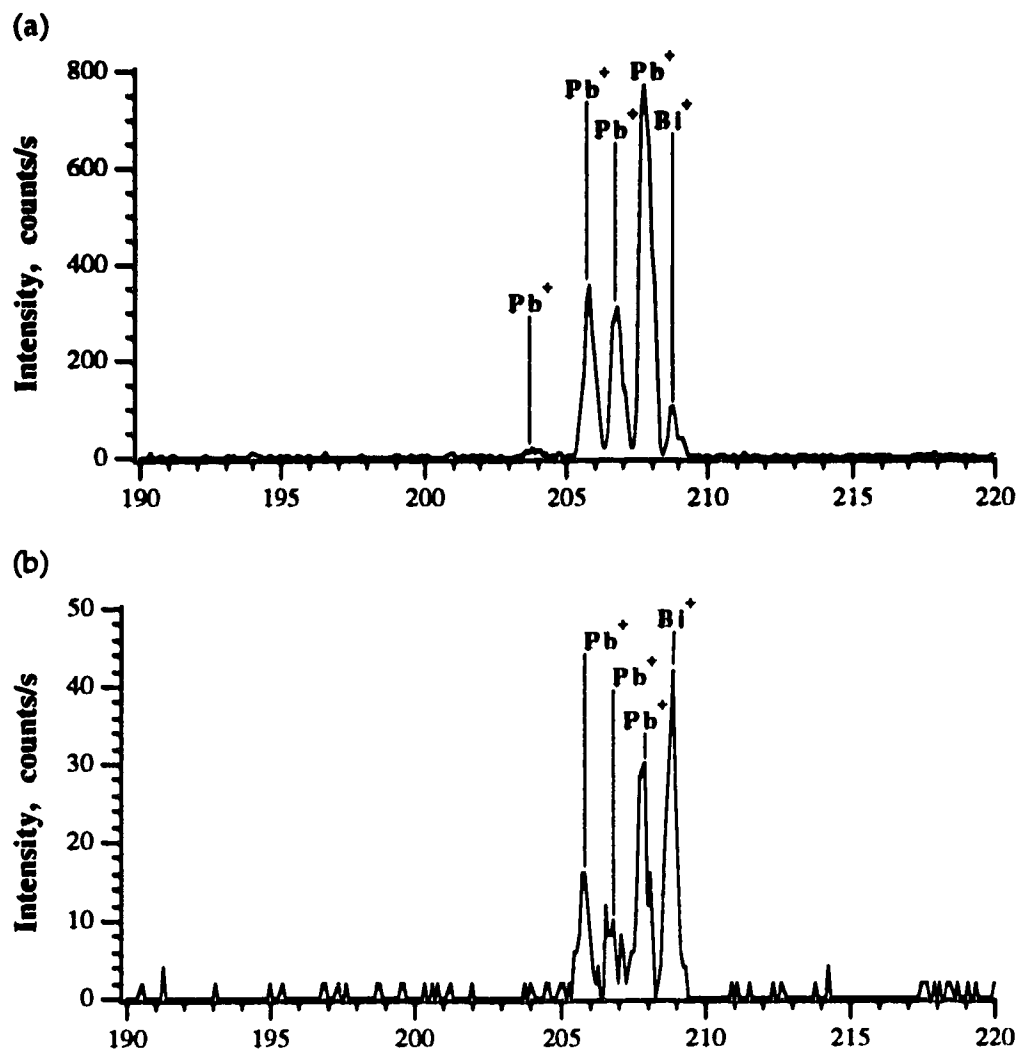


Figure 5.6 Mass spectra for (a) ICP-MS and (b) GD-MS of Alcan aluminum alloy (1SCXG) in the mass range 190-220 m/z .

zirconium in a glow discharge. Not only is the $^{93}\text{Nb}^+$ mono-isotopic signal observed in ICP-MS, but also the mono-oxide NbO^+ signal can be found at m/z 109 in a 9% level ($^{93}\text{NbO}^+ / ^{93}\text{Nb}^+$), which supports the presence of niobium. Although a number of possible molecular interferences (such as $^{23}\text{Na}^{35}\text{Cl}_2^+$, $^{58}\text{Ni}^{35}\text{Cl}^+$, $^{40}\text{Ar}^{37}\text{ClO}^+$, $^{40}\text{Ar}^{35}\text{Cl}\cdot\text{H}_2\text{O}^+$, $^{40}\text{Ar}^{36}\text{ArOH}^+$, $^{40}\text{Ar}_2^{12}\text{CH}^+$, $^{27}\text{AlO}_2(\text{OH})_2^+$ and $^{27}\text{AlClNOH}^+$) can be considered, there is no sound evidence to confirm that the signal at m/z 93 is coming from a background interference in ICP-MS. For Example, $^{23}\text{Na}^{35}\text{Cl}_2^+$ may be suspected, but both $^{23}\text{Na}^+$ and $^{35}\text{Cl}_2^+$ signals are very weak. In addition, in the spectrum, there is no $^{60}\text{Ni}^{35}\text{Cl}^+$ signal to support the presence of $^{58}\text{Ni}^{35}\text{Cl}^+$ and no $^{40}\text{Ar}^{35}\text{ClO}^+$ signal to support the presence of $^{40}\text{Ar}^{37}\text{ClO}^+$ from the point of view of isotopic information. Moreover, the $^{40}\text{Ar}^{35}\text{Cl}^+$ and $^{40}\text{Ar}^{36}\text{ArH}^+$ signals are very weak, it is impossible to produce a higher signal of $^{40}\text{Ar}^{35}\text{Cl}\cdot\text{H}_2\text{O}^+$ or $^{40}\text{Ar}^{36}\text{ArOH}^+$, and there is no $^{40}\text{Ar}^{36}\text{ArO}^+$ signal to support the presence of $^{40}\text{Ar}^{36}\text{ArOH}^+$ as well. Also, there is no evidence to prove the existence of $^{27}\text{AlO}_2(\text{OH})_2^+$ and $^{27}\text{AlClNOH}^+$ from the point of view of fragment ion information in the mass spectrum. On the other hand, the Nb could have come from contamination introduced during dissolution and/or the machining step used to cut some Al from the rod form standard.

5.3.3 Comparison of detection limits

Detection limits for ICP-MS are typically in the 0.001-0.01 p.p.b. range (ng/mL) for solution samples[9], while the detection limits for GD-MS are usually in the 10-100 p.p.b. range (ng/g) directly in the solid samples. Thus, the detection limits in ICP-MS are superior, even when dilution is taken into account, where the detection limits are 0.1-1 p.p.b. (ng/mL) for a dissolved solid

sample in 1% solutions. However, 1% solutions are still difficult to run in ICP-MS because of severe matrix effects. In this experiment, 0.01% Al solutions were aspirated for ICP-MS comparing with directly solid sampling in GD-MS. There was no significant difference in signal intensities for most elements between ICP-MS and GD-MS spectra, so that the detection limits became comparable for these two methods under ICP solution conditions that minimized matrix effects, *i.e.* diluted solutions.

5.4 Conclusions

Both inductively coupled plasma mass spectrometry (ICP-MS) and glow discharge mass spectrometry (GD-MS) can be considered as very useful methods to carry out elemental analyses with a broad coverage of the periodic table. With a direct solid sampling technique, glow discharge works as a "dry plasma" source into which almost no water or air is being introduced. Thus the solvent and/or air dependent background species are significantly reduced or even eliminated in GD-MS compared with ICP-MS. On the other hand, the argon-based background species (such as multiply ionized argon ions, argon dimers and argides) tend to be more complicated in GD-MS than those in ICP-MS, but these did not bring so many interference problems to the analysis. For 0.01% Al solutions aspirated in ICP-MS, the analyte signal intensities are comparable to or slightly higher than those in GD-MS.

References

1. Y. Shao and G. Horlick, *Spectrochimica Acta* **46B**, 165 (1991).
2. S. H. Tan and G. Horlick, *Appl. Spectrosc.* **40**, 445 (1986).
3. M. A. Vaughan and G. Horlick, *Appl. Spectrosc.* **40**, 434 (1986).
4. H. Evans and L. Ebdon, *J. Anal. At. Spectrom.* **4**, 299 (1989).
5. K. E. Jarvis, A. L. Gray and E. McCurdy, *J. Anal. At. Spectrom.* **4**, 743 (1989).
6. B. S. Sheppard, W. L. Shen, J. A. Caruso, D.T. Heitkemper and F. L. Fricke, *J. Anal. At. Spectrom.* **5**, 431 (1990).
7. W. W. Harrison and B. L. Bentz, *Prog. Anal. At. Spectrosc.* **11**, 53 (1988).
8. N. Furuta, *Spectrochimica Acta* **41B**, 1115 (1986).
9. G. Horlick, *Spectroscopy* **7**, 22 (1992).

Chapter 6

Alcan DataBase: A Computer Program for Management and Display of ICP-MS and GD-MS Spectral Data

6.1 Introduction

Both inductively coupled plasma mass spectrometry (ICP-MS) and glow discharge mass spectrometry (GD-MS) are very useful methods to carry out elemental analysis with a broad coverage of the periodic table. As has been shown in the last three chapters, ICP-MS and GD-MS can be used successfully for aluminum samples.

The simplicity of elemental mass spectra relative to atomic emission spectra is an important advantage of ICP-MS over ICP-AES. Both ICP and GD mass spectra are less complicated compared with optical emission methods and isotopic information is provided. However, the mass spectrometric methods are by no means interference free. For both ICP-MS and GD-MS, spectral interferences include isobaric interferences, interferences from the support gas and other background gases, and molecular interferences from matrix components in combination with other plasma species. Moreover, the spectral characteristics of ICP-MS and GD-MS for the analysis of aluminum samples are also quite different. Glow discharge works as a "dry plasma" source into which almost no water or air is introduced. Thus the solvent and/or air dependent background species are significantly reduced or even eliminated in GD-MS

compared to ICP-MS. On the other hand, the argon-based background species (such as multiply ionized argon ions, argon dimers and argides) tend to be more complicated in GD-MS than those in ICP-MS.

Computers have become an essential part of spectrochemical research for both data acquisition and data processing [1], and an effective computerized data base can be considered as one of the most useful tools for the management of analytical results and analytical information. A computer program, Alcan DataBase, for Microsoft Windows (386 or 486 computers) has been developed. Alcan DataBase is a graphically-oriented database for the analysis of aluminum alloy samples with both ICP-MS and GD-MS. Five low alloy aluminum samples from Alcan were analyzed by ICP-MS and GD-MS, and the spectral data (1-125 m/z) for these standards were installed in this program. Alcan DataBase provides the ability to compare and contrast the different spectral characteristics of ICP-MS and GD-MS, and also can be used to demonstrate the qualitative analysis capability of ICP-MS and GD-MS. The comparison windows of ICP-MS and GD-MS for the Alcan 1SCXG standard are displayed in Figure 6.1.

The background spectral features and the spectral interferences of both ICP-MS and GD-MS are also listed. Since hydrochloric acid was used to dissolve the aluminum samples which were run as 0.01% Al aqueous solutions for ICP-MS, while aluminum samples were directly determined by GD-MS, the background and spectral interferences can be quite different between the two techniques. The interferences can be divided into the following categories: isobarics, matrix dependent background, doubly charged species, oxides (including hydroxides and hydrides), acid dependent background for ICP, and argides and dimers especially for the glow discharge. The interference database

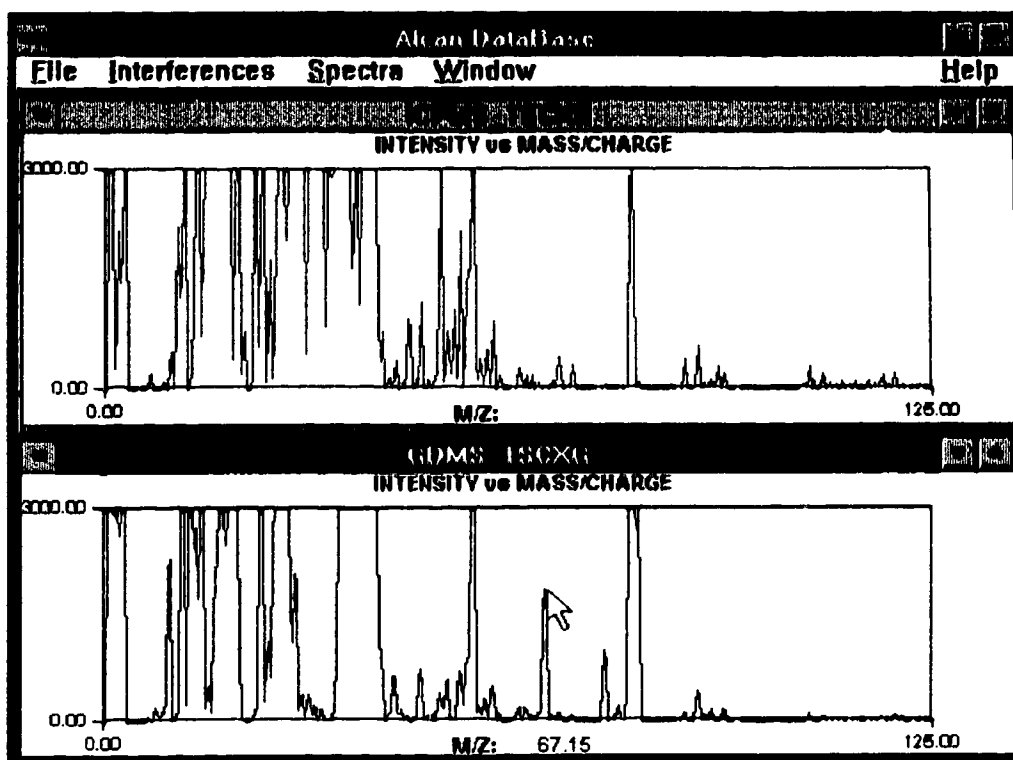


Figure 6.1 Comparison of spectral characteristics of ICP-MS and GD-MS windows

can be modified by the user and new interferences can be added or old ones deleted.

For qualitative elemental analysis, a mass spectrum window can be opened along with a periodic table, from which bar graphs of the isotope pattern and the tables of the isotopic abundance for all the elements can be obtained. This makes it easy to recognize the elements present in the spectrum that is displayed (see Figure 6.2). The program is written for users who are interested in inorganic mass spectrometry using a quadrupole mass analyzer. Thus, the largest mass for the program is 238 m/z , and all of the interferences are listed at their nominal mass positions.

The basic isobaric and background spectral interferences in ICP-MS have been well documented [2, 3] and a simple computer program for the Macintosh was developed to facilitate accessing interference data as early as 1987 [4]. However, the concept for the program Alcan DataBase is based on the software of MS InterView which was published as a Macintosh application in 1992 [5]. MS InterView shows the background interferences for ICP-MS with very limited data for GD-MS. Alcan DataBase focuses on the comparison of sample spectral characteristics of ICP-MS and GD-MS with respect to the analysis of aluminum samples, as well as providing a graphic platform for the qualitative analysis of unknown aluminum samples. In addition, the data for the natural abundances of the isotopes were updated using a recent IUPAC compilation [6]. Finally, the spectral interferences of both ICP-MS and GD-MS were updated with particular focus on the analysis of aluminum samples.

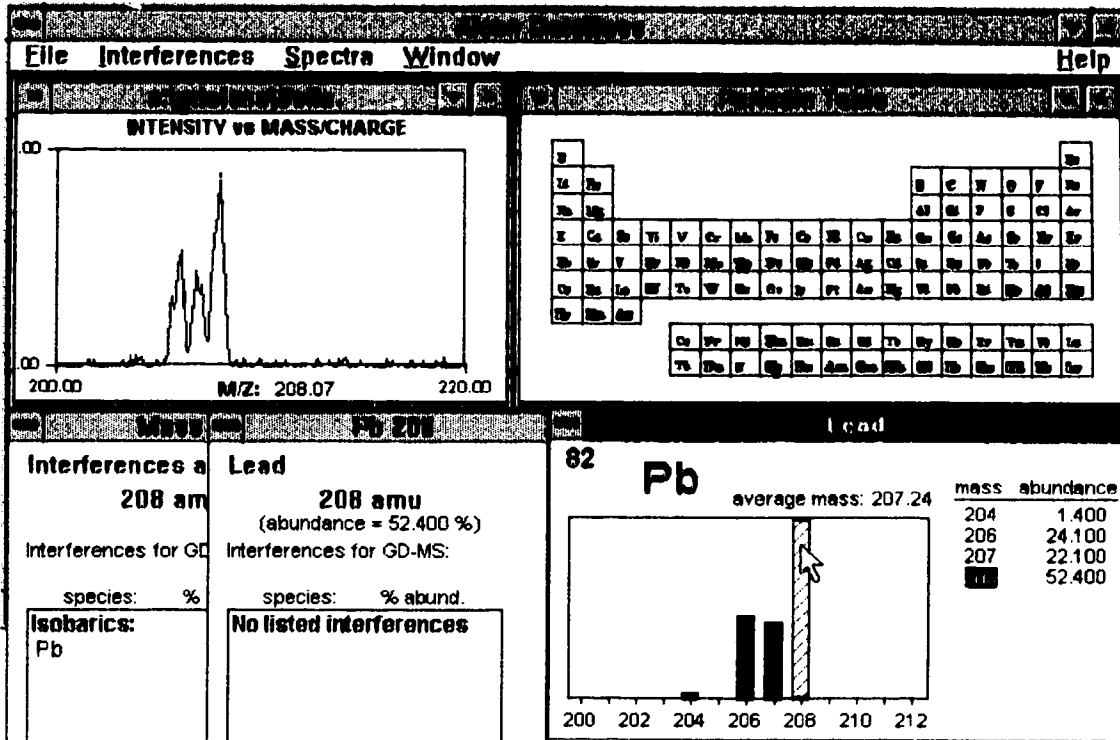


Figure 6.2 MDI windows for qualitative elemental analysis of lead

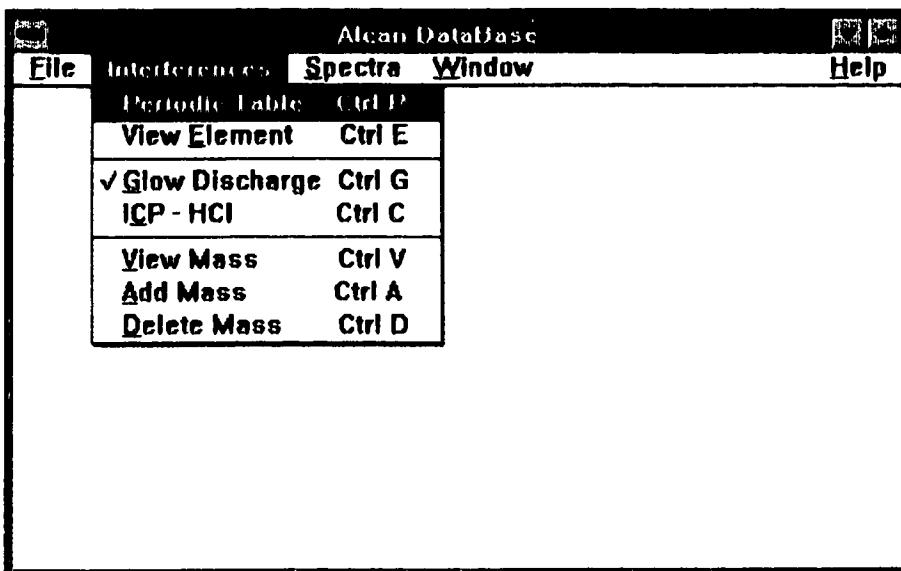
Object-oriented programming (OOP) was used to develop this program. OOP represents a recent stage in the development of programming technology. OOP language simplifies the task of programming for a window environment, allowing the application developer to focus on the application's function, rather than its form. OOP has the capability to manage very large programming projects by breaking up large problems into smaller, independently functioning, highly visible parts. It works in a truly modular programming environment where redundancies in coding are kept at an absolute minimum. It also provides the ability to spawn multiple instances of a given function or object from the same code without the codes, for the instances, interfering with one another [7]. As has been recently discussed [8], the OOP language makes it easier to evaluate and modify the program than non-OOP language. As a result, one can use the OOP to write Windows programs with much less time and effort than with non-object-oriented approaches.

6.2 Alcan DataBase

Alcan DataBase was written and compiled using Borland's Turbo Pascal for Microsoft Windows. The multiple document interface (MDI) window method was used to construct this program. The main frame window named Alcan DataBase contains a menu bar which includes *File*, *Interferences*, *Spectra*, *Window* and *Help* menus (see Figure 6.3a). These "pull-down" menus and the commands that the menus contain are shown in Figure 6.3b.

Alcan DataBase can be is described in two different environments. One is the Menus and another is the Windows.

(a)



(b)

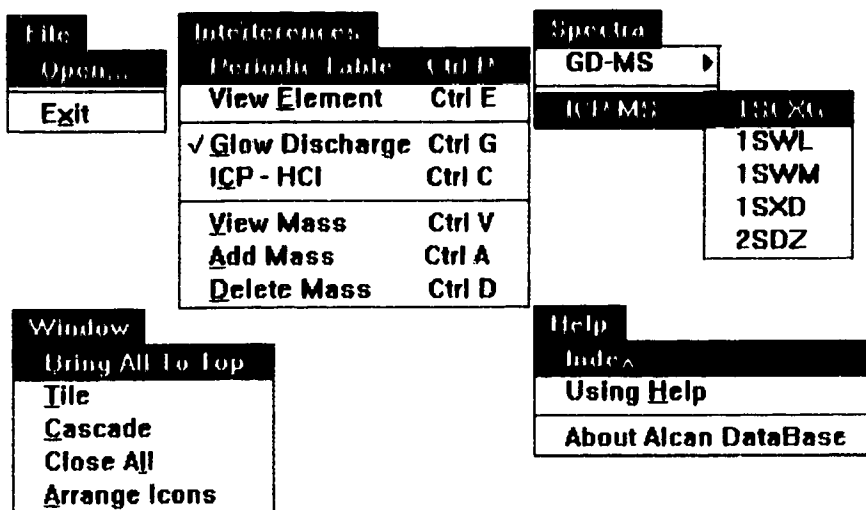


Figure 6.3 Alcan DataBase (a) main frame window and (b) pull down menus

6.2.1 Menus

6.2.1.1 File menu

The *File menu* includes *Open* and *Exit* commands. The *Open* command enables one to open stored spectrum files in which the data should be written in text format with mass in the first column and intensity in the second column. Thus a spectrum window can be opened containing an unknown aluminum sample spectrum which can then be analyzed by clicking on the unknown peaks in the spectrum or by comparison to a standard spectrum. The *Exit* command allows the user to cancel the *Alcan DataBase* application. The name of each opened MDI window (such as the periodic table window and spectrum windows) is automatically appended to the end of the *File Menu* and the currently selected window is marked with a check mark.

6.2.1.2 Interferences menu

The *Interferences menu* includes commands for opening a periodic table window, showing element windows, viewing a specific interference mass window, and selecting the spectrum background for either glow discharge or ICP. This menu is also used to add and/or delete interferences from the database. All of the commands in the *interferences menu* can be performed by using an accelerator method. An accelerator is a keystroke defined by the database to give the user a quick way to perform a task. For example, a periodic table window can also be opened simply by pressing "Ctrl + P" on the keyboard. The definitions of the accelerators are shown in the *interferences menu* (see Figure 6.3).

i. Change background

The interference background can be selected by choosing *ICP-HCl* or *Glow Discharge* Item. When hydrochloric acid is chosen as the background, several types of interferences are listed, such as 'Isobarics', 'Doubly charged', 'Oxides/Hydroxides/Hydrides' ('MO/MOH/MH') and 'Matrix dependent' background. When glow discharge is chosen as the background, the listed interferences will be: 'Isobarics', 'Doubly charged', 'Argides', 'Dimers' and 'GD background'.

ii. View a mass interference window

Choosing *View Mass Item* will prompt the user to enter a mass value at which to open a mass window listing the interferences. Since only one mass window can be opened, the *View Mass Item* is already turned to the *Change Mass Item*. A new mass window will be re-drawn after it is selected.

iii. Add a mass interference

In order to add a particular interference into the current interference file, choose *Add Mass Item* and you will be prompted for the mass, the name, the isotopic abundance of the species, and its 'category'. The name of the interference will be automatically formatted so that all numbers will be printed as subscripts unless immediately preceded by a '+' sign to indicate a multiply charged species (e.g. enter Ar(+2)). Note that you cannot add to the 'Isobarics' category. Any added interferences will automatically be saved to disk.

iv. Delete a mass interference

In order to delete a particular interference from the current interference file, you must first select the interference to be removed by clicking on it in any

open interference window and then immediately choosing *Delete Mass Item* from the Interferences menu. You will be asked to confirm the deletion, which will automatically be removed from the current interference file. Isobaric interferences cannot be deleted. Note that if you hold down the shift key before choosing *Delete Mass Item* the confirmation step will be skipped.

6.2.1.3 Spectra menu

The *Spectra menu* allows one to access the standard spectra. Spectra for five low alloy aluminum standards from Alcan are available (1SCXG, 1SWL, 1SWM, 1SXD and 2SDZ). Both ICP and glow discharge mass spectra for these standards are stored, and both ICP and GD mass spectra for one specific standard can be opened and compared.

6.2.1.4 Window menu

Window menu controls the MDI child windows with items such as *Tile*, *Cascade*, *Arrange Icons* and *Close All*. The periodic table window and spectrum windows belong to the MDI child windows. Each child window has some characteristics of an overlapped window. It can be tiled (all windows take up all the available space without overlapping) or cascaded (all windows overlap and display the title bar of each one). A child window also can be maximized to the full size of its parent window or minimized to an icon, which sits above the bottom edge of the frame window. MDI child windows tiled in their main frame window are shown in Figure 6.4. They never appear outside the borders of their frame window.

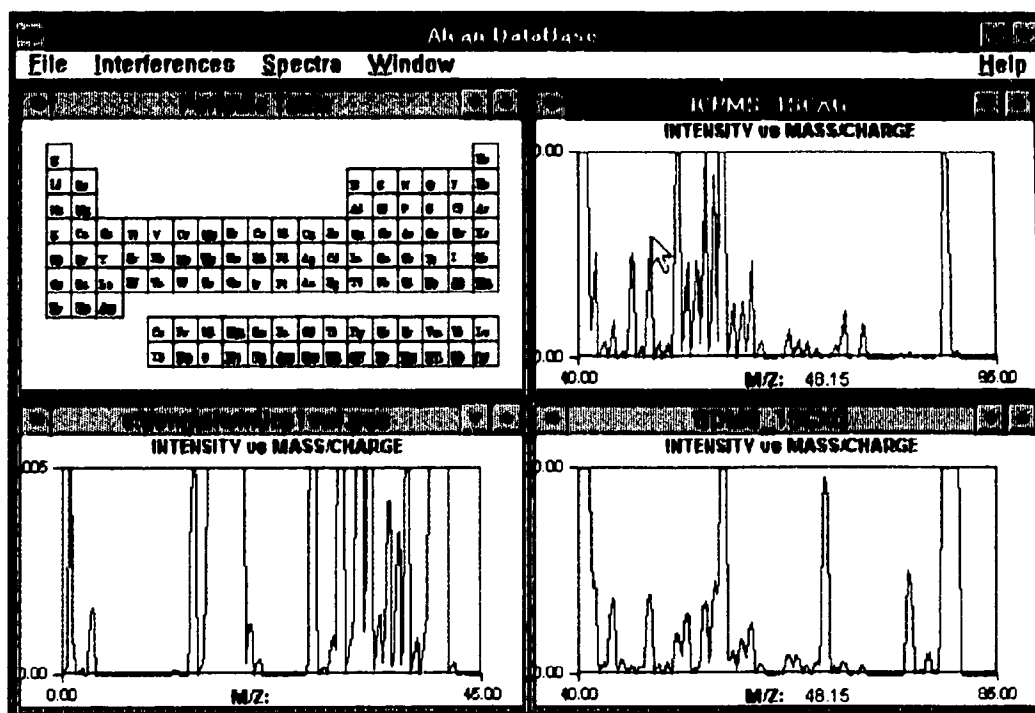


Figure 6.4 Tiled MDI Child windows in their main frame window

6.2.1.5 Help menu

The *Help Menu* provides the window-sensitive on-line help system for Alcan DataBase. A help index window is displayed in Figure 6.5. One may get help by pulling down the *Help Menu* or directly clicking the right button of the mouse on a specific window.

6.2.2 Windows

6.2.2.1 Spectrum windows

A spectrum window can be opened by selecting an item from the *Spectra Menu*. This menu item contains ICP and GD mass spectra for each standard sample (see Figure 6.3b). You can scale either of the two axes by double-clicking on them. Dialog boxes will be presented for the user to set the mass and/or intensity range. Mass/z (or m/z) value can be displayed on the bottom of the spectrum window by moving the cursor on the window. Double-clicking directly on the spectrum itself will open an interference window (or mass window) for the mass clicked on and, if necessary, will change the selected interference background to match that of the spectrum. Three spectrum windows are shown in Figure 6.4 with the cursor pointing at 48 m/z. Normally, red represents ICP-MS, blue represents GD-MS and black represents a spectrum read in from disk.

6.2.2.2 Periodic table window

The periodic table window displayed in Figures 6.4 and 6.6 is an interface leading to the isotopic abundance information of the elements as well as to the interference data. Isotopic abundance information is provided for 83 elements, but no isotopic information is available for the 20 elements written in outline

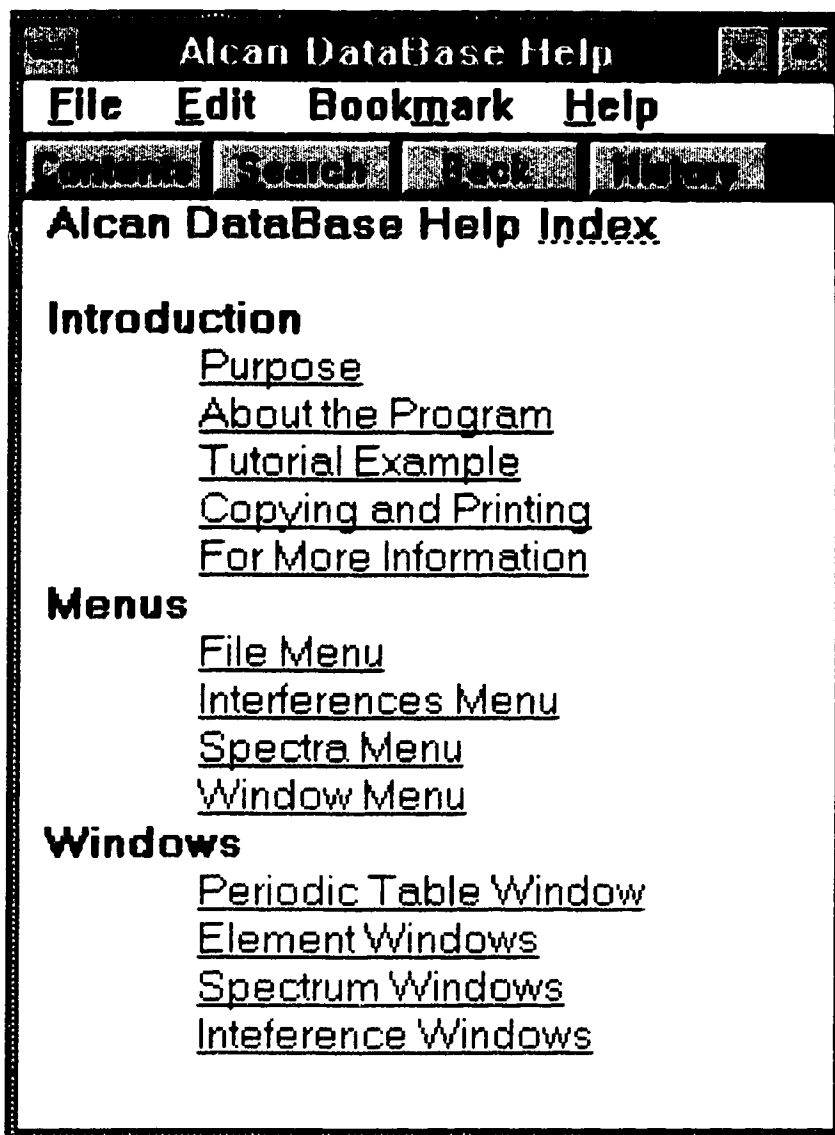


Figure 6.5 Alcan DataBase help index window

Alcan DataBase

File Interferences Spectra Window Help

Periodic Table

H																		He																												
Li	Be											B	C	N	O	F		Ne																												
Na	Mg											Al	Si	P	S	Cl		Ar																												
K	Ca	Sc	Ti	V	Cr	Mn	Fe	Co	Ni	Cu	Zn	Ga	Ge	As	Se	Br		Kr																												
Rb	Sr	Y	Zr	Nb	Mo	Tc	Ru	Rh	Pd	Ag	Cd	In	Sn	Sb	Te	I		Xe																												
Cs	Ba	La	Hf	Ta	W	Re	Os	Ir	Pt	Au	Hg	Tl	Pb	Bi	Po	At		Rn																												
Rf	Ra	Ac																																												
			<table border="1"> <tbody> <tr> <td>Ce</td> <td>Pr</td> <td>Nd</td> <td>Pm</td> <td>Sm</td> <td>Eu</td> <td>Gd</td> <td>Tb</td> <td>Dy</td> <td>Ho</td> <td>Er</td> <td>Tm</td> <td>Yb</td> <td>Lu</td> </tr> <tr> <td>Th</td> <td>Pa</td> <td>U</td> <td>Np</td> <td>Pu</td> <td>Am</td> <td>Cm</td> <td>Bk</td> <td>Cf</td> <td>Es</td> <td>Fm</td> <td>Mn</td> <td>Nb</td> <td>Lr</td> </tr> </tbody> </table>																Ce	Pr	Nd	Pm	Sm	Eu	Gd	Tb	Dy	Ho	Er	Tm	Yb	Lu	Th	Pa	U	Np	Pu	Am	Cm	Bk	Cf	Es	Fm	Mn	Nb	Lr
Ce	Pr	Nd	Pm	Sm	Eu	Gd	Tb	Dy	Ho	Er	Tm	Yb	Lu																																	
Th	Pa	U	Np	Pu	Am	Cm	Bk	Cf	Es	Fm	Mn	Nb	Lr																																	

Figure 6.6 Alcan DataBase main frame window and the periodic table window

type (see Figure 6.6). A single-click on an element in the periodic table will highlight it. Simply double-clicking on the element will open an element window which contains an isotopic abundance table and a bar graph of the mass spectrum of the element.

6.2.2.3 Element windows

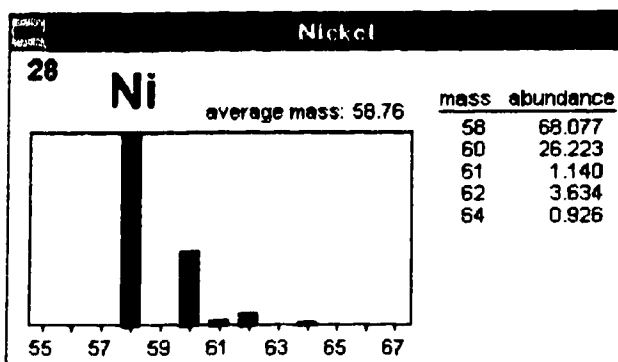
An element window contains a graph with isotope bars and an isotopic abundance table for that element. The element windows can also be accessed by double-clicking an element from the periodic table window or alternatively choosing the *View Element Item* under the *Interferences Menu* and entering the atomic symbol of a specific element. A nickel element window is shown as an example in Figure 6.7a. A single-click on an isotope bar will highlight the bar and the corresponding mass in the abundance table. Double-clicking on either an isotope bar or its corresponding mass in the table will open an isotope window listing the interferences at that mass. Figure 6.7b shows $^{58}\text{Ni}^+$ isotope windows for both ICP-HCl and GD backgrounds. You may have any number of both the element and isotope windows simultaneously open.

Double-clicking on the left vertical axis of the element window will open a dialog box which will allow you to scale the bar graph's vertical axis to 100% rather than to the default of the most abundant isotope.

6.2.2.4 Interference windows

Interference windows include a mass window and/or any isotope windows. The mass window can be opened by double-clicking a specific mass/z position on a spectrum window or alternatively selecting the *View Mass Item* under the *Interferences menu*, while the isotope windows only can be opened

(a)



(b)

Ni 58		Ni 58	
Nickel		Nickel	
58 amu (abundance = 68.077 %)		58 amu (abundance = 68.077 %)	
Interferences in HCl for ICP-MS:		Interferences for GD-MS:	
species:	% abund.	species:	% abund.
Isobarics:		Isobarics:	
Fe	0.280	Fe	0.000
Doubly charged:		Doubly charged:	
Cd	7.580	Cd	7.580
Background:			
ArO	0.199		
ArOH	0.040		
Matrix dependent:			
NaCl	75.800		
Oxides/Hydrides:			

Figure 6.7 (a) A nickel element window and (b) $^{58}\text{Ni}^+$ isotope windows for interferences in both ICP-MS and GD-MS

by double-clicking on isotope bars from an element window (see Figure 6.7). Both interference windows can show either the isobaric and background interferences which can be selected for ICP-MS or GD-MS. Figure 6.8 shows the mass window for mass 51 which displays ICP-MS interferences with HCl background. The "% abund." column in the interference window refers to the percentage natural abundance of the particular interfering species. For example, 75.648% of all ClO has a mass of 51 m/z. It can be seen that hydrochloric acid (ClO) would interfere with the determination of vanadium in ICP-MS, while there are no interferences for GD-MS at this mass.

In contrast to MDI Child windows, the element and interference windows cannot be resized. They may appear outside the borders of the main frame window or behind the main window. The name of the element and mass windows can be appended at the bottom of the *Window menu*. The *Bring All To Top* command under the *Window menu* will bring all of them in front of the main window.

Printing is not implemented for this database. However, all of the program's windows can be copied to the clipboard simply by pressing 'Print Screen' function key. After that, it is allowed to paste the image into another window-program (such as Microsoft Word 2.0) for printing.

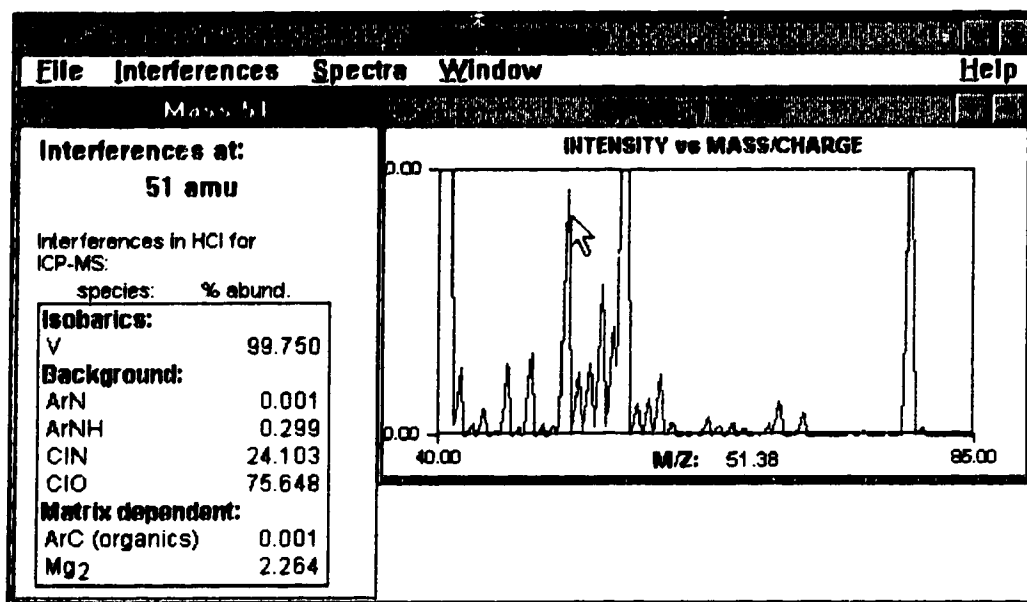


Figure 6.8 Mass 51 window is opened by double-clicking on the peak at m/z 51 in an ICP spectrum window

6.3 Conclusions

A computer database has been developed to help manage ICP-MS and GD-MS spectral data. Alcan DataBase provides the ability to compare and contrast the different spectral characteristics of ICP-MS and GD-MS, and also has the capability to assist in the qualitative analysis of unknown aluminum samples. Various customer spectrum windows can be opened and the data of the natural abundances has been updated to 1991. Moreover, a window-sensitive on-line help system for Alcan DataBase is also provided.

References

1. G. B. King and G. Horlick, *Spectrochimica Acta* **47B**, E353-E370 (1992).
2. M. A. Vaughan and G. Horlick, *Appl. Spectrosc.* **40**, 434 (1986).
3. S. H. Tan and G. Horlick, *Appl. Spectrosc.* **40**, 445 (1986).
4. M. A. Vaughan and G. Horlick, *Appl. Spectrosc.* **41**, 523 (1987).
5. L. L. Burton and G. Horlick, *Spectrochimica Acta* **47B**, E1621-E1627 (1992).
6. IUPAC New Isotopic Composition of the Elements, *Pure and Appl. Chem.* **63**, 991-1002 (1991).
7. Ernest R. Tello, *Object-Oriented Programming For Windows™*, John Wiley & Sons, Inc. New York, pp 29-42, (1991)
8. M. W. Borer, N. N. Sesi, T. K. Starn and G. M. Hieftje, *Spectrochimica Acta* **47B**, E1135-E1151 (1992).

Chapter 7

Analysis of Aluminum and Steel Samples Using Laser Ablation Inductively Coupled Plasma Mass Spectrometry

7.1 Introduction

Inductively coupled plasma mass spectrometry (ICP-MS) is usually used for the determination of trace and/or ultra trace amounts of elements in solution samples. However, direct solid sample analysis techniques using ICP-MS have been developed in recent years. These include: direct sample insertion (DSI-ICP-MS) [1-4], glow discharge (GD-MS) [5-9] and laser ablation (LA-ICP-MS) [10-13]. Interaction of laser radiation with a solid may cause ablation, vaporization, and excitation by processes that depend upon both the characteristics of the laser beam and the physical properties of the solid. The various species produced, including particulates, ground-state atoms, excited atoms and ions, have all been utilized for elemental analysis via atomic absorption (AA), atomic emission spectroscopy (AES), and mass spectrometry (MS). The advantages of using lasers for the analysis of solids include little or no sample preparation, resulting in high sample throughput; application to almost all materials including both conductors and non-conductors; and high spatial resolution, allowing analysis of small selected areas. Laser ablation has been combined with AA [14, 15], microwave induced plasmas (MIP-AES) [16, 17], ICP-AES [18-21], and ICP-MS [22]. LA-ICP-MS is normally carried out using an external ablation chamber

which separates the sample introduction from sample atomization, excitation and ionization in two steps. In external chamber LA-ICP-MS, the sample is first ablated in the chamber. The laser ablated material could contain atoms and particles. These are then carried by an argon transport-gas directly into the plasma where they are atomized, vaporized, excited and ionized.

As the solid is not dissolved, little or no sample preparation is necessary and the solid is not diluted. The direct analysis of solids can be carried out without the use of chemical reagents and without the processes of dissolution and dilution which could introduce contamination or cause loss of the analyte. As no acid or solvent is used, the polyatomic interferences are less problematic and contamination effects are unlikely in LA-ICP-MS. Dissolution will also dilute the low concentrations of the minor elements, lowering the power of detection. Solution nebulization delivers only a small percentage of the sample into the plasma whereas direct solid injection with laser ablation sends most of the sample into the plasma. The strength of LA-ICP-MS for a fast semiquantitative survey analysis of solids and pressed powders has been demonstrated [23]. Major and trace elements down to the sub-ppm level can be directly determined in this way. Sample preparation and any knowledge about the composition is not necessary. Non-conducting solids such as oxides, and geological refractory materials can be analyzed by laser ablation. For example, trace impurities in uranium oxide (U_3O_8) have been determined using LA-ICP-MS [24]. Zircon samples containing Hf, Y, Re, Th and U were analyzed by both laser ablation and solution ICP-MS [25]. A novel surface analytical technique, resonant laser ablation (RLA), has been investigated by detecting small quantities of aluminum in NIST SRM steel samples [26]. It has been estimated

that detection levels down to a few ppm were achievable by RLA-ICP-MS for aluminum in steel samples.

In this report, an external chamber laser ablation ICP-MS technique is investigated. Bulk metal samples were ablated and analyzed with this method. Simultaneously multielement analyses of aluminum and steel samples are presented with a particular emphasis placed on the utility of the minor isotope of iron (m/z 57) as an internal standard.

7.2 Experimental

A neodymium laser is a common solid-state ion laser that uses the Nd^{3+} ion in a host crystal such as yttrium aluminum garnet (YAG), $\text{Y}_3\text{Al}_5\text{O}_{12}$. A Nd:YAG Laser Photonics (12351 Research Pkwy Orlando, FL 32826) laser was used to ablate the disk samples. The laser was operated in a pulsed mode. The typical pulse width was 15 ns with a pulse energy of about 100 mJ/pulse and an output wavelength of 1.06 μm . The pulse repetition rate could be adjusted to 1, 5, 10, 15 or 20 Hz.

A schematic diagram of the external chamber laser ablation ICP-MS system is shown in Figure 7.1. A quartz ablation chamber was used as a site for vaporization of samples by the laser beam. The jacketed chamber is 35 mm in diameter and 75 mm in length. The inner tube is about 20 mm in diameter and 5 mm shorter than the outer quartz chamber. The inner diameter of the inner tube is 17 mm. The disk sample is pressed on the chamber and sealed by an o-ring. The argon gas is introduced through an inlet tube directly into the inner chamber and blows across the surface of the sample (see Figure 7.2). A lens with

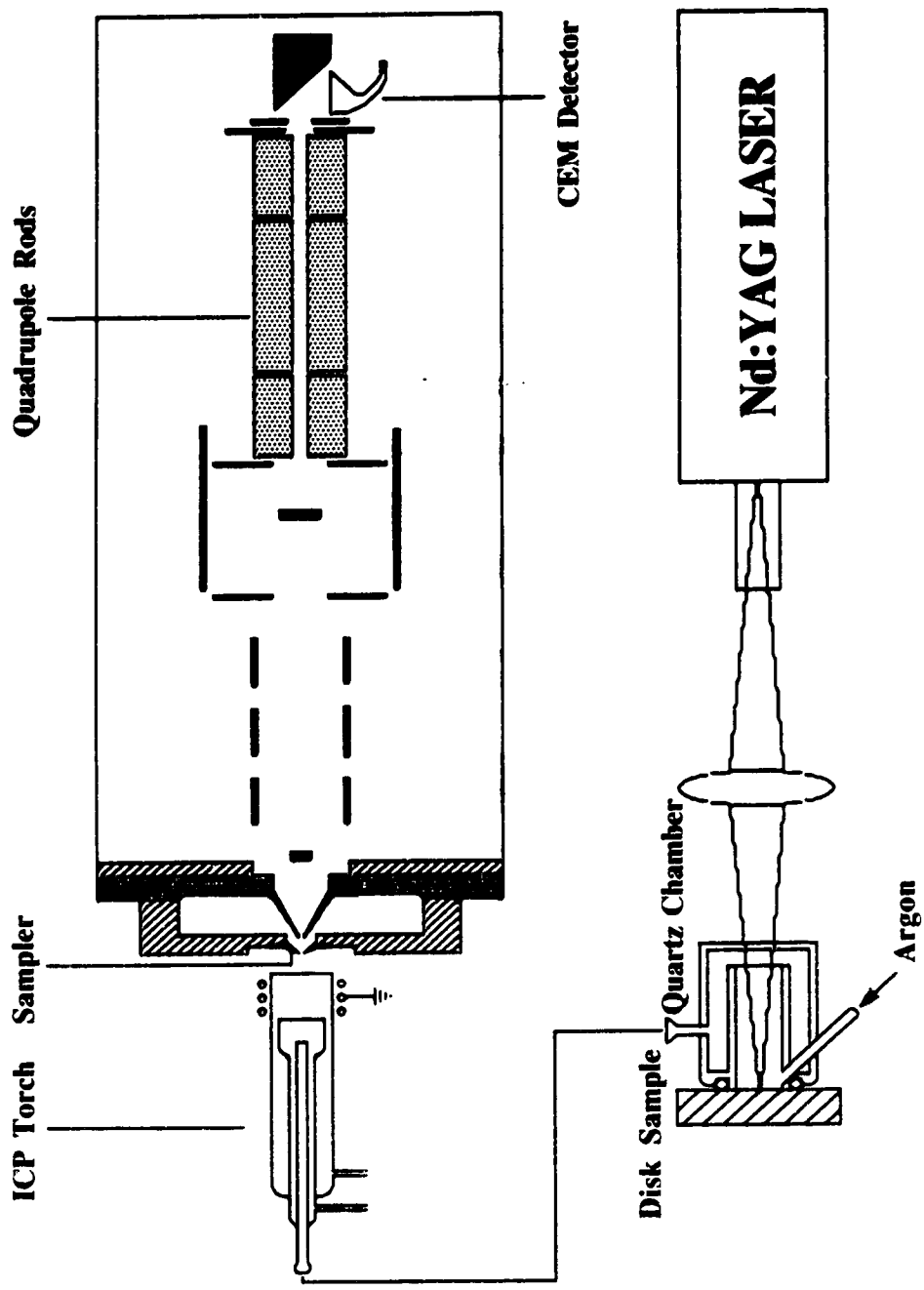


Figure 7.1 Schematic diagram of external chamber laser ablation ICP-MS system

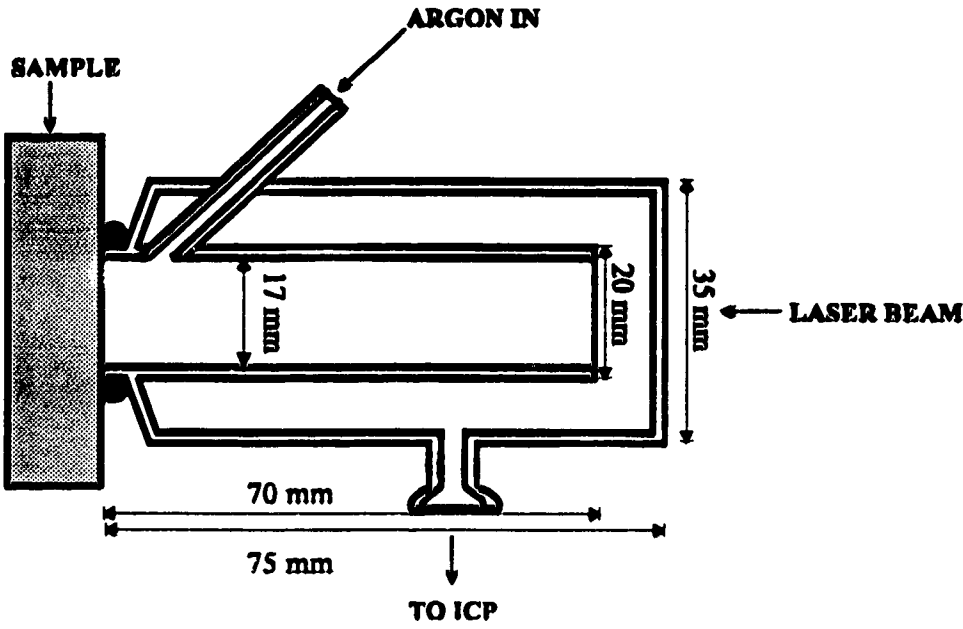


Figure 7.2 Schematic diagram of the quartz ablation chamber

a focal length of 10 cm is used to focus the laser beam directly onto the surface of the sample.

Eight standard aluminum samples from Alcoa and eight NIST SRM steel samples were chosen for this work. The aluminum samples included three low alloy and five high alloy Al standards, while the steel samples included four low alloy steels and four stainless steel samples. Both the aluminum and the steel samples were in disk form.

A standard SCIEX (Perkin Elmer) Elan Model 250 ICP mass spectrometer was used for all analyses and data acquisition. A standard length MAK optical emission ICP torch was used in conjunction with the external ablation chamber. Compromise conditions of power and central gas flow-rate can be easily obtained for a range of elements. The flow rate yielding the maximum ion count for a given power and sampling depth is essentially the same for most elements. For this work, a sampling depth of 16 mm from the load coil was chosen with a plasma forward power of 1.3 kW in order to obtain high sensitivity. The aerosol (central gas) flow-rate was selected at 0.90 L/min, which was controlled by a Matheson Model 8240-0423 mass-flow controller. The ion lens voltages were a compromise chosen to cover a large mass range. Typical operating parameters are summarized in Table 7.1.

Table 7.1 Typical operating parameters for the LA-ICP-MS system

Plasma---

r. f. forward power	1300 W
Outer gas flow-rate	12 L min ⁻¹ argon
Intermediate gas flow-rate	1.4 L min ⁻¹ argon
Central gas flow-rate	0.9 L min ⁻¹ argon

Mass Spectrometer--

Sampling depth	16 mm from load coil
Sampler, copper	0.9 mm orifice
Skimmer, nickel	0.8 mm orifice

Ion Lens Voltage Setting--

Bessel Box Barrel(B)	+ 5 volts
Bessel Box Plates(P)	-21 volts
Einzel Lens(E1)	-20 volts
Photon Stop(S2)	-23 volts

Laser---

Nd:YAG laser energy per pulse	100 mJ
Output wavelength	1064 nm
Laser pulse width	15 ns
Focal length of lens	10 cm
Repetition rate	15 Hz

7.3 Results and Discussion

7.3.1 Effect of Operating Parameters on Analyte Signals

In order to utilize the technique efficiently and take full advantage of its capability, it is necessary to know the effect of instrument operating parameters on analyte signals. The key variables for were found to be the central gas (carrier gas) flow rate and the forward power. The effect of the central gas flow-rate on the analyte ion signal for $^{24}\text{Mg}^+$, $^{58}\text{Ni}^+$, $^{63}\text{Cu}^+$ and $^{120}\text{Sn}^+$ at 1.3 kW is shown in Figure 7.3. Clearly all these elements exhibit similar behavior and the signal has a relatively sharp maximum value at the central gas flow-rate of 0.9 L/min. The effect of the central gas flow-rate and power on the $^{55}\text{Mn}^+$ signal is illustrated in Figure 7.4. The power is changed from 0.9 to 1.5 kW, and at all of the power settings, the element has its maximum signal value at a different central gas flow-rate. Thus changing the power from 1.3 to 1.5 kW does not increase the signal level unless the central gas flow-rate is also increased from 0.9 to 1.0 L/min.

It was found that the analyte signals are affected by changing the sampling depth (the distance from the load coil to the sampling cone). The effects of the sampling depth on the analyte ion signals for $^{24}\text{Mg}^+$, $^{55}\text{Mn}^+$, $^{63}\text{Cu}^+$ and $^{208}\text{Pb}^+$ at 1.3 kW and 0.9 L/min central gas flow-rate are shown in Figure 7.5. The sampling depth was varied from 15 to 18 mm from load coil. All these elements show the same behavior and the signal has a maximum value at a sampling depth of 16 mm from the load coil.

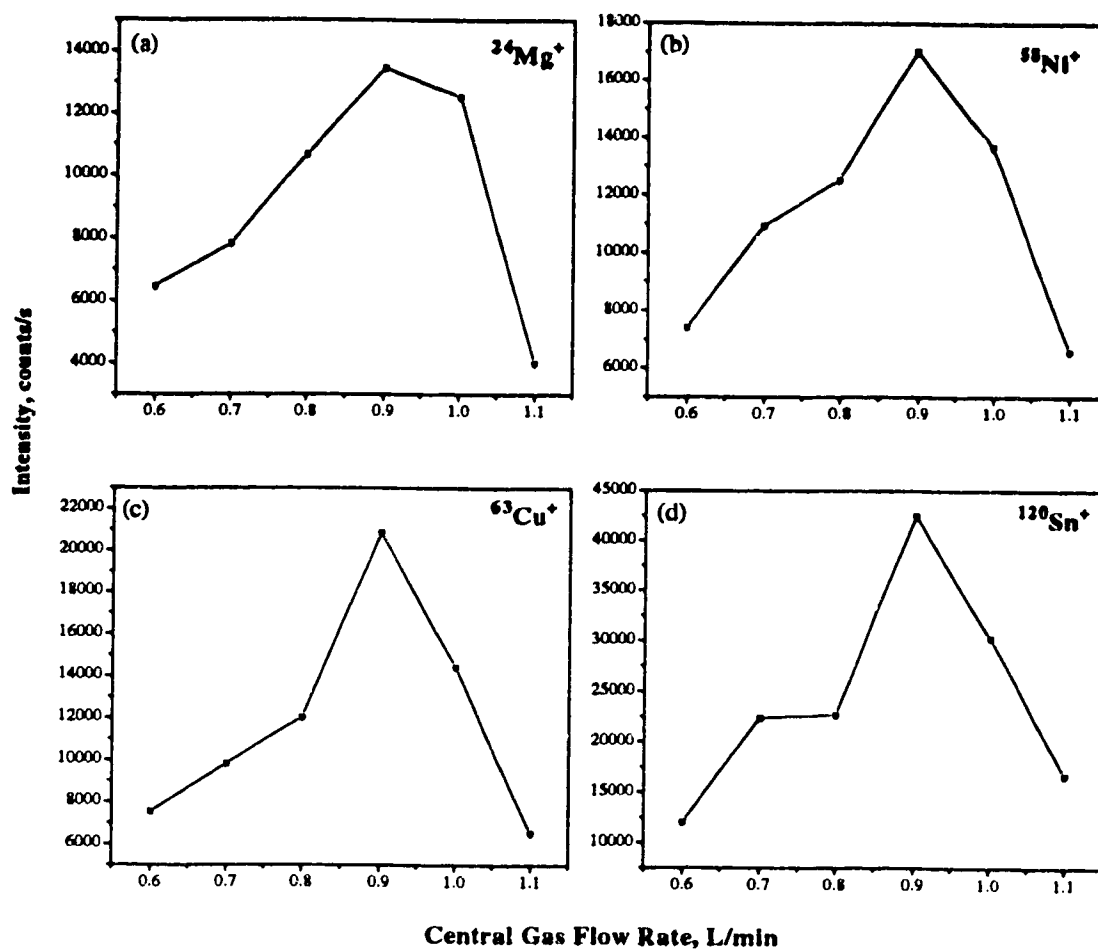


Figure 7.3 Dependence of signal intensity on the central gas flow-rate for (a) $^{24}\text{Mg}^+$, (b) $^{58}\text{Ni}^+$, (c) $^{63}\text{Cu}^+$ and (d) $^{120}\text{Sn}^+$

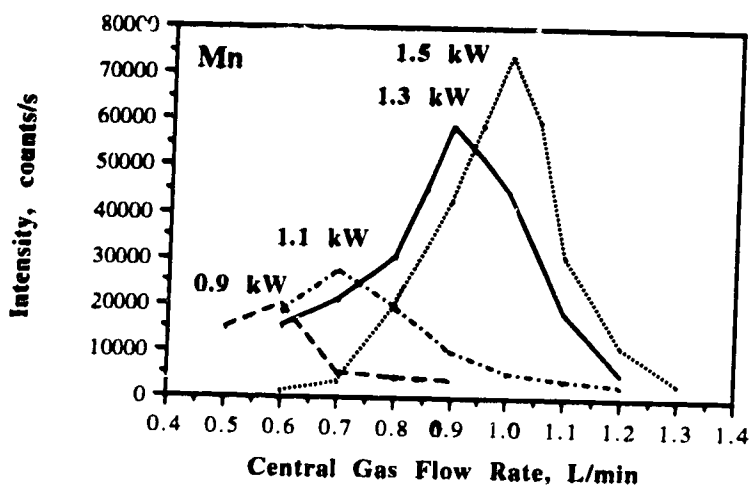


Figure 7.4 Central Gas Flow-Rate - Power parameter behavior graph for $^{55}\text{Mn}^+$ ion.

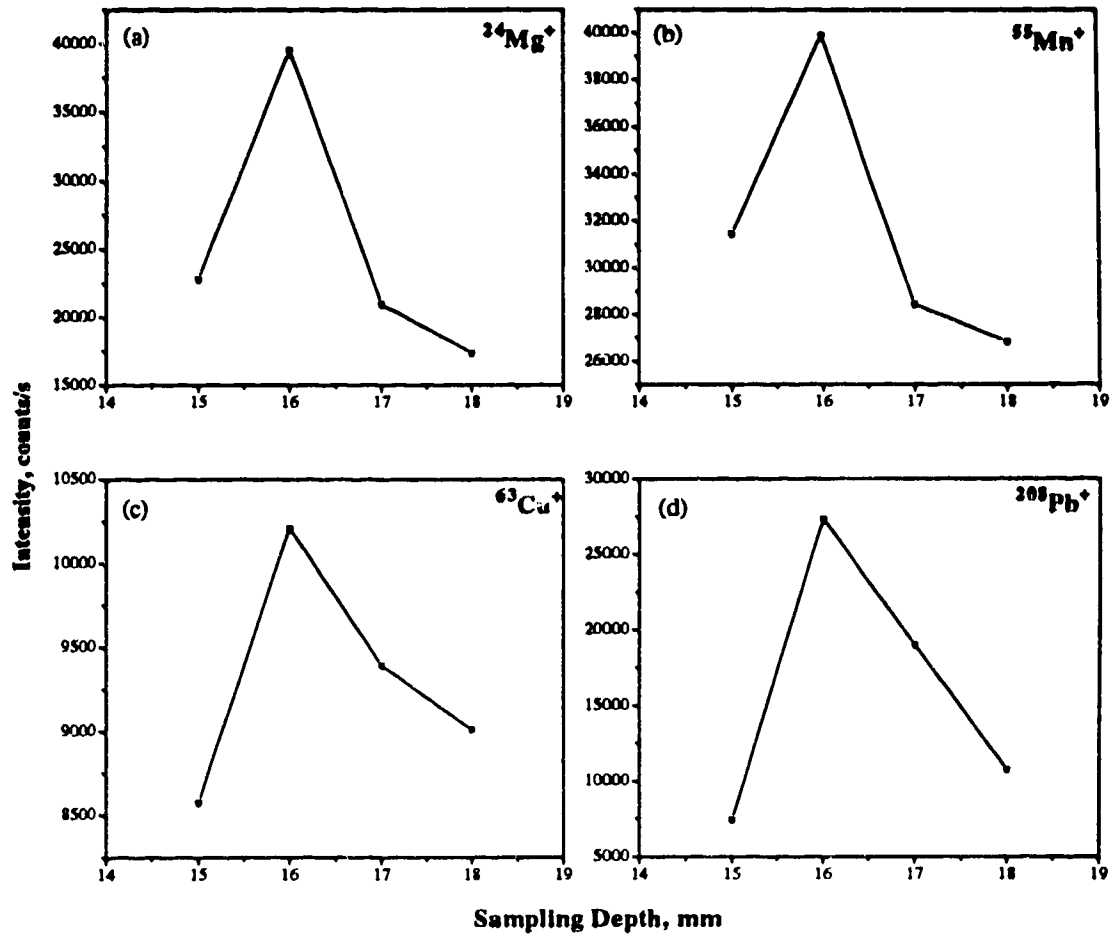


Figure 7.5 Dependence of signal intensity on sampling depth for (a) $^{24}\text{Mg}^+$, (b) $^{55}\text{Mn}^+$, (c) $^{63}\text{Cu}^+$ and (d) $^{208}\text{Pb}^+$

One of the most important variables for laser ablation is the pulse repetition rate of the laser. Only transient signals can be obtained when a single laser pulse is used [10]. The single pulse transient signal mode of operation is not normally used for quantitative analysis since the precision is limited by the number of data points acquired over the transient signal for each element to be determined [10]. The analyte signal can be made to be pseudo-continuous by raising the pulse repetition rate of the laser. The effects of the Nd:YAG laser pulse frequency on the analyte ion signals for $^{24}\text{Mg}^+$, $^{55}\text{Mn}^+$, $^{120}\text{Sn}^+$ and $^{208}\text{Pb}^+$ at 1.3 kW, 16 mm sampling depth and 0.9 L/min central gas flow-rate are shown in Figure 7.6. All of the elements exhibit similar behavior upon increasing the laser ablation frequency from 1 to 20 Hz. The analyte signals rise with an increase of the laser ablation frequency. Signal intensity seems to maximize at 15 Hz. The reason for the drop off 20 Hz is not understood, but perhaps the laser pulse energy reaching the surface is somewhat reduced at this repetition rate.

7.3.2 Evaluation of Potential Spectral Interferences

The plasma in LA-ICP-MS is a dry plasma in that solvent (*i.e.* H_2O) is not introduced into the ICP. This should reduced the intensity of many background species. This has been observed, for example, in direct sample insertion ICP-MS [3]. The background mass spectrum for the LA-ICP-MS system is shown in Figure 7.7. Significant signals for background species such as $^{14}\text{N}^+$, $^{16}\text{O}^+$, H_2O^+ , $^{14}\text{N}^{16}\text{O}^+$, N_2^+ , O_2^+ , $^{40}\text{Ar}^{14}\text{N}^+$, $^{40}\text{Ar}^{16}\text{O}^+$ and Ar_2^+ are observed in the dry ICP. Such species remain as air can still be entrained into a "dry" plasma. Because of these background interferences, some of the key elements of interest in ferrous metallurgy (Si, S, Ca and Fe) could not easily be determined. For instance, N_2^+ , O_2^+ , $^{40}\text{Ar}^+$, $^{40}\text{Ar}^{16}\text{O}^+$ would affect the major isotopes of Si, S, Ca and Fe.

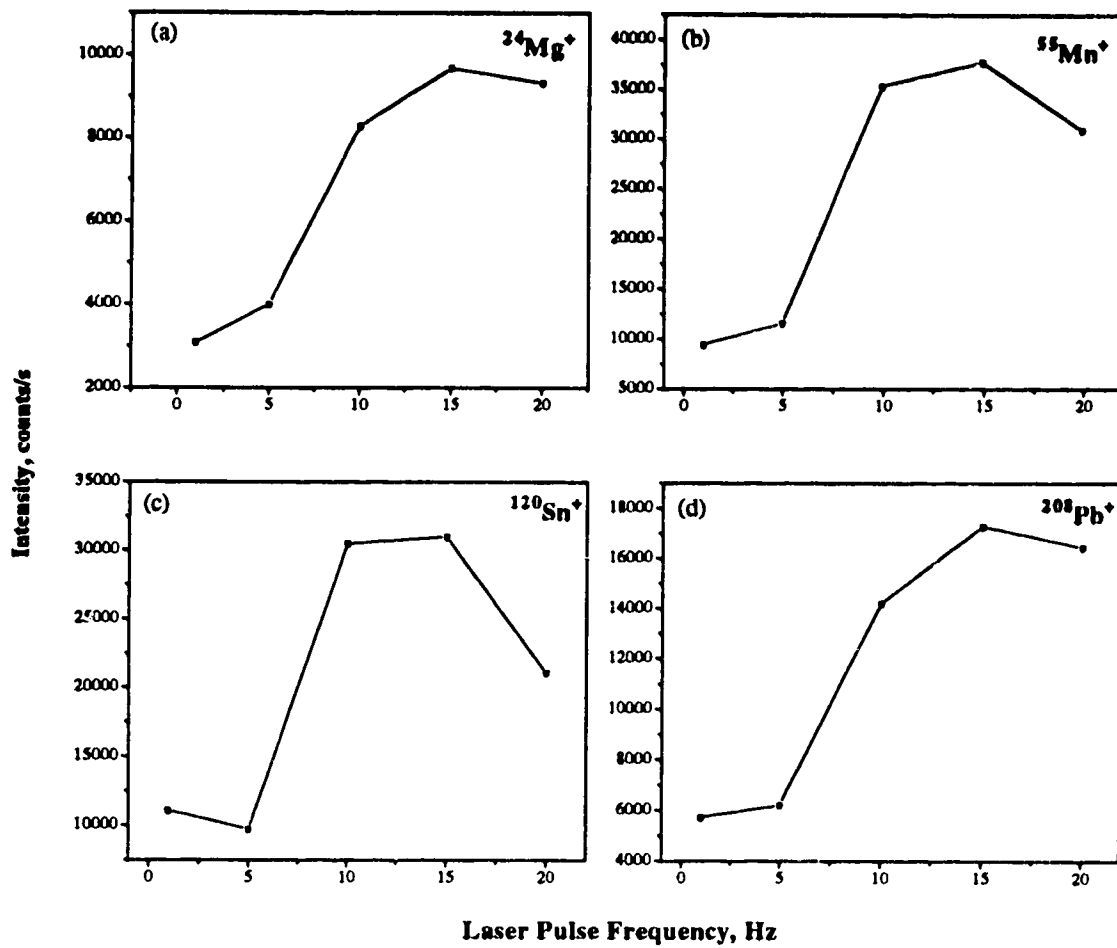


Figure 7.6 Dependence of signal intensity on the laser repetition rate for (a) $^{24}\text{Mg}^+$, (b) $^{55}\text{Mn}^+$, (c) $^{120}\text{Sn}^+$ and (d) $^{208}\text{Pb}^+$

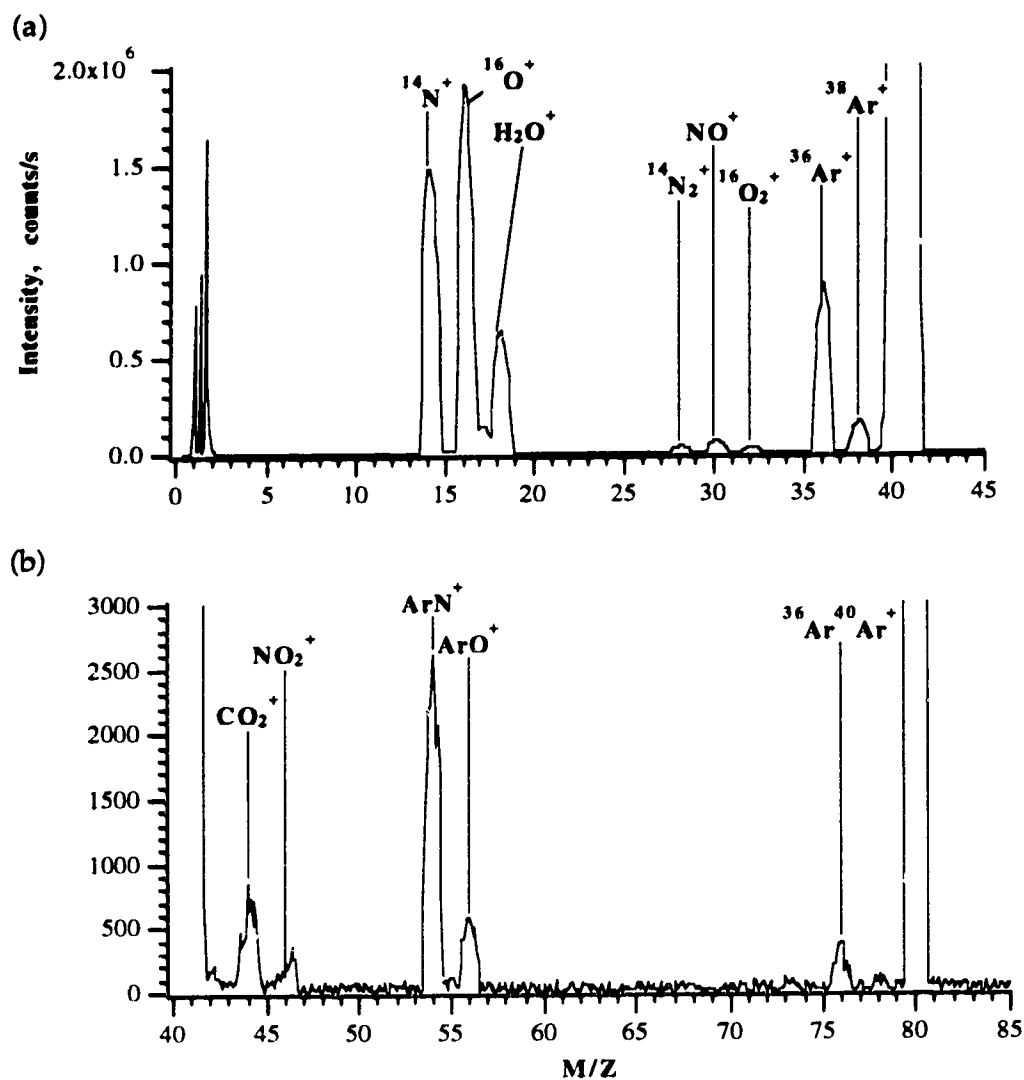


Figure 7.7 Background mass spectra for a dry ICP from (a) 0 to 45 m/z and (b) 40 to 85 m/z.

However, compared to the background spectra measured when aqueous solutions are nebulized into the plasma, the dry plasma background spectra are considerably simpler. Primarily due to the elimination of water in a dry ICP system there is a significant reduction and even elimination of numerous background species, especially, those containing oxygen and hydrogen. In addition, compared to the background spectra of GD-MS, the background of LA-ICP-MS was less complicated since the multiply charged argon species were absent. Molecular background from sulphur- and/or chlorine-containing components can be particularly troublesome in solution sample based ICP-MS, where the use of HCl presents some major potential problems. A chloride-containing matrix results in the formation of $^{35}\text{Cl}^{16}\text{O}^+$ and $^{40}\text{Ar}^{35}\text{Cl}^+$. $^{35}\text{Cl}^{16}\text{O}^+$ interferes with $^{51}\text{V}^+$ and $^{40}\text{Ar}^{35}\text{Cl}^+$ interferes with $^{75}\text{As}^+$, respectively. Since no HCl is used in the dry LA-ICP-MS, there are no such problems and that makes it possible to determine V and As in stainless steel samples.

7.3.3 Qualitative Spectral Scans for Aluminum Samples

Several segments of a LA-ICP-MS spectrum of a low alloy aluminum sample (Alcoa SA-909) are shown in Figure 7.8. This sample contains Mg (0.030), Si (0.061), Ti (0.030), Cr (0.027), Mn (0.031), Fe (0.082), Ni (0.034), Cu (0.031), Zn (0.030), Sn (0.026) and Pb (0.030). Values in parentheses are wt %. Signals for all these elements are readily observable although the $^{26}\text{Si}^+$ signal is interfered by N_2^+ or CO^+ at m/z 28, and the $^{56}\text{Fe}^+$ signal is overlapped with $^{40}\text{Ar}^{16}\text{O}^+$ at m/z 56. Moreover, Ga, Zr and perhaps a weak Nb signal can be observed, which are elements not reported by Alcoa. The presence of Ga and Zr was observed earlier by GD-MS. However, Nb was absent in the GD mass spectra. It was obviously present in ICP-MS, where the sample was dissolved

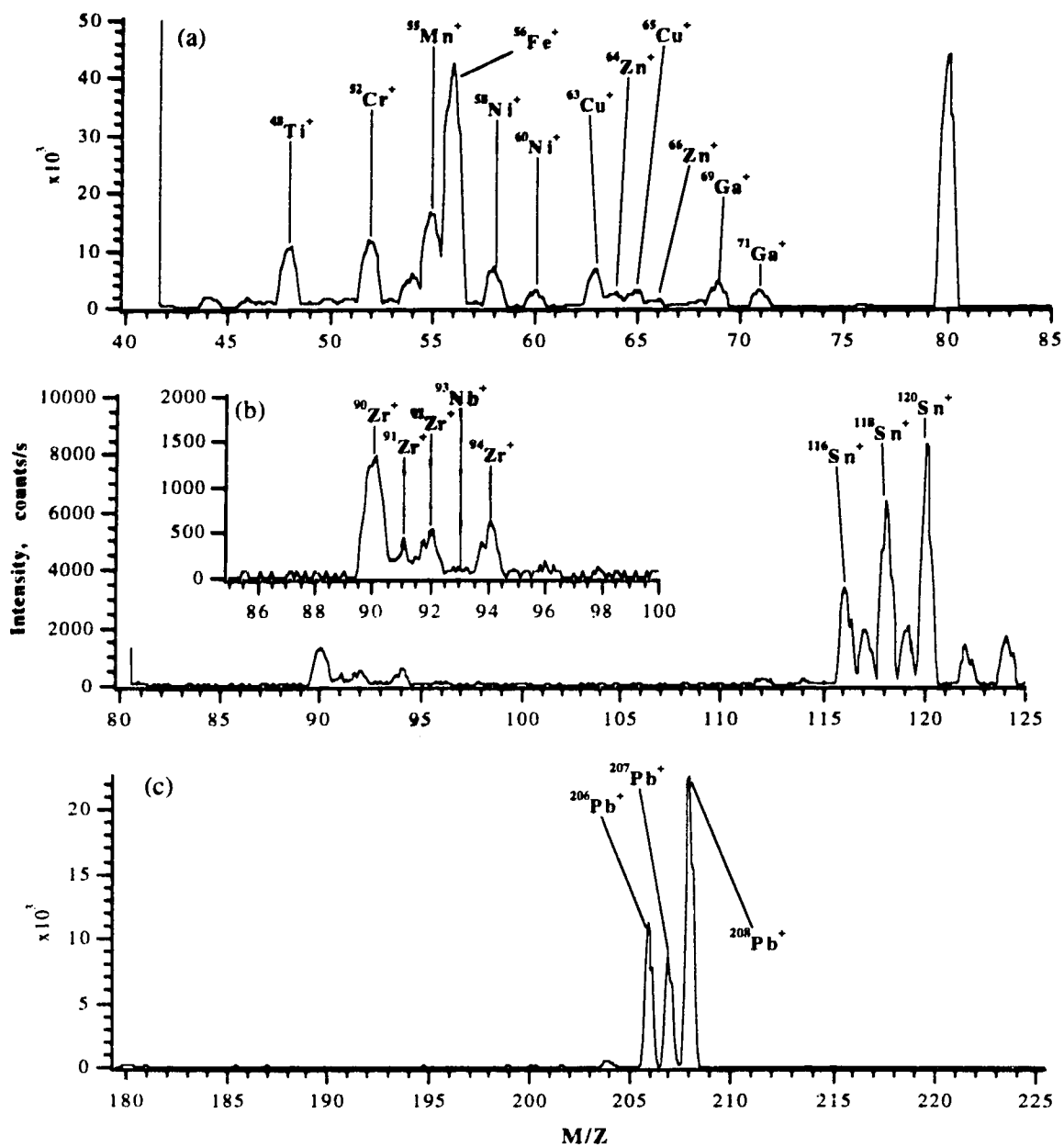


Figure 7.8 LA-ICP-MS spectra of a low alloy aluminum sample (Alcoa SA-909) in the (a) 40 to 85, (b) 80 to 125 and (c) 180 to 225 m/z range

and diluted to a 0.01% solution. Overall, the LA-ICP-MS spectrum is less complicated than either GD-MS or solution based ICP-MS. In particular, neither element-argide nor element-oxide species are observed in LA-ICP-MS.

7.3.4 Qualitative Spectral Scans for Steel Samples

Spectra for a NIST low alloy steel sample (1261) are shown in Figure 7.9 and 7.10. The spectra in Fig 7.9 and 7.10 illustrate the signal levels for several constituents of the steel sample (see Table 7.2). Essentially all elemental components can be observed including the rare earth elements with concentrations in the 4 $\mu\text{g/g}$ range. Compared to GD-MS, almost no element-argide and dimer can be found in LA-ICP-MS. However, only a very low level of mono-oxide such as $^{54}\text{Fe}^{16}\text{O}^+$ and $^{56}\text{Fe}^{16}\text{O}^+$ was observed in Figure 7.10a.

Table 7.2 Composition of NIST SRM 1261 low alloy steel

Element	Composition (%, by weight)	Element	Composition (%, by weight)	Element	Composition (%, by weight)
Ag	0.0004	La	0.0004	S	0.015
Al	0.21	Mg	0.0001	Sb	0.0042
As	0.017	Mn	0.66	Si	0.223
B	0.0005	Mo	0.19	Sn	0.011
Bi	0.0004	Nb	0.022	Ta	0.02
C	0.39	Nd	0.0003	Te	0.006
Ce	0.0013	Ni	1.99	Ti	0.020
Co	0.032	P	0.15	V	0.011
Cr	0.69	Pr	0.00014	W	0.017
Cu	0.042	Pb	0.00025	Zr	0.009

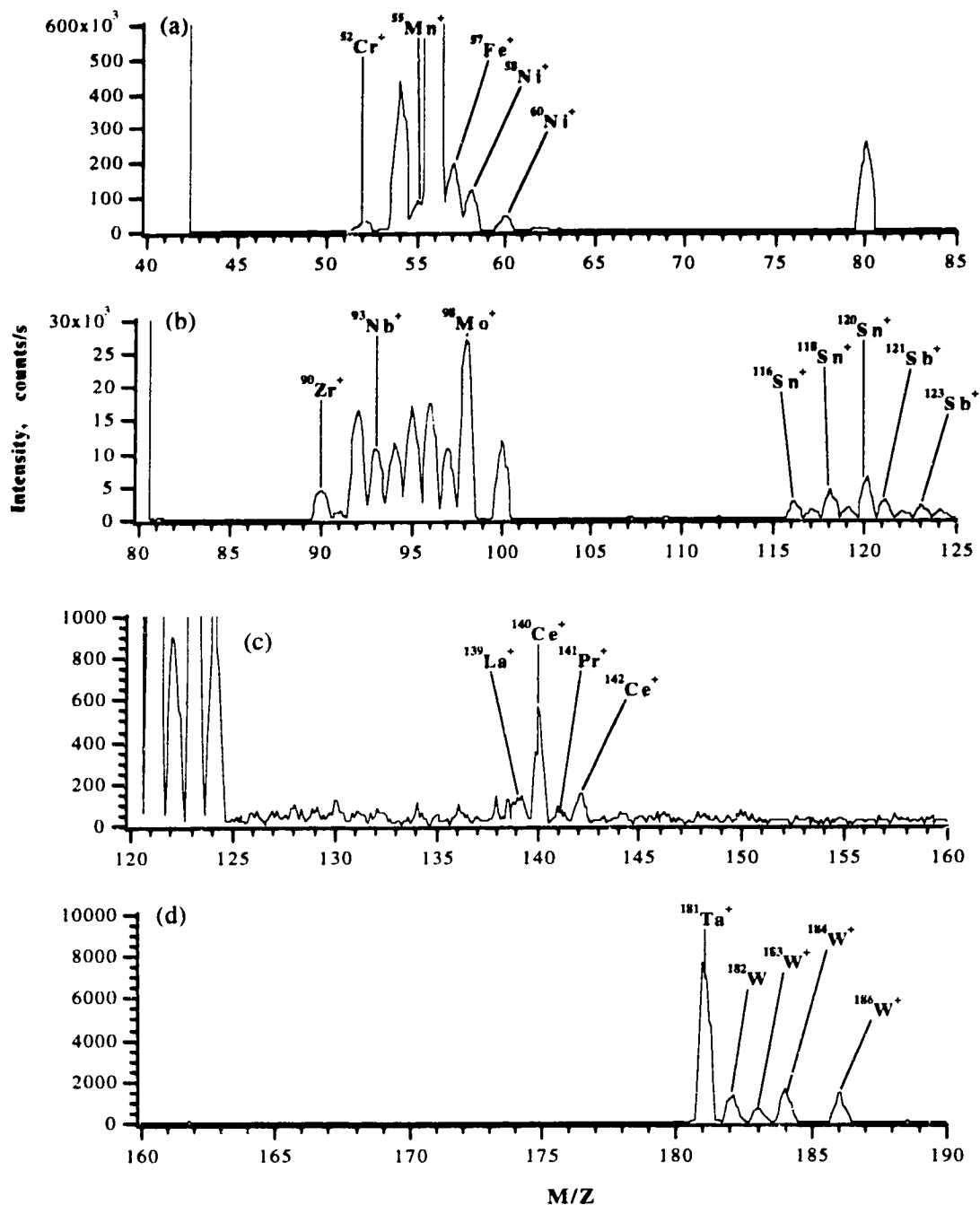


Figure 7.9 LA-ICP-MS spectra of a low alloy steel sample (NIST 1261) in the (a) 40 to 85, (b) 80 to 125, (c) 120 to 160 and (d) 160 to 190 m/z range

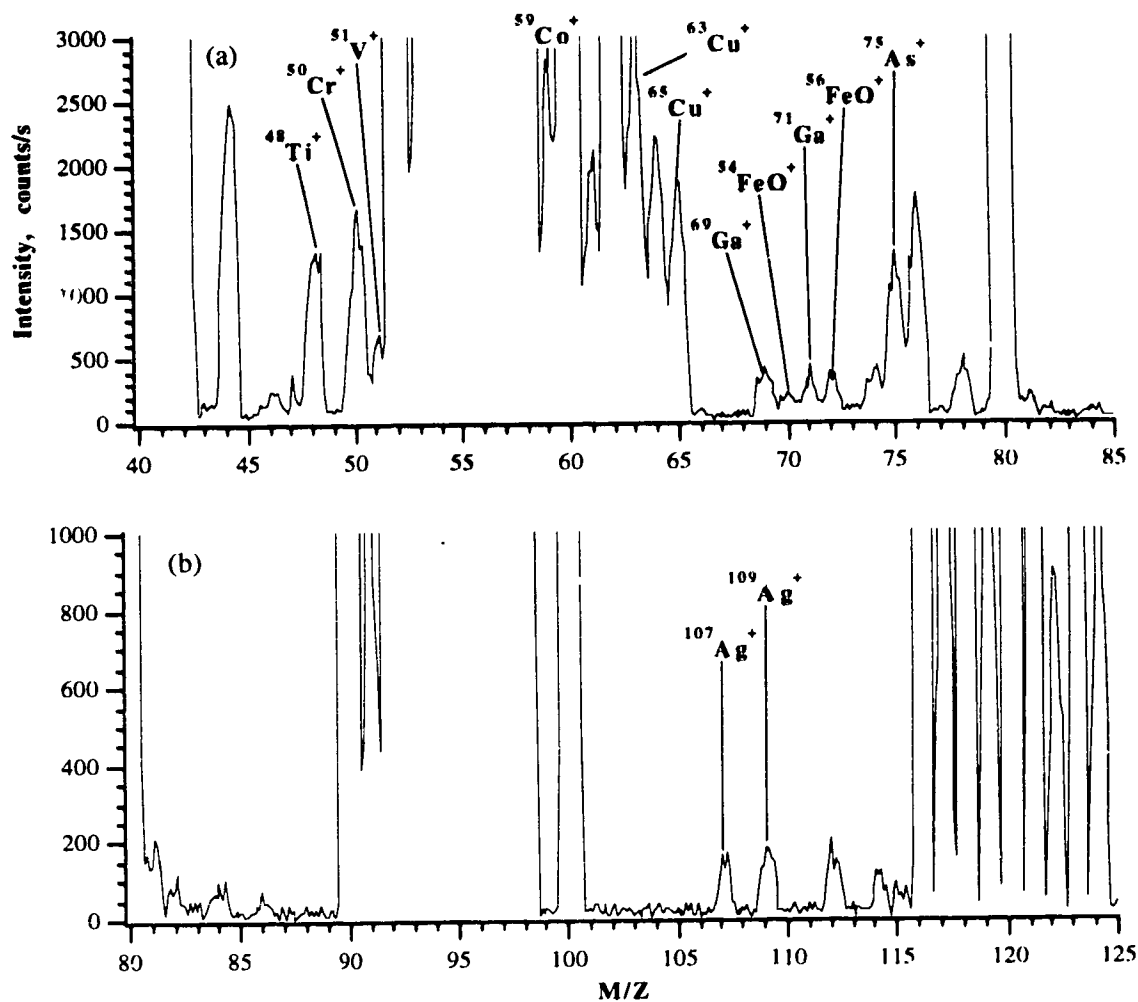


Figure 7.10 LA-ICP-MS spectra of a low alloy steel sample (NIST 1261) in the (a) 40 to 85 and (b) 80 to 125 m/z range

7.3.5 Quantitative Analysis

Laser ablation ICP-MS can be used for quantitative analysis and for semiquantitative screening applications. The accuracy that can be achieved in quantitation depends, to a large extent, on the availability of external standards and on the ability to perform internal standardization [27]. Several factors may cause variation in the amount of sample ablated and the observed signal. They include pulse-to-pulse variation in laser energy, defocusing of the beam during ablation or upon changing the sample, and differences in physical properties between samples. The first factor should not be too important due to the reasonable (~5%) reproducibility of Nd:YAG laser. A slow decline in signal may occur because of the gradual defocusing of the laser beam by hole-drilling. Continuous and steady signals were obtained at a 10 Hz repetition rate by using a small stepper motor to translate the sample back and forth along a single axis [10]. Thus, the problem of defocusing of the laser beam can be solved. In this experiment, a disk sample was fixed without translation and ablated at 15 Hz repetition rate. A short-term (4 minutes) $^{208}\text{Pb}^+$ signal from SA-909 low alloy aluminum was acquired with a integration time of 250 ms for each point and compared at 10, 15 and 20 Hz laser ablation repetition rates (see Figure 7.11). In terms of sensitivity and stability, the best signal was obtained at the 15 Hz rate.

Internal standardization should be used in LA-ICP-MS to correct for systematic and sample-to-sample variations in the signal. A primary advantage of this approach is that knowledge of the absolute amount of sample ablated is not required. Because of the solid sample form in LA-ICP-MS, the choice of an internal standard is restricted, as one is generally limited to a component of known composition or a minor isotope of a major component. This is workable

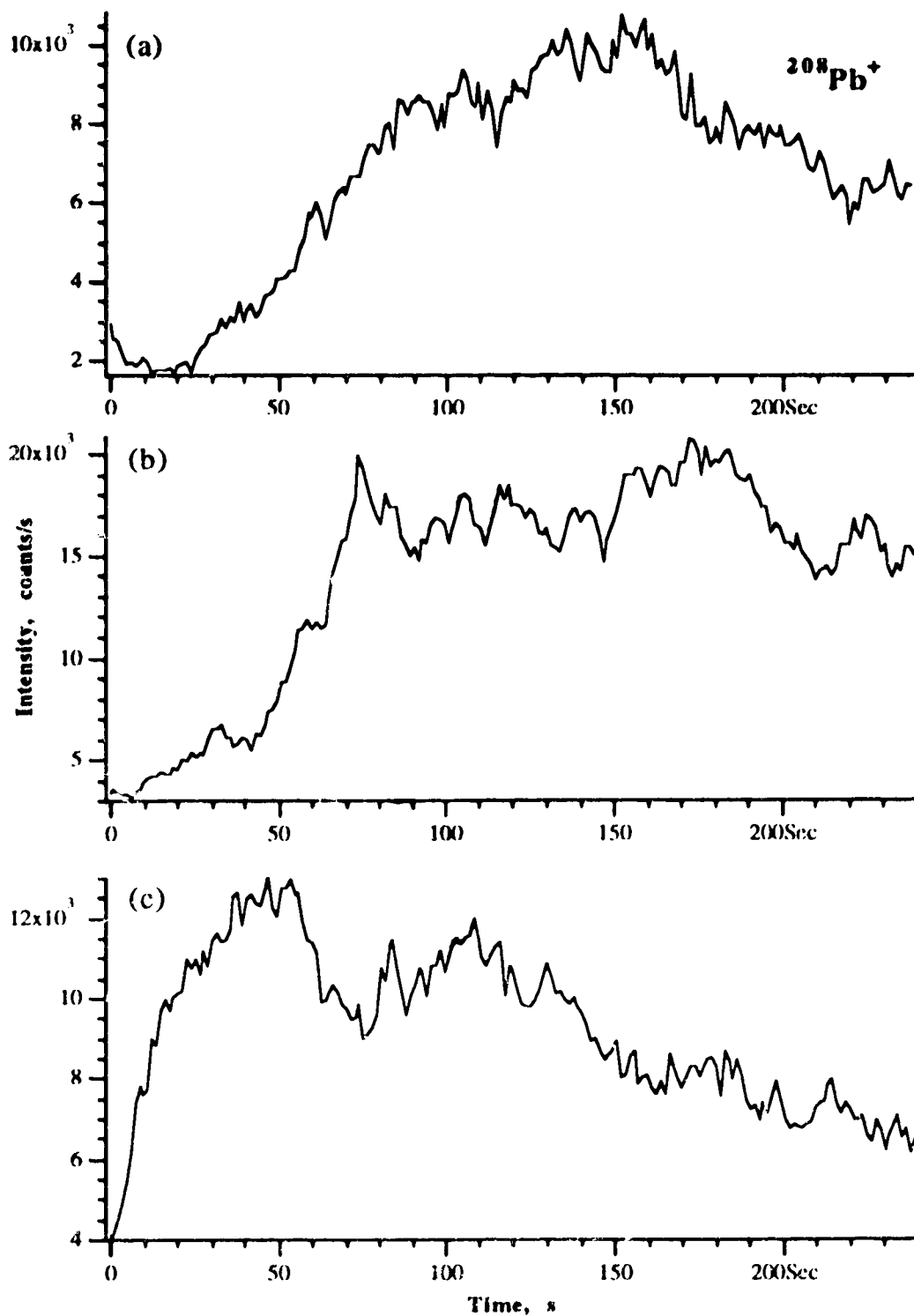


Figure 7.11 Dependence of lead signal intensity on different laser ablation repetition rates at (a) 10Hz, (b) 15 Hz and (d) 20 Hz.

for steel samples where $^{57}\text{Fe}^+$ might be used as an internal standard since iron is the matrix element in steel samples. However, there are some limitations for aluminum analyses because aluminum is monoisotopic. As aluminum is the major element in the samples the signal for $^{27}\text{Al}^+$ is too strong and overranges the dynamic range of the detector and detector electronics. For this study, since the samples were known standards, Fe was chosen as the internal standard for the aluminum analyses. For both aluminum and steel standards, in this experiment, $^{57}\text{Fe}^+$ the minor isotope of iron gave $^{57}\text{Fe}^+$ signals of 10^3 - 10^5 counts/s. Moreover, there is no significant interferences from either background or analyte species at m/z 57. For quantitative analysis, signal intensities for both analytes and internal standard were acquired with a signal integration time of 2 s for each mass.

7.3.5.1 Aluminum Alloys

A group of calibration curves was established by using both low and high alloy aluminum standards from Alcoa for the determination of $^{24}\text{Mg}^+$, $^{48}\text{Ti}^+$, $^{55}\text{Mn}^+$, $^{58}\text{Ni}^+$, $^{63}\text{Cu}^+$ and $^{66}\text{Zn}^+$. Seven standards named SA-909, SA-1170, SA-1169, SS-356-B, SS-A132AA, SS-D132-A and SS-319E were used to plot the standard curves. The composition of the components for Alcoa standards was in the range of 0.03% to 1.3% for magnesium, 0.03% to 2.5% for nickel and 0.03 to 3.8% for copper, and the slopes of the log-log plots for the standard curves were usually in the range of 0.99 to 1.1. Examples of four standard curves for $^{24}\text{Mg}^+$, $^{55}\text{Mn}^+$, $^{63}\text{Cu}^+$ and $^{66}\text{Zn}^+$ with $^{57}\text{Fe}^+$ as the internal standard are presented in Figure 7.12. The slopes of the log-log plots in Figure 7.12 are 0.99, 1.00, 1.00 and 0.99, respectively. A high alloy aluminum SS-360-C was analyzed as an

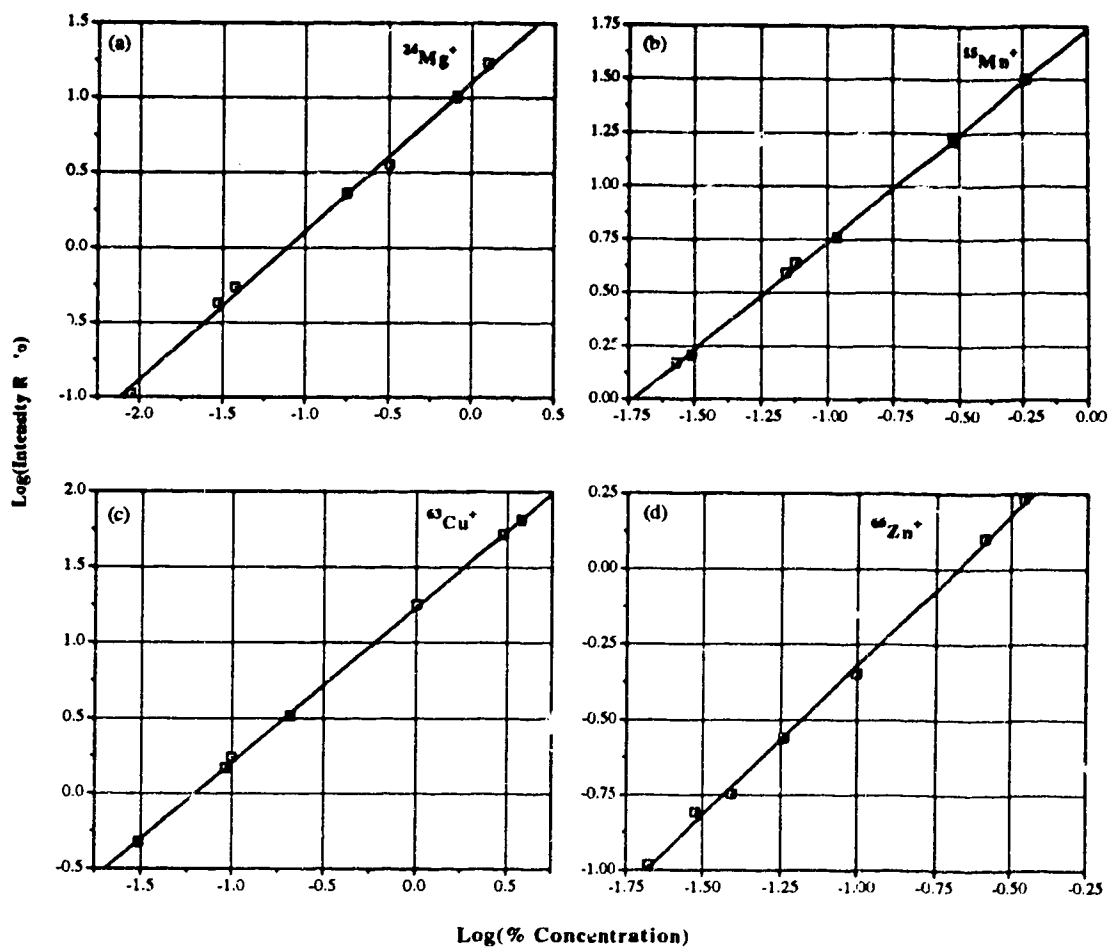


Figure 7.12 Calibration curves for (a) $^{24}\text{Mg}^+$, (b) $^{55}\text{Mn}^+$, (c) $^{63}\text{Cu}^+$ and (d) $^{66}\text{Zn}^+$ with $^{57}\text{Fe}^+$ as an internal standard in both high and low alloy aluminum standards

"unknown" sample. The results listed in Table 7.3 show excellent agreement with the certified values. The precision data were obtained based on $n=4$.

Table 7.3 Results for the analysis of SRM SS-360-C high alloy aluminum

Element	Certified Value (%)	Result (% \pm s)	% rsd
Mg	0.52	0.563 \pm 0.023	4.1
Ti	0.079	0.084 \pm 0.003	4.1
Mn	0.22	0.219 \pm 0.007	3.2
Ni	0.26	0.269 \pm 0.009	3.4
Cu	0.31	0.332 \pm 0.018	5.5
Zn	0.25	0.257 \pm 0.007	2.7

7.3.5.2 Steel Samples

LA-ICP-MS was also applied to the quantitative analysis of steel samples. Both low alloy and stainless steels were analyzed. The calibration curves were established using NIST low alloy steel standards 1261, 1263 1264, and stainless steel standards 1155, 1171, 1172, and 1185. The low alloy steels contain 94% to 97% iron and more than 20 minor or trace elements. However, the stainless steels only contain 60% to 70% iron, 17% to 18.5% chromium, 11% to 13% nickel, 1% to 2% manganese and about 2% molybdenum in some particular standards. The slopes of the log-log plots for the calibration curves were usually in the range of 0.99 to 1.1 except the slope of the plot for $^{58}\text{Ni}^+$ which was below 0.90. The minor isotope of the iron ($^{58}\text{Fe}^+$) affected the signal of $^{58}\text{Ni}^+$ for low alloy steel samples, so that the log-log plot of $^{58}\text{Ni}^+$ was curved at low concentrations. It was possible to do the correction by subtracting the signal intensity from iron at mass 58. The subtraction value is determined based on the isotope abundance ratio of $^{58}\text{Fe}^+ / ^{57}\text{Fe}^+$ (0.28/2.20) and the signal intensity of $^{57}\text{Fe}^+$ measured in the experiment. Two calibration curves for $^{58}\text{Ni}^+$ with $^{57}\text{Fe}^+$ as an internal standard

before and after the correction are shown in Figure 7.13. In order to avoid the interference from iron, on the other hand, the signal for $^{60}\text{Ni}^+$ could be utilized to establish the calibration curve. Examples of four calibration curves for $^{52}\text{Cr}^+$, $^{55}\text{Mn}^+$, $^{60}\text{Ni}^+$ and $^{98}\text{Mo}^+$ with $^{57}\text{Fe}^+$ as the internal standard are also illustrated in Figure 7.14, where the calibration curve for $^{60}\text{Ni}^+$ did not need correction. The slopes of the log-log plots in Fig 7.14 are 1.03, 1.04, 0.99 and 1.09, respectively. Low alloy steel NIST 1262 was analyzed for the metal elements as an "unknown" sample. The results are summarized in Table 7.4 and the standard deviations for the results were calculated based on $n=4$.

Table 7.4 Results for the analysis of NIST SRM 1262 low alloy steel

Element	Mass	Certified Value (%)	Results (% \pm s)	% rsd
Ti	48	0.084	0.0844 \pm 0.0029	3.5
V	51	0.041	0.0394 \pm 0.0019	4.7
Cr	52	0.30	0.303 \pm 0.012	4.0
Mn	55	1.05	1.010 \pm 0.016	1.5
Ni	58	0.60	0.560 \pm 0.019	3.3
Ni	60	0.60	0.660 \pm 0.0033	5.0
Co	59	0.30	0.299 \pm 0.007	2.4
Cu	63	0.51	0.526 \pm 0.016	3.1
As	75	0.092	0.0938 \pm 0.0046	4.9
Nb	93	0.30	0.294 \pm 0.012	4.0
Mo	98	0.070	0.0752 \pm 0.0034	4.5
Sb	121	0.012	0.0120 \pm 0.0004	3.3
W	184	0.21	0.221 \pm 0.005	2.3

7.3.6 Evaluation of Memory Effects

Memory effects for LA-ICP-MS were checked using the high alloy aluminum

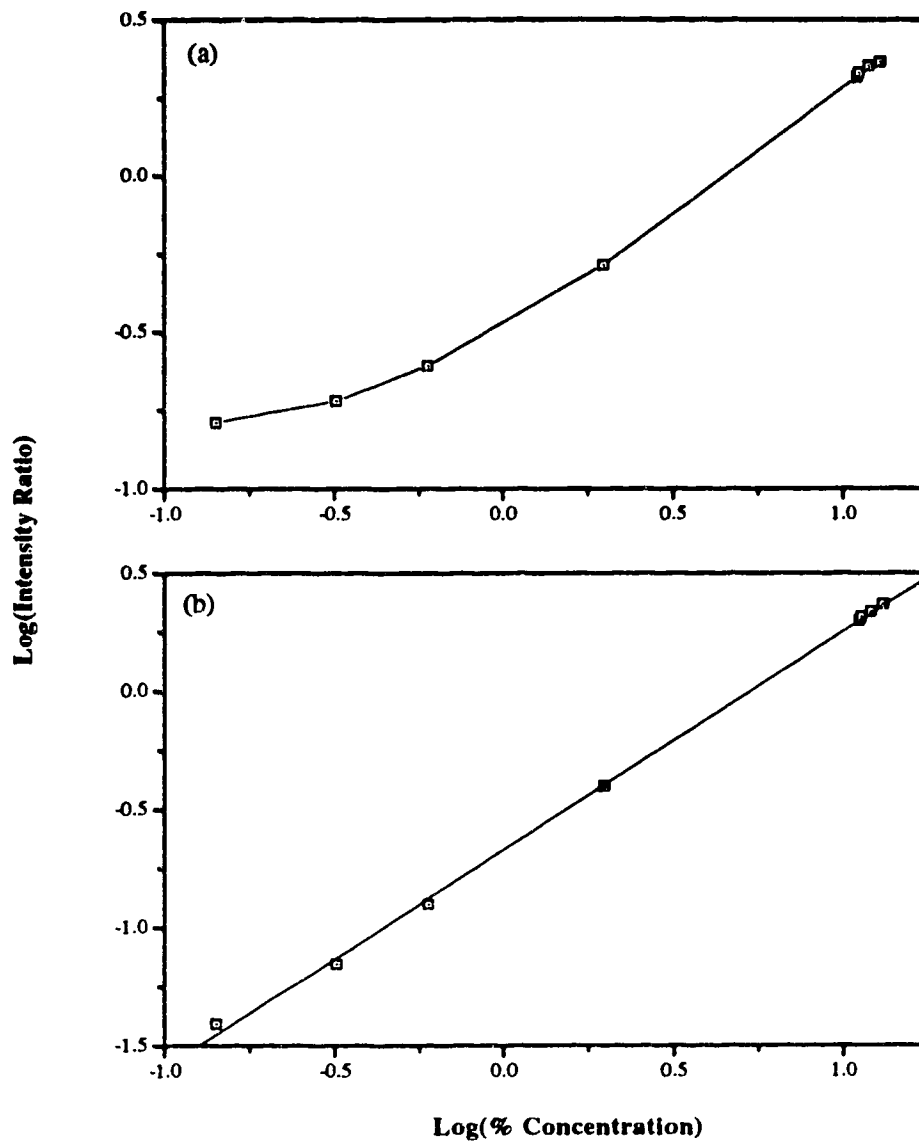


Figure 7.13 Calibration curves for $^{58}\text{Ni}^+$ with $^{57}\text{Fe}^+$ as an internal standard (a) before and (b) after correction for the interference of $^{58}\text{Fe}^+$

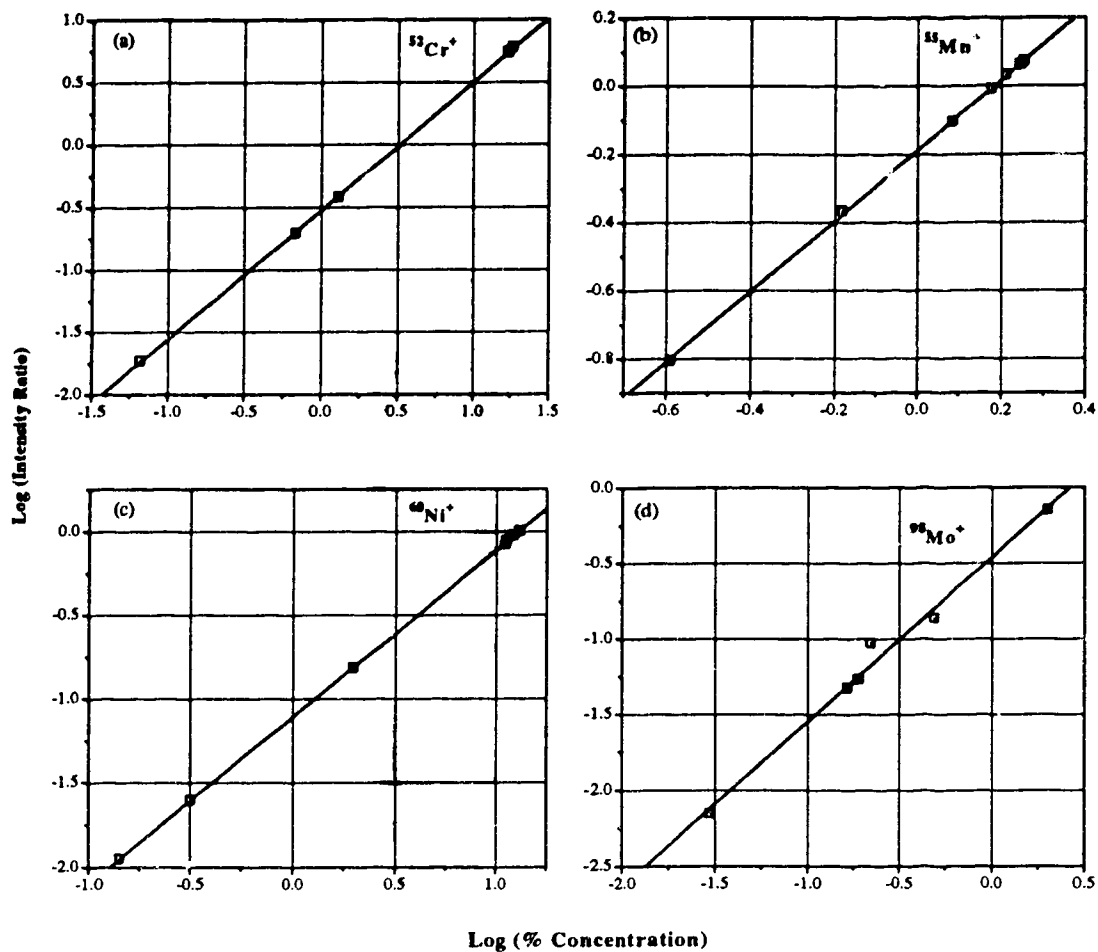


Figure 7.14 Calibration curves for (a) $^{52}\text{Cr}^+$, (b) $^{55}\text{Mn}^+$, (c) $^{60}\text{Ni}^+$ and (d) $^{98}\text{Mo}^+$ with $^{57}\text{Fe}^+$ as an internal standard in both low alloy and stainless steel standards

SS-319E and the low alloy aluminum SA-1507 standards. The samples were run in the sequence high alloy, low alloy, and then blank where no sample was ablated and introduced into the plasma. Strong signal levels for $^{24}\text{Mg}^+$, $^{48}\text{Ti}^+$, $^{55}\text{Mn}^+$, $^{57}\text{Fe}^+$, $^{60}\text{Ni}^+$, $^{63}\text{Cu}^+$ and $^{66}\text{Zn}^+$ ions were obtained in the first run. However, very weak signals were observed in the second run, when essentially pure aluminum was ablated. Only low level noise signals could be seen in the third run where no sample was ablated. The results are summarized in Table 7.5. Based on the data presented in this table there seems to be no significant memory effect present from run to run. Therefore, it is not necessary to clean the quartz chamber and the tubing for each run. It was usually cleaned every few days. The blank signal for ^{55}Mn seems a little bit higher than the rest of the elements (110 counts/sec) since it was affected by the background signals ArN^+ and ArO^+ .

Table 7.5 Results of memory effects check for external chamber LA-ICP-MS

Run		First Run (High Alloy SS-319E)		Second Run (Low Alloy SA-1507)		Third Run (Blank)
Element	Mass	% C	Intensity c/s	% C	Intensity c/s	Intensity c/s
Mg	24	0.18	13,900	< 0.0002	40	12
Ti	48	0.10	17,000	0.001	100	12
Mn	55	0.58	190,000	< 0.0002	200	110
Fe	57	0.68	4,000	0.001	90	20
Ni	60	0.20	8,000	< 0.0002	60	15
Cu	63	3.83	400,000	0.0013	300	55
Zn	66	0.35	10,000	0.001	25	12

7.3.7 Comparison to GD-MS

GD-MS has also been used for the quantitative analysis of both low alloy and stainless steels in the solid form [28, 29]. Both GD-MS and LA-ICP-MS are direct

methods for the analysis of steel samples in a dry plasma. Thus, the signal level of metal oxides could be very low in both GD-MS and LA-ICP-MS. Shao and Horlick reported that metal oxides such as $^{56}\text{Fe}^{16}\text{O}^+$, $^{90}\text{Zr}^{16}\text{O}^+$, $^{93}\text{Nb}^{16}\text{O}^+$, $^{181}\text{Ta}^{16}\text{O}^+$ and W^{16}O^+ were observed in steel spectrum of GD-MS [29]. However, these oxides could hardly be found in LA-ICP-MS except two very weak peaks at 70 and 72 m/z (see Figure 7.10a) that might arise from the isotopes of iron oxide ($^{54}\text{Fe}^{16}\text{O}^+$ and $^{56}\text{Fe}^{16}\text{O}^+$). The argon induced background spectrum for GD-MS seems more complicated than that for LA-ICP-MS. A group of metal argides such as $^{56}\text{Fe}^{40}\text{Ar}^+$, $^{52}\text{Cr}^{40}\text{Ar}^+$ (0.03%) and $^{58}\text{Ni}^{40}\text{Ar}^+$ (0.04%), and the multiply charged argon species such as $^{40}\text{Ar}^{2+}$ were reported in GD-MS [29], but they were absolutely absent in LA-ICP-MS. Furthermore, metal dimers such as $^{52}\text{Cr}_2^+$ (0.0005%) and $^{56}\text{Fe}_2^+$ (0.0002%) which correspond to Ru and Pd isotopes at m/z 104 and a Cd isotope at 112 m/z could be observed in GD mass spectrum [29], while no such problem could be found in LA-ICP-MS. Compared to GD-MS, moreover, LA-ICP-MS is a fast analytical method without the pre-burning procedure which is necessary for GD-MS [29].

7.4 Conclusion

Among the known techniques of direct solid sampling such as DSI, GD, electrothermal vaporization (ETV) and laser ablation (LA), LA-ICP-MS offers significant potential for the direct analysis of solids. External chamber laser ablation ICP-MS can be used successfully for the analysis of both aluminum and steel solid samples. It has been shown that the method is quite simple, rapid and effective, and matrix effects and memory effects are minimal. Such a system is applicable to the direct quantitative and qualitative analysis of metallic solid samples. The spectral complexity of LA-ICP-MS spectra seem to be on a par with GD-MS spectra, and tend to be much simpler than solvent-based ICP-MS, since no metal mono-oxides were observed in spectra for this dry plasma. Thus a quadrupole-based mass spectrometer is adequate for most analytical determinations. Internal standardization is very important in quantitative analysis. A minor isotope of iron ($^{57}\text{Fe}^+$) was chosen as the internal standard for analysis of both aluminum alloy and steel samples. The limitations of the LA-ICP-MS include that the laser is expensive, and that the knowledge of the iron composition in both standards and samples is necessary for the purpose of the internal standardization.

It is possible to perform semi-quantitative analysis for non-conducting samples such as macor, glaze, ceramics and porcelain. There are quite a few elements of possible interest in these non-conducting samples, but the composition is unknown in detail. A qualitative survey of the non-conducting samples including macor, glaze and a porcelain dish with LA-ICP-MS was carried out and will be presented in the next chapter.

References

1. S. A. Darke, S. E. Long, C. J. Pickford and J. F. Tyson, *J. Anal. At. Spectrom.* **4**, 715 (1989).
2. V. Karanassios and G. Horlick, *Spectrochim. Acta* **44B**, 1345 (1989).
3. V. Karanassios and G. Horlick, *Spectrochim. Acta* **44B**, 1361 (1989).
4. V. Karanassios and G. Horlick, *Spectrochim. Acta* **44B**, 1387 (1989).
5. W. W. Harrison and C. W. Magee, *Anal. Chem.* **46**, 461 (1974).
6. C. G. Bruhn, B. L. Bentz and W. W. Harrison, *Anal. Chem.* **50**, 373 (1978).
7. J. W. Coburn and W. W. Harrison, *Appl. Spectrosc. Rev.* **17**, 95 (1988).
8. N. Jakubowski, D. Stuewer and W. Vieth, *Anal. Chem.* **59**, 1825 (1987).
9. W.W. Harrison, *J. Anal. At. Spectrom.* **3**, 867 (1988).
10. P. Arrowsmith, *Anal. Chem.* **59**, 1437 (1987).
11. J. W. Hager, *Anal. Chem.* **61**, 1243 (1989).
12. S. A. Darke, S. E. Long, C. J. Pickford and J. F. Tyson, *Anal. Proc.* **26**, 159 (1989).
13. S. A. Darke, S. E. Long, C. J. Pickford and J. F. Tyson, *J. Anal. At. Spectrom.* **4**, 715 (1989).
14. T. Ishizuka, Y. Uwamino and H. Sunahara, *Anal. Chem.* **49**, 1339 (1977).
15. R. Wennrich and K. Dittrich, *Spectrochim. Acta* **37B**, 913 (1982).
16. T. Ishizuka and Y. Uwamino, *Anal. Chem.* **52**, 125 (1980).
17. F. Leis and K. Laqua, *Spectrochim. Acta* **33B**, 727 (1978).
18. M. Thomson, J. E. Goulter and F. Sieper, *Analyst* **106**, 32 (1981).
19. J. Carr and G. Horlick, *Spectrochim. Acta* **37B**, 1 (1982).
20. T. Ishizuka and Y. Uwamino, *Spectrochim. Acta* **38B**, 519 (1983).

21. M. Hale, M. Thomson and M. R. Wheatley, *J. Geochem. Explor.* **21**, 361 (1984).
22. A. L. Gray, *Analyst* **110**, 551 (1985).
23. P. van de Weijer, W. L. M. Baeten, M. H. J. Bekkers and P. J. M. G. Vullings, *J. Anal. At. Spectrom.* **7**, 599 (1992).
24. J. S. Crain and D. L. Gallimore, *J. Anal. At. Spectrom.* **7**, 605 (1992).
25. W. T. Perkins, N. J. G. Pearce and R. Fuge, *J. Anal. At. Spectrom.* **7**, 611 (1992).
26. I. S. Borthwick, K. W. D. Ledingham and R. P. Singhal, *Spectrochim. Acta* **47B** 1259 (1992).
27. L. Moenke-Blankenburg, *Spectrochimica Acta Reviews*, **15**, 1 (1993).
28. N. Jakubowski, D. Stuewer and W. Vieth, *Anal. Chem.* **59**, 1825 (1987).
29. Y. Shao and G. Horlick, *Spectrochim. Acta* **46B**, 165 (1991).

Chapter 8

Analysis of Non-Conducting Materials Using Laser Ablation Inductively Coupled Plasma Mass Spectrometry

8.1 Introduction

Both glow discharge-mass spectrometry (GD-MS) and external chamber laser ablation inductively coupled plasma mass spectrometry (LA-ICP-MS) can be used successfully for the analysis of both aluminum and steel solid samples. It has been shown that these methods are quite simple, rapid and effective, and matrix and memory effects are minimal. Such systems are applicable to the direct quantitative and qualitative analysis of metallic solid samples. However, there is some difficulty for dc GD-MS in the analysis of non-conducting materials since the sample must be used as a cathode. Methodology has been developed for the analysis of non-conducting powders or oxide samples by dc GD-MS [1]. The mixing of an oxide powder with a conducting host matrix (1:9) allows pressing of a sample pellet for glow discharge sputtering. Several conducting matrices including graphite, copper, silver, iron, aluminum and tantalum have been studied for analysis of non-conducting materials using GD-MS [2]. Different configurations of glow discharge sources were used for the analysis of powder materials. Geological and related

materials were sputtered with a hollow cathode plume [3] and a grimm-type glow discharge lamp [4]. Glass samples could also be sputtered by using a secondary cathode glow discharge [5]. Furthermore, radio frequency generated plasma discharge atomization/ionization sources [6-8] have also been introduced for direct non-conducting solid sampling GD-MS.

However, time is consumed in preparing and compressing the sample pellets for dc GD-MS. More impurities might be introduced into the GD system because of the addition of the conducting host matrix which makes the background spectrum more complicated. Time for pre-sputtering the sample is also necessary for GD-MS analysis. Among the known techniques of direct solid sampling of insulators such as DSI, GD, electrothermal vaporization (ETV) and laser ablation (LA), LA-ICP-MS is a simple, rapid and effective technique which is capable of ablating non-conducting samples such as macor, glass, ceramics, glaze, porcelain, oxides, and geological refractory materials. Sample preparation and knowledge about the composition is not required. The strength of LA-ICP-MS for a fast semiquantitative survey analysis of solids and pressed powders has been demonstrated [9]. Major and trace elements down to the sub-ppm level can be directly determined in this way. Non-conducting solids such as oxides and geological refractory materials can be analyzed by laser ablation. For example, trace impurities in uranium oxide (U_3O_8) have been determined using LA-ICP-MS [10], and elements such as Hf, Y, Re, Th and U in zircon samples have been determined by both laser ablation and solution based ICP-MS [11]. In this report, non-conducting solids such as macor, porcelain and glaze samples were analyzed by external chamber laser ablation ICP-MS.

8.2 Experimental

A Nd:YAG Photonics (12351 Research Pkwy Orlando, FL 32826) laser was used to ablate non-conducting samples. The laser was operated in a pulsed mode. The typical pulse width was 15 ns with a pulse energy of about 100 mJ/pulse and an output wavelength of 1.06 μm . The pulse repetition rate used in this experiment was 1 Hz.

The external chamber laser ablation ICP-MS system is shown in chapter 7. A quartz ablation chamber was used as a site for vaporization of non-conducting samples by the laser beam. The jacketed chamber is 35 mm in diameter and 75 mm in length. The inner tube is about 20 mm in diameter and 5 mm shorter than the outer quartz chamber. The inner diameter of the inner tube is 17 mm. The sample was pressed on the chamber and sealed by an o-ring. The argon gas was introduced through an inlet tube directly into the inner chamber and blows across the surface of the sample. A lens with a focal length of 10 cm was used to focus the laser beam directly onto the surface of the non-conducting sample.

A macor sample, a porcelain sample and eight glaze samples were chosen for this work. They were ablated using the Nd:YAG laser with the external quartz chamber. The vaporized sample was directly introduced into the ICP and detected by the quadrupole-based mass spectrometer. The porcelain sample was a dish. The dish-clay was covered with three different types of glazes: white glaze, yellow glaze and grey glaze. The glaze samples which were square in shape have eight different colors. The thickness of the glaze layer was about 0.1 mm. Each glaze and the dish-clay were ablated and analyzed separately. The glazes were ablated at a 1 Hz repetition rate because of the thickness of the

glazes on the porcelain dish clay so as not to ablate through to the underlying clay.

A standard Perkin Elmer /SCIEX ELAN Model 250 ICP mass spectrometer was used for all analyses and data acquisition. A standard length MAK optical emission ICP torch was used in conjunction with the external ablation chamber. Compromise conditions of power and central gas flow-rate can be easily obtained for a range of elements. The flow rate yielding the maximum ion count for a given power and sampling depth is essentially the same for most elements. For this work, a sampling depth of 16 mm from the load coil was chosen with a plasma forward power of 1.3 kW in order to obtain high sensitivity. The aerosol (central gas) flow-rate was selected at 0.90 L/min, which was controlled by a Matheson Model 8240-0423 mass-flow controller. The ion lens voltages were a compromise chosen to cover a large mass range. Typical operating parameters are summarized in Table 8.1.

8.3 Results and Discussion

8.3.1 Evaluation of Potential Spectral Interferences

LA-ICP-MS is a direct solid sampling technique, and no solvent (*i.e.* H₂O) is introduced into the plasma. Primarily due to the elimination of water in a dry ICP system there is a significant reduction and even elimination of numerous background species, especially, those containing oxygen and hydrogen. As shown in Chapter 7, the background spectrum was quite simple. The background interferences including $^{14}\text{N}^+$, $^{16}\text{O}^+$, H_2O^+ , $^{14}\text{N}^{16}\text{O}^+$, N_2^+ , O_2^+ , $^{40}\text{Ar}^{14}\text{N}^+$, $^{40}\text{Ar}^{16}\text{O}^+$ and Ar_2^+ might arise from impurities in the argon gas and

Table 8.1 Typical operating parameters for the LA-ICP-MS system

Plasma--	
r. f. forward power	1300 W
Outer gas flow-rate	12 L min ⁻¹ argon
Intermediate gas flow-rate	1.4 L min ⁻¹ argon
Central gas flow-rate	0.9 L min ⁻¹ argon
Mass Spectrometer--	
Sampling depth	16 mm from load coil
Sampler, copper	0.9 mm orifice
Skimmer, nickel	0.8 mm orifice
Ion Lens Voltage Setting---	
Bessel Box Barrel(B)	+5 volts
Bessel Box Plates(P)	-21 volts
Einzel Lens(E1)	-20 volts
Photon Stop(S2)	-23 volts
Laser---	
Nd:YAG laser energy per pulse	100 mJ
Output wavelength	1064 nm
Laser pulse width	15 ns
Focal length of lens	10 cm
Repetition rate	1 and 5 Hz

entrainment of air in the 10-mm gap between the end of the ICP torch and the tip of the sampler orifice. The levels of these background species were reduced by one order of magnitude compared to those obtained by nebulization of aqueous solutions. Especially, the signals of hydrides and hydroxides were much less intense than those obtained from solution-based ICP-MS. Some of the key elements of interest in non-conducting samples such as Si, S, Ca and Fe could not easily be determined since N_2^+ , O_2^+ , $^{40}Ar^+$ and $^{40}Ar^{16}O^+$ would affect the major isotopes of these elements.

8.3.2 Qualitative Spectral Scans for Non-Conducting Samples

8.3.2.1 Macor Sample

A group of mass spectra for a macor sample are displayed in Figure 8.1. Seventeen elements were observed in this sample (Table 8.2). Four major components found in the macor sample are Mg, Al, Si and K since their signal levels are very strong ($>10^6$, see Figure 8.1a). The medium components such as B, Na, Fe and Sn are less intense, and the rest of the elements such as Ti, Mn, Cu, Ga, Rb, Sr and Zr, *etc.* are at the trace level. The continuous signals of $^{24}Mg^+$, $^{11}B^+$, $^{56}Fe^+$ and $^{120}Sn^+$ obtained by laser ablation of the macor sample are shown in Figure 8.2. The data were acquired when the sample was ablated with 5 Hz repetition rate laser and the measurement time for each point was 250 ms. The signals appear continuous and constant over a period of 4 minutes. However, the signals will decay as the ablation cavity deepens. A sample translation method is necessary in order to avoid the decline of the signals [12].

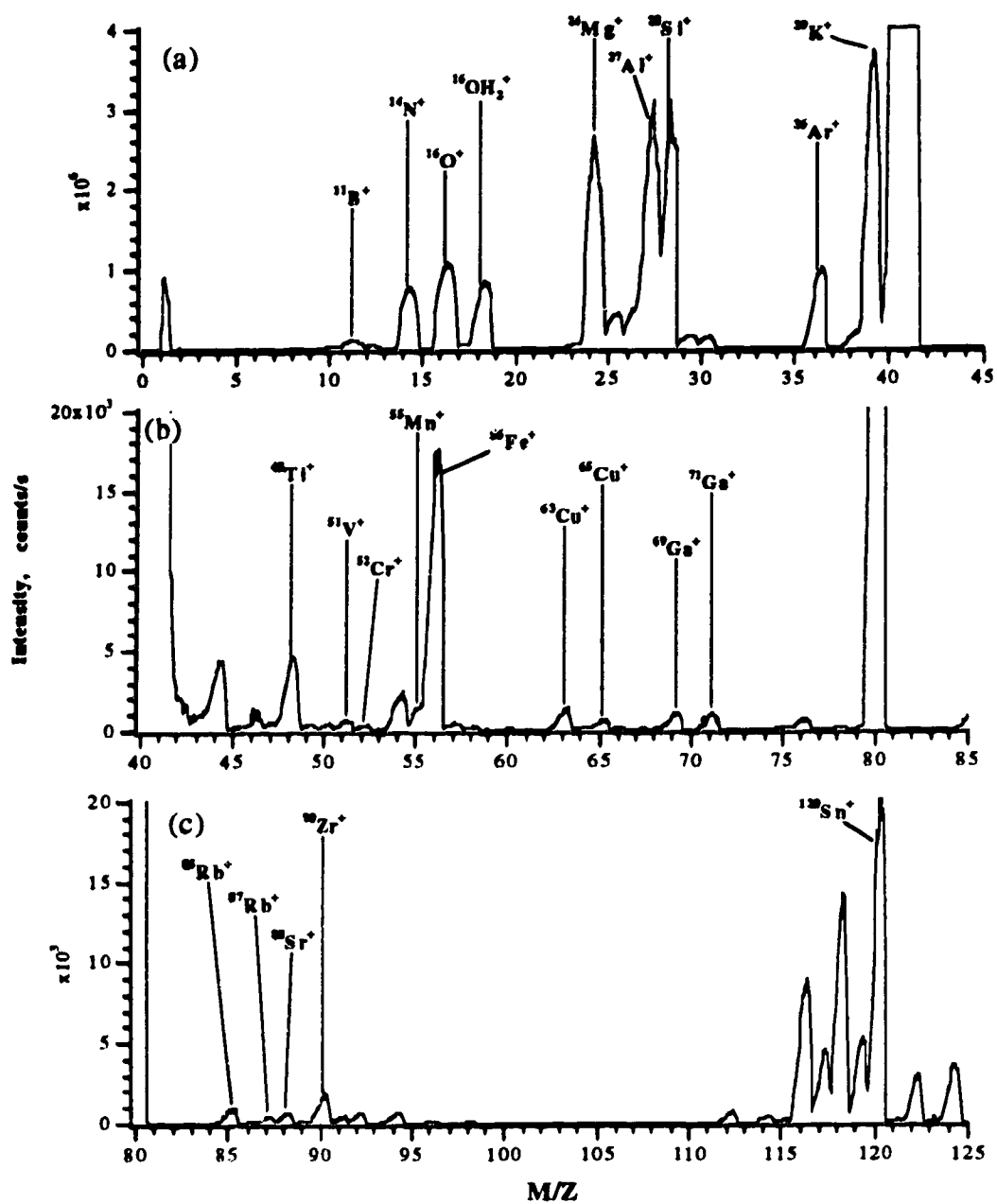


Figure 8.1 LA-ICP-MS spectra of a macor sample with a 5 Hz repetition rate of the Nd:YAG laser

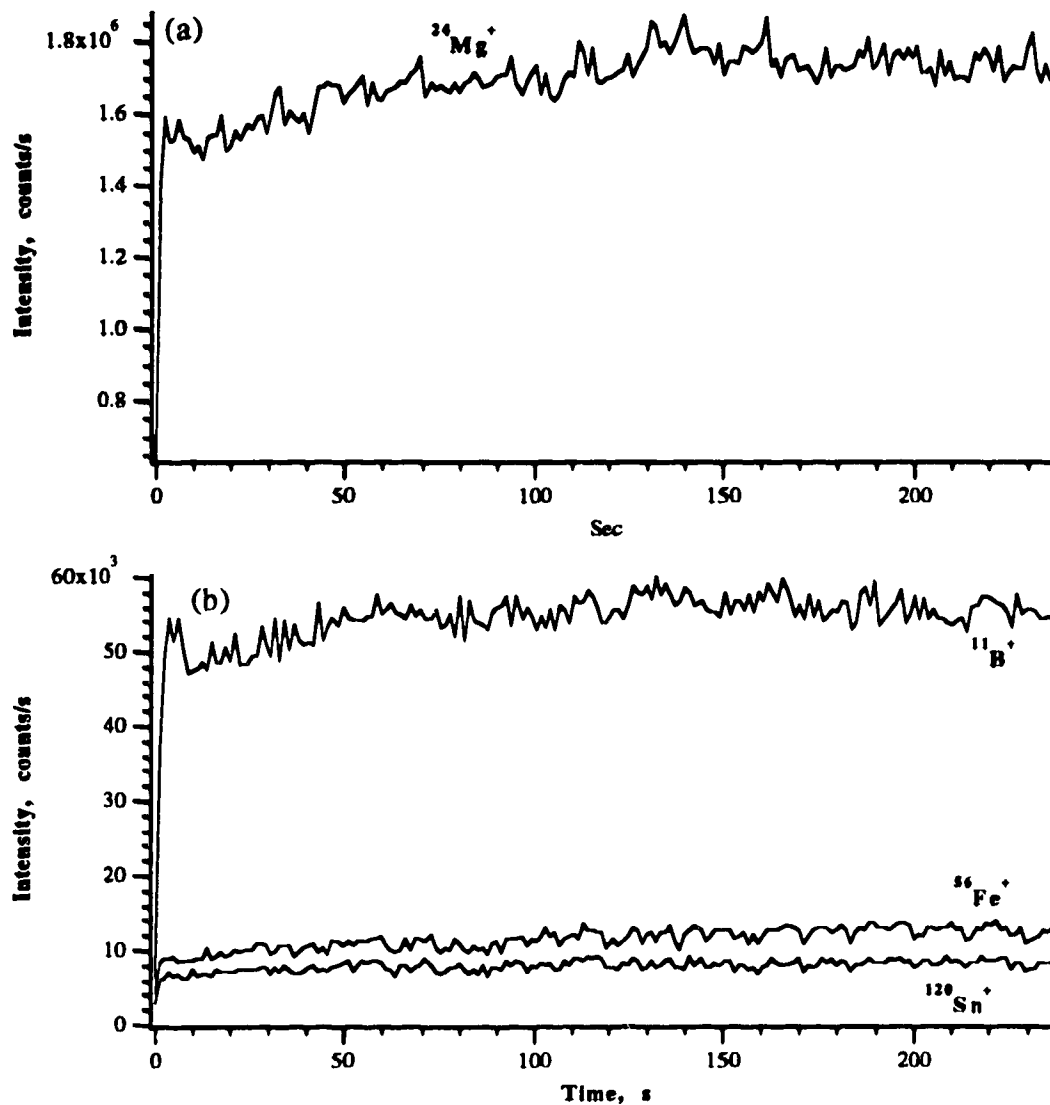


Figure 8.2 Continuous signals obtained by ablation of a macor sample with 5 Hz repetition rate of the Nd:YAG laser. Signals were observed at four m/z values (a) $^{24}\text{Mg}^+$, (b) $^{11}\text{B}^+$, $^{56}\text{Fe}^+$ and $^{120}\text{Sn}^+$

8.3.2.2 Porcelain Sample

A set of mass spectra for the yellow glaze on the porcelain dish sample are shown in Figure 8.3. Twenty-eight elements were found in the porcelain sample (Table 8.2). The intense signal of some elements suggests that Al, Si, Ti and Sn are the major elements in this glaze. Metal mono-oxides and metal argides could not be observed in these mass spectra. The dish sample including the dish-clay and three glazes contain high amounts of silicon and aluminum, while the glazes also contain large amounts of Ti and Sn besides Si and Al.

Table 8.2 Signal levels of elements in porcelain sample and macor sample.

Signal Levels	Dish-Clay	Grey Glaze	Yellow Glaze	White Glaze	Macor Sample
High >10 ⁶ c/s	Al, Si	Al, Si, Ti, Sn	Al, Si, Ti, Sn	Al, Si, Ti, Sn	Mg, Al, Si, K
Medium High 10 ⁵ -10 ⁶ c/s	Na, Mg, Ti, Fe, Ba	Mn, Zn	Na, Fe	Na, Zn	B, Na
Medium 10 ⁴ -10 ⁵ c/s	Rb, Sr, Zr	Na, Mg, Fe, Ba	Mg, Ba, Zn, B	Mg, Fe, Ba, Rb	Fe, Sn
Medium Low 10 ³ -10 ⁴ c/s	Li, V, Cr, Mn, Zn, Ga, Y, Nb, Cs, La, Ce, Pr, Nd, Pb	Rb, Zr, Cs, Ce, Pb	Li, Cs, Sr, Zr, Nb, La, Ce, Pb	Mn, Cs, Ce, Pb	Ti, Mn, Cu, Ga, Zr
Low < 10 ³ c/s	B, Sn, Tl, Bi	Li, B, Sr, Y, Nb, La, Pr, Nd	V, Cr, Ga, Y, Pr, Nd	Li, B, Sr, Zr, Y, Nb, La, Pr, Nd	V, Cr, Rb, Sr

Five different signal levels of elements in both macor and porcelain samples are listed in Table 8.2. High signal level means a major amount of the analyte in the sample (signal intensity greater than 10⁶ counts/s), while medium high represents a signal intensity in the range of 10⁵-10⁶ counts/s, medium in the

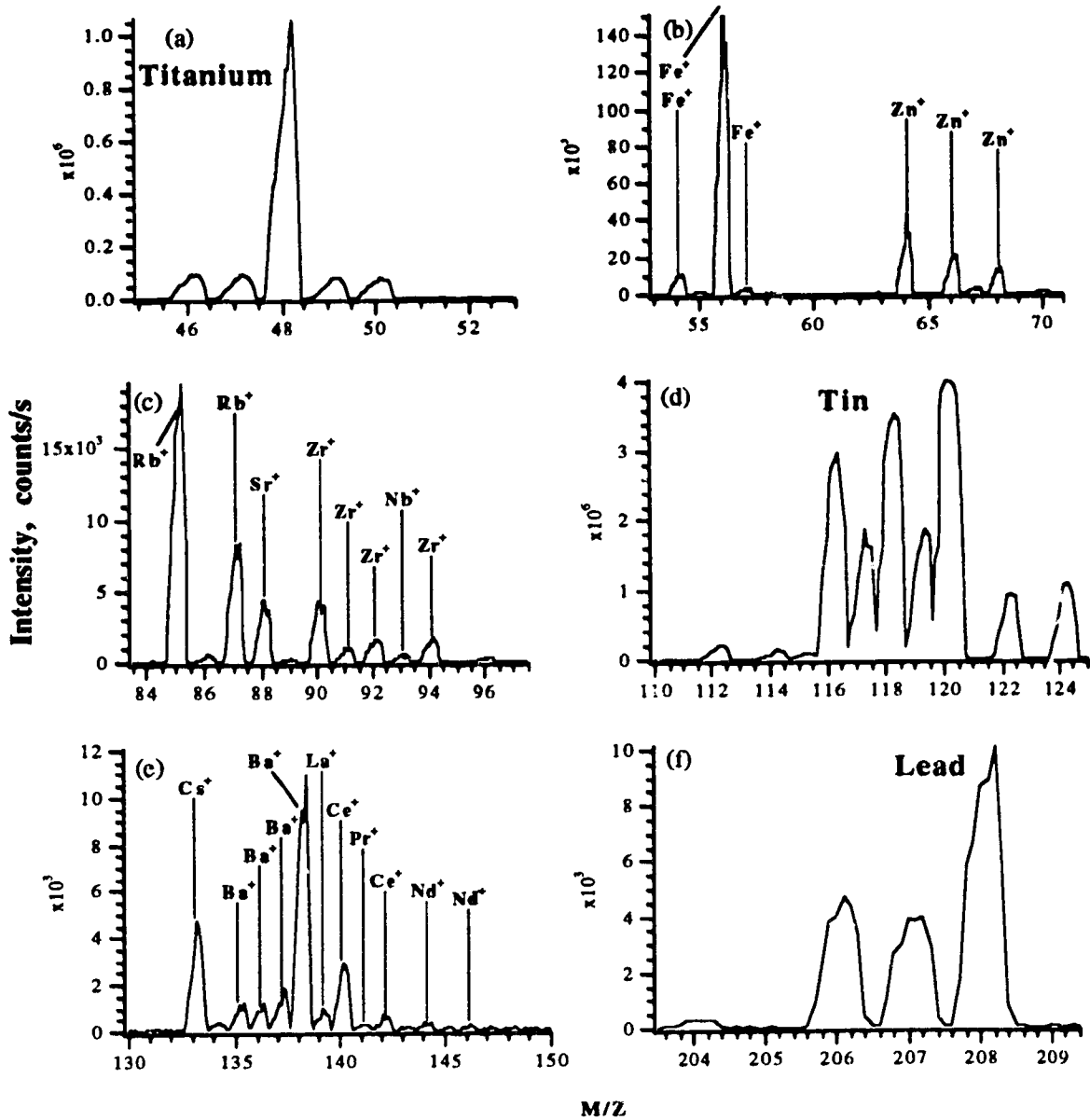


Figure 8.3 LA-ICP-MS spectra of the yellow glaze on a porcelain dish sample with 1 Hz repetition rate of the Nd:YAG laser

range of 10^4 - 10^5 and medium low in the range of 10^3 - 10^4 counts/s. Low signal level means that the elements are at the trace level (signal intensity is below 10^3 counts/s). Semi-quantitative estimation can be roughly carried out for the non-conducting samples. Normally, the amount of the element is greater than 10% when the signal intensity is greater than 10^6 counts/s, while 1-10% composition has a signal intensity in the range of 10^5 - 10^6 counts/s, 0.1-1% in the range of 10^4 - 10^5 counts/s and 0.01-0.1% in the range of 10^3 - 10^4 counts/s. Low signal level means that the elements are at trace level (<0.01%) and the signal intensity is below 10^3 counts/s. The signal levels of some elements such as Fe and Mn are quite different among these glazes. As a result, the different colors of the glazes could arise from Fe in the yellow glaze, Mn in the grey glaze and Zn in the white glaze.

8.3.2.3 Glaze Samples

A number of mass spectra for the white glaze sample (#2) are shown in Figures 8.4 and 8.5. Thirty-two elements were found in this glaze sample. The intense signal of some elements suggests that Al and Si are the major elements in this glaze. The rare earth elements such as La and Ce and heavy elements such as Hf and Pb can also be found (Figures 8.5b and 8.5c). The major components of the eight different color glazes are sodium, aluminum and silicon. The different colors of the glazes could arise from Mn and Co in the black glaze (#1), Zr and Zn in the white glaze (#2), Cu in the blue glaze (#4), Ni and Co in the grey glaze (#5), Cu and Fe in the green glaze (#6), Fe in the brown glaze (#7) and Ba and Fe in the creamy glaze (#8). A bar graph for the relative signal levels of eight elements in these glaze samples is shown in Figures 8.6. The signal levels of these elements are quite different among these glazes. That is why the glazes

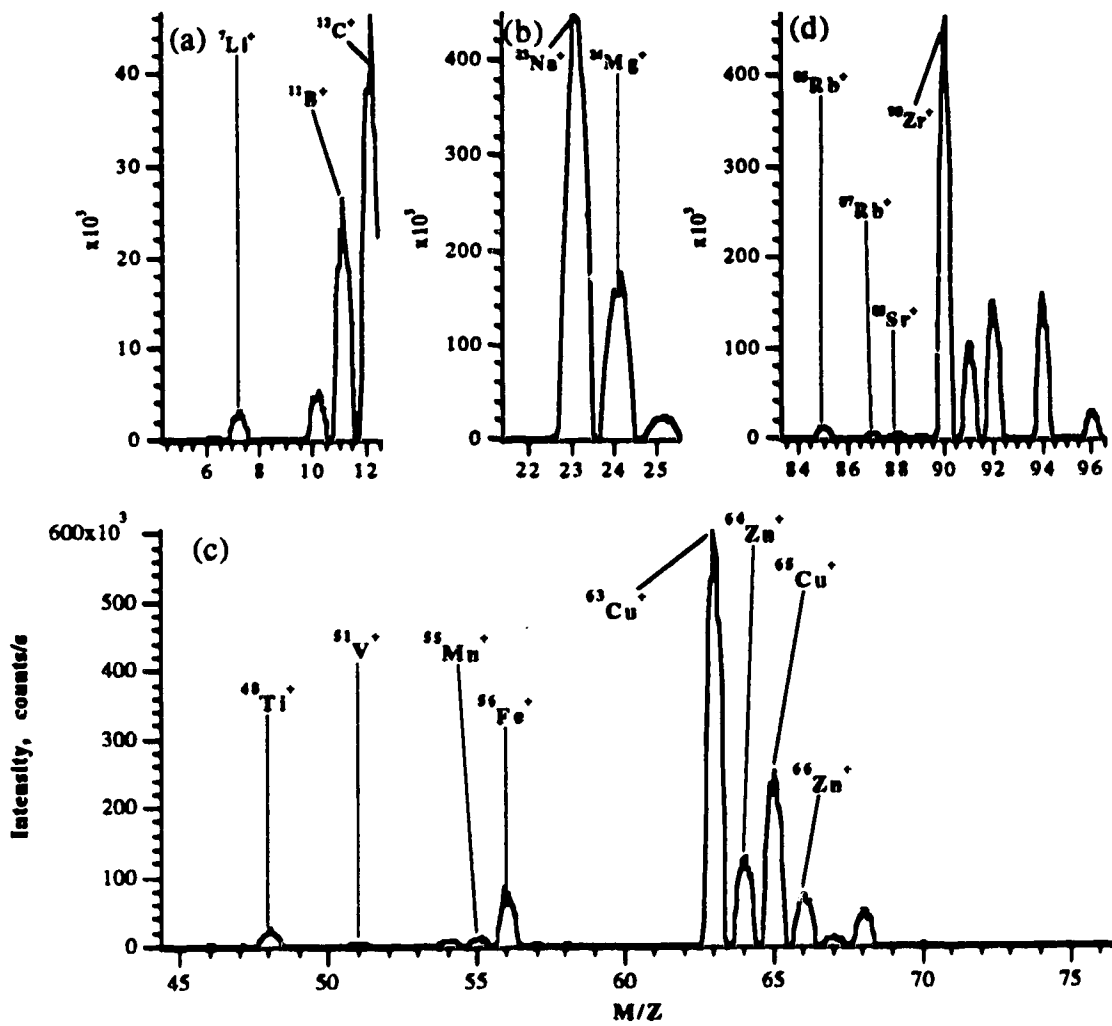


Figure 8.4 LA-ICP-MS spectra of a white glaze sample (#2) with 1 Hz repetition rate of the Nd:YAG laser

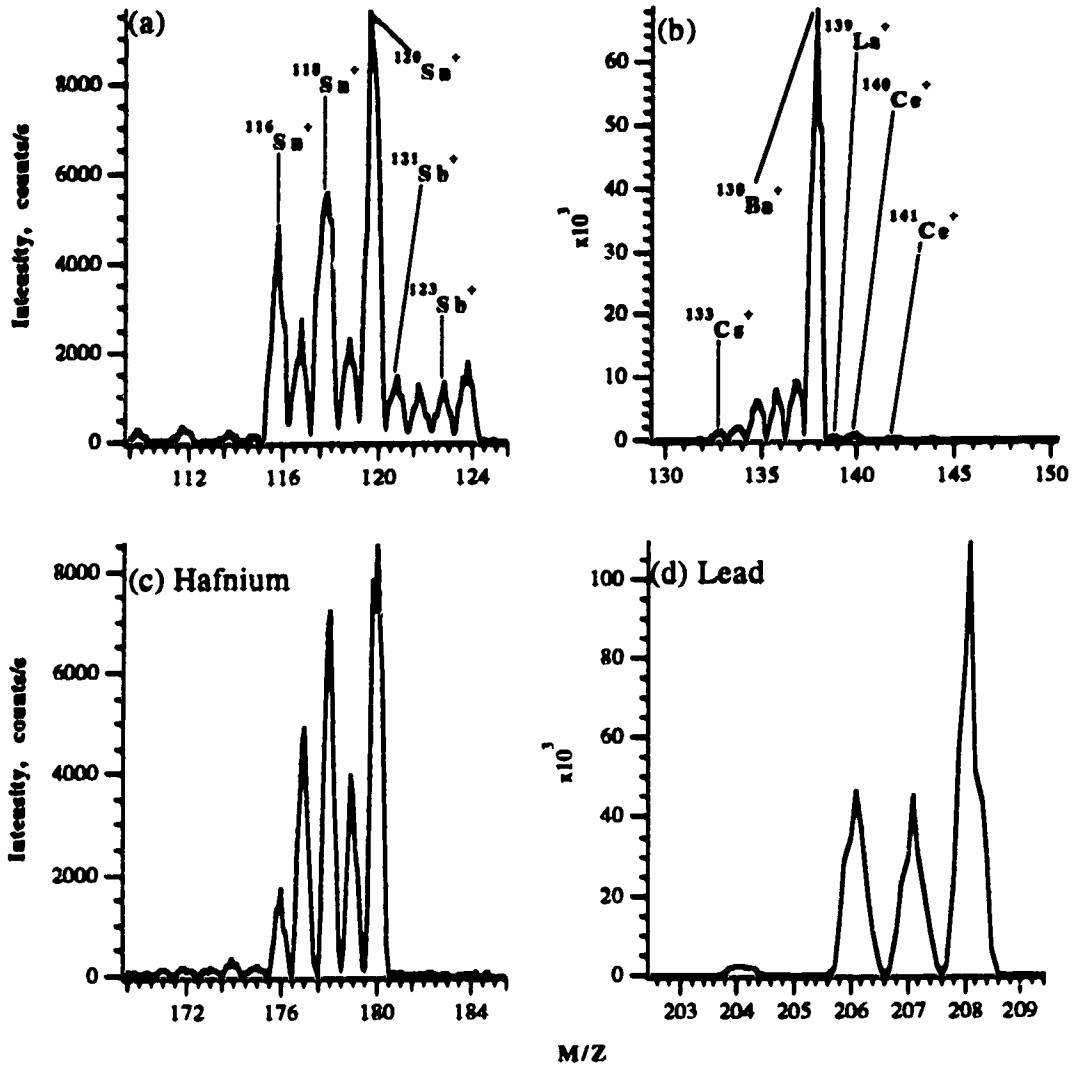


Figure 8.5 LA-ICP-MS spectra of a white glaze sample (#2) with 1 Hz repetition rate of the Nd:YAG laser

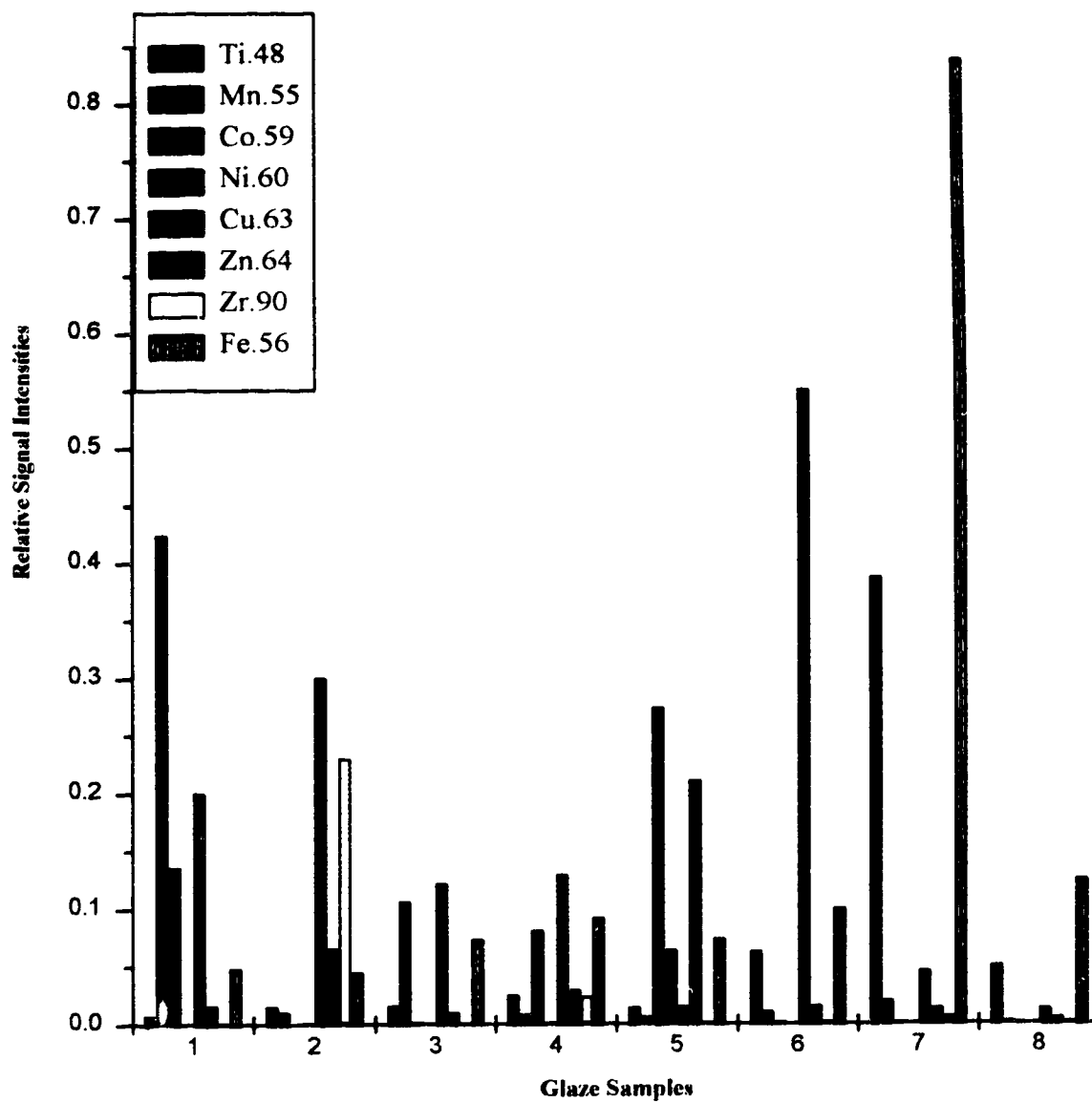


Figure 8.6 Relative signal levels of elements in glaze samples

show different colors. The relative signal intensities were obtained as the signal intensity ratio of the analytes to silicon at m/z 28. Elements found in these eight glaze samples for five different signal levels are also listed in Table 8.3.

Table 8.3 Signal levels of elements in the glaze samples with 1 Hz Nd:YAG LA-ICP-MS

Glaze Samples	High > 10^6 c/s	Medium High 10^5 - 10^6 c/s	Medium 10^4 - 10^5 c/s	Medium Low 10^3 - 10^4 c/s	Low (Trace) < 10^3 c/s
#1(Black)	Si	Na, Al, Mn, Co, Cu	B, C, Mg, Ti, Fe, Zn, Rb, Ba	Li, Sr, Zr, Sn, Cs, Pb	V, Cr, Ni, As, Nb, Sb, Ga, La, Ce, Pr, Bi
#2(White)	Al, Si	Na, Mg, Cu, Zn, Zr, Pb	B, C, Ti, Mn, Fe, Rb, Ba	Li, V, Sr, Sn, Sb, Cs, Ce, Hf	Pr, Bi, Cr, Ni, Co, Ga, As, La
#3(Turquoise)		Na, Al, Si	C, Mg, Mn, Fe, Cu, Ba	Li, B, Ti, Zn, Rb, Sr, Sn, Pb	V, Cr, Ga, La, Ce, Cs, Nb, Zr, Co, Bi
#4(Blue)	Si	Na, Al, Fe, Cu	C, Mg, Ti, Mn, Co, Zn, Zr, Ba	Li, B, Rb, Sr, Sn, Hf, Pb	V, Cr, Ga, Ni, Nb, Cs, Ta, W, Bi, La, Ce, Pr, Nd
#5(Grey)		Na, Al, Si, Ni, Co, Zn	C, Mg, Ti, Fe, Cu, Ba	Li, B, Mn, Rb, Sr, Cr, Pb	V, Zr, Nb, Sn, Cs, Ta, W, Bi, Ga, La, Ce, Pr, Nd
#6(Green)	Na, Al, Si, Cu	Mg, Ti, Fe	Li, B, C, Mn, Zn, Sr, Ba	V, Cr, Co, Zr, Rb, Ce, Pb	Ni, Ga, As, Cs, Nb, Sn, La, Ce, Pr, Nd, Hf
#7(Brown)	Si, Fe	Na, Mg, Al, Ti	B, C, Mn, Cu, Zn, Rb, Sr, Ba, Pb	Li, V, Cr, Zr, Nb, Sn, Cs, Ce, Ta	Ni, Co, Ga, As, Sb, La, Pr, Nd, Hf, W, Bi
#8(Creamy)	Al, Si	Na, Fe, Ba	C, Mg, Ti, Cu,	Li, B, Mn, V, Cr, Zn, Rb, Sr, Zr, Sn, La, Ce, Pb	Ni, Co, Ga, Cs, Nb, Pr, Nd, Hf, Ta, W, Bi

It is possible to perform semi-quantitative analysis for non-conducting samples such as macor, glaze and porcelain. There are quite a few elements of possible interest in these non-conducting samples, but the composition is unknown

in detail. It is important to get the signal intensities from a set of standards first. The instrument response factors for all elements could be calculated and stored in the instrument computer, after correcting for ionization energy and isotopic abundance, and then used to provide calibration sensitivities for elements not in the original standard [13].

8.4 Conclusion

A qualitative survey of non-conducting samples including macor, glaze and a porcelain dish with LA-ICP-MS was carried out and is presented in this chapter. The glaze samples were ablated with a 1 Hz repetition rate of a Nd:YAG laser since the glaze layer was quite thin. External chamber laser ablation ICP-MS can be used successfully for the analysis of both macor and glaze samples. It has been shown that the method is quite simple, rapid and effective, and matrix effects and memory effects are minimal. Such a system is applicable to the direct qualitative and semi-quantitative analysis of non-conducting solid samples. The spectral complexity of LA-ICP-MS spectra seem to be on a par with GD-MS spectra, and tends to be much simpler than solvent-based ICP-MS, since no metal mono-oxide can be observed in spectra for this dry plasma. Thus a quadrupole-based mass spectrometer is adequate for most analytical determinations.

References

1. Y. Mei and W. W. Harrison, *Spectrochimica Acta* **46B**, 175 (1991).
2. S. L. Tong and W. W. Harrison, *Spectrochimica Acta* **48B**, 1237 (1993).
3. D. C. Duckworth and R. K. Marcus, *Anal. Chem.* **61**, 1879 (1989).
4. I. B. Brenner, K. Laqua and M. Dvorachek, *J. Anal. At. Spectrom.* **2**, 623 (1987).
5. D. M. P. Milton and R. C. Hutton, *Spectrochimica Acta* **48B**, 39 (1993).
6. R. K. Marcus and W. W. Harrison, *Anal. Chem.* **59**, 2369 (1987).
7. M. R. Winchester, C. Lazik and R.K. Marcus, *Spectrochimica Acta* **46B**, 483 (1991).
8. R. K. Marcus, *J. Anal. At. Spectrom.* **8**, 935 (1993).
9. P. van de Weijer, W. L. M. Baeten, M. H. J. Bekkers and P. J. M. G. Vullings, *J. Anal. At. Spectrom.* **7**, 599 (1992).
10. J. S. Crain and D. L. Gallimore, *J. Anal. At. Spectrom.* **7**, 605 (1992).
11. W. T. Perkins, N. J. G. Pearce and R. Fuge, *J. Anal. At. Spectrom.* **7**, 611 (1992).
12. P. Arrowsmith, *Anal. Chem.*, **59**, 1437 (1987).
13. L. Moenke-Blankenburg, *Spectrochimica Acta Reviews*, **15**, 1 (1993).

Chapter 9

Conclusions and Future Directions

9.1 Conclusions

Among the known techniques for direct solid sampling such as direct sample insertion (DSI), glow discharge (GD), electrothermal vaporization (ETV) and laser ablation (LA), GD-MS and LA-ICP-MS offer significant potential for the direct analyses of solids. GD-MS has been available commercially for several years [1] and many of its features and limitations have been documented. It is a very sensitive technique with detection limits in the low parts-per-billion range [2] and the calibration curves are linear over 4-5 orders of magnitude. GD-MS is now well established for the direct analysis of conducting solid samples such as metals and alloys [3, 4] with little or no sample pre-treatment. The spectra are much simpler than optical emission spectra, and the majority of elements can be detected. The mass spectrum is responsive to both metallic and nonmetallic elements and minimal matrix effects have been observed. It provides a rapid qualitative scan of almost all elements in the periodic table and offers a wide dynamic range on the order of 10^9 for simultaneous multielemental determinations of major to trace or ultra-trace constituents. Quantitative analysis is possible with the application of internal standardization and/or relative sensitivity factors (RSF) since the sensitivities are generally uniform for most elements [2].

Both GD-MS and Inductively Coupled Plasma Mass Spectrometry (ICP-MS) have been successfully applied for the determination of trace amounts of elements in low alloy aluminum, low alloy steel and stainless steel samples [3-5]. An investigation was carried out by comparing both background and analyte spectral features between solution based ICP-MS and GD-MS with respect to the analysis of low alloy aluminum. By using ICP-MS, the samples were dissolved and analyzed as 0.01% Al solutions, whereas the samples were directly analyzed in a solid form by using GD-MS. Due to their different sampling methods, however, different spectral characteristics between ICP-MS and GD-MS were noticed. The interesting results include the higher basic background species originating from solvent and air in ICP-MS, formation of argides, dimers of argon and multiply charged argon ions in GD-MS, and the different intensity ratios of some elements observed between ICP-MS and GD-MS. It is also important to point out that even though dissolution involves dilution of the analyte by 100 to 10,000 fold when 1-0.01% sample solutions are prepared, ICP-MS still will have comparable or superior detection limits when referenced back to the solid composition; a consequence of the 1-10 pg/mL range of detection limits for ICP-MS vs. the 1-10 ng/g detection limits currently typical for GD-MS.

Laser ablation-Inductively Coupled Plasma-Mass Spectrometry (LA-ICP-MS), another different solid sampling method, was also used to determine elements in both the aluminum alloy and stainless steel samples. A Nd:YAG laser was used to ablate disk samples and a quartz external chamber functioned as a site for vaporization of samples by laser ablation. This system is applicable to the direct qualitative and quantitative analyses of metallic solid samples, as well the direct qualitative and semi-quantitative analyses of non-conducting materials. The spectral background character of LA-ICP-MS seems to be on a

par with GD-MS and is much simpler than solvent-based ICP-MS. Although significant intensities for background species such as $^{14}\text{N}^+$, $^{16}\text{O}^+$, H_2O^+ , $^{14}\text{N}^{16}\text{O}^+$, N_2^+ , O_2^+ , $^{40}\text{Ar}^{14}\text{N}^+$, $^{40}\text{Ar}^{16}\text{O}^+$ and Ar_2^+ were observed in the dry ICP, the signal levels of these interferences were much lower than those in solution based ICP-MS. The signal levels of hydrides such as NH^+ , OH^+ , OH_3^+ , N_2H^+ , NOH^+ and ArOH^+ were extremely low and even absent in LA-ICP-MS. On the other hand, the most important difference in spectral features between ICP-MS and GD-MS is the existence of metal argides in GD-MS. AlAr^+ can be observed clearly in GD-MS but not in ICP-MS. The level of the argides in GD-MS is in the range of 0.01-0.1%. Other argon species including argon dimers and multiply charged argon species can be found in GD-MS. However, the signals of argon dimers are much stronger in GD-MS than those in ICP-MS. The multiply charged argon species (Ar^{2+} , Ar^{3+} , Ar^{4+} , Ar^{5+} and even Ar^{6+}) are present in GD-MS, but they are absolutely absent in ICP-MS.

In addition to the interferences from the background, the interferences arising from hydrochloric acid could be observed, and the metal oxides (MO) could not be avoided in solution aspirated ICP-MS. Signals of $^{51}\text{V}^+$ and $^{75}\text{As}^+$ can be interfered by the presence of $^{35}\text{Cl}^{16}\text{O}^+$ and $^{40}\text{Ar}^{35}\text{Cl}^+$, while no such problem exists in GD-MS and LA-ICP-MS. It has been reported that the oxide levels in ICP-MS are in the range of 0.1-2.5% [6] and the rare earth elements form particularly strong oxides [7]. For steels, potential spectral interferences can occur as a result of FeO and FeOH formation in the plasma and an FeO/Fe ratio of 0.5% has been reported [5]. Under optimum conditions for controlling oxide levels, CeO^+/Ce^+ ratios of 2.5% and 2% [8] have been obtained. Consequently, the oxides of La, Ce, Pr and Nd are all readily observed in ICP-MS. Moreover, the oxides of Mo, Ta and W were also observed in analysis of steels using ICP-

MS [2]. These oxides can result in serious spectral interferences for the determination of some trace elements in steels. For a dry plasma, however, the signal level of the mono-oxides is much lower in GD-MS and they could hardly be found in LA-ICP-MS. That is one of the most important advantages for direct sample analysis.

Both GD-MS and LA-ICP-MS are direct sampling techniques which have been successfully applied for the determination of trace amounts of elements in both low and high alloy samples including aluminum and steels. Compared to ICP-MS and GD-MS, LA-ICP-MS is a simple, rapid and effective analytical method with minimal matrix effects and memory effects. No dissolution or pre-sputtering steps are required with LA-ICP-MS. Solution based ICP-MS typically requires dissolution of a sample which consumes time and may lead to contamination. However, GD-MS also has time-consuming steps involving sample form fabrication and pre-sputtering, especially for aluminum samples. Certainly some contamination is possible during fabrication although the pre-sputtering step should minimize surface transferred contamination. Because of difficulty in the dissolution of silicon in the samples, only low alloy aluminum samples were analyzed with solution based ICP-MS. On the other hand, a laser is expensive, while use of a glow discharge device is economical since less argon gas is consumed for GDs than that for ICPs.

9.2 Future directions

Non-conducting materials such as compacted powder samples can be analyzed with GD-MS, solution residues can be deposited onto the surface of an appropriate conducting electrode (high density pyrolytic graphite or vitreous

carbon electrodes) and sputtered in a glow discharge and analyzed with GD-MS [1] and solution sample can also be injected into a hollow cathode and analyzed with GD-MS. Some work is even under way in developing direct solution sample interfaces for GD devices [9]. Non-conducting samples can be ablated by a laser, and the vaporized samples can be introduced into a hollow cathode glow discharge device. On the other hand, alternative gas glow discharge devices are developed where Ne and mixtures of gases such as Ar-Ne and Ne-He [10, 11] are used to modify the ionization characteristics and background spectral features of glow discharge devices.

Mass spectrometry is now firmly established as a major technique for elemental analysis, and the ICP-MS implementation should be regarded merely as the beginning. Beyond ICPs and GDs, new and different ion sources for elemental MS are sure to be developed. Electrospray mass spectrometry (ES-MS) is a new ionization technique for the determination of solution species. Both molecular and metal ion clusters generated by ES have been studied. It is clear that ES-MS has the potential to evolve into a generic ion source for elemental MS. Ion-trap mass spectrometry may also prove to be a viable system. The combination of laser ablation-ion-trap MS is a potentially powerful technique for elemental analysis [12].

Finally, elemental speciation of inorganic and organic environmental samples with plasma mass spectrometry [13] is an area which comprises a major portion of my immediate research interests. Elemental speciation is defined as identification and quantitation of the chemical forms of an element, including metals and nonmetals. These chemical forms can be the oxidation state of an inorganic form or the metal associated with different ligands in the inner and

outer coordination spheres; it can also depend on the type and number of substituents of organometallic compounds. From a risk assessment perspective, it is no longer sufficient to quantitate the total elemental content of samples to define toxicity. Thus elemental speciation offers a continuing challenge for the analytical chemist. Both inductively coupled plasmas (ICPs) and microwave-induced plasmas (MIPs) are useful as ion sources for MS and easily utilized as ion detectors after coupling with various types of separation procedures. The ICP mass spectrometer and/or MIP mass spectrometer can be coupled with GC, LC, Supercritical Fluid Chromatography (SFC), Capillary Electrophoresis (CE) or even Flow Injection Analysis (FIA) to determine different chemical forms of an element in environmental or bio-inorganic samples. Efficient interface methods need to be considered and studied. The sample can be directly introduced into an ICP source with a specific nebulizer after separation or even use of an electrospray interface to couple CE-MS where one end of the electrophoretic capillary functions as an electrospray source [14]. With these developments, mass spectrometric techniques conceivably will provide the dominant methods for elemental analysis by the beginning of the next century.

References

1. W. W. Harrison and B. L. Bentz, *Prog. Analyt. Spectrosc.* **11**, 53 (1988).
2. W. W. Harrison, *J. Anal. At. Spectrom.* **3**, 867 (1988).
3. Y. Shao and G. Horlick, *Spectrochimica Acta* **46B**, 165 (1991).
4. N. Jakubowski, D. Stuewer and W. Vieth, *Anal. Chem.* **59**, 1825 (1987).
5. M. A. Vaughan and G. Horlick, *J. Anal. At. Spectrom.* **4**, 45 (1989).
6. J. W. McLaren, D. Beauchemin and S. S. Berman, *Anal. Chem.* **59**, 610 (1987).
7. H. P. Longerich, B. J. Fryer and D. F. Strong, *Spectrochimica Acta* **42B**, 101 (1987).
8. G. Zhu and R. F. Browner, *Appl. spectrosc.* **41**, 349 (1987).
9. C. M. Strange and R. K. Marcus, *Spectrochimica Acta* **46B**, 517 (1991).
10. K. Wagatsuma and K. Hirokawa, *Spectrochimica Acta* **46B**, 269 (1991).
11. N. Jakubowski and D. Stuewer, *Fresenius' Z. Anal. Chem.* **335**, 680 (1989).
12. C. G. Gill, B. Daigle and M. W. Blades, *Spectrochimica Acta* **46B**, 1227 (1991).
13. N. P. Vela, L. K. Olson and J. A. Caruso, *Anal Chem*, **65**, 585A (1993).
14. R. D. Smith, J. H. Wahl, D. R. Goodlett and S. A. Hofstadler, *Anal Chem*, **65**, 574A (1993).